The Western Australian School of Mines
Department of Spatial Sciences

An Artificial Neural Network Approach For Soil Moisture Retrieval Using Passive Microwave Data

Soo See Chai

This thesis is presented for the Degree of
Doctor of Philosophy
of
Curtin University of Technology

March 2010

Declaration

To the best of my knowledge and belief this thesis contains no material previously published by any other person except where due acknowledgement has been made.

This thesis contains no material which has been accepted for the award of any other degree or diploma in any university.

Signature: .....

Date: .....

Abstract

Soil moisture is a key variable that defines land surface-atmosphere (boundary layer) interactions, by contributing directly to the surface energy and water balance. Soil moisture values derived from remote sensing platforms only accounts for the near surface soil layers, generally the top 5cm. Passive microwave data at L-band (1.4 GHz, 21cm wavelength) measurements are shown to be a very effective observation for surface soil moisture retrieval. The first space-borne L-band mission dedicated to observing soil moisture, the European Space Agency's (ESA) Soil Moisture and Ocean Salinity (SMOS) mission, was launched on 2nd November 2009.

Artificial Neural Network (ANN) methods have been used to empirically ascertain the complex statistical relationship between soil moisture and brightness temperature in the presence of vegetation cover. The current problem faced by this method is its inability to predict soil moisture values that are "out-of-range" of the training data.

In this research, an optimization model is developed for the Backpropagation Neural Network model. This optimization model utilizes the combination of the mean and standard deviation of the soil moisture values, together with the prediction process at different pre-determined, equal size regions to cope with the spatial and temporal variation of soil moisture values. This optimized model coupled with an ANN of optimum architecture, in terms of inputs and the number of neurons in the hidden layers, is developed to predict scale-to-scale and downscaling of soil moisture values. The dependency on the accuracy of the mean and standard deviation values of soil moisture data is also studied in this research by simulating the soil moisture values using a multiple regression model. This model obtains very encouraging results for these research problems.

The data used to develop and evaluate the model in this research has been obtained from the National Airborne Field Experiments in 2005.

Acknowledgement

I am greatly in debited to many people throughout the three years of my postgraduate research study in the Department of Spatial Sciences. To name a few:

First and foremost, I would like to thank my supervisors, Professor Bert Veenendaal and Professor Geoff West for their time and efforts in helping me to complete this research study. Thank you for the calm patience you have shown towards me.

I would also like to extend my thanks to my associate supervisor, Associate Professor Jeffrey P. Walker of University of Melbourne for the data used in this research study and also for his comments and help at the different stages of my research. This appreciation also goes to Mr. Rocco Panciera and Dr. Oliver Merlin for giving me valuable suggestions throughout my study.

I also would like to thank my friends in the Department of Spatial Sciences: Mr. Mulalu, Mr. Saud Aboshiqah, Mr. Jacob Delfos, Miss Ira Anjasmara, Dr. Cecilia Xia, Dr. Rob Corner and Dr. Joseph Awange. I really enjoy the time talking to you people. I would also like to thank Dr. Kevin Fleming for his help to proof read this thesis.

I am indebted with the Malaysia's Ministry of Higher Education Malaysia (MOHE) for giving me the scholarship for my study. Without the financial support, I would not have gone so far.

Last but not least, I also would like to thank my beloved parents who have supported all my decisions throughout my life. Their love and patience are the main drive of my life.

Credits

Portions of the material in this thesis have previously appeared in the following publications:

Journal:

- Chai, S.-S.; Walker, J.P.; Makarynskyy, O.; Kuhn, M.; Veenendaal, B.; West, G. Use of Soil Moisture Variability in Artificial Neural Network Retrieval of Soil Moisture. *Remote Sens.* 2010, *2*, 166-190. [Chapter 7]

- Chai, S.-S.; Walker, J.P.; Veenendaal, B.; West, G. Artificial Neural Network Downscaling of Passive Microwave Soil Moisture. *Computers and Electronics in Agriculture*. Under Review. [Chapter 8]

Conference Proceedings:

- Chai, S.-S., B. Veenendaal, G. West, and J.P. Walker. *Explicit Inverse of Soil Moisture Retrieval with an Artificial Neural Network Using Passive Microwave Remote Sensing Data* in *IEEE International Geoscience and Remote Sensing Symposium, 2008 (IGARSS 2008)*. 2008: Boston, Massachusetts, U.S.A. p. II-687-II-690. [Chapter 5]

- Chai, S.-S., B. Veenendaal, G. West, and J.P. Walker, *Input Pattern According to Standard Deviation of Backpropagation Neural Network: Influence on Accuracy of Soil Moisture Retrieval*, in *IEEE International Geoscience and Remote Sensing Symposium, 2008 (IGARSS 2008)* 2008: Boston, Massachusetts, U.S.A. p. II-691-II-694. [Chapter 7]

- Chai, S.-S., B. Veenendaal, G. West, and J.P. Walker, *Backpropagation Neural Network for Soil Moisture Retrieval Using Nafe'05 Data : A Comparison of Different Training Algorithms*, in *The International Archives of the Photogrammetry, Remote Sensing and Spatial Information Sciences (ISPRS)*. 2008: Beijing, China. p. 1345-1349. [Chapter 7]

- Chai, S.-S., B. Veenendaal, G. West, and J.P. Walker, *Input Parameters Selection for Soil Moisture Retrieval Using an Artificial Neural Network*, in *Surveying & Spatial Sciences Institute Biennial International Conference Adelaide 2009*, B. Ostendorf, P. Baldock, D. Bruce, M. Burdett, and P. Corcoran, Editors. 2009: Adelaide Convention Centre, Adelaide, Australia. p. 1181-1194. [Chapter 7]

Table of Contents

List of Figures

List of Tables

List of Abbreviations

AEF	Actual Evaporative Fraction
ANN	Artificial Neural Network
AMSR-E	Advanced Microwave Scanning Radiometer for EOS
ASL	Above Sea Level
AVHRR	Advanced Very High Resolution Radiometer
BP	Backpropagation
DEM	Digital Elevation Model
EF	Evaporative Fraction
EOS	Earth Observing System
ESA	European Space Agency
ESTAR	Electronically Scanned Thinned Array Radiometer
FNN	Feedforward Neural Network
IEM	Integral Equation Model
L-MEB	L-band Microwave Emission of the Biosphere
LST	Land Surface Temperature
MODIS	MODerate Resolution Imaging Spectrometer
NAFE	National Airborne Field Experiments
NDVI	Normalized Difference Vegetation Index
NN	Neural Network
NOAA	National Oceanic and Atmospheric Administration
PALS	Passive/Active L-band System
RMSE	Root Mean Square Error
SM	Soil Moisture
SMM/I	Special Sensor Microwave Imager
SMOS	Soil Moisture and Ocean Salinity Mission
Tb	Brightness temperature
TbH	H-polarized brightness temperature
TbV	V-polarized brightness temperature
VTCI	Vegetation Temperature Condition Index
WDI	Water Deficit Index

Chapter 1

Introduction

This thesis focuses on the investigation and development of a methodology using Artificial Neural Network (ANN) for both scale-to-scale and downscaling prediction of soil moisture from passive microwave remote sensing data. The scale-to-scale methodology predicts soil moisture at the same scale as the input parameters, while downscaling uses data at a coarser scale to predict soil moisture at finer resolution.

1.1 Background

Within a remote sensing context, surface soil moisture refers to the amount of water in the top layer of the soil surface; generally in the upper 5 to 10 cm below the natural ground surface. Although the volume of soil moisture is small compared to other components in the hydrological cycle, it is of fundamental importance to many hydrological, biological and biogeochemical processes. It is one of the few directly observable hydrological variables that plays an important role in the water and energy budgets necessary for climate study (Jackson and Schmugge 1995).

The variability of soil moisture changes in space (i.e. spatial variation) and time (i.e. temporal variation) and the behaviour of these two parameters is important for various hydrological modelling processes, such as rainfall-runoff models (Wei *et al.* 2007) and snow melting models (Vinnikov *et al.* 1996). Moreover, the spatial distribution of soil moisture is being increasingly used as an input to these models (Lakhankar *et al.* 2006b). Therefore, the accurate estimation or prediction of the spatial distribution of soil moisture becomes increasingly important. The most common and accurate way of measuring the spatial distribution of soil moisture is through actual field measurement techniques that acquire data at discrete, although usually sparse, locations. The disadvantage of these techniques is that, as the

soil moisture values are generally affected by the heterogeneity of soil properties, topography, land cover, evapotranspiration and precipitation, their use is limited to a small geographic area and within a limited time period. Many environmental phenomena such as drought and flooding cannot be captured by ground measurements alone and methods are sought that can capture full coverage information over wide areas regularly. Remote sensing can satisfy these desires as it allows rapid collection of spatial data over large areas on a routine basis. Although remote sensing offers better data coverage, soil moisture measurements at distinct points are still important for calibration and verification of the results from remote sensing.

Microwave remote sensing has the potential for soil moisture retrieval due to the pronounced effect of the soil dielectric properties on the microwave signal. Passive microwave observation allows for larger area coverage at higher temporal frequencies for retrieving surface soil moisture. The Soil Moisture and Ocean Salinity (SMOS) mission, the first ever space borne radiometer which was launched in November 2009, has a resolution of ~40 km. Thus, methods need to be developed for reducing the coarse scale measurements of the data from such a satellite to a finer scale at which soil moisture knowledge is desired (~1 km) (Tsegaye *et al.* 2003).

1.2 Motivation

The research reported in this thesis is motivated by recent intense research activities currently underway by the European community in producing an upcoming satellite mission fully dedicated to soil moisture mapping from space: the European Space Agency's (ESA)'s Soil Moisture and Ocean Salinity Mission (SMOS) (Kerr *et al.* 2001). SMOS was launched in November 2009 and will use an L-band interferometric radiometer to make measurements at a spatial resolution of around 40 km with a temporal resolution of 1 to 3 days. The accuracy of the soil moisture measurements of

this mission is expected to be 0.04 (4% v/v) volume of water over total volume (i.e. soil volume + water volume + void space) (Kerr *et al.* 2001).

Soil moisture predictions from passive microwave remote sensing involve the measurement of the self emitted and/or reflected electromagnetic radiation in the microwave region of the electromagnetic spectrum from the Earth's surface. The measured intensity is termed the "brightness temperature". At passive microwave radiation frequencies in the L-band (1.4 GHz frequency, 21 cm wavelength), vegetation and atmospheric effects are minimized, but are still non-negligible (Sandells *et al.* 2008). For soil moisture prediction from passive microwave data, ancillary data like land cover and soil information are necessary (Schlenz *et al.* 2008). Due to the complex approximation function relating brightness temperature and soil moisture, non-parametric methods like neural networks have been used to empirically ascertain the statistical relationship between soil moisture and brightness temperature in the presence of vegetation cover (Del Frate *et al.* 1999; Atluri *et al.* 1999; Yuei-An *et al.* 1999b; Maier and Dandy 2000; Chang and Islam 2000; Yuei-An *et al.* 2001; Paloscia *et al.* 2002; Del Frate *et al.* 2003; Angiuli *et al.* 2008; Junlei *et al.* 2008; Elshorbagy and Parasuraman 2008; Lakhankar *et al.* 2009). Other non-parametric methods used include fuzzy logic (Lakhankar *et al.* 2006a) and maximum likelihood (Li and Gaiser 2007). The neural network methods do not require prior assumptions about the statistical behaviour of the data or about any specific relationship between the variables. The relationship between the inputs and outputs are determined by the network itself. The major advantages of the neural network method are (Ghedira *et al.* 2004):

i. Easy adaptation to different types of data and input configurations. Neural networks can easily incorporate ancillary data that would be difficult or impossible to do with conventional techniques. Although mechanistic models, sometimes called process models, can easily incorporate ancillary data as well, these models are usually data

intensive and frequently over-parameterized comparing to neural network models.

ii. A neural network uses its complex configuration to find the best nonlinear function between the input and output data without the constraint of linearity or pre-specified non-linearity which is required in regression analysis.

ANN methods for soil moisture prediction using passive microwave remote sensing data have been investigated in this thesis. From the review, for scale-to-scale retrieval, data used for the testing of the "trained" ANN is either a sub-set of the training data (Yuei-An *et al.* 1999a; Yuei-An *et al.* 2001; Shou-Fang *et al.* 2002) or simulated data (Del Frate *et al.* 2003). The problem with simulated data is its incapability of covering all the unforseen conditions. This issue has been reported by Angiuli *et al.*(2008) and Lakhankar *et al.*(2009) who found that the "trained" neural network models were unable to predict soil moisture values, which are outside the range of the training data.

One of the most popular and important types of neural network architectures are Feedforward Neural Networks (FNNs). A FNN is a static network with a single signal flow direction from input to output and no feedback loop. The training of the FNNs is mainly undertaken using Backpropagation (BP) based learning algorithms. There has been much research activity directed to improving the conventional BP algorithm, which has resulted in many different training algorithms. Researchers in soil moisture prediction have been utilizing some of these training algorithms in BP for their works. This includes the conventional BP algorithm (Paloscia *et al.* 2002), Levenberg-Marquardt BP algorithms (Atluri *et al.* 1999; Posa *et al.* 2004) and the Scaled Conjugate Gradient algorithm (Del Frate *et al.* 1999). Note the justification for the choice of the particular BP training algorithm has not been documented by these researchers. Although the different variations of BP algorithms are aimed at improving the learning efficiency of

the conventional BP algorithm, the impacts of them in improving the soil moisture prediction has yet to be analysed.

Apart from the brightness temperature, other spatial data may be used to aid the predictions. Angiuli *et al.* (2008) used brightness temperature, surface temperature and soil roughness as the inputs while Atluri *et al.* (1999) used surface temperature and brightness temperature as inputs. On the other hand, Yuei-An *et al.* (1999a; 2001) used only brightness temperature as an input. The effects of incorporating ancillary data with the brightness temperature values as the inputs of the neural network have not been previously analysed and discussed. Shou-Fang *et al.* (2002) claimed that, ancillary information such as vegetation biomass, surface temperature, and surface roughness is not needed when using a neural network as a prediction method. However, ancillary data, which provides information on the surface characteristics, should help a neural network in improving the soil moisture prediction, especially in building a neural network model that can capture the spatial and temporal nature of soil moisture variations. For space borne operational applications over large heterogeneous regions, the retrieval of accurate ancillary data, especially field-based, can be problematic or impractical. Therefore, the requirements for ancillary data for moisture prediction using ANN should be analysed properly to avoid unnecessary efforts in obtaining such data.

A scale disparity exists between the resolution of the passive microwave satellite missions, e.g. ESA's SMOS mission (40 km), and the much finer resolution at which soil moisture is desired (~1 km). There is therefore a need to address such coarse spatial resolutions before important potential applications, such as the incorporation of soil moisture estimates in precision agriculture derived from L-band passive microwave data, can become possible (Voltz 1997). In the research by Schamschula *et al.* (2002) and Tsegaye *et al.* (2003), much ancillary data were used, which included low resolution emissivity, antecedent rainfall, soil texture, vegetation water content and upstream contributing area. The downscaling was carried out

from a resolution of 12.8 km to 0.8 km. While these papers were restricted to only linear neural network models, i.e. the activation function is linear function, this thesis will explore more complex non-linear neural network models, i.e. the activation function is non-linear.

1.3 Research Objectives

The main aim of this thesis is to investigate and develop ANN based soil moisture prediction approaches. Specific objectives of the research include:

i. To investigate and develop a scale-to-scale soil moisture prediction solution. The developed solution must be able to produce consistent and accurate results for data that are totally new and independent from the training data. The developed solution must also be able to capture the spatial and temporal variation of soil moisture.

ii. To determine the appropriate ancillary data to improve soil moisture prediction. It is most efficient if the ancillary data are based on satellite observations. For this reason, the ancillary data being studied are limited to the Normalized Difference Vegetation Index (NDVI) and the surface temperature obtained from the **MOD**erate Resolution **I**maging **S**pectrometer (MODIS).

iii. To develop a soil moisture prediction solution using a neural network for the downscaling of soil moisture to bridge the gap of scale disparity between the resolutions of space-borne passive microwave remote sensors and the much finer scales at which soil moisture estimates are required (~1km).

In addition, the scope of this thesis is constrained as follows:

i. The proposed methodology will be evaluated using data from a target area 40km×40km in size, located at Goulburn River Catchment in south-eastern Australia.

ii. Only data available for the field trip of 40km×40 km, which is the target study area of this research, will be used.

iii. An analysis of the computational performance of the proposed methodology in terms of execution time is worthwhile, but is not within the scope of this thesis.

1.4 General Methodology

The methodology involves developing solutions to achieve the objectives in **Section 1.3**. The data used in this research is obtained from the National Airborne Field Experiments conducted in 2005 (NAFE'05). During the first part of this research, soil moisture prediction is focused on scale-to-scale prediction (**Figure 1.1**), while the focus in the second part is on downscaling problems of soil moisture prediction (**Figure 1.1**). The data will be divided into training, validation and testing sets. The developed ANN solutions will then be evaluated using an independent data set, i.e. data from a new date, to verify the accuracy of this model.

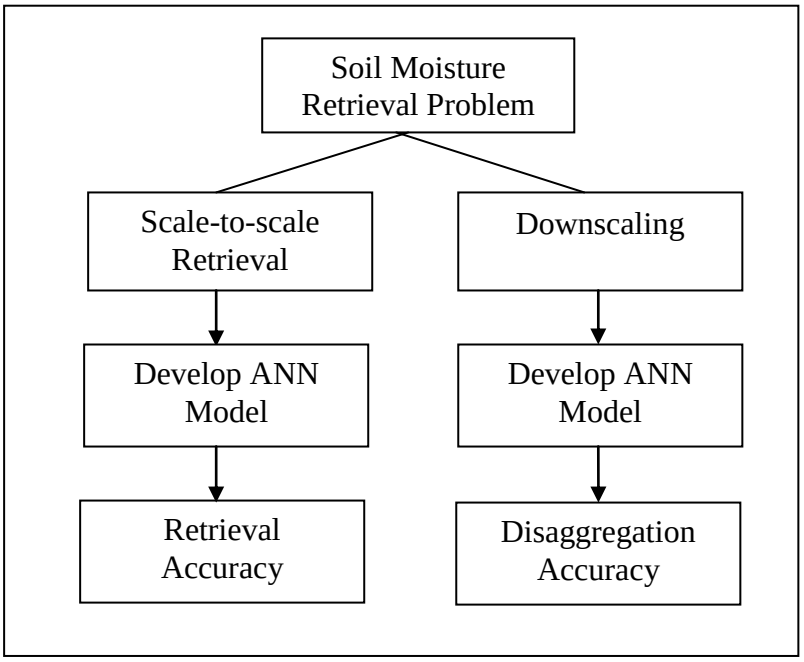

Figure 1.1. Overview of the methodology followed in this research study.

1.5 Overview of the Thesis

This thesis is divided into nine chapters. **Chapter 2** presents the background information and theory related to soil moisture and soil moisture measurements that are necessary for this research. A review of soil moisture prediction using passive microwave data is also presented in this chapter. **Chapter 3** gives a brief overview of Artificial Neural Networks (ANNs) that includes the theory and examples of ANN models. The terminologies and components that are important for this research are explained in this chapter.

The data used in this research was obtained during the field campaign NAFE 2005 (National Airborne Field Experiment) conducted in New South Wales, Australia during the month of November 2005. Details on this field campaign are in **Chapter 4** of this thesis. The description will cover the objectives of the campaign, ground sampling strategy and the airborne monitoring.

The literature review on the use of Artificial Neural Networks (ANNs) in the field of soil moisture prediction using passive microwaves is presented in **Chapter 5**. This chapter will include a review of both scale-to-scale and downscaling of soil moisture predictions. The general methodology of the approach developed in this thesis is also presented in this chapter.

The data pre-processing and analysis of the data used in this thesis are presented in **Chapter 6**. This is followed by a detailed description of the methodology developed for scale-to-scale soil moisture prediction using the ANN in **Chapter 7** and downscaling in **Chapter 8**. Finally, the conclusions and proposed future directions are presented in **Chapter 9**.

Chapter 2

Soil Moisture Measurement

This chapter outlines the different methods and most recent research on soil moisture measurements, the theory of microwave dielectric behaviour, and the different sensors in remote sensing used for soil moisture retrieval. The use of L-band passive microwaves and the different satellite observing systems for soil moisture retrieval are also covered.

2.1 Types of Soil Moisture Measurement

Information about soil moisture can be obtained either through point measurements or remote sensing techniques. Point-based measurements of soil moisture, which are categorized as ground-based measurements, produce accurate information but gathering such data is costly and time consuming (Walker 1999). Being point-based, only sparse measurements can practically be taken. Point-based measurement methods can be further divided into direct and indirect methods (Navarkhele *et al.* 2006). For direct measurements, a sample of soil is taken and the water removed, by either evaporation or a chemical process, and measured. The thermo-gravimetric method, the standard direct method of measuring volumetric soil moisture content, removes water from the soil sample by evaporating the sample at 105°C using an oven (Walker *et al.* 2004). The soil moisture measurement obtained can be expressed as a fraction or as a percentage of a gravimetric or volumetric basis. The volumetric soil moisture θ is obtained using the formula (Walker *et al.* 2004):

$$\theta = \frac{W_w \rho_b}{W_d \rho_w} \tag{2.1}$$

where W_w is the weight of the water contained in the voids (gaps) in the moist soil, W_d is the weight of the dry soil, ρ_b is the soil bulk density of a known volume of soil, and ρ_w is the density of the water. Equation (2.1) can be rewritten as:

$$\theta = \frac{V_w}{V_T} \tag{2.2}$$

where V_w is the volume of water, and V_T is the total volume (i.e. soil volume, water volume and void space. The unit used for $\boldsymbol{\theta}$ is either m^3/m^3 or v/v (i.e. volume/volume). A direct point-based measurement is simple, inexpensive and the soil moisture can be easily calculated. However, this method is also destructive and it would not be possible to repeatedly carry out the point-based measurement at the same location (Roth *et al.* 1990).

Indirect methods are non-destructive and monitor soil properties that are a function of water content. The use of Time Domain Reflectometry (TDR) probes is based on the measurement of the dielectric properties of soil (Robinson *et al.* 2003). Indirect methods normally involve inserting instruments into the soil, or placing them on the surface. This method promises in-situ measurements of soil moisture and can be repeated at the same location a number of times, although it requires one time calibration for the same location to determine soil moisture.

The disadvantages of using point-based measurements are that this type of measurement is rarely representative of the spatial distribution of moisture required for mapping large areas. This is because accurate spatial estimates of soil moisture require samples that are closely spaced, relative to the correlation length of the spatial soil moisture fields, meaning that this method is impractical to determine large scale areal estimation of soil moisture.

Remote sensing, on the other hand, provides a mean of measuring soil moisture in both higher spatial and temporal dimensions and can provide readings for the top few centimetres of soil for areas with moderate to low vegetation cover. Platforms supporting remote sensing instruments can be

either ground-based, aircraft-based or space-based (Wu 1996). For ground-based remote sensing systems, the sensors can be mounted on vehicles like trucks to allow the movement of the sensors. The advantage of this type of measurement is the relatively small footprint of the sensor, allowing for easier control of the conditions under which the measurements are made (Jackson and Schmugge 1996). However, the footprint covered is usually only a few metres in size, so this method is again limited when coverage of a larger area is needed. Aircraft-based systems overcome such a limitation, allowing the mapping of larger areas to be carried out. This method can also be used to investigate the performance and feasibility of future satellite sensors that will typically be of a lower resolution.

In most cases, aerial measurements offer better spatial resolution than those from satellite systems. Although aircraft data have more control over the frequency and timing of the coverage (Jackson and Schmugge 1996), the data are only available for limited areas and at times of intensive field experiments.

The optimal solution in terms of mapping large areas and long term repetition coverage involves space-borne satellite systems. However, for studies which involve rapidly changing conditions, like surface soil moisture where the time interval between measurements can be critical, aerial systems are still needed (Jackson and Schmugge 1996).

2.2 Microwave Dielectric Behaviour

The dielectric constant, ε which is dimensionless, is also known as permittivity or specific induction capacity, and can be used to determine soil moisture. It is a measure of an object's ability to polarize in response to an electric field (Walker 1999; Escorihuela *et al.* 2007). This material property is usually measured relative to that of free space and is referred to as the relative dielectric constant ε_r.

A wet soil medium is a mixture of soil particles, air voids and liquid water (i.e. both bound and free water) (Hallikainen *et al.* 1985). Therefore, the relative dielectric constant of soil is a composite of its components (Jackson and Schmugge 1996). **Table 2.1** shows the dielectric constants of soil constituents and the major types of soil. As the contrast between the dielectric properties of liquid water (~80) and dry soil (~4) is large, soil moisture content can be determined from the measurement of the soil's dielectric constant (Wang and Schmugge 1980; Jackson and Schmugge 1989). As the moisture increases, the dielectric constant of the soil-water mixture increases and this change is detectable by microwave sensors (Njoku and Entekhabi 1996).

Table 2.1. Dielectric constant of soil constitutes and of major soil types (Noborio 2001).

Material	Dielectric Constant
Air	1
Water	80 at 20°C
Ice	3 at -5°C
Basalt	12
Granite	7 – 9
Sandstone	9 – 11
Dry loam	3.5
Dry sand	2.5

The dielectric constant, ε is a complex number representing the response of the material to an applied electrical field, such as electromagnetic waves (Behari 2005). This property can be calculated from the real and imaginary parts:

$$\varepsilon = \varepsilon' + i\varepsilon'' \tag{2.3}$$

usually measured relative to that of the free space ($\varepsilon_r = \varepsilon / \varepsilon_0$). The real component, ε' in ε determines the propagation characteristics of the electromagnetic wave in the material. The imaginary component, which is often referred to as the dielectric loss factor, determines the energy losses or

absorption as the electromagnetic wave travels through the material (Engman and Chauhan 1995).

For dry soil particles, depending on the bulk soil density, the real part of the relative dielectric constant ε_r' varies from 2 to 5 independent of frequency (Dobson and Ulaby 1986) with the imaginary component ε_r'' typically less than 0.05 (Ulaby *et al.* 1996). For free water, the relative dielectric constant at room temperature for 1 GHz radiation is approximately 80 for ε_r', and 4 for ε_r'' (Ulaby *et al.* 1996). This large contrast makes the use of a microwave technique possible for the measurement of the soil moisture content with the addition of water to the soil causing the relative dielectric constant of the mixture to increase to a value of 20 or greater. However, the dielectric constant of moist soil is not simply a weighted average over its components. The mixing model is complex and there are many influencing factors (Jackson and Schmugge 1989). Apart from the total soil moisture content, the magnitude of ε is also a function of the observation frequency, soil temperature, soil texture and soil salinity (Ulaby *et al.* 1996; Dobson *et al.* 1985).

The most sensitive frequency range for soil moisture content determination from the measurement of the soil dielectric constant lies between 50 MHz to 10 GHz (Curtis 2001), with the dielectric constant having a relatively weak sensitivity to soil type at the normal microwave range (0.4 to 10 GHz). **Figure 2.1** shows the relationship between the dielectric constant and volumetric soil moisture at a frequency of 1.4 GHz for different soil types. The dependence on soil type (or 'texture') is due to the different percentages of water bound to the particle surfaces in the different soils (Njoku and Entekhabi 1996; Dobson and Ulaby 1986) and the soil porosity (Dobson and Ulaby 1986). When soil moisture content is greater than 5%v/v, the soil porosity does not influence the soil dielectric constant as long as the moisture content is expressed in terms of volume (Ulaby *et al.* 1996).

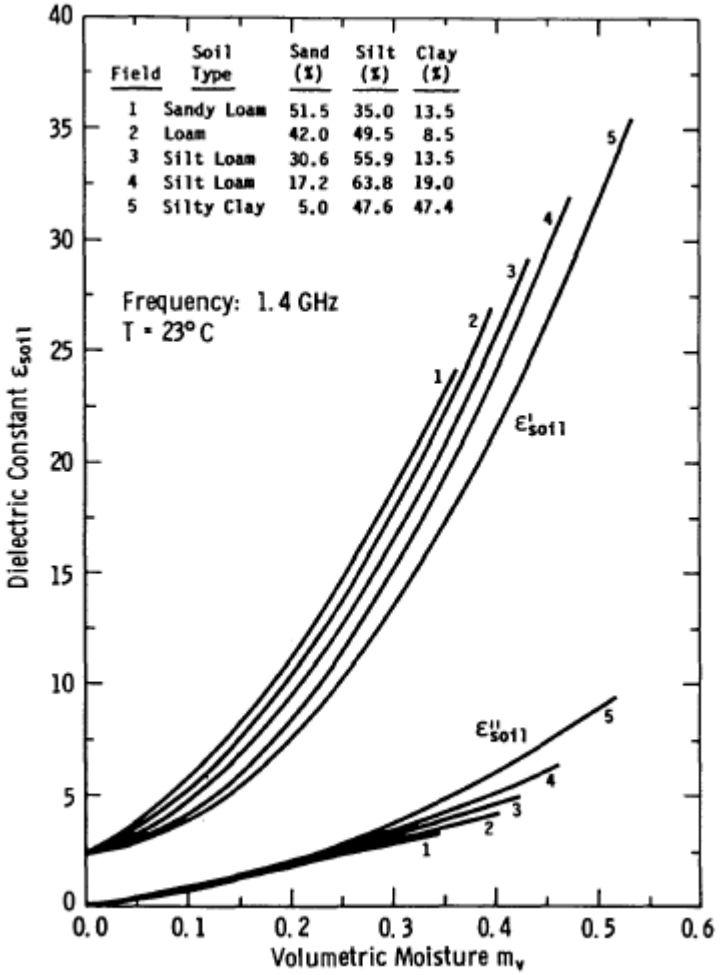

Figure 2.1. Dielectric constant as a function of volumetric soil moisture content for five different soil types and a soil temperature of 23°C (Ulaby et al. 1986).

As soil temperature increases, the decrease in the dipole of alignment resulting from thermal agitation causes ε' to decrease (Walker 1999). The effect of salinity on the dielectric constant is to add an ionic conductivity term to ε'' (Walker 1999). This results in the following (Jackson and O'Neill 1987):

i. Salinity decreases the real part of the dielectric constant ε' and increases the imaginary part ε'' at a given microwave frequency.

ii. For frequencies in the 1 – 10 GHz range, the sensitivity of the real part ε' is relatively constant regardless of the frequency.

iii. As frequency increases, the sensitivity of the imaginary part of the dielectric constant ε'' changes as salinity increases.

Salinity, frequency and temperature play only a minor role in determining the dielectric constant of soil. The frequency dependence up to 5 GHz is low because there is little variability in the real part of the dielectric constant (Njoku and Entekhabi 1996). The imaginary part of the dielectric constant in this range of frequencies, however, exhibits marked frequency dependence. This dependence influences only the penetration depth, with smaller penetration depths for higher frequencies (Njoku and Entekhabi 1996). The temperature dependence of the dielectric constant of wet soil is weak and for the range of soil temperatures encountered, it may be ignored (Njoku and Entekhabi 1996). Salinity becomes an important factor in more saline environments, such as when sea water is present in the soil, but for non-saline soil, this factor can be neglected.

It is therefore first and foremost the amount of water present in the soil that affects its dielectric properties. The dielectric properties, along with several other physical characteristics determine the microwave measurements. This is explained in **Section 2.3.3.5**.

2.3 Remote Sensing For Near Surface Soil Moisture

The measuring of soil moisture using remote sensing is dependent on a relationship between the remote sensing parameter and soil moisture. For example, the measurement of soil moisture using radar data is dependent on the relationship between the radar data and soil moisture. If a relationship can be determined, the amount of radiation reflected or emitted from the land surface that is captured by the sensor at particular wavelengths can be used to quickly obtain an estimate of the soil moisture (Wang and Zhang 2005). Research on near-surface soil moisture retrieval has shown that suitable remote sensing signals are at visible, thermal infrared, active and passive microwave wavelengths. These four signals differ in terms of the region of the electromagnetic spectrum that is used by the sensor and the

source of the electromagnetic energy. A brief review of these four types of remote sensing measurements for near surface soil moisture is presented next.

2.3.1 Visible Remote Sensing

Remote sensing of soil moisture content using the visible regions of the electromagnetic spectrum (from 350 nm to 700 nm) is measured through the reflected radiation of the Sun from the Earth's surface. In general, wet surfaces have lower reflectance values compared to dry surfaces (Singh and Fiorentino 1996). The reflected solar radiation is not only dependent on soil moisture conditions, but also on other factors such as the amount and type of organic matter, soil texture, surface roughness, angle of incidence, plant cover and colour (Engman 1991). In other words, the relationship between soil moisture and solar reflectance is only unique if these factors are known. As well as these limitations, reflected solar energy only responds to the top few millimetres of the soil profile (Moran *et al.* 2004). These factors, therefore, have limited the utility of visible light for surface soil moisture retrieval.

2.3.2 Thermal Infra-red Remote Sensing

Thermal infrared radiation (approximately 3.0 μm and 14.0 μm) sensors measure the soil surface temperature using thermal infrared data. As soil moisture influences the thermal properties of the soil, near surface soil moisture content can be inferred from the thermal infrared data. Soil moisture has a strong influence on the thermal properties of the Earth's surface, hence, relatively small changes in moisture content have a large effect on the thermal properties of the ground. As the radiation from the soil surface depends on the surface temperature and emissivity, inferring soil moisture from thermal infrared will need knowledge of, or assumptions about, the soil surface emissivity (Ottlé *et al.* 1989).

2.3.3 Microwave Remote Sensing

Microwaves have wavelengths ranging from 1 mm to 1 m, with frequencies between 0.3 GHz and 300 GHz. Microwave remote sensing is currently being actively researched for soil moisture measurement (Okamura 2000). The theoretical basis for measuring soil moisture by microwave techniques is the large contrast between the dielectric properties of liquid water and of dry soil (Engman 1991). The large dielectric constant for water is the result of the alignment of the electric dipoles of the water molecules in response to an applied electromagnetic field (Schmugge 1983b; Engman 1991). Over bare fields, the measured microwave emissivity is almost linearly related to the moisture content of the soil layer that has a thickness dependent on the frequency of the observing signal (between 1cm at 5 GHz and 5cm at 1.4 GHz) (Wang 1987). The sensitivity of microwave responses to soil moisture variations and the relative transparency of microwaves to the atmosphere, make microwave sensors especially well suited for remote sensing of soil moisture (Schmugge 1983b). In addition and importantly, microwave signals can penetrate, to a certain extent, the vegetation canopy and retrieve information from the ground (Engman 1991; Oldak *et al.* 2002; Kasischke *et al.* 1997). The sensitivity of the soil's emissivity and reflectivity to its moisture content has been demonstrated with microwave systems operating from field/tower, aircraft and spacecraft platforms (Schmugge 1983b).

Microwave techniques for measuring soil moisture include both active (radar) and passive (radiometry) approaches. Active microwave systems generate their own radiation that is transmitted toward the Earth's surface, and measure the reflected energy, which is dependent on the backscatter coefficient. Passive microwave sensors measure the natural thermal emission, termed the *brightness temperature*, from the land surface. Active and passive microwave approaches to sensing soil moisture share certain physical processes, but they are also different with regards to the quantities they sense and the image products they generate (Du *et al.* 2000). The following subsections describe the principles for both active and passive microwave

remote sensing. This is followed by a discussion of both the system and target parameters affecting these two types of microwave sensing methods.

2.3.3.1 Active Microwave Remote Sensing

Active microwave sensors use the well-known RaDaR, (Radio Detection and Ranging) method. This type of system generates its own radiation which is transmitted towards the Earth's surface and measures the returning backscattered radiation. The strength of the backscattered signal, measured to discriminate between different targets and the time delay between the transmitted and reflected signals, determines the distance (or **range**) to the target. The information that can be extracted is two-fold: the distance from the target to the radar and the backscattering coefficient (Barbier 2003). The ratio of the strength of the received and transmitted signals, termed the backscattering coefficient σ , depends on the surface reflectivity (itself dependent on surface geometry, surface roughness and dielectric properties) and the antenna characteristics (incidence angle, wavelength and polarization) (Behari 2005).

Over bare fields, the radar backscatter σ_s is related directly to soil moisture and is written in its functional form as (Engman and Chauhan 1995):

$$\sigma_s = f(R, a, M_v) \tag{2.4}$$

where R is the surface roughness term, a is the soil moisture sensitivity term, and M_v is the volumetric soil moisture. Although R and a are known to vary with wavelength, polarization and incidence angle, there is no satisfactory theoretical model suitable for estimating these terms independently. Thus, the relationship between measured backscatter and soil moisture requires the determination of an empirical relationship with ground truth data, even for the simplest case of bare soils.

2.3.3.2 Passive Microwave Remote Sensing

Passive microwave sensors are radiometers that measure the thermal emission from the surface (Schmugge 1998). Over bare surfaces, a radiometer measures the intensity of emissions from the soil surface, which is proportional to the product of the surface temperature and the surface emissivity, referred to as the microwave brightness temperature (T_B) (Engman and Chauhan 1995). The soil emissivity is subject to atmospheric, vegetation and surface features, as shown in **Figure 2.2** (Thomas 1993).

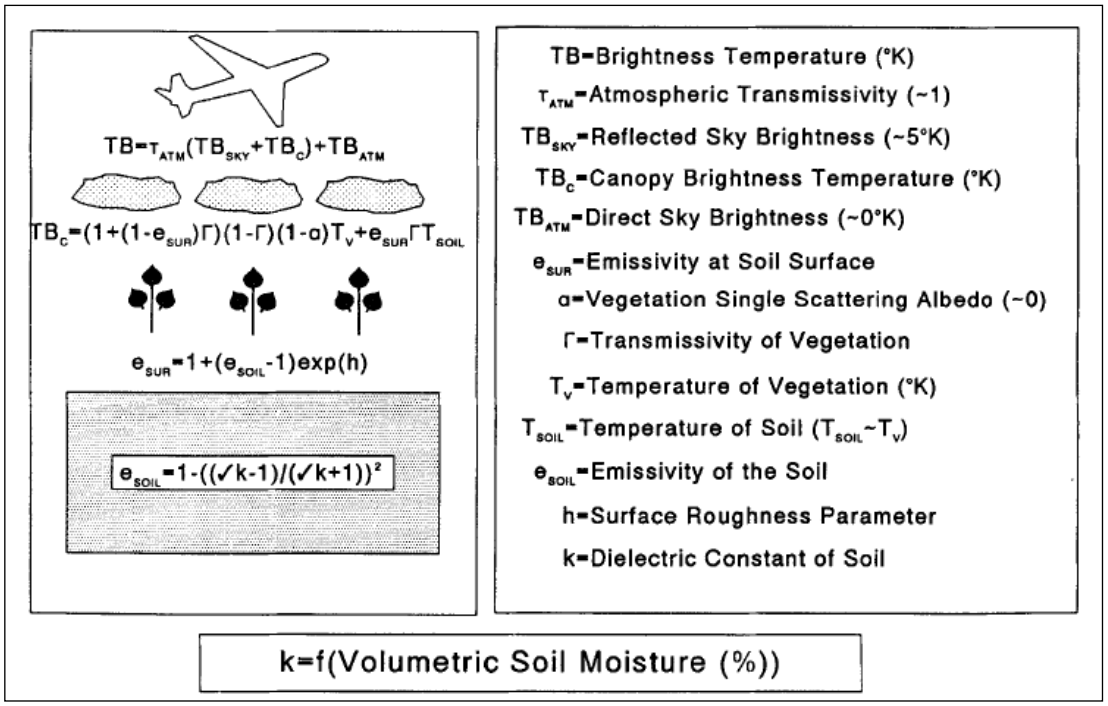

Figure 2.2. Schematic diagram of a passive microwave emission model for land surfaces (Thomas 1993).

Mathematically, T_B can be expressed as (Schmugge 1990):

$$T_B = t(H) * \left[rT_{sky} + (1 - r\ )T_{soil} \right] + T_{atm} \qquad (2.5)$$

where:

- $t(H)$: is the atmospheric transmissivity for a radiometer at height H above the soil
- r : smooth surface reflectivity
- T_{soil} : thermometric temperature of the soil
- T_{atm} : average thermometric temperature of the atmosphere
- T_{sky} : contribution from the reflected sky brightness

At wavelengths greater than 5cm, the atmospheric T_{atm} and sky T_{sky} contributions are small (less than 5˚K) compared to the soil contribution. Thus, the brightness temperature of an emitter of microwave radiation is related to the physical temperature of the source through emissivity such that (Schmugge 1990):

$$T_B = (1-r)T_{soil} = eT_{soil} \tag{2.6}$$

where e = (1 - r) is the emissivity and is dependent on the dielectric constant of the soil and the surface roughness. Although Equation 2.6 indicates the relationship between T_B and e is linear, soil moisture has a non-linear dependence on reflectivity because the reflection coefficient of the ground is related in a nonlinear way to the dielectric constant ε of the ground. For horizontal polarization, the reflection coefficient is given by:

$$R = \frac{\cos\theta - \beta}{\cos\theta + \beta} \tag{2.7}$$

where $\beta = \left(\varepsilon - \sin^2\theta\right)^{\frac{1}{2}}$ and θ is the angle of incidence. Empirical relationships between the dielectric constant and soil moisture derived by Dobson *et al.* (1985) show that the dielectric constant has a nonlinear dependence on soil moisture. Even though the brightness temperature and soil moisture relation has a strong theoretical basis, most algorithms are empirical in that they depend on ground truth data to determine the relationship (Engman and Chauhan 1995).

2.3.3.3 Active and Passive Microwave Remote Sensing: A comparison

Figure 2.3 shows the difference between active and passive microwave sensors. Both active and passive microwave remote sensing techniques utilize the large contrast between the dielectric constant of dry soil and water (Zhen *et al.* 2002) and can be used in all weathers for land-surface monitoring (Robinson 2000). Active microwave systems offer the advantage of high

resolution, but this comes at the expense of higher data rates and more complex processing, while passive microwave systems have the advantages of frequent coverage, low data rates and simpler data processing (Zhen *et al.* 2002). Due to the long wavelengths required for soil moisture remote sensing, space-borne passive microwave radiometers (both current and planned) have a coarse spatial resolution of the order of 25 to 50 km. Active microwave remote sensing, on the other hand, can supply resolutions of the order of tens of metres.

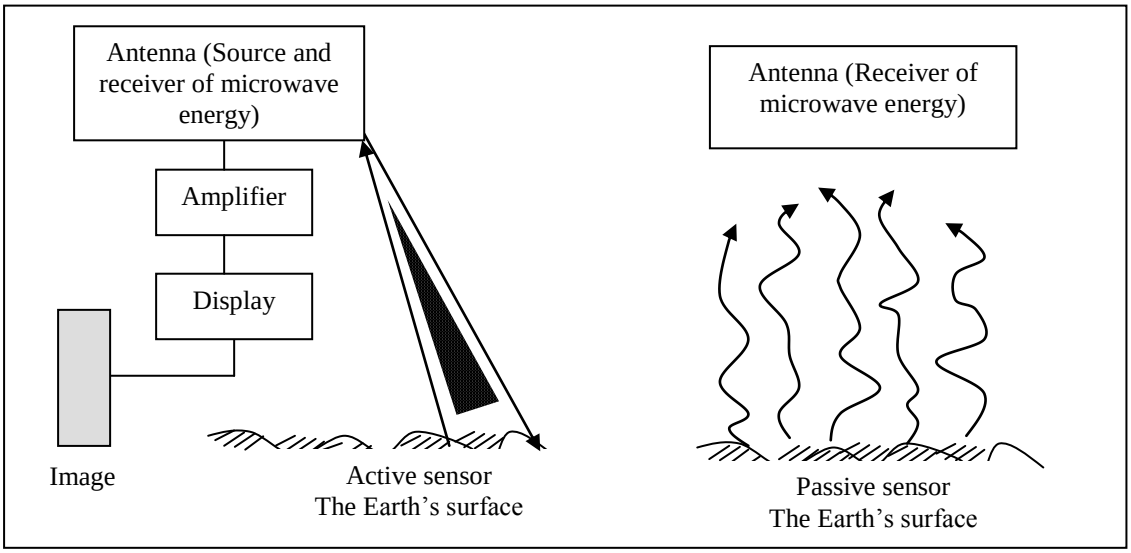

Figure 2.3. Active and passive microwave system (Behari 2005).

The signal-to-noise ratio from dry to wet soils is significantly higher for passive radiometers than for active radars (Berger *et al.* 2003). In addition, the radar signal is more sensitive to structural features such as soil roughness or vegetation canopy geometry than to soil moisture variations. The radiometer response appears to be less disturbed by the geometrical features of the scene and hence, more sensitive to soil moisture (Chauhan 1997). Even under the ideal scenario where effects due to roughness and vegetation cover can be estimated (which is generally not the case), active microwave systems generally fail to provide spatially distributed soil moisture at small scales. This is because the radar systems get strongly coupled to the variations of the surface. If there are no surface features, i.e., the surface is smooth, the radar

is unable to sense the surface in the backscatter direction, whereas a radiometer can (Chauhan 1997). This results in high resolution active microwave data only being able to assess mean soil moisture at the catchment scale. These particular disadvantages of active microwave remote sensing have meant that passive microwave systems are preferred when dealing with soil moisture measurement (Jackson and Schmugge 1989; Thomas 1993; Schmugge 1998; Simmonds 1998; Owe and Rathbun 1999; Jackson 2001; Tien *et al.* 2004; Calla *et al.* 2008).

2.3.3.4 System Parameters Affecting Microwave Signature

System design considerations for radiometers used in soil moisture sensing include the optimum choice of frequency or wavelength, polarisation and the incidence angle based on trade-offs between requirements for high vegetation penetration capability, freedom from electromagnetic interference and manageable antenna size (Njoku and Entekhabi 1996).

i. Frequency

The potential of passive microwave remote sensing for measuring surface soil moisture has been demonstrated over a range of microwave frequencies (Choudhury and Golus 1988; Drusch *et al.* 2001) and a variety of platforms (Jackson *et al.* 1999; Jackson and Hsu 2001). These studies clearly show the advantages of low-frequency (<5 GHz) (thus longer wavelength) microwave sensors for this application (Jackson *et al.* 2002). At low frequencies, attenuation from clouds and vegetation is lower than for higher frequencies (Drusch *et al.* 2001) and the soil sensing depth is increased. The contrast between wet and dry soil is also larger at low frequencies (Bolten *et al.* 2003). The longest wavelength, i.e. most deeply penetrating, generally used for remote sensing of soil water is L-band (1.4 GHz or a wavelength of 21 cm) (Simmonds 1998).

ii. Incidence Angle

The incidence angle affects the sensitivity to soil moisture content. With larger incidence angle, the sensitivity to soil moisture content increases. Moreover, an increase in the incidence angle increases the path length through the canopy; consequently, the optical depth will be increased (Owe and de Jeu 2001). As the incidence angle increases, the influence of surface roughness also increases and the spatial resolution decreases (Mission Objectives and Scientific Requirements of the SMOS Mission 2003; Thomas 1993).

iii. Polarisation

The orientation or polarisation of the electric field of electromagnetic waves is typically either horizontal (H) or vertical (V). The H polarized waves travel parallel to the soil surface and the V polarized waves travel perpendicular to the soil surface (**Figure 2.4**) (Lakhankar 2006).

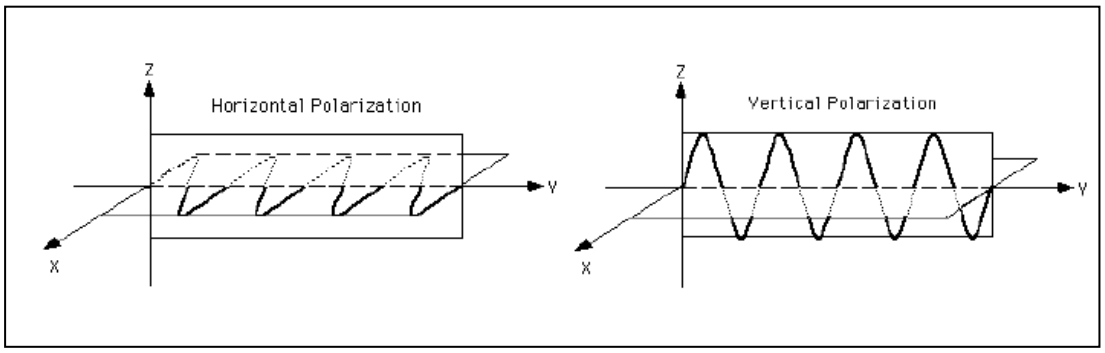

Figure 2.4. Horizontal and vertical polarization (Lakhankar 2006).

For a homogenous soil with a smooth surface, the reflectivity at vertical and horizontal polarizations, R_V and R_H are given by the Fresnel expressions (Schmugge *et al.* 1986):

$$R_H = \left| \frac{\cos\theta - \sqrt{k - \sin^2\theta}}{\cos\theta + \sqrt{k - \sin^2\theta}} \right|^2 \tag{2.8}$$

$$R_V = \left| \frac{k\cos\theta - \sqrt{k - \sin^2\theta}}{k\cos\theta + \sqrt{k - \sin^2\theta}} \right|^2 \quad (2.9)$$

where θ is the incidence angle and k is the absolute value of the soil bulk dielectric constant (ε_b). Equations (2.8) and (2.9) show that the absolute magnitude of the soil emissivity ($e = 1 - R$) is lower for horizontal polarization. The sensitivity to changes in surface moisture is significantly greater for horizontal polarization than for vertical polarization (Owe and de Jeu 2001). Vertical polarization of microwave measurements were found to be influenced by some external disturbances (Grant *et al.* 2007b). Most research and applications involving microwave remote sensing of soil moisture have emphasized the use of low frequencies (L-band) and, at this frequency, it is possible to develop a soil moisture measurement based on a single H polarization signal (Thomas 1993).

2.3.3.5 Target Parameters Influencing Microwave Signature

There are a number of factors other than soil moisture that influences the intensity of the emission from the soil. These include, amongst others, surface roughness, vegetation cover and soil texture (Schmugge *et al.* 1986).

i. Roughness

Surface roughness increases the apparent emissivity due to an increase in the surface area of the emitting surface (Schmugge 1983b). In order to modify the emissivity for a rough surface, an empirical roughness model has been developed (Choudhury *et al.* 1979) and is expressed as:

$$e_{r(i)} = 1 - R_{(i)} \exp(-h\cos^2\theta) \quad (2.10)$$

where e_r is the emissivity of the rough surface at polarization (i) (H or V), h is an empirical roughness parameter which is related to the root mean square (RMS) height variation of the surface and the correlation length, R is

the reflection coefficient and θ is the incidence angle. The effect of a rough surface is to increase the surface emissivity and thus to decrease the sensitivity to soil moisture (Newton and Rouse 1980). It was found that for microwave emissions, the effect of the surface roughness is less significant compared to that of the amount and type of vegetation (Wang *et al.* 1987).

ii. Vegetation

Vegetation absorbs, emits, and scatters microwave radiation (Njoku and Entekhabi 1996). The brightness temperature measured above the canopy therefore contains not only information about the soil moisture, but also the vegetation characteristics. A method based on radiative transfer theory described in Mo *et al.* (1982) is a simple but physically based model that can effectively estimate the radiation by the soil surface even under vegetation (Owe *et al.* 2001):

$$T_B = (e_s\Gamma)T_s + (1-\omega)(1-\Gamma)T_c + (1-e_s)(1-\omega)(1-\Gamma)T_c \qquad (2.11)$$

where :

e_s	smooth surface emissivity
Γ	transmissivity of the vegetation layer
ω	single scattering albedo
T_s	soil surface temperature
T_c	canopy temperature

The first term on the right of Equation (2.11) represents the emission contribution from the soil corrected for the energy absorbed by the vegetation layer (labelled 1 in **Figure 2.5**). The second component is the direct microwave emission from the vegetation layer (labelled 2 in **Figure 2.6**). The last term quantifies the vegetation emitted radiation travelling via the soil surface to the sensor (labelled 3 in **Figure 2.5**) (Su 2006).

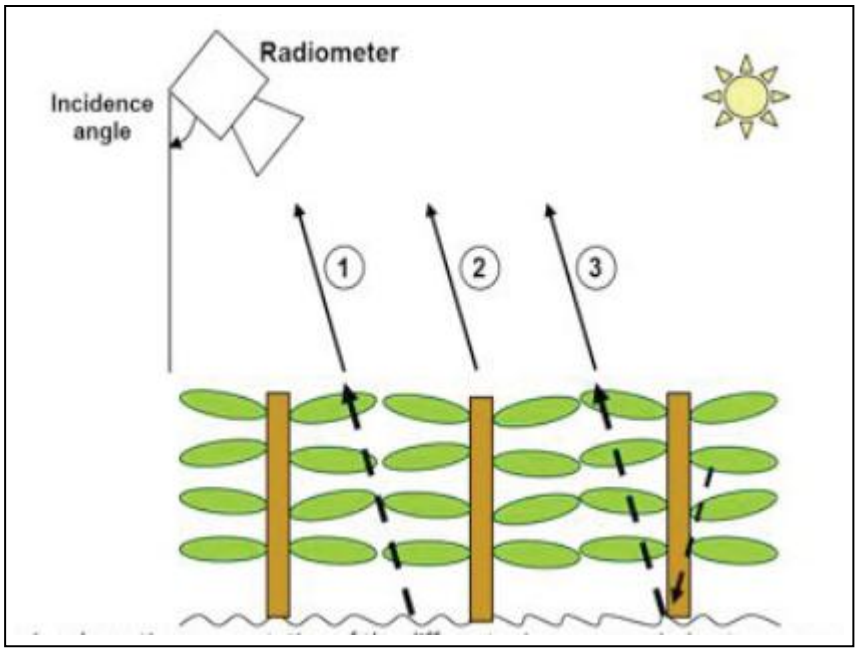

Figure 2.5. Schematic representation of the different microwave emission terms over a vegetated surface (Su 2006).

The single scattering albedo describes the scattering of the emitted radiation by the vegetation and is a function of plant geometry. The transmissivity is defined in term of optical depth τ such that:

$$\Gamma = \exp(-\tau / \cos\theta) \tag{2.12}$$

Optical depth is related to the vegetation density and the frequency. With increasing optical depth, the sensitivity of the above-canopy brightness temperature to soil emissivity decreases as the vegetation weakens the soil emission. However, towards the longer wavelength region of the microwave spectrum (wavelength ≥10 cm), the effects of vegetation and roughness are much reduced. At these wavelengths, and in areas of low to moderate vegetation, soil moisture has a dominant effect on the brightness temperature (Wang and Choudhury 1995).

iii. Soil Texture

The dependence on soil type or texture is due to the different percentages of water bound to the particle surfaces in the different soils (Njoku and Entekhabi 1996). Bound water exhibits molecular rotation less freely at microwave frequencies, and hence has a smaller dielectric effect than the

free water in the pore space or voids between the particles. The dielectric constant changes with the relative amounts of sand, silt and clay in the soil and this affects the microwave sensing of soil moisture (Engman and Chauhan 1995). Laboratory data and an empirical model developed by Wang and Schmugge (1980) show that the effect of soil texture is relatively small and can be neglected in practice (Engman and Chauhan 1995).

2.3.4 L-band Passive Microwave Soil Moisture Retrieval

Results of studies with L-band radiometers on trucks (Jackson *et al.* 1995b; Burke and Simmonds 2001), aircraft (Schmugge 1996; Mattikalli *et al.* 1998; Jackson 2001) and satellite platforms (St. Germain and Gaiser 2000; Njoku *et al.* 2003; Jackson *et al.* 2008) have shown a strong relationship between brightness temperature and surface soil moisture. The attenuation from vegetation and surface roughness is lower at L-band frequencies. Moreover, the penetration depth is approximately 5 cm, which is deeper than for shorter wavelengths (Jackson and Schmugge 1989). These conclusions are supported by much research and experiments into passive L-band microwaves (Schultz 1988; Thomas 1993; Jackson *et al.* 1995b; Jackson and Le Vine 1996; Chanzy *et al.* 1997; Simmonds and Burke 1998; Schmugge 1998; Yuei-An *et al.* 1999b; Fischman and England 1999; Crosson *et al.* 2002; Shou-Fang *et al.* 2002; Schneeberger *et al.* 2003; Bolten *et al.* 2003; Uitdewilligen *et al.* 2003; Jackson *et al.* 2004; Schneeberger *et al.* 2004; Limaye *et al.* 2004; Behari 2005; Paloscia *et al.* 2006; Angiuli *et al.* 2008). The physical basis of microwave emission from bare soil and vegetated area is next presented.

2.3.4.1 Soil Emission: Smooth Soil

For rather smooth soil surfaces, the soil microwave emissivity e can be approximated from the soil reflectivity R of a plane surface:

$$\begin{aligned} e &= 1 - R \\ &= 1 - \left| R(\varepsilon, \theta) \right|^2 \end{aligned} \tag{2.13}$$

The soil reflectivity, R, can be written as a function of soil dielectric permittivity ε and viewing angle θ using the Fresnel equation. For soil, ε is mainly dependent on the soil moisture content, and to a smaller extent, on the soil textural and the structural properties. Although from Equation (2.13), the emissivity of the smooth soil can be related to soil moisture through ε and θ, there are other factors, including the surface roughness and the volume of soil, which should also be taken into account.

For simple applications, the p-polarized soil reflectivity R can be written as:

$$R_p = \left[1 - Q_{soil} R_p^{\,*} + Q_{soil} R_q^{\,*}\right] \exp\left(-h_{soil} \cos^{N_{soil}}(\theta)\right) \tag{2.14}$$

where Q_{soil} (polarization-mixing effect) and h_{soil} (roughness effect) are obtained via a semi-empirical method; R^* is the soil specular reflectivity at polarization p or q; $\cos^{N_{soil}}(\theta)$ is a function accounting for the observed dependence on the incidence angle where the exponent N_{soil} is adjusted to fit the data. At L-band frequencies, it had been shown that N_{soil} can be set to zero and Q_{soil} can be disregarded. Therefore, at L-band frequencies:

$$e_p = 1 - R_p^{\,*} \exp(-h_{soil}) \tag{2.15}$$

Equation (2.15) is referred to as the h-parameter correction for soil roughness effects. The volumetric soil moisture w_s can be considered as a decreasing function of the emissivity e_p of bare soil. In general, the soil roughness conditions do not change much during the observations, so equation (2.15) can be approximated by a linear equation:

$$e_p = a_0 - a_1 w_s \tag{2.16}$$

where a_0 represents the value 1, a_1 represents $R_p^{\,*}$, and w_s represents the $\exp(-h_{soil})$. This function has been shown to be true under a wide range of soil moisture and roughness conditions (Newton *et al.* 1982; Wang *et al.* 1983; Schmugge 1983a; Jackson and O'Neill 1987).

2.3.4.2 Soil Emission: Vegetation-covered

The vegetation layer over the soil surface attenuates the soil emissions and adds its own contribution to the emitted radiation. At low frequencies, these effects are well approximated by a simple radiative transfer (RT) model which is normally referred to as the tau-omega (τ—ω) model. This model uses the optical depth τ and the single scattering albedo ω to parameterize the vegetation attenuation properties and the scattering effects within the canopy layer, respectively. Using the τ—ω model, the emission from the soil and vegetation is the sum of three terms:

a. the direct vegetation emission,
b. the vegetation emission reflected by the soil and attenuated by the canopy layer, and
c. the soil emission attenuated by the canopy layer.

The soil (T_{soil}) and vegetation (T_{veg}) temperature are approximately equal ($T_s \approx T_{soil} \approx T_{veg}$). The canopy brightness temperature $T_{B(p)}$, where p is either *H*- or *V*-polarization, can be estimated as a function of the attenuation factor γ_p:

$$T_{B(p)} = e_p T_s \tag{2.17}$$

where the emissivity e_p is given by:

$$e_p = (1-\omega)(1-\gamma_p)(1+\gamma_p R_{s(p)}) + (1-R_{s(p)})\gamma_p \tag{2.18}$$

where $R_{s(p)}$ is the soil reflectivity at p-polarization.

The attenuation factor can be computed from the optical depth:

$$\gamma_p = \exp(-\tau_p / \cos\,\theta) \tag{2.19}$$

Studies have shown that τ_p is linearly related to the total vegetation water content W_c (kg/m^2) through the parameter b_p which can be calibrated for each crop type or for large categories of canopy, i.e. leaf-dominated, stem-dominated and grasses (Pampaloni and Paloscia 1986; Jackson and Schmugge 1989; Schmugge and Jackson 1992; Thomas 1993; Owe *et al.* 2001):

$$\tau_p = b_p W_c \tag{2.20}$$

From Equations (2.17) and (2.18), it can be seen that the canopy brightness temperature can be computed as a function of three main surface variables: surface soil moisture (through its effects on surface reflectivity $R_{s(p)}$), vegetation optical depth τ_p (which can be related to W_c and canopy type), and canopy temperature T_c. Therefore, several measurements are required to determine the different effects of these variables. These data can be obtained from measurements of several configurations of the systems in term of polarization, view angle and frequency.

2.3.5 Satellite Observing System

This section provides a short description of satellite observing systems and is limited to those observing systems that provide data of potential relevance to soil moisture remote sensing.

i. Advanced Microwave Scanning Radiometer for EOS (AMRS-E)

The Earth Observing System (EOS) Aqua satellite containing the AMSR-E was launched on May 4, 2002 to provide observations of several geophysical parameters of interest to hydrology, ecology and climate (Kawanishi *et al.* 2003). It uses a dual-polarized microwave radiometer with frequency channels at 6.9, 10.6, 18.7, 23.8, 36.5 and 89 GHz (Paloscia *et al.* 2006). Aqua is in a polar orbit with 1.30 A.M./P.M. equatorial crossing times (Jones *et al.* 2007). The viewing angle of AMSR-E is fixed at 54.8° and the mean footprint diameter ranges from 56 km at 6.9 GHz to 5 km at 89 GHz (Bolten *et al.* 2006). The revisit time for the global swath coverage is two days or less (Njoku *et al.* 2003). The most appropriate frequency of AMSR-E for soil moisture retrieval is the C-band or the 6.9 GHz channel, which can measure to an accuracy of 6%v/v under vegetated conditions or better with vegetation water content up to 1.5 kg m^{-2} (Njoku *et al.* 2003). Passive microwave measurements at frequencies below L-band are susceptible to man-made radio-frequency

interference (RFI) and the AMSR-E C-band centred at 6.9 GHz, which it shares with fixed and mobile communication services, is subject to RFI contamination, particularly near large urban land areas (Njoku *et al.* 2003).

ii. Moderate Resolution Imaging Spectroradiometer (MODIS)

The Terra and Aqua satellites carry MODIS sensors. These two satellites provide observations in the late morning (10.30 A.M./P.M) and early afternoon (1.30 A.M./P.M) (Savtchenko *et al.* 2004), meaning that the data is available on a daily basis. MODIS acquires data in 36 spectral bands between 0.41 μ m (visible) and 14.2 μ m (thermal infrared) with spatial resolutions of 250m, 500m and 1000m (Barnes *et al.* 2003; Savtchenko *et al.* 2004). There are many products derived from MODIS observations to describe features of land, ocean and atmosphere, and these can be divided into the following:

a. MODIS Level 1 data: geo-location, cloud mask, and atmosphere products,
b. MODIS land products,
c. MODIS cryosphere products, and
d. MODIS ocean colour and sea surface temperature products.

iii. Advanced Spaceborne Thermal Emission and Reflection Radiometer (ASTER)

ASTER is a sensor flying on the Terra satellite used to obtain detailed maps of land surface temperature, reflectance and elevation (Tan 2004). It has a unique combination of wide spectral coverage and high spatial resolution in the visible near-infrared through shortwave infrared to the thermal infrared regions (*LP DAAC: Land Processes Distributed Active Archive Center* 1999).

iv. WindSat

WindSat, launched in 2003, is a space borne multi-frequency polarimetric microwave radiometer operating at 6.8, 10.7, 18.7, 23.8 and 37.0 GHz (Connor

et al. 2004). The earth incidence angle is not the same for all frequencies with the nominal range approximately 50˚ to 55˚ (Gaiser *et al.* 2004). The spatial resolution for 6.8 GHz is around 40km×60km and around 8km×13km for 37.0 GHz.

v. Soil Moisture and Ocean Salinity (SMOS)

The main objective of the SMOS mission is to deliver key variables of the land surface (soil moisture fields), and of the ocean surface (sea surface salinity fields) (Kerr *et al.* 2001). This mission is based on a revisit time of one to three days and uses a dual polarized L-band radiometer to achieve a ground resolution between 35 and 50 km with a swath width of 1000 km coupled with multi-angular (between 0˚ to 55˚) acquisitions (Mecklenburg *et al.* 2008). The satellite has a 6.00 A.M./P.M. equator overpass time. It was launched in November 2009 (*ESA Water Mission SMOS* 2009).

vi. Hydrospheric States (Hydros) Mission

The objective of this mission is to provide exploratory global measurements of the Earth's soil moisture with two to three days revisit time (Jackson *et al.* 2005). The Hydros instrument is a combination of a radar system (1.26 GHz with VV, HH and HV polarizations) and a radiometer system (1.41 GHz with H and V polarizations). The radiometer system allows retrieval of soil moisture in non-forested landscapes with a resolution of 40 km while the radar measurements will retrieve soil moisture at 3 km resolution, both at a constant look angle of 39˚ with respect to nadir (Entekhabi *et al.* 2004). The Hydros satellite is scheduled to be launched in 2010 (Xiwu *et al.* 2006).

2.4 Research Review: Passive Microwave Soil Moisture Retrieval

Different soil moisture retrieval approaches have been developed to account for the various parameters contributing to the surface microwave emission (Wigneron *et al.* 2003). In this review, three main approaches of soil moisture

retrieval are identified and classified, namely: i) statistical approaches, ii) forward model inversion, and iii) explicit inverse (use of neural networks) are identified and described.

2.4.1 Statistical Approaches

This is an approach whereby the algorithms directly manipulate the remotely sensed signal to retrieve information on land surfaces through empirical relationships of the type:

$$x_j = F_j\left(T_{B,1}, T_{B,2}, \ldots . T_{B,n}\right) \tag{2.21}$$

where $T_{B,i}$ corresponds to the brightness temperature measurements made for various configurations of the sensor in terms of incidence angle θ, polarization, or frequency; and x_j is the relevant land surface variable (Wigneron *et al.* 2003).

Surface soil moisture is statistically related to a combination of microwave emissivities and vegetation microwave indices that are used to correct the vegetation and roughness effects. Over bare soil (Lixin *et al.* 2002), the linear relationship of Equation (2.16) has proven to be valid under a large range of conditions, provided that sufficient ground data are available to calibrate the coefficients a_0 and a_1 (Wigneron *et al.* 2003). Using Equation (2.16), the soil moisture value can be retrieved by inverting the linear equation. The emissivity in Equation (2.16) is often replaced by the normalized brightness temperature T_{BN}:

$$T_{BN} = T_B / T_s \tag{2.22}$$

where T_s is the estimated surface temperature.

For vegetation covered areas, some studies have shown that, for a given level of vegetation biomass, the relationship between T_B and soil moisture w_c can be approximated by a linear function for soil moisture between 0.1 to 0.4 m^3/m^3 (Ulaby *et al.* 1983; Pellarin *et al.* 2003). The slope and intercept of the relationship are a function of the vegetation

characteristics, i.e. canopy type, biomass or water content, and of the viewing configuration in terms of view angle, polarization, and frequency. The vegetation index has been used to quantify the effects of the vegetation cover. The vegetation index can be computed either from passive microwave observations (Microwave Polarization Difference Index (MPDI), Polarization Difference (PD), etc.) or from data acquired by optical remote sensing systems (Normalized Difference Vegetation Indices (NDVI), Perpendicular Vegetation Index (PVI), etc).

2.4.2 Forward Model Inversion

Forward model inversion is a technique whereby a radiative transfer model is used to simulate the microwave radiometric measurement. The microwave radiometric measurement, $(T_B)_i$ (where $i = 1,2,\ldots.q$ corresponds to measurements made for various configurations of the sensors in term of incidence angle θ, polarization or frequency f) can be written as a function of land surface characteristics x_j ($j = 1,2,\ldots p$):

$$\left(T_B\right)_i = \Phi_i\left(x_1, x_2, \ldots.. x_p; s_{1_i}, s_{2i}, \ldots.. s_{p_i}\right) + \varepsilon_i \qquad (2.23)$$

for $i = 1,2,\ldots.. q$ where s_{k_i} $(i = 1,2,\ldots,r; i = 1,2,\ldots,q)$ represents the configuration parameters which determine the observation conditions, and ε_i are the residual errors between the simulated and measured brightness temperature values. Inverting the model consists of finding the set of variables under examination $x_j\,(j = 1,2,\ldots,p)$ that provides the minimum value of residual errors ε_i. In other words, a model is used to simulate remotely sensed signatures (output) on the basis of land surface parameters (input). The inversion methods are developed to produce an 'inverse model' in which the outputs are represented by the relevant land surface variables. The inversion methods are usually based on iterative minimization routines using the Root Mean Square Error (RMSE) between the forward model simulations and observations. In short, forward model inversion consists of

two steps: 1. selection of a forward model, and 2. selection of an inversion model that minimizes the residual errors ε_i.

There are different forward modelling approaches that can be categorized into:

i. Non-parametric data driven models that are either based on statistical regression analysis or the neural network model (Yuei-An *et al.* 2001). Non-parametric regression is regression without an assumption of linearity.

ii. Parametric data driven models in which the model parameters are adjusted by comparison with observations. In this approach, prior knowledge of the functional form of the processes that are being modelled is required (Mätzler C and Standley 2000).

iii. Physical models that include a physical description of the radiative transfer process and where the model parameters can be directly related to the land surface characteristics. In this approach, a number of surfaces can be modelled as a continuous medium or as a discrete medium containing randomly distributed scatterers characterized in terms of size, shape, density, and distribution orientation (Ferrazzoli and Guerriero 1995; Ferrazzoli *et al.* 2000). This is a complex model that requires many input parameters, and which cannot be implemented easily to retrieve the surface characteristics.

After the particular forward model has been selected, the method to invert the model needs to be defined. A very common method of inverting the forward model is the statistical inversion approach, which searches for the input parameters $x_1, x_2, \ldots, x_p$ consisting of the relevant geophysical parameters that minimize the square error between the brightness temperatures as measured from space $(T_B)_i$ and the actual outputs of the model $\Phi_i\left(x_1, x_2, \ldots\ldots x_p\right)$ (Pulliainen *et al.* 1993).

2.4.3 Explicit Inverse

The explicit inverse of the physical process can be built by mapping the input (remote sensing measurements) into the output (the land surface parameters). Some of these applications include the estimation of snow characteristics (Davis *et al.* 1993; Tsang *et al.* 1992), surface wind speed over the ocean (Stogryn *et al.*), clouds and precipitation (Li *et al.* 1997), etc. Artificial Neural Networks (ANNs) are used to produce the explicit inverse function. The ANN is used to train an inverse model by reversing the roles of the inputs and outputs: the input nodes of the ANN are the measured brightness temperatures and the output nodes are the land surface characteristics. The advantage of the ANN is that once the ANN is trained, the parameter inversion can be accomplished quickly. Other advantages of ANNs include (Ghedira *et al.* 2000):

- **Adaptability:** ANNs are easily adaptable to different types of data and input configurations. Moreover, ANNs can easily incorporate ancillary data, which would be difficult or impossible with conventional techniques.
- **No assumption about data distribution**: The traditional parametric classification methods, such as the Maximum Likelihood classifier, make unreasonable assumptions about the statistical proprieties of the data, specifically that they are normally (or Gaussian) distributed for each ground cover class. However, this assumption is not always satisfied.
- **Problem and model complexity**: ANNs can deal with large amounts of training data and their complex configuration can find the best nonlinear mapping function between the input and the output data without the constraint of linearity or pre-specified nonlinearity which is required in regression analysis.

ANNs have been utilized in many applications in the field of hydrology and water resources and the results obtained have been very promising. One of these applications is in the field of soil moisture retrieval. Soil moisture is linked to radiometric signatures through its influence on microwave emission of land surfaces (Jackson *et al.* 1999; Yuei-An *et al.* 1999a;

Njoku and Entekhabi 1996; Njoku and Li 1999) and the linkage is often extremely non-linear. It is in general difficult to develop a physically-based retrieval approach due to the problem of understanding the behaviour of all the data involved. To resolve the non-linearity the ANNs approach which is known for its ability to handle non-linear mapping problem, is a good scheme.

2.5 Chapter Summary

This chapter has discussed the two methods commonly used for measuring soil moisture content over the soil profile: discretely at specific locations and by using remote sensing observations. The use of remote sensing observations is better in terms of area and temporal coverage compared to point measurements.

It is concluded that of the remote sensing observations used, microwave observations have the greatest ability for soil moisture retrieval due to its all weather capabilities. In addition, passive microwave observation has the best capability for measuring soil moisture content compared to active microwave observation as passive microwave observations are less sensitive to surface roughness, vegetation and topographic influences.

This chapter has also discussed the different categories of methods for retrieving soil moisture using passive microwave observations. From the three different approaches, the statistical and ANN approaches promise simpler and more efficient methods than the forward modelling approach. The ANN is superior to the statistical approach as it does not require explicit mathematical functions. The ANN will map the function between the input and output using the data provided during its training process. Once this function is successfully mapped, inverse mapping can be accomplished quickly.

The ANN approach has been applied to the soil moisture retrieval problem. **Chapter 3** will present the basics of ANN theory before reviewing the application of ANNs for soil moisture prediction in **Chapter 5**.

Chapter 3

Artificial Neural Networks

A brief overview of Artificial Neural Networks (ANNs) including the theory and some examples is presented in this chapter. The knowledge presented in this chapter is then used to build the methodology in the following chapters that are concerned with using ANNs to enhance surface moisture retrieval from remotely sensed data.

3.1 Introduction

ANNs are used to generate a mapping between some input data and some required output. ANNs are model free estimators in that they do not rely on an assumed form for the underlying data (Chang and Islam 2000). Rather, based on some observed data, they attempt to obtain an approximation of the underlying system that generated the observed data. They use a non-linear data driven self-adaptive approach as opposed to the traditional model based methods. They are powerful tools for modelling, especially when the underlying data relationships are unknown (Jha 2007). ANNs can identify and learn the correlated patterns between the input data set and the corresponding target outputs. After training, the ANNs can be used to predict the outcome of new, unseen independent input data. ANNs imitate some aspects of the structure and learning of the human brain and can process problems involving non-linear and complex data even when the data are imprecise and noisy (Jha 2007). One of the appealing features of ANNs is that "learning by example" replaces "programming" in solving problems. This feature makes such computational models very useful in applications where one has little or incomplete understanding of the problem to be solved,

but where training data is readily available. ANNs are not intelligent, but they are good at recognizing patterns and making simple rules for complex problems (Nissen 2007).

In general, one can look at the computation in an ANN from the perspective of estimating an unknown function based on some observations. However, this does not imply that the ANN is a heuristic technique. ANNs have a rich theory underlying them and are based on sound mathematical principles. The technique has proved very popular and criticisms of the technique primarily arise from attempts to use ANNs as off-the-shelf black boxes (Chang and Islam 2000) without understanding their underlying theory.

3.2 Basic ANN Model

The neural network was historically inspired by the biological functioning of a human brain. Specifically, it attempts to mimic the fault-tolerance and capacity to learn of biological neural systems by modelling the low-level structure of the brain (Patterson 1996).

The brain is composed of a very large number of interconnected neurons. The neuron has a branching input structure (the dendrites), a cell body (the soma), and a branching output structure (the axon). The axon of one cell connects to the dendrites of another through a synapse (**Figure 3.1**).

When a neuron is activated, it fires an electrochemical signal along the axon. The signal crosses the synapses to the other neurons, which may in turn fire. A neuron fires only if the total signal received at the cell body from the dendrites exceeds a certain level (the firing threshold). The chance of firing, i.e. the strength of the signal received by a neuron, depends on the efficacy of the synapses.

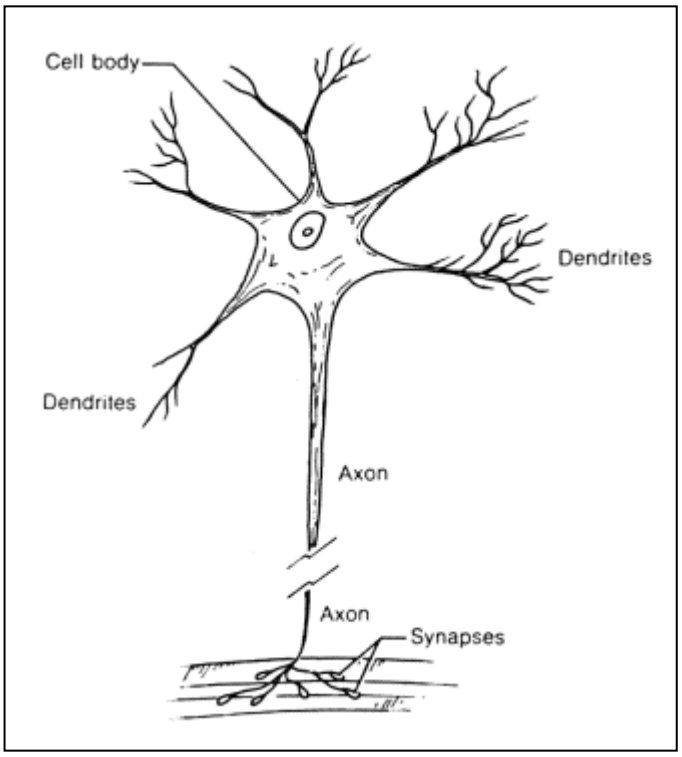

Figure 3.1. Structure of a neuron (Turchin 1977).

When creating a functional model of the biological neuron, there are three basic components of importance (Haykin 1994):

i. Synapses. This is modelled as weights in ANNs. The strength of the connection between an input and a neuron is represented by the value of the weight. Unlike the synapses in the brain, the synapse weight of the artificial neuron lies within the range of positive and negative values. Positive weight values designate excitatory connections while negative values reflect inhibitory connections;

The next two components model the actual activity within the neuron cell:

ii. An adder to sum up the input signal modified by their respective weights. This is referred to as a linear combination;

iii. An activation function that controls the amplitude of the output of the neuron. An acceptable range of output is usually between 0 and 1, or -1 and 1.

This model is described schematically in **Figure 3.2**.

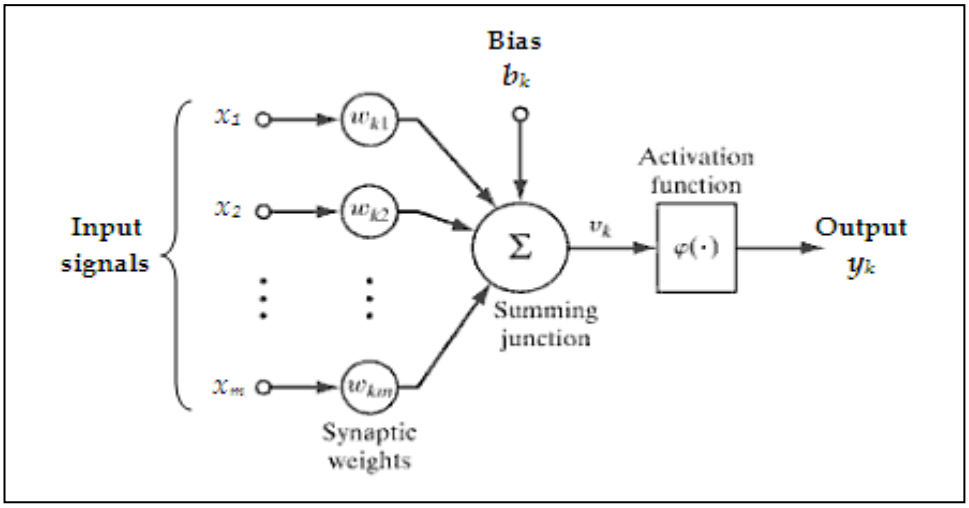

Figure 3.2. An artificial neuron model (Haykin 1994).

The model illustrated in **Figure 3.2** also includes an externally applied bias, b_k, which has the effect of increasing or lowering the net input of the activation function, depending on whether it is positive or negative, respectively. Mathematically, using **Figure 3.2,** a neuron k can be written as:

$$u_k = \sum_{j=1}^{m} w_{k_j} x_j \tag{3.1}$$

and

$$y_k = \varphi(u_k + b_k) \tag{3.2}$$

where $x_1, x_2, \ldots, x_m$ are the input signals; $w_{k_1}, w_{k_2}, \ldots, w_{k_m}$ are the respective synaptic weights of neuron k; u_k is the linear combination output due to the input signal; b_k is the bias; $\varphi(.)$ is the activation function and y_k is the output signal of the neuron. The use of bias b_k has the effect of applying an affine transformation to the output u_k:

$$v_k = u_k + b_k \tag{3.3}$$

where v_k is termed as the induced local field or activation field of neuron k. The linear combiner u_k is modified by b_k in the manner shown in **Figure 3.3**.

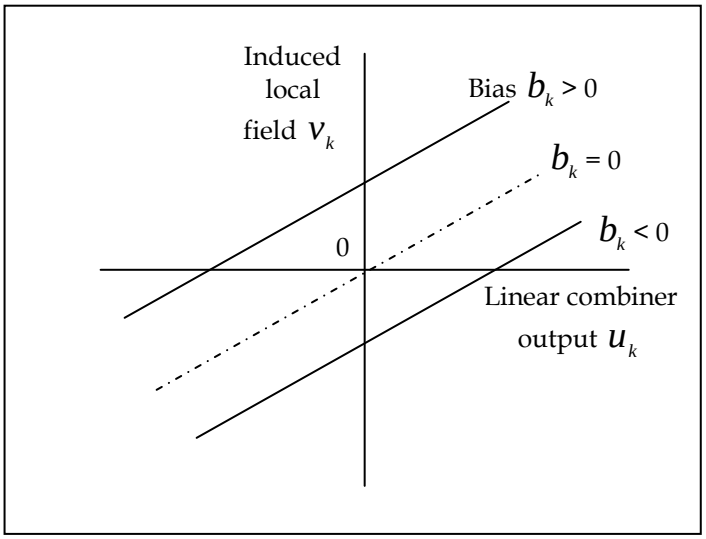

Figure 3.3. Affine transformation produced by the presence of a bias (reproduced from (Haykin 1994)).

A bias is similar in function to a threshold and is treated as a weight connected to a node that is always on (Meyer and Maul 1991). The weights determine where this hyperplane lies in the input space. Without a bias term, this separating hyperplane is constrained to pass through the origin of the space defined by the inputs. For some problems this is acceptable, but in many problems the hyperplane would produce increased performance away from the origin. If you have many units in a layer, they share the same input space and without bias they would ALL be constrained to pass through the origin (Sarle 1997).

3.3 ANN Data Pre- and Post-Processing

Preprocessing aims at transforming the data into a better form for the network to use (Demuth *et al.* 2009). This process, normally known as normalization or normalization, can speed up the training process of the ANN and reduce the chances that the ANN gets stuck in a local minima. By normalizing the data, the effects of outliers in the data are reduced and with this, the density of the local minima (due to the outliers) is also reduced. The use of normalization is mainly to transform the input features into the same

range of values in order to minimize the possibility of bias within the ANN towards one feature over another (Priddy and Keller 2005). The training time will be reduced because each feature has the same range of data values as each other and the gradient descent process will treat each feature the same. The normalization process is especially useful when the inputs of an application vary over widely different scales. There are different ways to normalize the data, and a popular one is the statistical or Z-score normalization technique which uses the mean and standard deviation for each feature across a set of training data to normalize each input feature vector.

The usual way of data preprocessing for ANNs is to obtain the standard deviation and mean from the training data, but not from the validation and testing data (Sarle 1997). The means and standard deviations are computed for each feature over the set of training data, and used to scale each sample of the validation and testing data (Priddy and Keller 2005). The performance of the ANN will vary significantly as the data was trained on a different data representation.

The ANNs predictions will be in the normalized format. These values must subsequently be "de-normalized" to provide meaningful results by reversing the normalization process (Dawson and Wilby 1998).

3.4 Activation Function

The activation function or transfer function works as a "squashing" function so that the output of a neuron in the neural network falls between certain values. In general, there are two types of activation function:

i. Threshold Function: This function will limit the output of the neuron to either 0 or 1 as illustrated in **Figure 3.4**.

$$y_k = \begin{cases} 1 \ \ if \ v_k \geq 0 \\ 0 \ \ if \ v_k < 0 \end{cases} \tag{3.4}$$

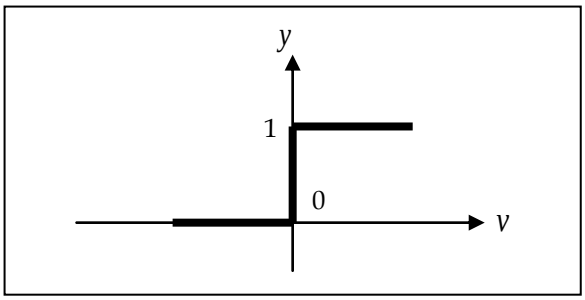

Figure 3.4. Threshold function.

ii. Sigmoid Function: This is by far the most common form of activation function used in the construction of ANNs. It is defined as a strictly increasing function that exhibits a graceful balance between linear and non-linear behaviour (Haykin 1994). This function will limit the output of a neuron to a range between 0 and 1. The hyperbolic tangent function, on the other hand, limits the outputs to fall between -1 and +1 (**Figure 3.5**).

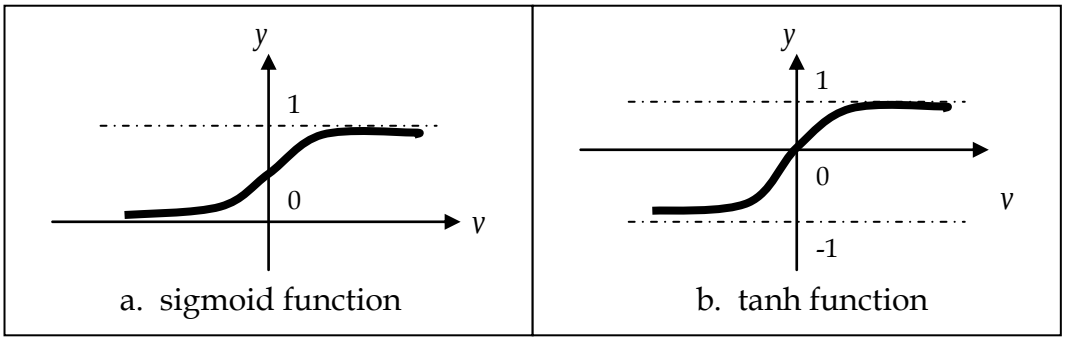

Figure 3.5. Common non-linear functions.

3.5 Network Architectures

There are two fundamentally different classes of network architecture (Sarle 1997):

i. Feedforward ANNs

In this type of topology, the connections between the neurons in an ANN flow from input to output only. These ANNs can be further divided into either single-layer feedforward ANNs or multi-layer

feedforward ANNs. The single-layer network is the simplest form of a layered network that has only one input layer that links directly to the output layer. **Figure 3.6(a)** shows a one-layer network with the single layer referring to the output layer. With multi-layer feedforward ANNs, one or more hidden layers are present between the input and output layers, as shown in **Figure 3.6(b)**. By adding one or more hidden layers, the network can extract higher-order statistics from its input and model more complex non-linear and linear models.

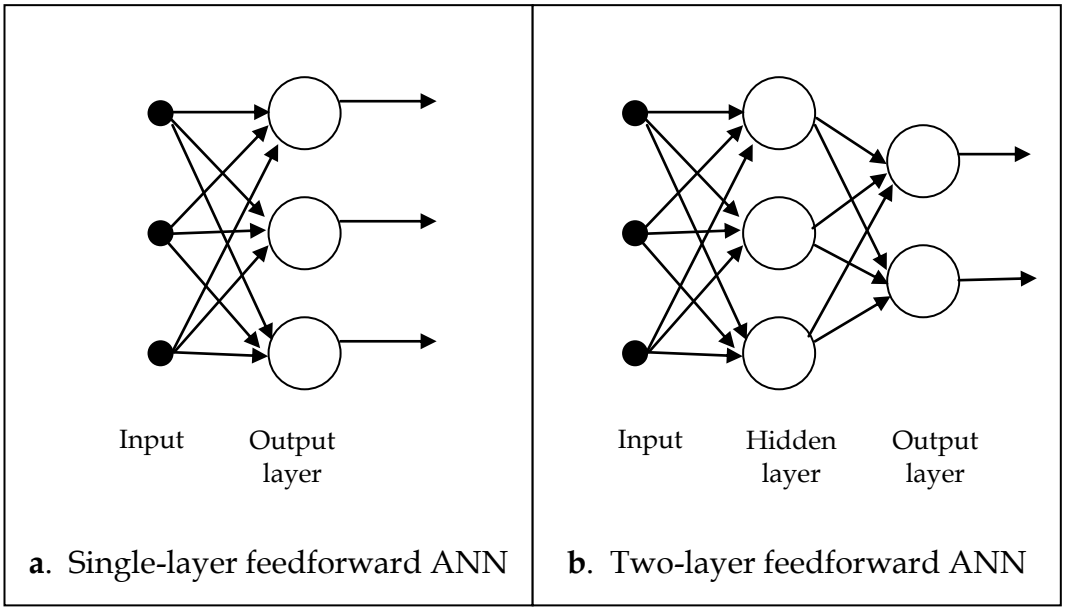

a. Single-layer feedforward ANN **b**. Two-layer feedforward ANN

Figure 3.6. Feedforward ANNs topology

ii. Feedback/Recurrent ANNs

In feedback or recurrent ANNs, there are connections from later layers back to earlier layers of neurons. There is at least one feedback loop in this type of network. Either the network's hidden neuron unit activation or the output values are fed back into the network as inputs as shown in **Figure 3.7**. The internal states of the network allow this type of network to exhibit dynamic behaviour when modelling the data's dependence on time or space (Timm *et al.* 2006). With one or more feedback links whose state varies with time, the network has

adjustable weights. This results in the state of its neuron being dependent not only on the current input signal, but also on the previous states of the neuron (Chiang *et al.* 2004). In other words, the network behaviour is based on the current input and the results of processing previous inputs. Some applications that use this type of network are (Orr *et al.* 1999):

a. Learning formal grammars: Language *L* is represented with a set of strings *S*. Each string *S* is composed of a series of symbols. A recurrent ANN is used to identify the strings that belong to language *L*. An example is $L = \{a^n b^n\}$, where *L* is a string of any number of *a*'s, followed by the same number of *b*'s. Strings belonging to *L* include: *ab*, *aabb*, *aaabbb*, *aaaaabbbbb*. Strings not belonging to *L* include: *aab*, *abb*, and *aabbbb*. Strings which belong to a language *L* are said to be grammatical, and ungrammatical otherwise.

b. Speech recognition: For this type of application, speech is first represented as a series of spectral slices to a recurrent ANN. Each output of the network represents the probability of a specific phoneme, given both present and recent input. The probabilities are then interpreted to recognize the whole utterance.

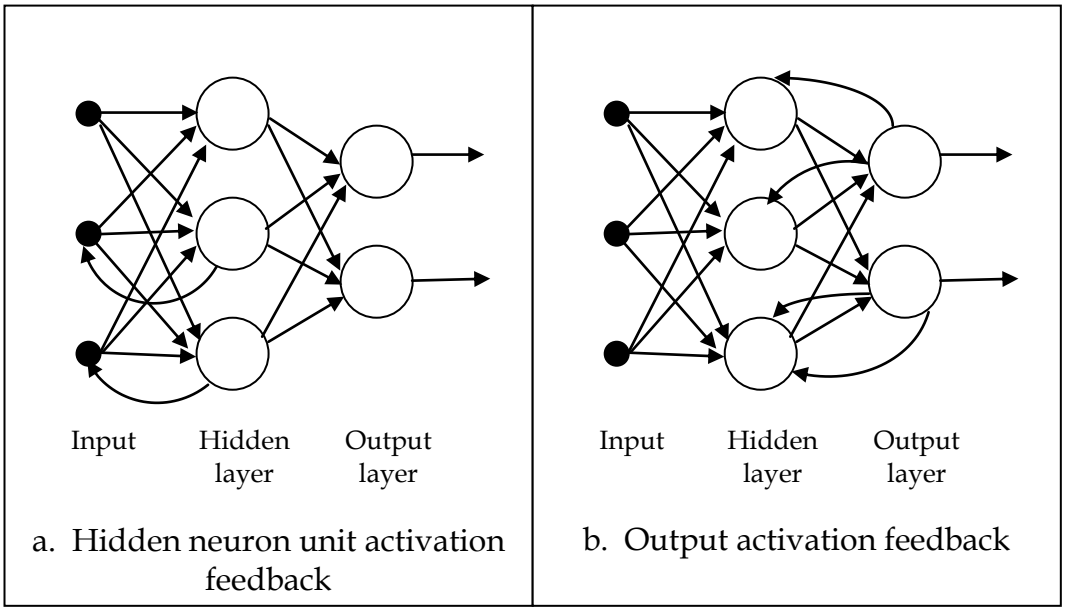

a. Hidden neuron unit activation feedback

b. Output activation feedback

Figure 3.7. Recurrent ANN topologies (O'Brien 2008).

3.6 Learning Processes

The learning processes are the processes through which ANNs function can be categorized as supervised learning, or unsupervised learning.

3.6.1 Supervised Learning

This form of learning can be regarded as analogous to learning with a teacher, whereby the teacher has the knowledge of the environment. The knowledge is represented as input-output combinations. This environment is unknown to the neural network system. The teacher who has the knowledge of the environment will provide the neural network with desired responses for the training vectors. The network parameters are adjusted step by step under the combined influence of the training vector until the network emulates the teacher, producing the desired outputs for the corresponding inputs. At this stage, the network is presumed to be optimum in some statistical sense. In this way, the knowledge of the environment available to the teacher (ANN parameters frozen) is transferred to the neural network through training and stored in the form of fixed synaptic weights, representing long-term memory. When this condition is reached, the network is released from the teacher to deal with the environment by itself. With an adequate set of input-output examples, and enough time in which to do the training, a supervised learning system is usually able to approximate an unknown input-output mapping reasonably well (Haykin 1994). Some of the categories of well-known supervised learning ANN models are listed in **Table 3.1**.

3.6.2 Unsupervised Learning

In this form of learning, the networks learn on their own as a kind of self study. When a set of data is presented to the network, it will learn to recognize patterns in the data. To perform unsupervised learning, a competitive-learning rule may be applied e.g. by creating a neural network with two layers – an input layer and a competitive layer. The input layer will

receive the available data. The competitive layer consists of neurons that compete with others for the opportunity to respond to features contained in the input data. The output of the network is not compared with the desired output. Instead, the input vector is compared with the weight vectors leading to the competitive layer. The neuron with the weight vectors most closely matching the input vector is the winning neuron (Best 1990). In another words, the network operates in accordance with a "winner-takes-all" strategy (Haykin 1994).

Table 3.1. Some well-known supervised ANNs (Sarle 1997).

Supervised Learning
a. ***Feedforward NN***
i. Linear
• Hebbian (Hebb 1949)
• Perceptron (Rosenblatt 1957)
• Adaline (Widrow and Hoff 1960)
ii. Multilayer Perceptron (MLP)
• Backpropagation (Rumelhart *et al.* 1986)
iii. Classification only
• Learning Vector Quantization (LVW) (Kohonen 1982)
• Probabilities Neural Network (PNN) (Specht 1988)
iv. Regression only
• General Regression Neural Network (Specht 1991)
b. ***Feedback NN***
• Backpropagation through time (Werbos 1990)
• Elman network (Elman 1990)
• Recurrent Backpropagation (Fernando 1988)
• Time Delay Neural Network (TDNN) (Kevin *et al.* 1990)
• Real-time Recurrent Network (Williams and Zipser 1989)
• Hopfield network (Hopfield 1982)

3.7 ANN Methodology: Training, Validation and Testing Datasets

Once the network architecture is decided and the data needed are collected, the next phase of the ANN methodology is the training of the ANN model. The training goal is to find the training parameters that result in the best

performance, as judged by the ANN's performance with unfamiliar data. This measures how well the ANN will generalize. To find the optimum ANN configuration, an ideal approach is to divide the data into three independent sets: training, validation and testing. The definition of these terminologies as discussed by Priddy and Keller (2005) are taken:

i. Training set: A set of samples used to adjust or train the weights in the ANN to produce the desired outcome.
ii. Validation set: The validation error is used to stop the training. The validation error is monitored to determine the optimum point to stop training. Normally, the validation error will decrease during the initial phase of training. However, when the ANN begins to overfit the data, the output error produced by the validation set will begin to rise. When the validation error increases for an appreciable number of iterations, thus indicating the trend is rising, the training is halted, and the weights that were generated at the minimum validation error are used in the ANN for the operation.
iii. Testing set: To assess the performance (generalization) of the ANN.

As the real prediction accuracy will be generally worse than that for the holdout sample (Zhang 2007), there is a need to evaluate the developed model with some real problem. In this research, the sets of independent data used will be termed "evaluation sets". The "evaluation sets" used in this research represent two real problems, i.e. predicting soil moisture from two different dates which was not used during the training process.

3.8 Classification and Function Approximation

Neural networks are mainly used to learn for two main tasks (Swingler 1996):

i. **Classification**: Where the input is the description of a number of objects to be recognized and the output is the identification of the class to which the objects belong. In other words, this is a task whereby the target output cannot be arranged along a meaningful continuum; each

possible output of the network is a separate entity, discrete from all the others.

ii. **Continuous Numeric Functions**: These functions describe the relationship between different sets of variables. This is where the target output falls along a meaningful continuum and each possible output of the network has its place along that continuum. This problem is called function approximation or function mapping.

If the output of a function approximation problem is discrete, then the problem becomes a classification task.

3.8.1 Example: Function Approximation Using ANN

ANNs are widely used to model non-linear functions. The ability of an ANN in fitting a non-linear function when given training data will be demonstrated using an example. In this example, a set of training data was generated from the function $y = x^2 + x$:

Table 3.2. Data created from function $y = x^2 + x$.

x	1	2	3	4	5	6	7	8	9	10
x^2	1	4	9	16	25	36	49	64	81	100
y	2	6	12	20	30	42	56	72	90	110

As an example, a feedforward backpropagation neural network with two layers is created. The transfer function between the input and the hidden layer is a sigmoid function and the function between the hidden layer and the output layer is the linear function. There are 10 neurons in the hidden layer (**Figure 3.8**). The input of the neural network are the x and x^2 values and the target is the y value. These input-output combinations are provided to the neural network to "learn" to fit a function to the two inputs and the

one output. The learning process involves the setting of the weights and bias values in the neural network architecture.

Table 3.3. Predicted y values obtained using the neural network.

x	Actual y	Predicted y
1	2	1.97
2	6	5.75
3	12	12.71
4	20	19.20
5	30	30.07
6	42	42.47
7	56	55.74
8	72	72.07
9	90	89.06
10	110	110.02

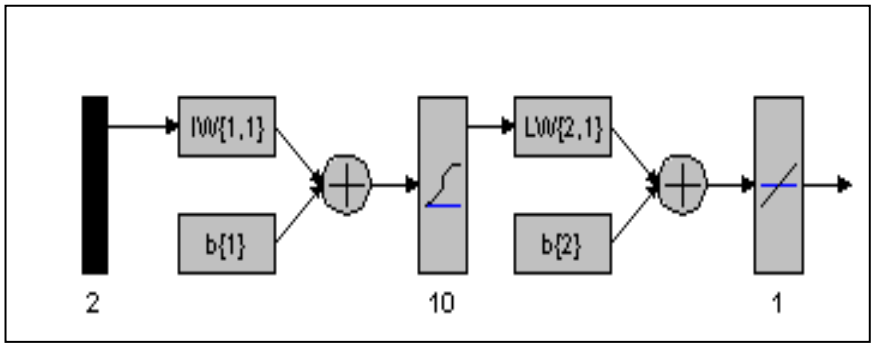

Figure 3.8. Architecture of the neural network being applied.

Figure 3.9 shows the relationship between the actual y and the predicted y values for given values of x, while **Table 3.3** shows the numerical and predicted values of y using the neural network. From the graph (**Figure 3.9**), it can be seen that the predicted y values are very close to the actual value y. These results demonstrate that the ANN can map a non-linear equation from a small set of input-output combinations. More complex non-linear relationships can be learned with more complex ANN structures and with enough input-output pairs for the ANN to adequately learn the relationship.

It is the function approximation property of ANNs that is explored in this thesis. The ANN model is expected to build the relationship between the input parameters, i.e. brightness temperature and/or ancillary data and the soil moisture value.

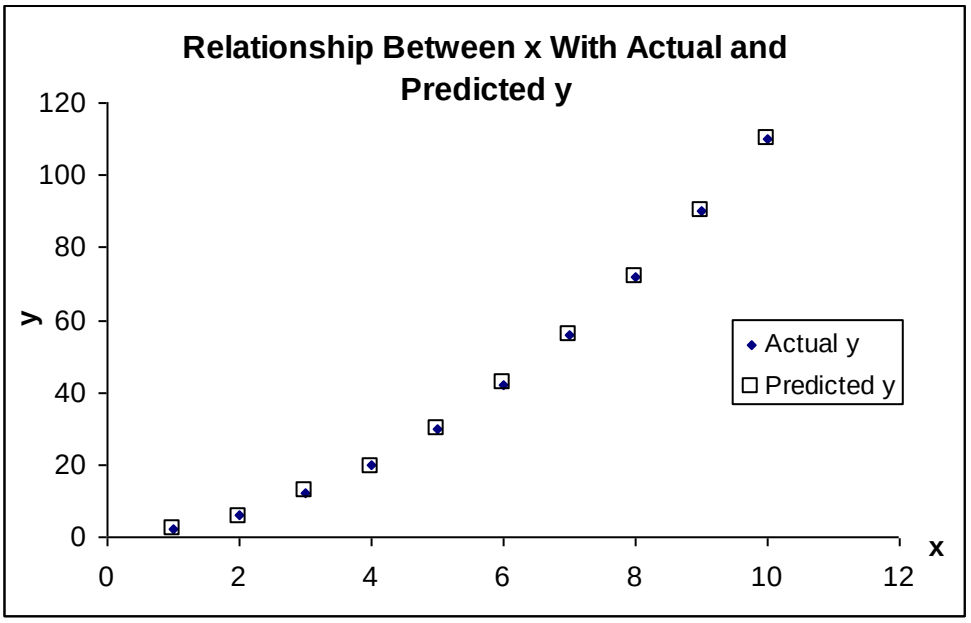

Figure 3.9. Actual and Predicted y values given x.

3.9 Chapter Summary

This chapter presents the basis and theory of ANNs models. The terminologies of training, validation, testing and evaluation sets are introduced in this chapter. Moreover, the normalization process of preparing the data for ANN in the data pre-processing is also presented. The difference between classification and function mapping problem is discussed. An example of using ANN for non-linear function mapping is also presented. This example shows that ANN is capable of solving non-linear problems. The information presented in this chapter and **Chapter 2** will be utilized in the research of passive microwave data for soil moisture prediction using ANNs. The data used for this research study is next presented in **Chapter 4**.

Chapter 4

NAFE'05: Study Area & Data Acquisition

This chapter describes the field campaign NAFE 2005 (National Airborne Field Experiment) conducted in New South Wales, Australia, during November 2005. The description will cover information relevant to this thesis, namely the objectives of the campaign, the ground sampling strategy and the airborne monitoring during this field campaign. A more detailed description regarding this field campaign can be found in Walker and Panciera (2005) and Panciera *et al.* (2008). The data are available at www.nafe.unimelb.edu.au.

4.1 Overview and Objectives

The purpose of NAFE was to map near surface soil moisture at different resolutions making use of passive microwave airborne and space borne remote sensors. The ultimate goal was to provide reliable near-surface soil moisture observations at paddock scale over a large area. Specifically, it involves capitalizing on remote sensing missions such as the European Space Agency's (ESA's) Soil Moisture and Ocean Salinity (SMOS) satellite that was launched in November 2009. SMOS carries the first-ever space borne 2-D interferometric radiometer operating at 1.4 GHz (L-band) with V- and H-polarized observations at a range of incidence angles (Kerr *et al.* 2001).

To utilize SMOS, there are still unanswered questions that need to be addressed. These include: (i.) the correct interpretation of the large-scale spatially averaged passive microwave observations provided by the remote sensors (i.e. brightness temperatures), (ii.) the inconsistency between the

scales at which the variables are measured and predictions are needed, and (iii.) the applicability of soil moisture retrieval algorithms from brightness temperatures developed using radiometers mounted on towers or trucks, whose field of view is limited to tens of meters, to satellite sensors characterised by large footprints (Panciera *et al.* 2006). Consequently, to utilize data from the SMOS mission requires coordinated airborne and ground data collection campaigns to verify and refine the soil moisture retrieval algorithms (Panciera *et al.* 2008).

4.2 Study Area

The study area of NAFE'05 was the Goulburn River catchment, a sub-humid to temperate area located in south eastern Australia, approximately 300 km north-west of the city of Sydney (**Figure 4.1**). This catchment extends from $31^{0}46'$S to $32^{0}51'$S and $149^{0}40'$E to $150^{0}36'$E, with elevations ranging from 106 m in the floodplains to 1257 m in the northern and southern mountain ranges. The catchment was chosen for: (i.) its relatively large area of predominantly low to moderate vegetation cover in the north of the catchment (useful for satellite soil moisture remote sensing studies), and (ii.) the lack of maritime effects in order to avoid mixed pixel responses from ocean and land data within the satellite measurements.

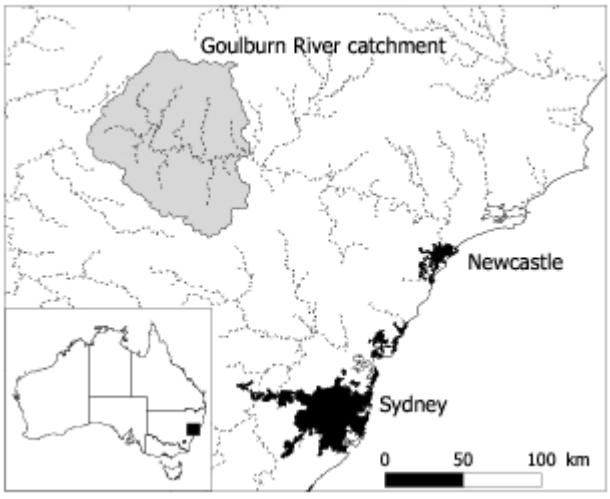

Figure 4.1. Location of the Goulburn River Catchment (Rüdiger *et al.* 2007).

This catchment has two intensively monitored sub-catchments, the Krui River (562 km^2) and Merriwa River (651 km^2) in the northern half of the catchment (**Figure 4.2**).

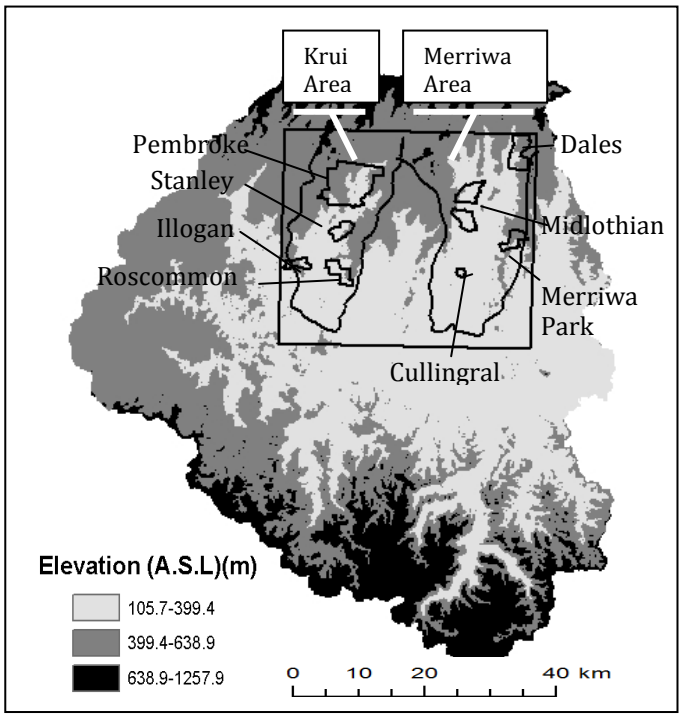

Figure 4.2. Overview of NAFE'05 focus farms within the Krui and Merriwa areas.

4.2.1 Climate

The general climate within the region can be described as sub-humid or temperate with significant variation in the annual rainfall and evaporation during the year, and a high variability of rainfall throughout the catchment. While the average annual rainfall in the Goulburn River catchment is approximately 650 mm, it varies from 500 to 1100 mm depending on altitude. Major rainfall events generally occur from November to March with an average monthly precipitation of 68 mm, while the monthly average precipitation in June is 32 mm. Monthly mean maximum temperatures reach approximately 30˚C in summer and 14˚C in winter, with mean minimum values of 16˚C and 2˚C, respectively. Except for elevated areas, frost is unlikely to occur during daytime in winter, but night time minimum temperatures in winter are frequently less than 0˚C (Rüdiger *et al.* 2007).

4.2.2 Geology and Soil

The geology of the Goulburn River catchment can be divided into two types: the north, which is predominantly Tertiary basalt, a product of the Cainozoic volcanism that took place throughout much of eastern Australia; and the south, which is dominated by rocks of Triassic age laid down as sediments in lagoons and consisting of sandstone, conglomerate, and shale. The actual NAFE'05 study area falls in the northern part of the Goulburn catchment, across the Liverpool Range and the Merriwa Plateau. The northern part of the NAFE '05 study area is characterized by black basalt derived cracking clays, while the very southern part of the study area is characterized by sandstone derived soils. Red basalt derived clays also exist in southern regions of the study area.

4.2.3 Vegetation

Much of the original vegetation in the northern part of the Goulburn catchment has been cleared, the extent of which has largely been influenced by topography and soil type. In the north where the terrain is rugged (the Liverpool Range), accessibility is restricted and the area has thus remained highly vegetated. To the south, clearing has been more extensive due to the rolling to hilly terrain, ensuring greater accessibility (the Merriwa Plateau). Grazing and cropping activities dominate the cleared areas due to the high fertility of basaltic soils. The sandstone derived soils to the far south are largely uncleared as they are less fertile and hence expected to be less productive.

4.3 Ground Monitoring

Eight focus farms within the Krui and Merriwa sub-catchments were chosen according to the spatial distribution and characteristics of each farm for detailed measurements. This region is very suitable for soil moisture remote sensing studies due to the moderate vegetation cover arising from grazing and cropping activities in the region. **Table 4.1** summarizes the main

characteristics of each farm. From **Table 4.1**, it can be seen that for a grid cell of 1 km spatial resolution for example, there is sub-grid heterogeneity either in terms of the vegetation or the topography.

Table 4.1. Main characteristics of the focus farms during the NAFE'05 campaign.

Farm Name	Area(ha)	Topography	Landuses	Soils
Pembroke	6400	Hilly/Gently rolling	• Grazing • Crop (wheat)	• Black basaltic clays
Stanley	720	Hilly	• Grazing	• Black basalts on flat; red basaltic clays on crests
Roscommon	940	Flat/Gently rolling	• Grazing	• Black basaltic clays and sandy soils
Illogan	560	Flat/Gently rolling	• Crop (Barley, Oats, Wheat)	• Black basaltic clays with patches of red basaltic clays
Dales	1500	Flat/Hilly	• Grazing	• Black basaltic clays
Midlothian	2000	Flat/Hilly	• Grazing • Crops (Sorghum, Lucerne, Wheat)	• Black basaltic clays
Merriwa Park	750	Hilly	• Grazing • Crop (wheat)	• Black basaltic clays
Cullingral	220	Flat	• Grazing	• Black basaltic clays

Spatial ground sampling was concentrated in the 40 km × 40 km region and the eight focus farms, with soil moisture data to 5 cm depth soil profiles collected at a range of spatial scales. The spatial soil moisture sampling is divided into: (i.) regional scale sampling, and (ii.) focus farm measurements. **Figure 4.3** shows the calendar for ground sampling for the NAFE'05 campaign. In this figure, the shading shows when the sampling took place. The soil moisture within the top 5 cm of the soil profile was monitored coincident with aircraft flight either across the entire site or across the focus farms. During regional sampling, the entire 40km×40km study area was sampled on a grid of approximately 1 km. Regional sampling was carried out once a week. On all other days (**Figure 4.3**), the sampling was

focused on the two focus farms, with each farm mapped one or two times per week.

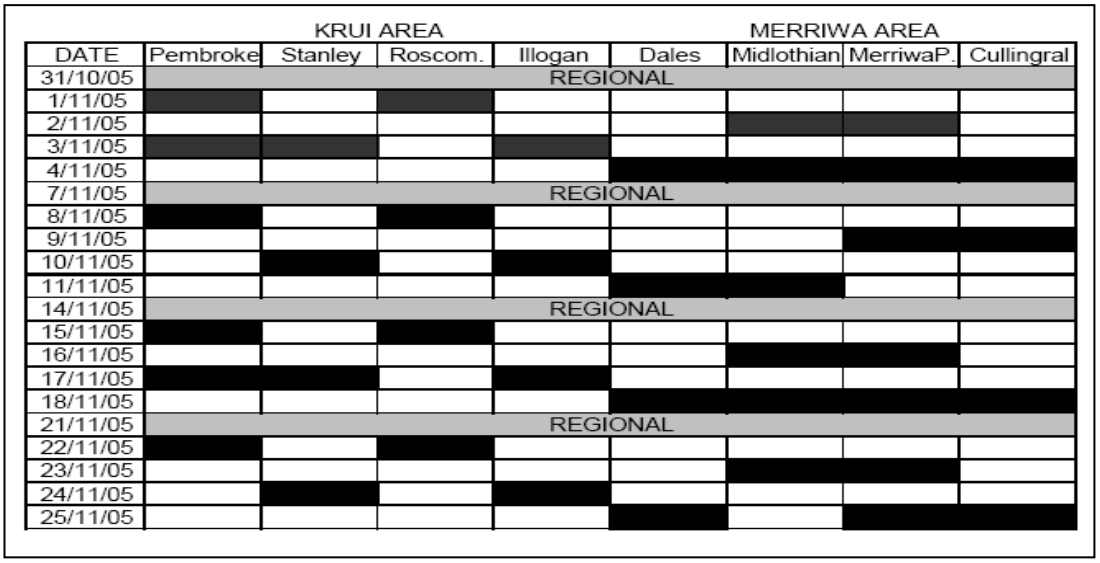

	KRUI AREA					MERRIWA AREA		
DATE	Pembroke	Stanley	Roscom.	Illogan	Dales	Midlothian	MerriwaP.	Cullingral
31/10/05	REGIONAL							
1/11/05								
2/11/05								
3/11/05								
4/11/05								
7/11/05	REGIONAL							
8/11/05								
9/11/05								
10/11/05								
11/11/05								
14/11/05	REGIONAL							
15/11/05								
16/11/05								
17/11/05								
18/11/05								
21/11/05	REGIONAL							
22/11/05								
23/11/05								
24/11/05								
25/11/05								

Figure 4.3. Ground sampling calendar for NAFE'05 (Walker and Panciera 2005).

Soil moisture measurements within the focus farms were taken at 500 m, 250 m, 125 m and 62.5 m resolutions, covering as much as possible the range of land uses, topography, soil types and soil wetness conditions present across the farms. **Figure 4.4** shows the ground sampling strategy within the focus farms.

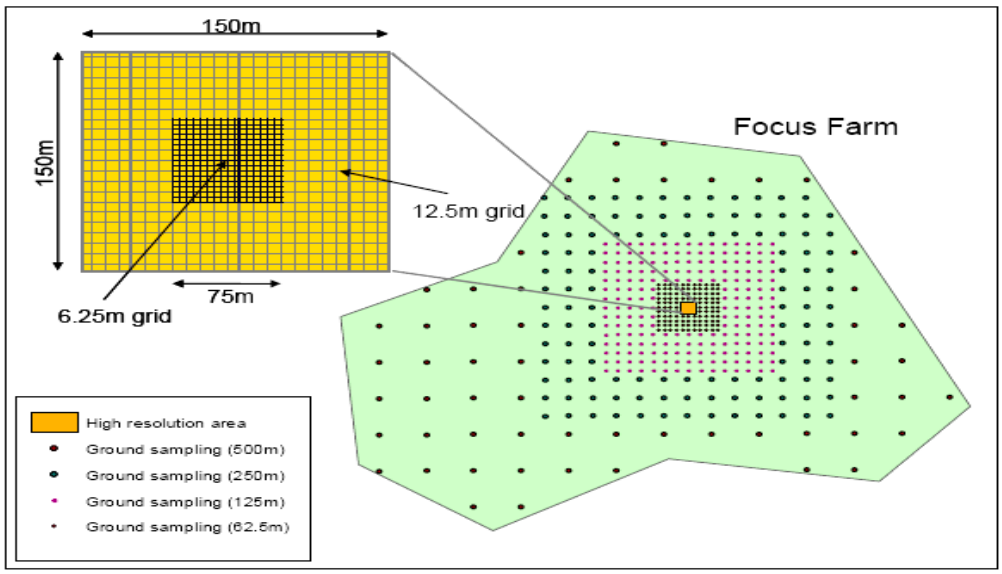

Figure 4.4. Schematic of farm scale soil moisture sampling strategy (Walker and Panciera 2005).

Within each farm, a small area of 150m × 150m was chosen for intensive soil moisture sampling. These small "high resolution" areas were sampled at 12.5 m and 6.25 m to provide highly detailed information about the variability expected from point soil moisture and vegetation biomass measurements.

Apart from soil moisture measurements, the following supporting data were also collected at the focus farms during each sampling day for each focus farm:

i. Gravimetric soil moisture samples

ii. Vegetation water content samples

iii. Leaf wetness observation and dew amount

A number of auxiliary data sets are needed to characterize the surface conditions of the study area. This information is needed to model the soil microwave emission and to calibrate the ground sensors that were used during the campaign. The supporting data include:

i. Thermogravimetric soil moisture samples

ii. Vegetation biomass and water content

iii. Dominant vegetation type

iv. Visual observation of land use and classification

v. Normalized Difference Vegetation Index (NDVI)

v. Surface roughness

4.4 Airborne Monitoring

Airborne measurements have been made using a two-seater motor glider called the Small Environmental Research Aircraft (SERA). This aircraft is instrumented with the Polarimetric L-band Multibeam Radiometer (PLMR), which allows very high resolution passive microwave (down to 50 m) observations to be made across the entire study areas.

The PLMR measures both V- and H-polarized brightness temperatures with polarization switched at incidence angles +/-7°, +/-21.5° and +/-38.5° in either across track (pushbroom) or along track configurations. The beamwidth is 17° resulting in an overall 90° field of view. This instrument has a frequency of 1.413 GHz and bandwidth of 24 MHz.

A total of around 100 hours of NAFE mission flights were conducted during the campaign. All flights were north-south oriented to be parallel to the geomorphology of the area and to avoid the strong variation in terrain elevation, as well as direct sun glint in the outermost beams. Importantly, this orientation is similar to the planned SMOS flight path. Full coverage of the same ground area was guaranteed by allowing a full PLMR pixel overlap between adjacent flight lines for the median ground altitude of the area. A schematic view of the PLMR flights during this field campaign is shown in **Figure 4.5**.

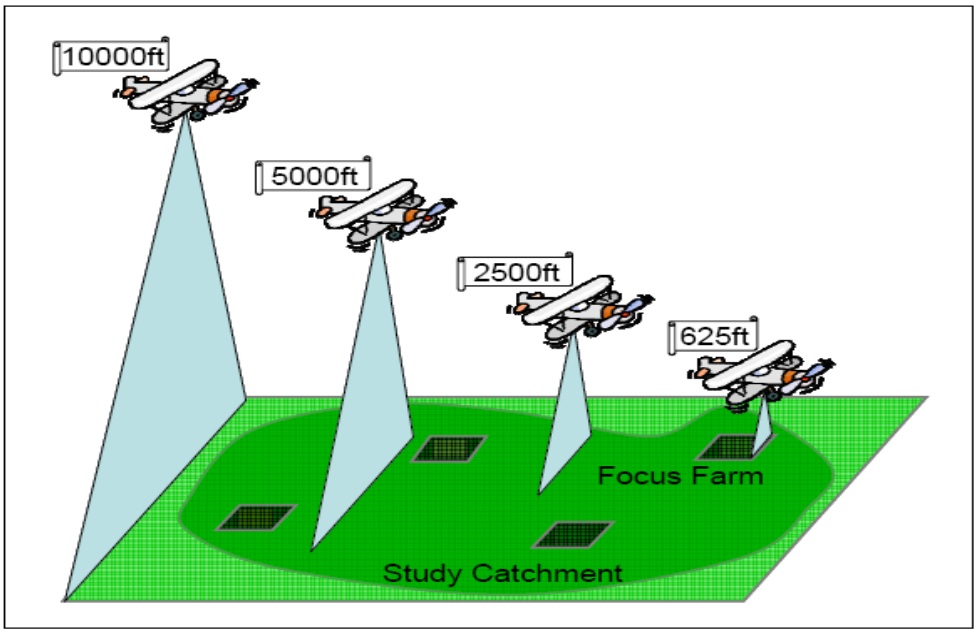

Figure 4.5. Schematic view of PLMR flights during NAFE'05. The flight heights are nominal mean altitudes above ground level (Walker and Panciera 2005).

During each flight, the study area was covered at four different altitudes in descending order: 3000m, 1500m, ~750m and ~200m Above Sea Level (ASL), which results in L-band maps at approximately 1000, 500, 250 and 62.5 m spatial resolution (**Table 4.2**).

Table 4.2. PLMR flight description.

Flight Names	Flight Altitude (AGL)	Flight Altitude (ASL)	Nominal Ground Resolution	Swath	Coverage
Low Resolution	10000 ft	3430 m	1000 m	6000 m	• Regional • Krui • Merriwa
Intermediate Resolution	5000 ft	1910 m	500 m	3000 m	• Krui • Merriwa
Medium Resolution	2500 ft	1050 – 1270 m	250 m	1500 m	• Farms
High Resolution	625 ft	480 – 700 m	62.5 m	375 m	• Farms

4.5 1-km Soil Moisture Product

In this section, a description of the 1 km soil moisture product is presented. The 1 km soil product was produced and validated using the L-MEB (L-band Microwave Emission of the Biosphere) model applying the brightness temperature observations made with the PLMR radiometer (at incidence angle of ±38.5^{o}) across the NAFE'05 study area. A detail description of this retrieval can be found in Panciera (2009). For the purpose of this thesis, only the pertinent details from Panciera (2009) are presented. The product, termed the 1-km soil moisture product hereafter, is used as the soil moisture ground truth for the analysis in **Chapters 7** and **8** of this thesis.

The soil moisture maps derived from the 1 km airborne data have two major advantages with respect to ground point measurements, which make them desirable for the objective of ground-truthing coarse-scale soil moisture retrieval: (i.) they have a larger extent, covering the entire study area and therefore characterizing the soil moisture variability within all the coarse-scale pixels, and (ii.) each soil moisture observation represents an integrated value over a 1km area, therefore overcoming the limitation of point data, which only provide information for the domain sensed by the ground probe (a few centimetres depth) at specific locations.

The L-MEB model (Wigneron *et al.* 2007) is based on a simplified zero-ordered radiative transfer model, called the "tau-omega $(\tau-\omega)$" model (Grant *et al.* 2007a). The model takes into account the effect of vegetation cover on soil emission. The ancillary data on land cover, near surface soil moisture and canopy temperature, and soil textural properties for the L-MEB model used in this study were obtained from either existing databases or derived from available satellite imagery. The L-MEB model, which is used as a forward emission model to simulate the L-band emission of the soil-canopy layer at H- and V-polarization according to incident angle, is the core component of the SMOS soil moisture retrieval algorithm (Panciera *et al.* 2009). In principle, ground collected data were given priority where possible. In the case where satellite imagery had been used, the dataset with

the finest available resolution were chosen. This choice aims at avoiding as much as possible any errors associated with the ancillary data so that the effects of land surface heterogeneity can be isolated. A summary of the ancillary data is presented in **Table 4.3**.

A direct comparison is carried out of the L-MEB model determined soil moisture with the soil moisture from ground-based measurements. The average accuracy of this soil moisture product is reported to be 3.8% v/v and in all cases better than 6% v/v over the variety of land surface conditions typical of the study area (Panciera 2009). Soil moisture was retrieved for each cell of the 1 km brightness temperatures (Tb) grid using the L-MEB model together with the ancillary data described in **Table 4.3**. The soil moisture output of the L-MEB algorithm was limited to a maximum soil moisture value of 58%v/v, derived from the analysis of the maximum soil moisture achieved at the monitoring stations. Conversely, no lower limit was imposed on the retrieved soil moisture.

Table 4.3. Summary of the ancillary data used for the L-MEB model.

Ancillary Data	Source	Resolution	Description
Land cover	Landsat 5 Thermatic Mapper	30m	Supervised classification and defined five land cover types: • Native grass (50.7%) • Dense forest (24.3%) • Bare soil/vegetation with low Leaf Area Index (LAI) (12%) • Open woodland (8.5%) • Cropped area (4.5%)
Soil Texture	Ground sampling (Malvern Mastersizer 2000)	88 soil samples (7cm wide, 5cm deep) on two regional sampling	Very variable, ranging from black basalt derived cracking clays in the northern part to sandstone derived soils in the southern part. An exact

		days	inverse distance technique was used to interpolate and upscale soil texture point data to the entire study area.
Soil Temperature	Monitoring stations	2.5cm and 15cm depth	Daily average obtained from the monitoring stations was used.
Canopy Temperature	Thermal infrared sensors	Four thermal infrared stations	Sensors were mounted on 2m high towers pointing vertically down towards the vegetation canopy of four different land covers: bare soil, lucerne crop, wheat crop and native grass.

4.6 Conclusions

This chapter described the field campaign NAFE 2005 (National Airborne Field Experiment) conducted in New South Wales, Australia during November 2005. Only details of the data pertinent to this thesis are presented. These details include an introduction of the study area, the airborne and ground monitoring data obtained from this field experiment. For the purpose of this research, the 1 km soil moisture product will be used as the ground truth. The average accuracy of the ground truth is 3.8%v/v, which is considered very accurate according to the SMOS mission. Full details can be obtained from the NAFE data website: http://www.nafe.unimelb.edu.au and from Panciera *et al.* (2008). The website provides all the information needed for the full interpretation of these data, along with general information on the Goulburn catchment, photographs of the landscape, sampling methods and a full experiment plan.

Chapter 5

Literature Review and General Methodology

A review of the use of Artificial Neural Networks (ANNs) for soil moisture retrieval, focusing particularly on passive microwave data, is presented in this chapter. The description starts with an explanation of the inverse problem. For clarity, the research is categorized according to the number of parameters, including the soil moisture values retrieved using ANNs. In addition to this, the use of the ANN for solving the downscaling of the soil moisture retrieval problem is also presented in this chapter. Following an analysis of possible solutions, a new solution is proposed to solve the current issues at the end of the chapter.

5.1 The Inverse Problem

When we have a measurement vector **m** arising from some physical process **Ø( )** acting on a parameter vector **x** which we wish to infer, it is called an inverse problem (Davis *et al.* 1995). In soil moisture retrieval, the radiative transfer model can be used to calculate the brightness temperature from geophysical parameters in a forward model. In an inverse model, the soil moisture can be estimated from the brightness temperature values. In other words, the inverse problem involves restoring the values of the physical parameters of a natural medium from the data of remote sensing instruments (Sharkov 2003).

Inverse problems are usually ill-posed and complicated as inverse mapping is often a many-to-one mapping, with more than one parameter set **x** which could account for the observed measurement set **m**. Moreover, the relationship between the sensing measurements and the geophysical

parameters is often highly nonlinear (Davis and Jenq-Neng 1997). **Figure 5.1** shows more than one forward mapping and the explicit inverse mapping. Multiple parameter values X_1 and X_2 are mapped to the same measurement m. An explicit inverse can immediately invert a measurement m and estimate its associated parameter $\hat{x}$ (Davis and Jenq-Neng 1997).

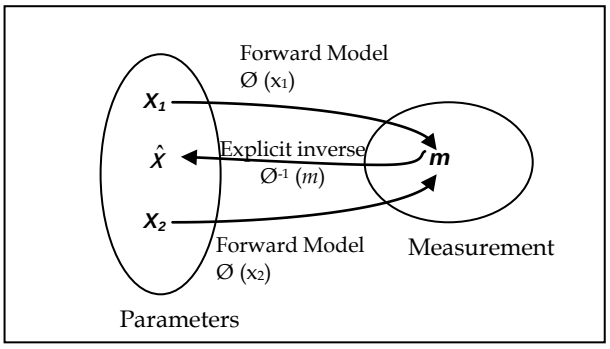

Figure 5.1. Representation of a common forward model and the explicit inverse relationship. (Davis and Jenq-Neng 1997).

5.1.1 The ANN as an Explicit Inverse Solution

From **Figure 5.1**, it is clear that the explicit inverse is a process whereby for a given measurement set **m**, a unique inverse $\boldsymbol{Ø^{-1}(m)}$ exists that will yield $\hat{x}$. The explicit inverse of the physical process can be built by transferring input (remote sensing measurements) into output (land surface parameters) (Wigneron *et al.* 2003). In most studies (Yuei-An *et al.* 1999b; Atluri *et al.* 1999; Shou-Fang *et al.* 2002; Posa *et al.* 2004) an ANN may be used to create this explicit inverse function. The input of the ANN is the measured brightness temperature and the output nodes are the land surface parameters such as soil temperature, soil roughness and soil texture (**Figure 5.2**). After the inversion, the ANN provides an explicit retrieval algorithm, which is a solution of the inverse problem and can be used for retrieval.

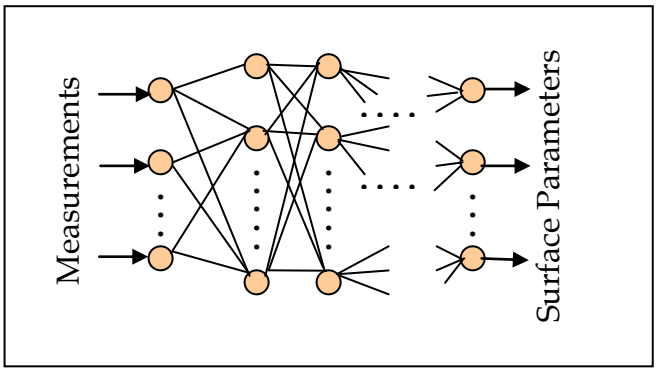

Figure 5.2. An ANN model based on inversion where the inputs are the measurements and the outputs are the surface parameters.

For a given set of training data and with sufficient training, a feedforward ANN is ideally able to synthesize a mapping akin to the process that is responsible for generating the training data (Jensen *et al.* 1999). The output of the trained neural network x can be characterized by:

$$x = f(m, w) \tag{5.1}$$

where f corresponds to the memory-less function describing the mapping from the input to the output, m is the input vector, and w is the vector of the weights internal to the network. Inversion of a neural network consists of clamping the weights and the neural network output while adjusting the input in equation (5.1) until an equality or a best possible fit occurs for one or more values of m (Jensen *et al.* 1999).

The advantage of using an ANN is that all surface parameters can be included and the ANN will act as an empirical mapping between the brightness temperature measurements and the surface parameters. The disadvantage of such a method is that the empirical mapping is not easy to write down explicitly from the ANN parameters once the ANN has been trained (Dawson *et al.* 1997). This is because of the inherent complexity of the ANN. Each node (hidden and visible) sums the responses of a number of linear equations, each described by a number of parameters or weights. It is this complexity that gives the ANN the flexibility to learn in many different

domains. **Figure 5.2** shows one particular ANN architecture from the many that can be used.

Importantly, the number of nodes and layers can significantly affect the performance and these parameters have to be chosen carefully with respect to the data, the model of the process, and the required performance. Ideally, the simplest ANN architecture that gives the required performance is the best as compared to a complicated architecture.

5.2 Review: Soil Moisture Using ANN

The research in this thesis looks into the problems of: (i.) scale-to-scale, and (ii.) downscaling of soil moisture prediction. The discussion on previous research into soil moisture prediction using ANN particularly using passive microwave data, is presented according to these two categories.

5.2.1 Scale-To-Scale Soil Moisture Prediction

To simplify the discussion, the research under this category is divided into (i) single- and (ii) multi-parameter retrieval. Single parameter retrieval is only concerned with obtaining soil moisture whereas multi-parameter retrieval uses one ANN to obtain the values of soil moisture and other land surface parameters.

5.2.1.1 Single Parameter Retrieval

For single parameter retrieval, the only target of retrieval is the soil moisture. Yuei-An *et al.* (2001), Paloscia, *et al*. (2002), Del Frate, *et al.* (1999; 2003), Macelloni, *et al.* (2003) and Angiuli *et al.* (2008) have used either a model-based approach, field experimental data or a combination of these two as the input for the ANN they used for the retrieval of soil moisture.

Yuei-An *et al.* (2001) used only simulated data from the Land Surface Process/Radiobrightness (LSP/R) model during a two-month dry-down of a prairie grassland with vegetation wet biomass of 3.7kg/m^2 to train and test

the ANN. The LSP module in the LSP/R model simulates land-air interactions and estimates surface fluxes, temperature, and moisture profiles in soil and vegetation when forced with observed weather. These estimates are used by a microwave emission model, called the R module, that predicts terrain brightness temperatures (Judge *et al.* 2003). From the total of 8640 paired Tb-SM samples, 5% were randomly chosen to train the developed Error Propagation Learning Back Propagation (EPLBP) network model. Another 5% were randomly chosen for testing. Experiments were conducted for combinations of different frequencies of brightness temperature (Tb) with either single or multiple viewing angles. The retrieval result saw less than 1% v/v Root Mean Square Error (RMSE) for all cases and the correlation coefficient between the retrieved and reference SM was better than 0.9 for all cases. The noise was assumed to have a Gaussian distribution with standard deviations of 1K and 2K. It was found that L-band with a single look angle is more sensitive to soil moisture retrieval, producing a RMSE as low as 0.412% v/v for the no noise case at an incident angle of 10˚, 0.614% v/v for the 1K noise case at an incidence angle of 20˚, and 0.955% v/v for the 2K noise case at an incidence angle of 50˚.

Paloscia, *et al.* (2002) used both model simulations and experimental data as input for their ANN. Their results showed that the retrieval performance is encouraging if the ANN is trained using the physical model together with the experimental data. The microwave bands used for these studies were the L, C, and X bands. Dual polarizations, i.e. H- and V-polarization data, were used as the input for the ANN. In addition to the brightness temperature, Paloscia, *et al.* (2002) also used the incident angle as input to the ANN for soil moisture retrieval. It was verified that L-band emission correlated well with the soil moisture content of a greater depth (≈10cm) compared with the C and X bands. Apart from the frequency of the data, researchers were also trying to verify whether single or multi-angular data are more suitable for soil moisture retrieval. Saleh *et al.* (2006) in their research on investigating the development and assessment of the

performance of statistical regressions linking passive microwave measurements to surface soil moisture over natural grass land, reported that rather small accuracy differences in the surface soil moisture retrievals should be found between single and multiple angles configuration approaches when the L band emission of standing vegetation and the mixed layer is small.

An ANN trained with a physical vegetation model was used to retrieve soil moisture of a wheat crop during the whole crop cycle by Del Frate *et al.* (1999). The network was next tested by using extensive field measurements carried out in 1993. The frequencies studied included 1.4 GHz (L band), 5.3 GHz (C band), 10.65 GHz (X band) 23.8 GHz (K band), 36.5 GHz (Ka band) and 90 Ghz. The dual-polarization data at various observation angles (between 0^o and 50^o) together with the corresponding soil moisture content values were used to train and test the network. Using L band data, the RMSE obtained was approximately 3% v/v.

Macelloni *et al.* (2003) trained two different neural networks (ANN1 and ANN2) with different set of inputs. For ANN1, the data used were generated using the Integral Equation Model (IEM) only, while ANN2 used both IEM and field measurements data. The Integral Equation Model (IEM) (Fung 1994) is a theoretical method to model microwave emission. This model provides a good prediction of surface scattering coefficients for a wide range of surface profiles (Zhao *et al.* 2003). The frequencies being investigated included L, X, and Ka bands. Only H polarized data were used as the input for the ANNs. Their results showed that ANN1, which was only trained with data from the IEM, was not very good, compared to ANN2, with a correlation coefficient between the actual and predicted soil moisture of around 0.7 for all cases. ANN2, which was trained with data from both IEM and experiment data, showed a better result with an average correlation coefficient of around 0.9.

Del Frate *et al.* (2003) retrieved soil moisture using multiangular L band observations at both H and V polarizations for each date of radiometric

acquisition in 1993 and 1996 for the whole wheat cycle using the Scaled Conjugate Gradient (SCG) algorithm with sigmoid functions as the activation function of the networks units. The training data were generated using an electromagnetic model by using the detailed biophysical and geometrical information of year 1993 as the input of the model. A variety of conditions within the established range of 6.25% to 37.5% of soil moisture and surface standard deviations of 0.5 cm, 1 cm, and 1.5 cm were covered by using the dual polarized L band brightness temperature with incidence angles between 10^{o} and 50^{o} in steps of 10^{o}. A total of 180280 samples were used for training. The RMSE values obtained were between 4 and 5% v/v for 1993 and slightly lower for 1996.

In the work by Angiuli *et al.* (2008), an ANN based on the standard backpropagation algorithm was applied to train the data simulated using the land emission model and tested with L band radiometric data of bare soils obtained during two field experiments: T-REX and MOUSE. A total of 2000 samples were simulated with 1400 used for training and 600 for testing. The data were simulated for soil moisture ranging from 0.0 to 0.4% v/v, standard deviation of roughness from 0 to 5 cm, correlation lengths from 1 cm to 50 cm, incidence angles from 25˚ to 65˚, and soil temperatures from 10˚C to 45˚C. In terms of the topology, a two hidden layer ANN with sigmoid activation function was used. The simulated data were divided into training and testing sets. The input vector consisted of the brightness temperatures at different incidence angles (with no noise added), surface temperature and soil roughness. The output of the neural network was the soil moisture content corresponding to the brightness temperature in the simulation. The performance of the ANN during the learning phase was monitored simultaneously both on the training and the testing set. Once the error on the test set reached the minimum value, indicated by an increase in error if learning continues, the learning process ended. At this point, the ANN is regarded as trained. The trained ANN was tested using L band radiometric data of bare soils at different antenna elevation angles obtained during the

two different field experiments. The maximum Root Mean Square Error (RMSE) obtained was 7% v/v, and being 5% v/v for soil moisture in the 0-5 cm soil layer. The ANN was found to underestimate for cases of soil moisture content of more than 15% v/v as the network was trained with the simulation data of soil water content, in a large percentage lower than this value.

5.2.1.2 Multi-parameter Retrieval

For multi-parameter retrieval, the ANN is used to retrieve other parameters of interest, e.g. soil temperature as well as the soil moisture. Yuei-An *et al.* (1999b) utilized both simulated H and V polarized brightness temperature at 1.4, 19.0, and 37.0 GHz for a single incidence angle at 53˚ as input for the ANN. The parameters retrieved were the land surface parameters: canopy temperature, water content, soil temperature and moisture of the uppermost 5 mm of the ground. In their research, the LSP/R model and the ANN model were integrated to retrieve these parameters from the terrain brightness temperature. The two ANN architectures with their inputs and outputs configurations are shown in **Figure 5.3**.

For the four channels ANN model, the RMSE of soil moisture retrieval was around 0.05% v/v while for the six channels ANN model, the RMSE of soil moisture retrieval was around 0.1% v/v (Yuei-An *et al.* 1999b).

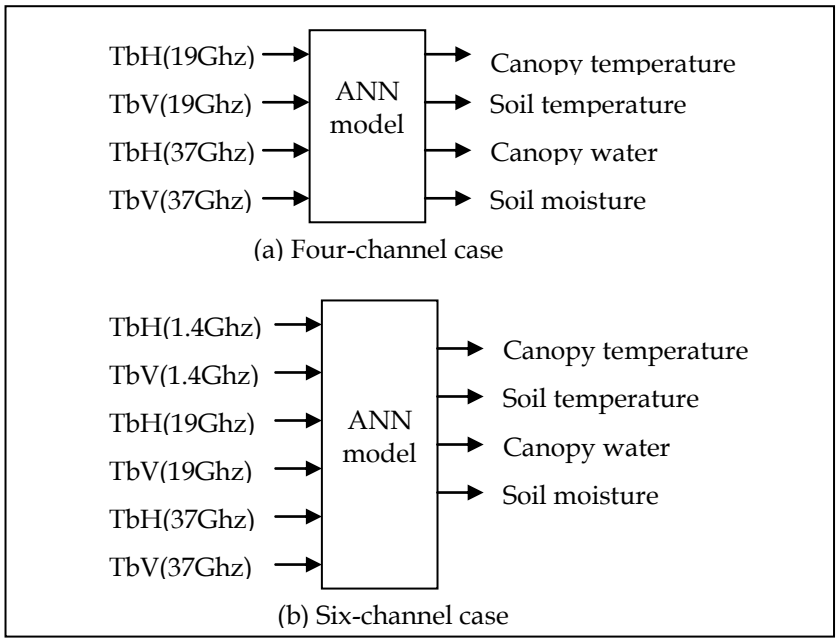

Figure 5.3. ANN input-output configuration of Yuei-An *et al.* (1999b).

Shou-Fang *et al.* (2002) used the measured H and V polarized brightness temperatures at 1.4 and 10.65 GHz to retrieve both soil moisture content and vegetation water content of wheat at multiple look angles. The brightness temperatures were taken over wheat fields through the three months growth cycle. The soil moisture was measured at depths of 5 cm and 10 cm. The input of the ANN was divided according to either one or two look angles. It was found that, retrieval of soil moisture content and vegetation water content can be obtained if two look angles for the L band signal are utilized, with an average RMSE error of ≈4% v/v for soil moisture retrieval.

Atluri *et al.* (1999) used field experiment data to retrieve soil moisture and soil temperature using a backpropagation ANN trained with the Levenberg-Marquardt algorithm. Ground-based microwave remote sensing instruments were used to measure soil moisture. The brightness temperature data were collected using two radiometers mounted on a crane and moved by a truck. The inputs of this network were the surface temperature together with the brightness temperature in the L and S bands. Angular data was not considered. The two-layer feed-forward ANN was

able to predict the soil moisture with an error of 0.02% to 0.95% v/v with respect to the ground truth values.

Zhao *et al.* (2003) tried to retrieve soil moisture and surface roughness of bare soil using a simulation of a validated IEM model of dual-polarized data. The simulation was of the satellite-based Advanced Microwave Scanning Radiometer (AMSR/E) for a viewing angle of 55˚. Sensitivity analysis with respect to the input noise was carried out in order to determine the effect of random noise on the results from the simulated data. The ANN consisted of two hidden layers, each made up of 100 neurons or nodes. For the 6 GHz data for both polarizations, the RMSE of soil moisture retrieval was 1.54% v/v. For both the 6 GHz and 10 GHz data of both polarizations, the RMSE was 0.0891% v/v without noise. When Gaussian distribution noise with a standard deviation σ of 0.02 and 0.06 was added, the results for the 6 GHz data with both polarizations gave a RMSE of 1.97% v/v, and for the 6 GHz and 10GHz data with both polarizations, the RMSE was 5.91% v/v.

5.2.2 Spatial Downscaling of Soil Moisture

Passive microwave in the L band (1.4 Ghz) has been proved to be more sensitive to soil moisture measurement up to 5 cm in depth compared to higher frequencies, and more direct methods such as radar backscatter and thermal data (Kerr 2007; Wagner *et al.* 2007). Despite the high sensitivity of microwave radiometers to near-surface soil moisture, their spatial resolution is about 10 to 500 times coarser than that of active microwave and optical systems (Merlin *et al.* 2008b). For example, the L-band Phased Array type L-band Synthetic Aperture Radar (PALSAR) can achieve a spatial resolution of about 100 m and the Advanced Visible and Near Infrared Radiometer type-2 (AVNIR-2) has a spatial resolution of 10 m. On the other hand, the Soil Moisture and Ocean Salinity (SMOS) mission, provides data at around 40 km resolution globally. While this spatial resolution is suitable for some broad scale applications, it is not useful for small scale applications such as on-farm

water management, flood prediction or meso-scale climate and weather prediction (Walker and Panciera 2005). To use this passive microwave data for small scale applications, it is important to explore ways to disaggregate low-resolution passive radiometry data to a finer scale resolution which is more suitable for use in hydrologic studies and water management.

Despite the low spatial resolution of passive microwave data, the repeat cycle of SMOS is 3 days, while the current and planned radar observations have repeat cycles of about 30 days for high resolution products (eg. PALSAR has a repeat cycle of 46 days) and about 6 days with medium resolution products (eg. 1 km resolution for the C-band of the Advanced Synthetic Aperture Radar (ASAR) data) (Merlin *et al.* 2008b). For optical sensors, high resolution data are acquired sparsely with a 16 days repeat cycle for ASTER, and optical sensors at intermediate spatial resolution, such as the MODerate resolution Imaging Spectroradiometer (MODIS), which has a 1 km spatial resolution, provides global coverage every 1 to 2 days (Merlin *et al.* 2008b). With the high soil moisture sensitivity, but low spatial resolution of passive microwave data, and the high spatial resolution but low temporal resolution of optical/thermal data, the combination of these two sources of information needs to be explored to determine if reliable soil moisture data can be determined at an intermediate spatial resolution.

5.3.2.1 Related Research

Several downscaling approaches with different degrees of complexity have been developed. These approaches can be categorized into three groups:

i. **Methods that used topography, soil depth and other land surface parameter information**

   In the research carried out by Pellenq *et al.* (2003), a disaggregation scheme based on simulated values of topography and soil depth was developed. This scheme was based on the assumption that topography was the dominant source of heterogeneity in soil water dynamics and that soil depth was the dominant source of heterogeneity in soil water

storage capacity. The catchment scale of 0.06 km² was disaggregated to a Digital Elevation Model (DEM) scale of 20 m. The main goal of this research was not to retrieve the local soil moisture values at the fine scale, but rather to predict satisfactory patterns of soil moisture at a coarse scale of three to five DEM pixels. The results showed that, given the DEM resolution of 20m×20m, an adequate level of correlation between observed and predicted near-surface soil water content may be obtained by averaging point values over more than 100m×100m.

Kim and Barros (Kim and Barros 2002) performed empirical scaling analysis using the linkage between the spatial and temporal variability of soil moisture and ancillary data such as topography, vegetation water content and soil texture indices (e.g. sand and clay content). They found that the variance of soil moisture fields was multi-scaling consistent with the scaling of soil hydraulic properties (related to the percent of sand content) and vegetation cover while the multi-fractal behaviour was associated with the temporal evolution of soil moisture fields. From their findings, they developed an algorithm to downscale from 10 km to 0.825 km (Kim and Barros 2002) with field experimental data. The scaling functions were a linear combination of spatial distributions of the ancillary data.

Kaheil *et al.* (2008) developed a method to reconcile information from coarse resolution images with point measurements. This approach was applied and validated by downscaling images for two cases. In the first case, a synthetically generated random field was reproduced at fine scale. The downscaled data was shown to match the spatial properties of the true image with goodness-to-fit measure of $R^2 = 0.91$. In the second case, a soil moisture field from a field experiment was downscaled from a resolution of 800m×800m to a resolution of 50m×50m. The algorithm was claimed to preserve the coarse resolution image, i.e. the algorithm managed to "rebuild" the coarse image.

Schamschula *et al.*(2002) and Tsegaye *et al.*(2003) developed a disaggregation algorithm using a linear ANN consisting of only one neuron. The input and output mapping functions were linear. The data used to train and validate the ANN was generated using a hydrology model. The input of the ANN included: low resolution emissivity, antecedent rainfall, soil texture, vegetation water content and upstream contributing area. Downscaling was done from a resolution of 12.8 km to 0.8 km and the algorithm showed encouraging results. Outside of the wettest season, the RMSE values for the 1.6 and 12.8 km resolutions were between 3% v/v to 7% v/v. However, during and immediately following the rain period, RMSE was greater than 7% v/v and occasionally 8% v/v for the 1.6 km case, and above 12% for the 12.8 km case.

ii. Methods based on the combination of passive microwave data with high spatial resolution active microwave data or optical data such as surface temperature and vegetation index

Narayan *et al.* (2004) and Xiwu *et al.* (2006) used a combination of passive microwave data with high spatial resolution active microwave data for disaggregation purposes. In the study by Narayan *et al.* (2004), the Passive/Active L-band System (PALS) radiometer and radar data obtained during a field experiment were used to disaggregate from 400 m resolution to a resolution of 90 m and the results showed good spatial agreement between the spatial patterns of soil moisture. The basis for this downscaling method was the linear relationship developed by performing statistical regression between PALS radiometer observations and the *in situ* surface soil moisture (0–6 cm. depth).

Xiwu *et al.* (2006) investigated a Bayesian method, using the simulation of the Hydrosphere State (Hydros) satellite data, and successfully merged the 36 km radiometer brightness temperature

with 3 km radar backscatter data to retrieve soil moisture at 3 km and 9 km resolutions. They found that the Bayesian method performed better than direct inversion of either the brightness temperature or radar backscatter alone. The average RMSE of 3 km soil moisture retrieval using the Bayesian method was 2.8% v/v and 5.0% v/v at 9 km resolution.

In terms of disaggregation using passive microwave and optical data, Chauhan *et al.* (2003) developed a two-step algorithm by which soil moisture at low resolution (~25 km) was estimated using a passive microwave remote sensing technique. This was followed by relating the microwave-derived soil moisture to NDVI, surface albedo, and Land Surface Temperature (LST) through a regression relation. This technique was applied to data obtained from the Special Sensor Microwave Imager (SSM/I) and Advanced Very High Resolution Radiometer (AVHRR). The RMSE showed that the estimated soil moisture was approximately 5% v/v. Hemakumara *et al.* (2004) used the Water Deficit Index (WDI) and Vegetation Temperature Condition Index (VTCI) which are both surface wetness indices from AVHRR and MODIS imagery to downscale low resolution AMSR-E near-surface product from 25 km to 1 km resolution. Their results concluded that AMSR-E is capable of providing reasonable estimates of near surface soil moisture content when compared with point observation averages.

iii. Methods based on the combination of coarse-resolution passive microwave data, with fine-scale optical data and a surface process model

Merlin *et al.* (2005) used a disaggregation method which involved three models: a L band radiative transfer model to simulate the angular and bipolarized SMOS brightness temperature, the thermal infrared radiative transfer model to invert the radiometric soil

temperature from the surface temperature, and the land surface model to simulate the radiometric soil temperature under different surface conditions within the SMOS pixel. This physically based disaggregation methodology combined multi-angular brightness temperature at a coarse scale (~40 km) along with fine scale auxiliary data (1 km) to estimate soil moisture at a fine scale. The basis of this disaggregation strategy was the correlation between the inverse of the radiometric soil temperature from the thermal infrared, and the microwave soil moisture. This method was then tested on real data from AVHRR and ESTAR for a field experiment. The input data was the surface temperature and fractional vegetation cover derived from AVHRR and the output was the inverse of the soil moisture from ESTAR. The result of this disaggregation showed that the standard deviation between the soil moisture disaggregated and the inverse of the soil moisture from ESTAR was less than 4% v/v.

The potential use of satellite-based estimates of instantaneous evapotranspiration on clear-sky days for downscaling the coarse resolution passive microwave soil moisture was studied by Merlin *et al.* (2008a). This model used two different soil moisture indices: Evaporative Fraction (EF) and Actual Evaporative Fraction (AEF). A land surface model was used to account for the heterogeneity of vegetation cover, soil type and atmospheric conditions. L-band airborne brightness temperatures obtained during a field experiment was first aggregated to a low resolution of ~500 m which was then disaggregated to 180 m. In their study, the authors suggested that although ground-based soil moisture indexes were used, these could be replaced with high resolution optical data such as that from NOAA/AVHRR and MODIS. The overall accuracy in the downscaled values was evaluated to be 3% v/v for EF and 2% v/v for AEF under cloud-free conditions.

5.3. Discussion on the Related Research

5.3.1 Scale-To-Scale Prediction

The most common ANN that has been used for soil moisture retrieval is the feedforward ANN with the backpropagation learning algorithm. This has been widely investigated for inversion modeling to obtain soil moisture information from the brightness temperature data. All the research considered in this chapter used either simulated or field based measurement data. The SMOS mission is the first ever satellite providing such data. However, as the satellite was recently launched, the data available is still limited. Hence, model simulations have been widely used for the verification of passive microwave systems for soil moisture retrieval, with the aim of developing methods for processing satellite data when it becomes available. Although model simulations show very encouraging results, the models present well-defined relationships between soil moisture and brightness temperature that may not be valid. On the other hand, field measurements typically obtained from ground-based radiometers are more representative of the true model, but are less representative of spatial resolution when compared to the proposed satellite systems. Hence, much care is needed when deciding on the best approach for the prediction of the performance of such satellite systems for soil moisture retrieval.

Shou-Fang *et al.* (2002) argued that there is no requirement to consider ancillary information of the complex surface parameters, such as vegetation biomass, surface temperature, and surface roughness, to aid in the retrieval of soil moisture from the brightness temperature. However, other researchers (Atluri *et al.* 1999; Angiuli *et al.* 2008) investigated ancillary information for input to an ANN together with the brightness temperature with the objective of improving the performance. The effect of the ancillary data in improving the soil moisture retrieval using ANN models should be further analyzed. A further research issue is the choice of the best architecture to use for the ANN.

ANNs require an initial training period to establish the weights of each neuron. Moreover, the number of data for training must be large enough in order for the ANNs to learn to map well the function between the inputs and outputs. To overcome the usual problem of data shortage for training, and to make sure the data used for training is representative of the testing data, there are basically two options: (i) sub-divide the available data into training and testing data, and (ii) simulate data using electromagnetic models to cover as much as possible the real-life conditions of the target. The use of option (i) was utilized by Yuei-An *et al.* (2001) and Shou-Fang *et al.* (2002) as discussed in **Section 5.3.1**. However, the weakness of this method is that the testing data is part of the data used for the training of the ANN. This is not practical for real-life problems, especially for soil moisture retrieval application as the retrieval is generally needed on an unknown future date. Consequently, method (ii) is a better option whereby data can be simulated to cover a variety of conditions, but a lot of ancillary data are needed for the simulation process.

The ANN used in most of the reported papers is trained and tested using data from specific geographic regions for specific times or dates. In this aspect, the ANN is calibrated for this problem domain for a specific time and place. Ideally the ANN should generalize across the spatial locations and for different times of the year so that it does not have to be re-trained for each set of measurements.

The potential of ANN applications within the context of ESA's SMOS mission (Wigneron *et al.* 2000) over land has been studied by Angiuli *et al.* (2008). Their results were claimed to be in accordance with the result obtained when an optimal estimation approach was applied. Moreover, their work also found that the neural network tends to "memorize" the pattern during the training, i.e. overtraining where the ANN does very well using the training data, but the prediction is poor on unseen data. In another words, the ANN does not generalize well. The mapping between the reference and predicted soil moisture was graphed and shown to be very

poor although the correlation coefficients were not being reported. The weakness of the neural network, i.e. being only able to retrieve soil moisture of the same pattern as the training data, will be the main challenge for this approach to be applied successfully in practice.

5.3.2 Spatial Downscaling

The review on spatial downscaling of soil moisture (**Section 5.3.2**) clearly showed that to fully utilize future satellite missions, the use of high resolution data from other sensors is needed. Category i. of **Section 5.3.2.1**, which used topography, soil depth, and other land surface parameter information were methods that used mainly ground-based parameters together with low resolution passive microwave data for downscaling purposes. The other two categories utilized high resolution data from either active microwave and/or optical data and ground measured parameters, by applying either statistical or deterministic methods. For statistical methods, regression (Narayan *et al.* 2004) and Bayesian (Chauhan *et al.* 2003; Xiwu *et al.* 2006) approaches were used. These approaches demonstrated that less ancillary data were needed compared with the deterministic methods and the downscaling can be done with the combination of passive microwave data and data from either high resolution active microwave or optical data. The deterministic method developed by Merlin *et al.* (2005; 2008a) utilized data from optical sensors and land surface model. For this type of approach, a larger number of surface parameters are required.

For the problem of soil moisture retrieval, ancillary data usually consist of surface parameters that can provide valuable information. To obtain this information, field experiments need to be conducted. However, capturing these data over large areas may not be practical. To overcome this issue, a statistical method is preferred. In the regression method, the slope of the linear law is not exactly constant from one watershed to another as the land regions associated with each watershed can be different. Therefore, calibration is needed each time this method is applied. The Bayesian method,

on the other hand, requires prior probability distributions, which are estimated from the training data sets. These are then used to find posterior probabilities using Bayes' method.

Compared to these statistical methods, ANNs have the advantage of being able to identify and accommodate subtle and non-linear patterns, which is not always the case for traditional statistical methods such as for Bayes' method. In addition to this, ANNs do not require normally distributed continuous data and may be used to integrate data from different sources with poorly defined or unknown contributions (Notarnicola *et al.* 2008).

5.4 General Methodology

This research study will look into developing a method to optimize a backpropagation ANN to predict soil moisture across geographic space and time within an area of 40 km×40 km for both scale-to-scale and downscaling issues (see **Section 1.4** and **Figure 1.1**). The desired target error for this research is ≤ 4%v/v, following the SMOS mission. The upper bound of the RMSE value will therefore be 4% v/v.

5.4.1 Scale-To-Scale Soil Moisture Prediction

The scale-to-scale soil moisture prediction will predict 1 km resolution soil moisure values from 1 km input data. **Figure 5.4** shows the overall of the scale-scale soil moisture prediction process. For this problem, the inputs used include the dual-polarized brightness temperatures data, i.e. TbH and TbV, the Normalized Difference Vegetation Index (NDVI) and Land Surface Temperature (LST) from MODIS (**Figure 5.4**). The combination of these inputs will undergo an input parameters selection process to determine the optimum combination of inputs for the soil moisture prediction purpose.

The brightness temperature data will undergo preprocessing to correct the data to an incidence angle of 38^{o} (**Figure 5..4**). As the MODIS

NDVI data were calculated from band 1 (red) and band 2 (near-infrared) at 250 m resolution, the NDVI data will be resampled to 1 km resolution (see **Section 1.3**). A number of studies (Sandholt *et al.* 2002; Carlson 2007; Nemani *et al.* 1993) have suggested that the combined information from land surface temperature (LST) and NDVI can provide better information on vegetation stress and moisture conditions at the surface. Moreover, research by Hossain and Easson (2008) showed it is possible to retrieve quantitative soil moisture by combining the universal triangle model (Carlson *et al.* 1994) of NDVI and LST from MODIS with reference soil moisture data from AMSR-E. Therefore in this study, only NDVI and LST are considered. The pre-processing of these data is discussed in **Chapter 6 Section 6.1**.

After the parameter selection process, the optimum combinations of inputs will be used in the ANN for soil moisture prediction. Preliminary experiments using the standard backpropagation neural network will be first carried out. The retrieval accuracy achieve from the prelimanary experiments show that the standard backpropagation ANN model fails to achieve the SMOS mission of ≤ 4%v/v accuracy (see **Section 7.1**). This leads to the development of the proposed solution. An optimization model is developed for the ANN model. The optimization model developed in this research study solves the spatial and temporal issues of the soil moisture prediction problem. The predicted soil moisture values are then compared with the 1-km soil moisture product from the NAFE'05 data in order to calculate the retrieval accuracy. .

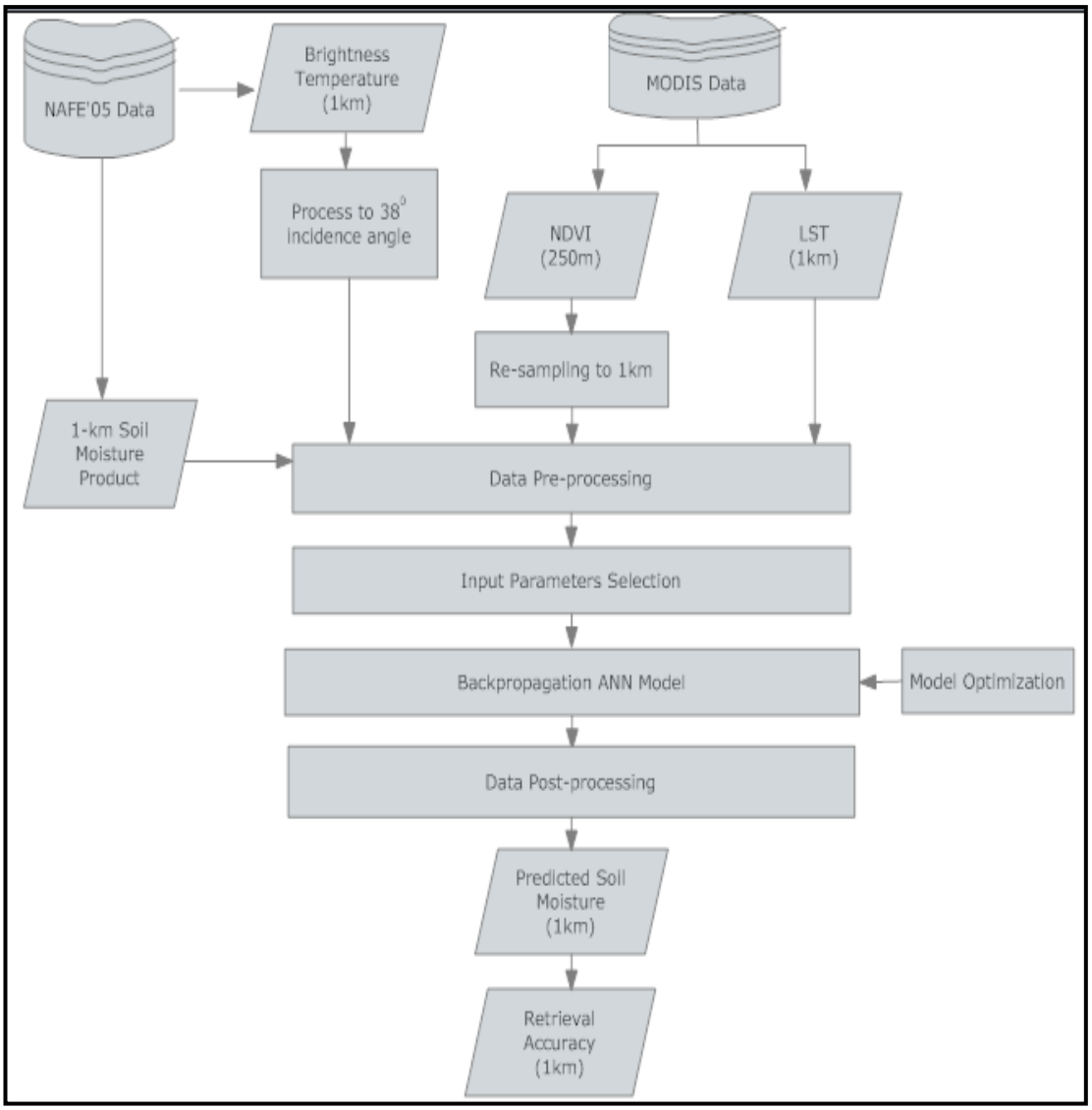

Figure 5.4 General processes involve in the scale-to-scale prediction.

5.4.2 Downscaling of Soil Moisture

For the issue of downscaling, the ANN model will predict soil moisture values at 1 km resolution (see **Section 1.3**) from a coarse resolution of 20 km (see **Section 8.3.1**). The model developed by Merlin *et al.* (2008b) is adapted to be used with the ANN model in this research. The processes carried out for the downscaling approach in this study is shown in **Figure 5.5**. Using this model, a few indices will need to be calculated from the MODIS data, mainly using the information from NDVI and LST data. These indices include the vegetation fraction cover, skin surface temperature, characteristic

volume fraction and the soil evaporative efficiency (see **Section 8.2.1**). The relationships of these parameters form the downscaling relationship by Merlin *et al.* (2008b). The use of the appropriate parameters for the ANN model for downscaling purpose is discussed in **Section 8.3**. The 1-km soil moisture product will be aggregated to 20 km resolution. This information, together with the indices calculated using the NDVI and LST from Merlin *et al.* (2008b) model, will be used in the backpropagation ANN model. The ANN model will be optimized using the methodology developed in this research study to improve the prediction results. The predicted soil moisture values at 1 km resolution will be compared with the 1-km soil moisture products from NAFE'05 data to calculate the retrieval accuracy.

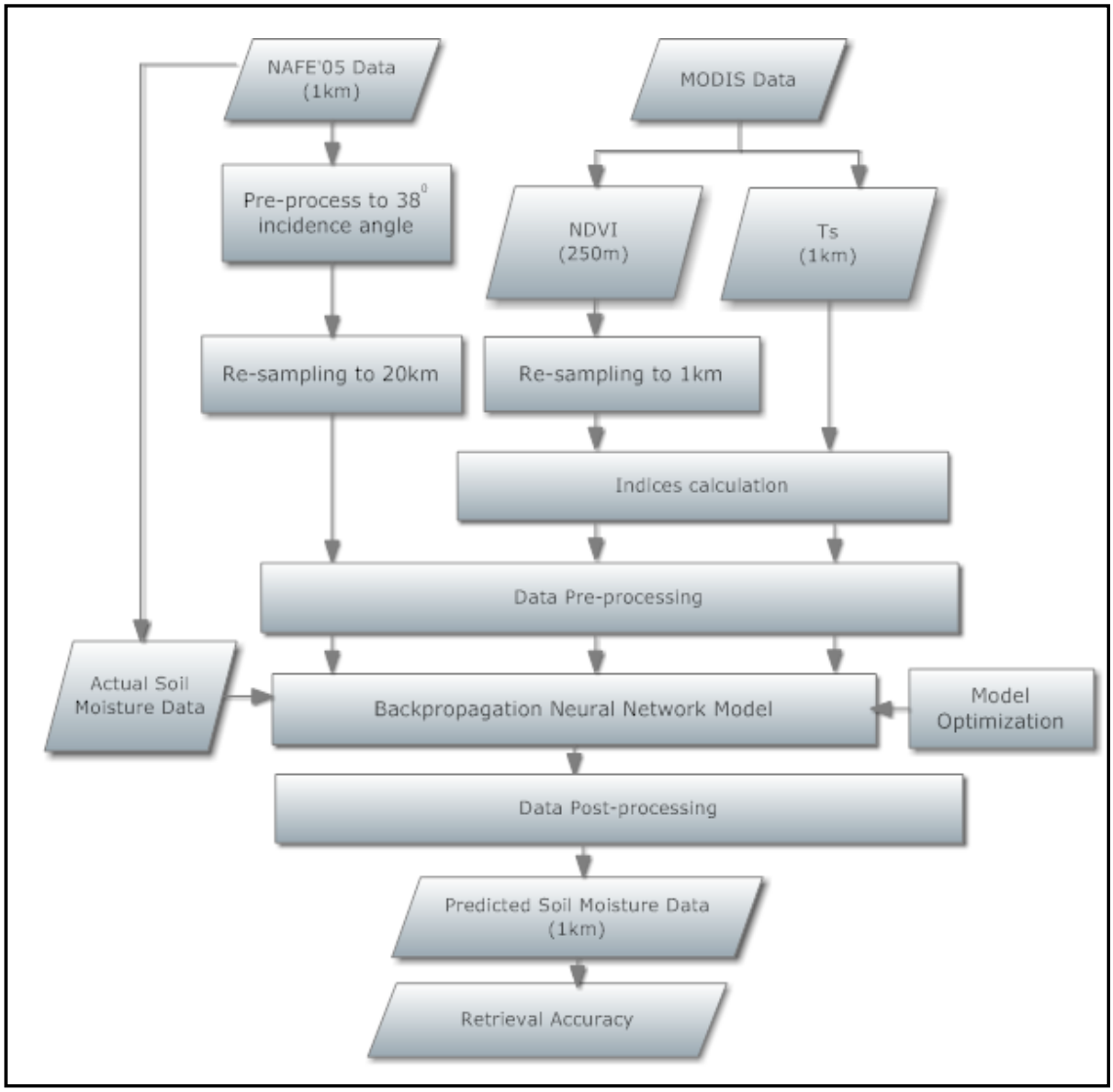

Figure 5.5. Overview of the downscaling process.

5.5 Chapter Summary

This chapter gave an analysis of the work that has been done on passive microwave soil moisture retrieval using ANN models. The review of the scale-to-scale soil moisture retrieval was categorized into either single or multiple parameter retrieval. For both of these categories, the inputs for the ANN model are either the dual-polarized brightness temperature or the brightness temperature together with ancillary information. Therefore, there is a need to verify the need for ancillary information. For supervised learning, the ANN needs to provide with adequate data for training. Data is either simulated from electromagnetic model or by dividing the training data into training and testing set. Moreover, the ANN used in most of the reported papers is trained and tested using data from specific geographic regions for specific times or dates. In addition to this, the ANN model has not been considered for the downscaling problem. Thus, the practicality of the ANN model developed using this practice is questionable.

The general methodology of this research study is divided into scale-to-scale and downscaling problems. The overall processes for each of these problems were introduced. The pre-processing process and analysis of the data being used in the methodology is presented in the next chapter, **Chapter 6: Data Pre-processing and Analysis**. Details of the developed methodology in optimizing the backpropagation ANN model used for both scale-to-scale and downscaling of soil moisture are presented in **Chapter 7: Scale-to-scale Soil Moisture Prediction** and **Chapter 8: Spatial Downscaling of Soil Moisture**.

Chapter 6

Data Pre-processing and Analysis

This chapter presents the data analysis and pre-processing steps in preparing the data for the experiments described in the following chapters. The pre-processing steps will process the raw data obtained from the NAFE'05 field experiment (**Chapter 4**). The analysis of the data obtained from this field experiment is useful to show the properties of the data.

6.1 Airborne Data

During the NAFE'05, the regional airborne observations were undertaken at 1 km nominal resolution over the entire study area on October 31st, November 7th, 14th and 21st 2005 (see **Section 4.4**). The data on October 31st were omitted from this research due to imperfections in the data acquisition that occurred partly because it was the first day of data acquisition. Hence, to maintain consistency, only data from the later three dates were used. The 40 km long, north-south oriented flight lines were flown at 10,000 ft between approximately 7.00 A.M. and 9.30 A.M. This time window was chosen as it is close to the SMOS overpass time (6.00 A.M.) and therefore will give measurements that will closely correspond to those that are planned to be acquired from this satellite. The radiometer was flown in 'pushbroom' configuration, yielding the following six across track observations at each aircraft location: brightness temperature (Tb) at H- and V-polarization at incidence angles ±7°, ±21.5° and ±38.5°. The PLMR data used in this thesis were already geo-referenced at H and V polarizations and internally calibrated (Panciera *et al.* 2006).

In order to effectively use pushbroom radiometer data for soil moisture mapping, it is desirable to account for the effects of varying beam

angles through a normalization procedure and for the effects of varying soil temperature during the acquisition (Panciera 2009). Over a homogeneous bare soil target, it is well-known that the measured Tb is affected by the viewing angle (Schmugge *et al.* 1992). This angular variation can be described by the Fresnel equations. Previous studies (Schmugge *et al.* 1992; Jackson *et al.* 1995a; Jackson *et al.* 1999) showed that a normalization procedure can be realised for mixed land covers. This procedure normalizes the data into an equivalent angle of choice, by assuming that the deviation between beam positions is due to the Fresnel effect and calibration errors for the individual beam positions, and that for a given day, the Fresnel effect for a particular beam is assumed constant for the range of soil moisture and vegetation present. There are some circumstances in which using a limited data set for this correction, say a single flight line, can lead to errors. This can occur when there is an anomaly in a particular beam that is not present in the others (such as a small water body). From the previous studies mentioned above, it was shown that by using a daily average for all data in an area, potential errors due to anomalies would be minimized. The normalization is applied as follows and summarized in **Figure 6.1**. First, the daily average Tb over the land target is computed for each beam. Next, a correction factor is computed by taking the ratio between the averages of each beam to the average of the reference beam. All the data for each beam on each day are then corrected using the following correction factor:

$$Tb_i^N = Tb_i \times \left(\overline{Tb_i} \Big/ \overline{Tb_{ref}} \right) \tag{6.1}$$

where Tb_i is the individual Tb value to be normalized, Tb_i^N is the normalized value, and $\overline{Tb_i}$ and $\overline{Tb_{ref}}$ are the daily averages of the Tb values of the beam to be normalized and the beam taken as the reference beam, respectively.

The reference beam was the radiometer's outermost beams ($\pm 38.5^0$). This choice of angle was motivated by the fact that at close-to-nadir incidence angles, H and V polarized Tb values are very similar, while at off nadir, the

V polarized Tb data at higher incidence angles have values generally higher than the H polarized values (the amount of difference varies depending on the land surface conditions). The polarization difference yields information about the polarizing effect of the vegetation canopy when using a wider incidence angle (Wigneron *et al.* 2000). With the NAFE'05 data, experiments were carried out by Panciera (2009) using multi-angle Tb observations to study the normalization procedure. The results obtained showed that there was an excellent agreement between normalized and observed Tb values with Root Mean Square Errors (RMSE) of less than 1.5 K in all cases. The experiments showed that the normalization procedures adopted can be used to produce Tb maps at a constant reference angle from pushbroom radiometer data, under the assumption that for a given day the Fresnel effect for a particular beam is constant for the range of soil moisture and vegetation conditions present (Panciera 2009).

The normalized Tb is gridded into a reference grid with uniform resolution. After averaging several individual Tb acquisitions into one Tb value for each cell in the grid, anomalies in individual readings and the signal noise are reduced. To determine if there was a good representation of pixel values across the various resolutions i.e. that specific resolutions did not produce any artifacts, a pixel-by-pixel comparison between the averaged high resolution Tb observations (sampled at 62.5m) and the individual low resolution Tb observations (sampled at 1 km) collected over the entire area was carried out by Panciera *et al.* (2006) for the NAFE'05 data. In their experiments, the Tb values for each pixel at each resolution (250 m, 500 m and 1000 m) were compared with the Tb values observed at higher resolutions (62.5 m, 250 m, 500 m) aggregated within each grid.

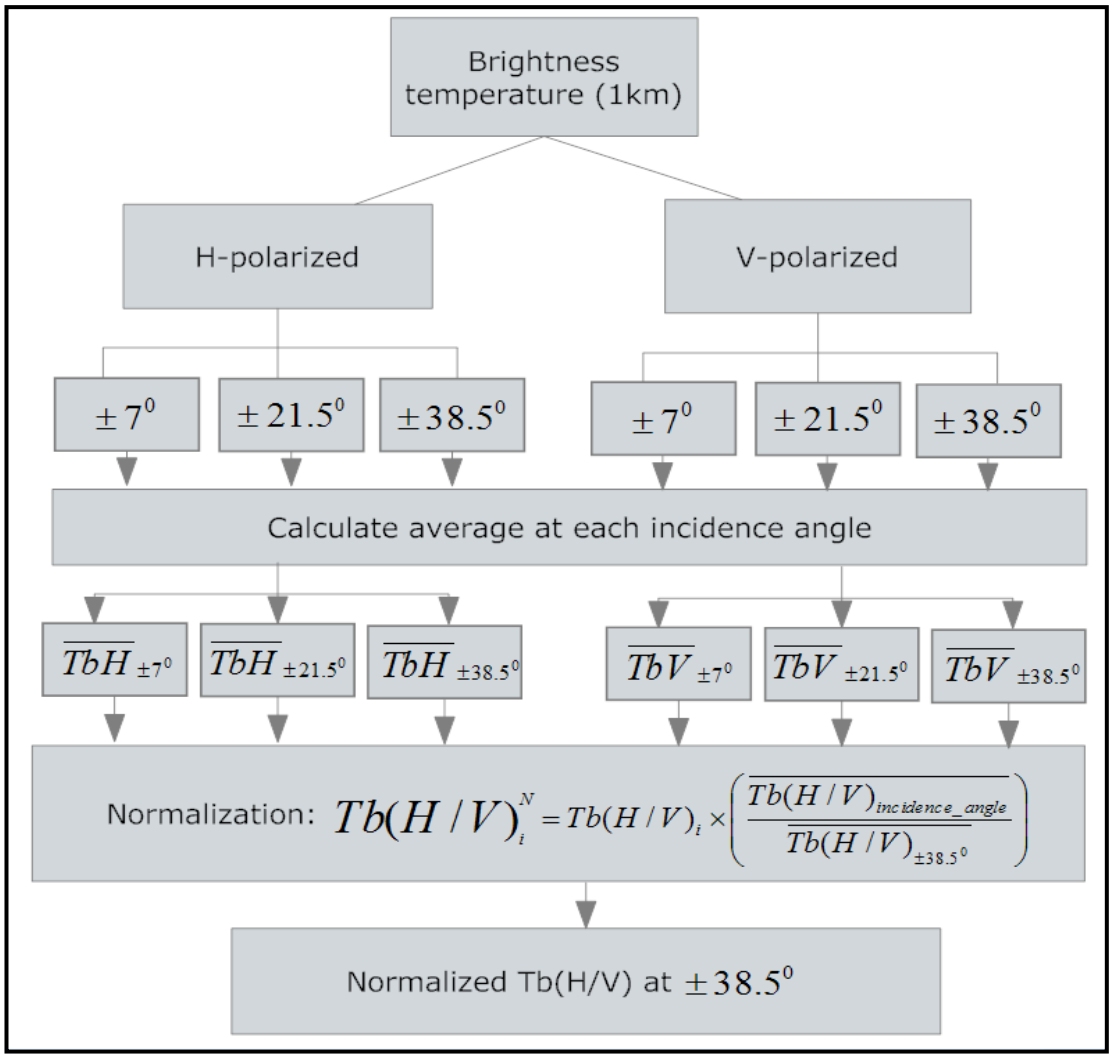

Figure 6.1. Normalization of the brightness temperature data to the reference incidence angle of ±38.5°.

For example, measurements at 62.5 m resolution were aggregated to 250 m resolution and compared with the corresponding single measurement at 250 m resolution. The comparison showed excellent correlation between the Tb values observed and the aggregated values for each pixel at all resolutions. The results indicated a linear scaling characteristic of passive microwave signatures across most land surface conditions for NAFE'05 data (Panciera *et al.* 2006).

Figure 6.2 shows the aggregated normalized brightness temperature for H polarized data for Nov 7th, 14th and 21st.

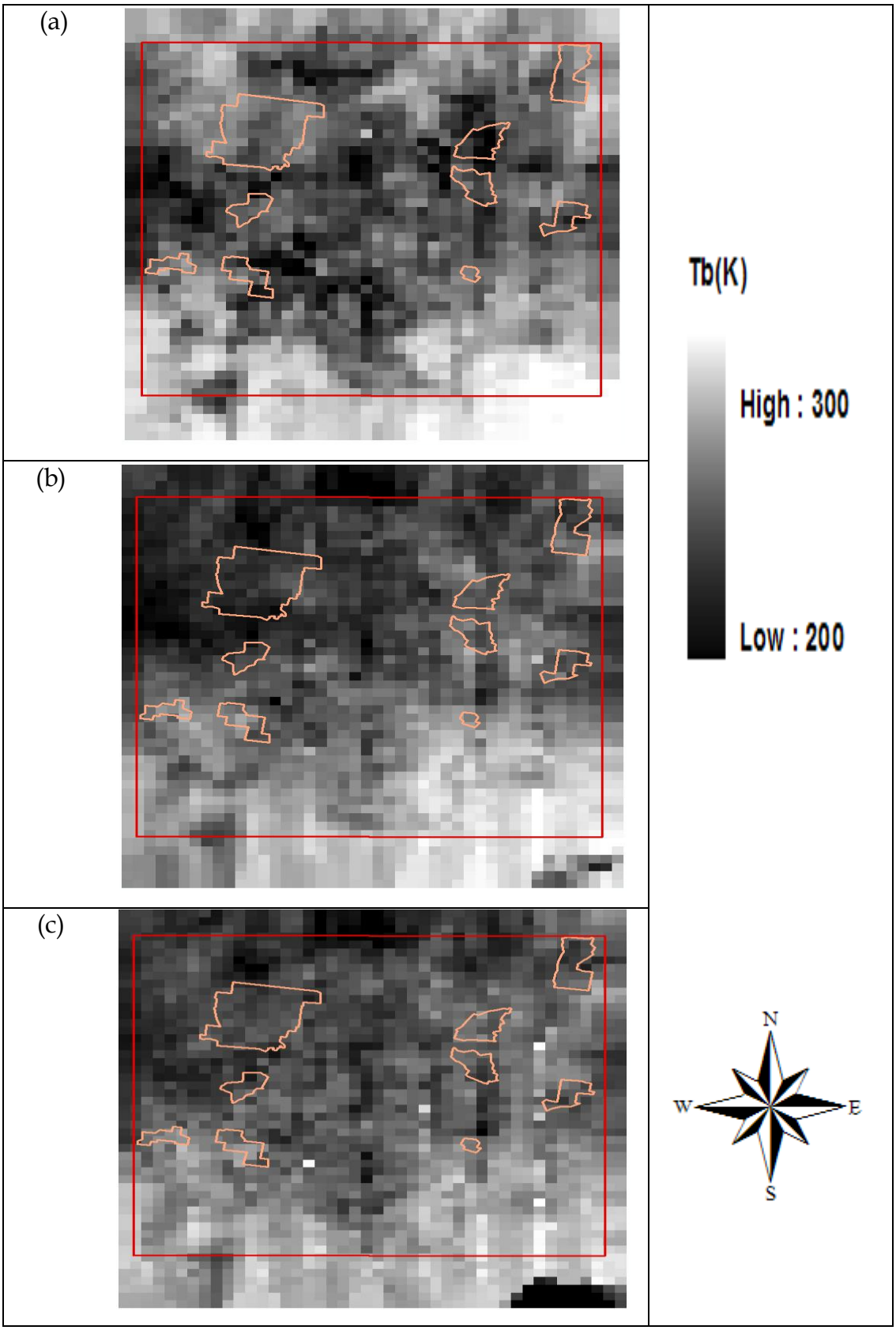

Figure 6.2. Normalized H-polarized brightness temperature for (a) November 7th, (b) November 14th , and (c) November 21st at 1 km resolution. The boundaries for the focus farms are shown in orange while the boundary for the study area is shown in red.

6.2 1-km Soil Moisture Data

The 1-km soil moisture data described in **Chapter 4** (section **4.5**) are shown in **Figure 6.3**. The retrieved soil moisture shows interesting spatio-temporal dynamics that reflects the rainfall regime experienced by the area during the field experiments. The high soil moisture values for November 7th were due to the heavy rainstorms that crossed the study area at the beginning of the experiment (20 mm over October 30th and 31st), followed by more intense rainfall on November 5th (21 mm). The period between November 5th and 23rd was characterized by little or no rainfall and accordingly drier soil moisture conditions were retrieved for November 14th and the 21st.

The spatial distribution of the retrieved soil moisture across the study area shows a significant association with land cover and soil texture. In particular, the large forested area in the southern part of the study area exhibited drier conditions than the rest, while the cropped areas, more dense in the western part of the study area, maintained wet conditions throughout the month.

The large native grass areas that cover the greatest fraction of the study area exhibited highly variable patterns where the influence of soil texture and some influence of topography can be identified. This is illustrated by comparing **Figure 6.4** to the soil moisture of **Figure 6.3**. During the drydown period between November 14th and the 21st, the southern part of the study area, which is characterized by a low, flat plateau with sandstone derived soils, dried more quickly than the northern part, which is characterized by steeper hills and black clay soils. This could be due to the higher water retention properties of the clay with respect to sandy soils, as well as surface shading effects due to topographic aspects in the northern part, reducing evaporation.

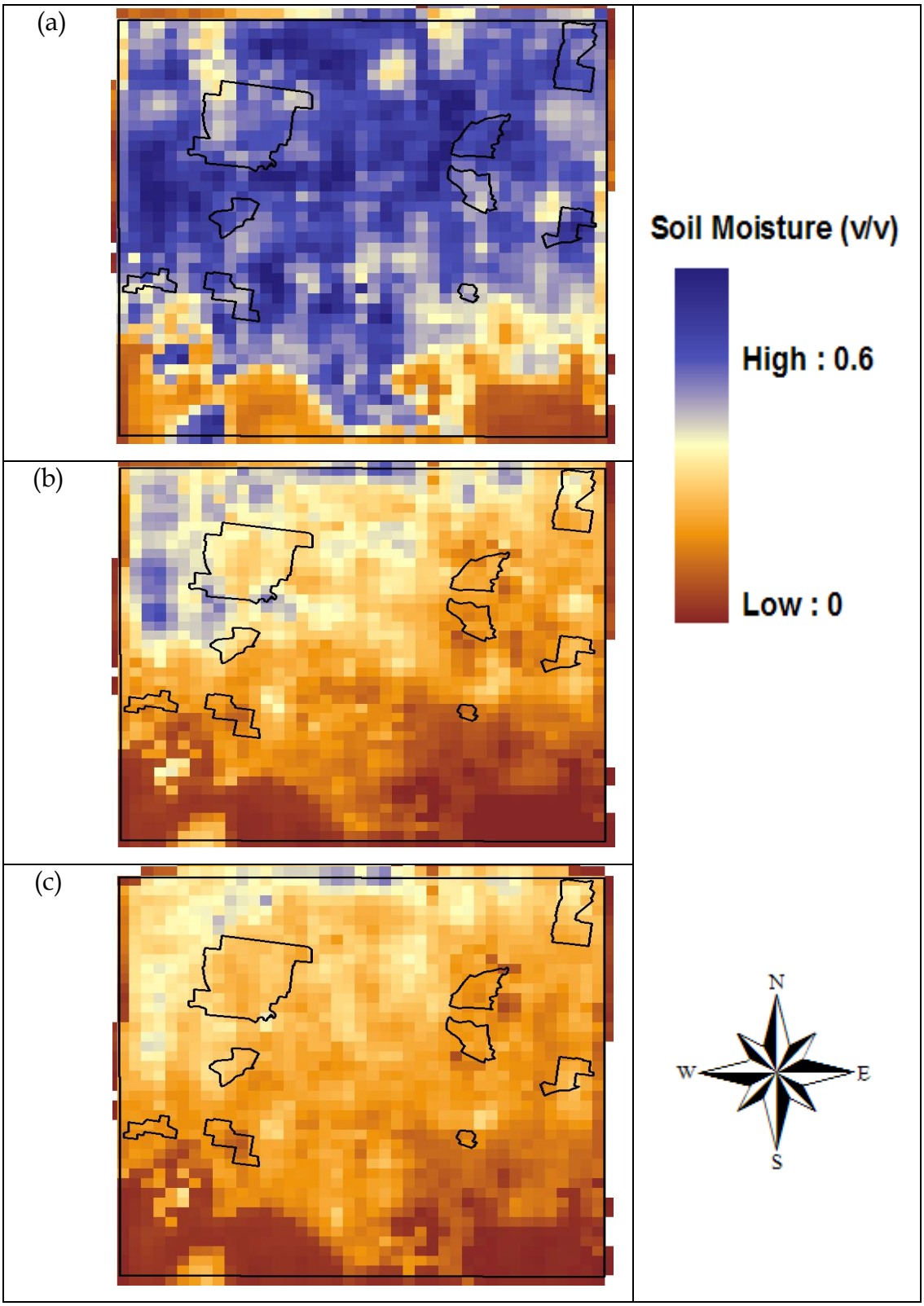

Figure 6.3. L-MEB retrieved soil moisture from regional airborne observations (1 km) on (a) 7th Nov, (b) 14th Nov and (c) 21st Nov 2005. The boundaries of the focus farms and the whole study area are shown as polygons.

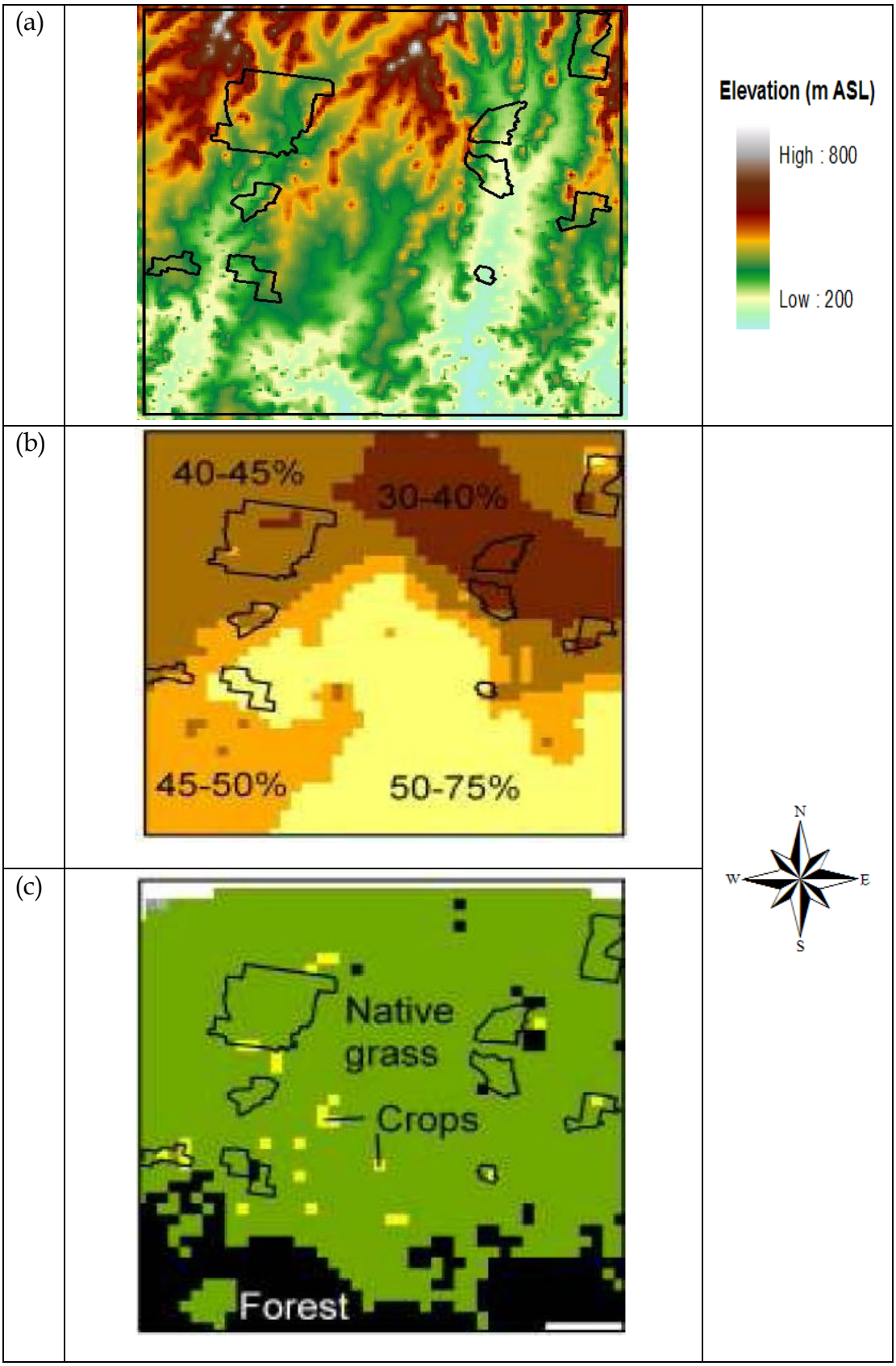

Figure 6.4. Spatial distribution across the study area: (a) terrain elevation map, (b) sand content, and (c) Landsat land cover map (Panciera 2009). The boundaries of the focus farms and the whole study area are shown as polygons.

6.3 Statistical Properties

The statistics of the L-MEB derived soil moisture data and for the Tb observations are shown in **Table 6.1** for each date when data acquisition occurred.

Table 6.1. Statistics of the regional L-MEB soil moisture product at 1 km resolution together with the brightness temperature at H and V polarized (TbH and TbV) and the amount of rain. For each date, the mean and standard deviation values are shown.

Date	TbH (K)	TbV (K)	Soil Moisture (v/v)	Rain (mm)
7th Nov	241.5±10.1	261.4±7.8	0.39±0.12	21.3 two days previously
14th Nov	266.0±6.5	279.3±5.4	0.17±0.10	4.1 five days previously
21st Nov	271.3±3.9	282.6±3.1	0.16±0.08	0

From Table 6.1, it is seen that the average soil moisture decreased from 39% v/v (7th Nov) to 16%v/v (21st Nov), with the soil moisture standard deviation across the 40km×40km study area decreasing from 12% v/v in wet conditions to 8% v/v in dry conditions. The average brightness temperature values show increment for both H and V-polarization. The wet to dry condition was the result of the amount of rain fell on the study area during the field experiment. It is seen that the amount of rain was getting less. This dataset is therefore representative as it covers the full soil moisture range to be considered, i.e. the dry and wet conditions.

6.4 Chapter Summary

This chapter covered the analysis and pre-processing that were carried out on the NAFE'05 dataset for the use of the methodology in this thesis. The L-MEB soil moisture product (**Section 4.5**) has the advantage of overcoming the limitations of the point measurements and limited extent achievable with traditional ground sampling methods. The L-MEB soil moisture product used in this research is representative of the soil moisture obtained from SMOS as the core component of SMOS soil moisture retrieval algorithm is the model which simulates the microwave emission at L-band from the soil–vegetation layer (Panciera *et al.* 2009). The data used in this thesis is representative as it covers the full soil moisture range from wet to dry conditions. From the review in **Section 5.3.1** and the analysis in **Section 5.3.3.1**, the practicality of ANN for soil moisture retrieval is that it can only predict soil moisture that is in the range of the training data. In this research study, a model is needed to solve this issue as predictions for a different date from that date when the training data was obtained will be used. Moreover, for coverage of an area of 40km×40km, the developed ANN methodology should be able to cope with the spatial variability of the soil moisture values. This methodology will need to solve both the scale-to-scale and downscaling of soil moisture problems. In the next two chapters (**Chapter 7** and **Chapter 8**), the methodology developed to solve these issues is presented.

Chapter 7

Scale-to-scale Soil Moisture Prediction

This chapter presents a methodology developed to optimize the most widely used backpropagation Artificial Neural Network (ANN) model to capture the spatial and temporal variability of soil moisture. Preliminary results on the experiments using high resolution data with the standard Backpropagation ANN are first presented. High resolution data is tackled first because they will give an upper bound on the results. It would be expected that lower resolution data will produce worse results. The preliminary results show that the standard ANN model is not able to achieve the desired 4%v/v of Root Mean Square Error (RMSE). Therefore, a methodology is developed to improve the accuracy of the retrieval of the standard ANN model. A discussion on the strengths and limitations of this model optimization methodology is presented at the end of the chapter.

7.1 Standard Backpropagation ANN model: Preliminary Results

In this section, the standard backpropagation neural network algorithm is used for soil moisture retrieval. The objective of the preliminary testing is to assess the ability of the standard backpropagation neural network algorithm on soil moisture retrieval. The effects of different variations of the standard backpropagation neural network model and the combination of different inputs are assessed.

The NAFE'05 data has different resolutions. However, as high resolution data (250m and 500m) consists of higher detailed information of the soil surface, they were chosen for testing. With such high resolution data,

the accuracy of the soil moisture retrieval will be higher compared to low resolution data.

7.1.1 Backpropagation Training Algorithms

As discussed in **Section 1.2**, there is a need to evaluate the impacts of the different variations of backpropagation algorithms to improve soil moisture predictions using ANNs. Soil moisture was retrieved at eight focus farms in the NAFE study area, corresponding to high resolution ground sampling sites that were intensively monitored for the top 5 cm soil moisture, soil temperature, surface roughness, soil texture, vegetation biomass and vegetation water content (refer to **Section 4.3)**. The Roscommon site was considered as the "control" site as it exhibits uniform, flat and short grass conditions. All other sites were characterized by either heterogeneous land cover (Midlothian, Cullingral, Illogan and Pembroke) or significant topography (Stanley, Dales and Merriwa Park) (Panciera *et al.* 2009). As there was little variability across the Roscommon farm, soil moisture is the dominant effect on the received passive microwave signal. Therefore, for the purpose of analysing the impacts of different variations of backpropagation algorithms, Roscommon was selected. As discussed in **Section 1.2**, there were different variations on the basic backpropagation algorithm. The major problem of the basic backpropagation neural network is its slow rate of convergence. The slow convergence rate prompted many proposed variations to the original backpropagation learning technique to address this problem. The effect of these different variations of the basic backpropagation neural network on soil moisture retrieval is the main objective of the testing in this section.

The information on the soil surface is more detailed at higher resolutions. Therefore, the airborne data at 250 m resolution is utilized for this section.

The inputs of the backpropagation ANN model are the H and V polarized brightness temperature values while the output is the volumetric soil moisture data. As the Roscommon farm exhibits uniform, flat and short grass conditions, the dominant effect on the brightness temperature is the soil moisture values. Therefore, only the dual-polarized brightness temperature values are used as the inputs for the neural network model. As H-polarization has a higher sensitivity to soil moisture, the Roscommon data were first divided into three different classes: low, medium and high, according to the maximum and minimum values of the TbH data. The corresponding TbV data were also grouped. As Roscommon is flat, uniform with low vegetation, the soil moisture variations for nearer locations were similar compared to data for further locations. Therefore, the data division method ensured that the final data are distributed throughout the spatial location and are not gathered only for a certain TbH range. For each of the classes, the data were manually sampled in a stratified manner into 60% for training, 30% for validation and 10% for testing the trained network. For example, the 60% training set consisted of the same number of samples from the high, medium and low classes and distributed across the site. There is no hard and fast rule on the proportions used for data partition, but more data should be allocated to training. A general schematic of the division of the data is shown in **Figure 7.1**. The training, validation and testing set each contain values from the low, medium and high classes.

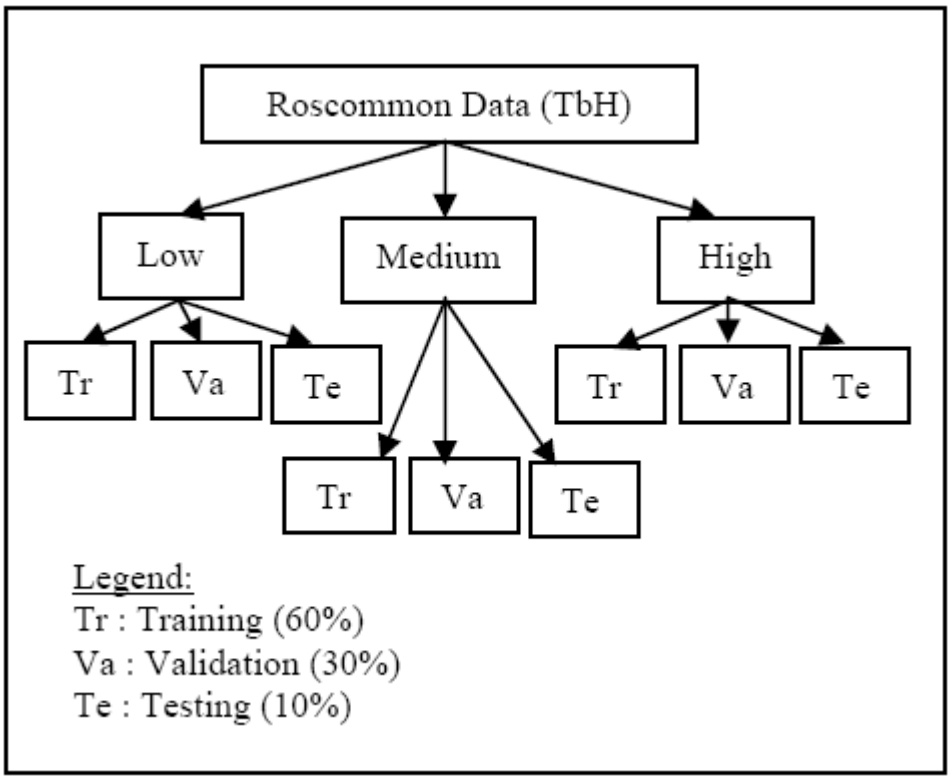

Figure 7.1. Schematic diagram shows the partition of the H polarized brightness temperature (TbH) for the Roscommon area. The corresponding V polarized brightness temperatures and the ground sampling volumetric soil moisture data are obtained together with the TbH data.

During the training and validation processes, 10-fold cross validation was carried out whereby the training and validation sets were combined. In 10-fold cross validation, the data were partitioned randomly into 10 partitions. During each run of the training process, a section of the 10 partitions was used for validation while the remaining 9 partitions of data were used for training. As the variations of the backpropagation neural network were developed based on the basic gradient descent algorithm, therefore, the network was trained and validated using a basic ANN that used backpropagation with gradient descent. The bias, layer weights and output weights of the network were obtained where it produced the lowest RMSE for both the training and validation data sets. These bias, layer, and output weights were then used for initialising the training, validation, and testing of the other backpropagation training algorithms using MATLAB. With these

bias, layer weights, and output weights, the ANN starts from a good configuration for the testing of the variations of the backpropagation algorithm.

As the inputs of the network consist of only two inputs, only a single hidden layer neural network is considered. Before running the experiment using different variations of backpropagation training algorithms, the optimum number of hidden neurons in the single hidden layer was first examined. With the standard gradient descent algorithm, the neural network was trained and validated using a number of hidden neurons starting from 1, in steps of 1. The results obtained when these networks were tested with the testing data are shown in **Figure 7.2**. It can be seen that the RMSE values increased for 5 hidden neurons and increased for 6 hidden neurons. Therefore, the training and validation were stopped at 6 hidden neurons. From **Figure 7.2**, it can be concluded that the optimum number of hidden neurons was four.

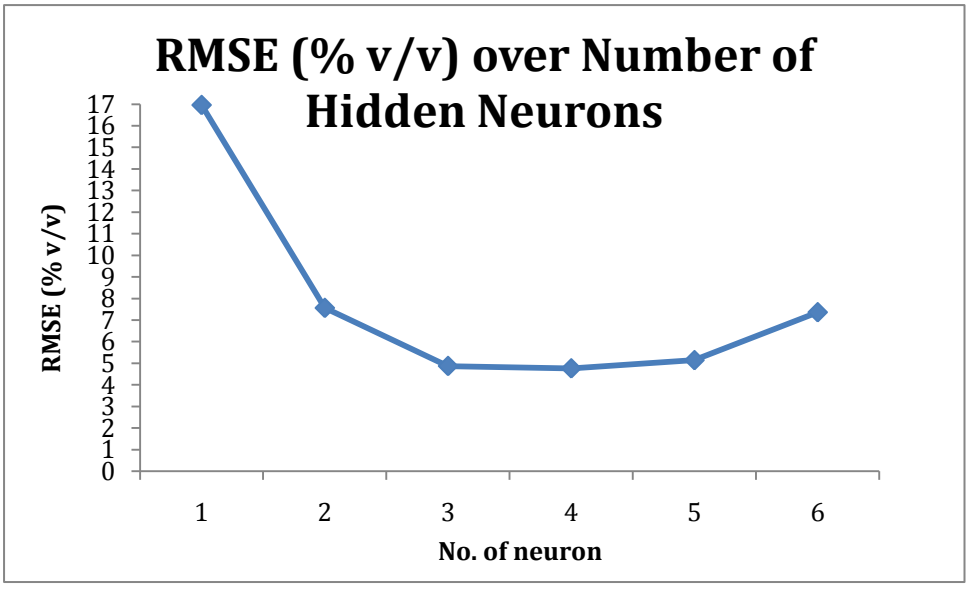

Figure 7.2. Experiment for selecting the optimum number of hidden neurons in the ANN model.

With two inputs (TbH and TbV), a single hidden layer of 4 neurons and one output, the ANN was tested with different variations of

backpropagation training algorithms. **Table 7.1** shows the results of each of the backpropagation training algorithms.

Table 7.1. RMSE of soil moisture retrieval of various backpropagation training algorithms.

No.	Backpropagation Algorithm	RMSE (%v/v)
1.	Batch Gradient with Momentum	4.86
2.	Gradient Descent with Adaptive Learning Rate	5.34
3.	Gradient descent with momentum and adaptive learning rate	4.88
4.	Resilient backpropagation	4.93
5.	Conjugate gradient backpropagation with Fletcher-Reeves updates	4.82
6.	Conjugate gradient backpropagation with Polak-Ribiére updates	4.83
7.	Conjugate gradient backpropagation with Powell-Beale restarts	4.83
8.	Scaled conjugate gradient backpropagation	5.77
9.	Quasi-Newton Algorithm : BFGS	3.93
10.	Quasi-Newton Algorithm :One step Secant Algorithm	5.51
11.	Levenberg-Marquardt	4.04

Results obtained are between the ranges of 3.93% to 5.77% of RMSE for soil moisture prediction using 11 different backpropagation ANN training algorithms. The globally accepted accuracy of soil moisture is less than or equal to 4% v/v of error. With the same backpropagation ANN architecture, it is seen that the Broyden, Fletcher, Goldfarb, and Shanno (BFGS) Quasi-Newton algorithm manages to retrieve soil moisture most accurately while the scaled-conjugate algorithm obtains the lowest soil moisture prediction accuracy using the same architecture of backpropagation ANN and with the same data set. By looking at the ranges of RMSE values, it is concluded that different variations of backpropagation neural network algorithm affect the retrieval accuracy. Therefore, it is important to carefully decide on the type of backpropagation training algorithm to be used.

7.1.2 Generalization Abilities of ANN across Different Dates and Sites

As discussed in **Section 5.3.3.1**, ideally the ANN should generalize across the spatial locations and for different times of the year so it does not have to be re-trained for each set of measurements. For this purpose, a combination of the different farms with different dates is used for training while testing will use data from different focus farms. The Krui area consists of four focus farms; Illogan, Pembroke, and Roscommon are used for training while Stanley is the area for testing. From **Table 4.1** (refer to **Section 4.3**), the training data of the three focus farms covers the different topography (flat, gently rolling to hilly). The land uses of the training data include grazing and different crops (wheat, barley and oats). Stanley, the testing site, is hilly with grazing as the main land use, which are a sub-set of the topography and land uses of the training data. The experiments in this section test the hypotheses that the ANN is able to capture these characteristics from the training data. As explained in the previous section, data at higher resolution is preferable. Therefore, data at 250 m resolution are used. The soil moisture variability ranges from 0.039 v/v to 0.47 v/v over these four focus farms. This shows that the farms cover the range of dry to wet conditions and the ANN is tested for its ability to learn such conditions. The ground sampling dates for each of these focus farms are shown in **Table 7.2**.

Table 7.2. The ground sampling dates where there are complete sets of required ancillary information.

No.	Focus Farm	Date
1.	Illogan	10th Nov, 17th Nov, 24th Nov 2005
2.	Pembroke	15th Nov, 22nd Nov 2005
3.	Roscommon	1st Nov, 8th Nov, 15th Nov 2005
4.	Stanley	10th Nov, 17th Nov, 24th Nov 2005

As shown in **Section 7.1.1**, the network: four neurons in one hidden layer with the BFGS Quasi-Newton training algorithm, is the best to use. With only TbH and TbV values as the input, the trained ANN achieves a RMSE of

6.75%v/v of soil moisture prediction accuracy. As the prediction accuracy is greater than the desired error of 4% v/v of SMOS mission, a further analysis on the use of the ancillary information, which provides information about the surface characteristics, is carried out to investigate whether the use of ancillary information would further improve the retrieval accuracy.

7.1.3 Prediction Accuracy Obtained By Incorporating Ancillary Data

Following **Section 7.1.2**, input data of TbH and TbV, together with ancillary information including soil temperature, vegetation water content (VWC) and soil texture properties ratio, are used in the ANN model. The retrieval for the control farm (Roscommon) in **Section 7.1.1** was seen to achieve an accuracy of 3.93% v/v with proper selection of the appropriate backpropagation training algorithm. However, when more farms of different topography and land use properties were used, the retrieval accuracy deteriorated to 6.75% v/v. This shows that the ANN model was not able to incorporate the topography and land use properties in the model. Ancillary information, which provides information about the surface characteristics, is next incorporated in the ANN model. The incorporation of the ancillary information is done by adding them as the inputs for the ANN model. The source of training and testing data are the same as in **Section 7.1.2**. The architecture of the ANN model as shown in **Figure 7.3** is used. The BFGS Quasi-Newton algorithm is used for the ANN learning.

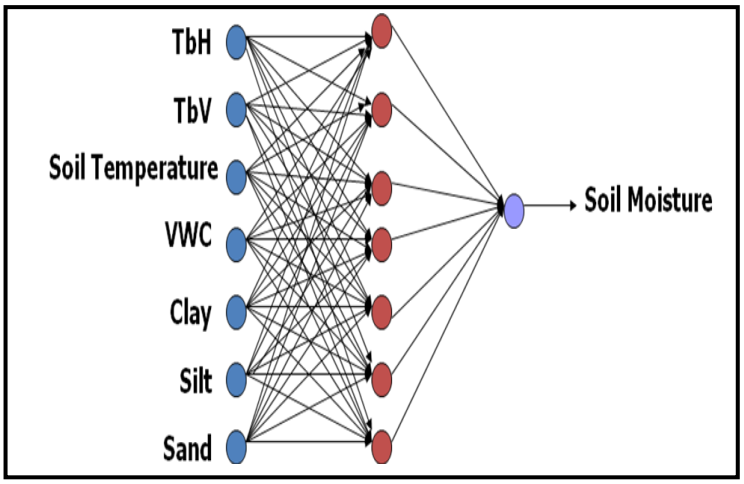

Figure 7.3. The ANN architecture used for the input of TbH and TbV and their corresponding ancillary data, including the soil temperature, vegetation water content (VWC) and the ratio of soil texture properties (clay:silt:sand).

The prediction result obtained is 5.65% v/v. Although this result is still greater than the desired 4% v/v for the SMOS mission, it shows that ancillary data aids in improving the prediction accuracy. In this experiment, the inputs are all of the available supporting data from the field experiment. There is no proper decision on whether the data provided are unnecessary or redundant for the ANN model. Since an ANN is a data driven model, proper input selection is a crucial step in its implementation as the presence of redundant or unnecessary inputs can severely impair the ability of the network to learn the target patterns. Therefore, a proper input selection method is explored in the next section.

7.1.4 Incremental Contribution of Variables: Ancillary Data Selection

To evaluate which information was redundant and not necessary for the ANN model used, the incremental contribution of variables was explored. When considering what inputs to use for an ANN, the effect of adding/removing an input can be used as an indication. The incremental contribution of an input can be explained by the reduction of the explained variance of the dependent variable (output) when we exclude an explanatory

variable (input) (Kaashoek and Van Dijk 2002). A natural candidate for quantification of the network performance is the square of the correlation, R^2. The network performance with only one input deleted can be measured in a similar way.

For the purposes of this study, the ANN architecture is first optimized using all available features as input. The optimization produces a correlation of R_y^2. When the contribution of an input of a feature is set to zero, the same network after this first optimization without this particular input produces a correlation of R_i^2. The incremental contribution of this particular input is then defined as:

$$R_y^2 - R_i^2 \tag{7.1}$$

If the value of Equation (7.1) is low for some input *n* compared to all other inputs, then this input is a candidate for exclusion from the network. In the research by Kaashoek and Van Dijk (2002), a feature is to be considered for exclusion if the value of Equation （7.1） is less than one tenth of the feature with the highest contribution. This criterium is used in the analysis below for selecting inputs.

For this study, experiments are carried out to select the input factors from the available inputs for the study area: H and V polarized brightness temperatures (TbH and TbV), surface temperature (Ts), vegetation water content (VWC), Normalized Difference Vegetation Index (NDVI), average RMS roughness value (Rs), and percentage of silt (%Si), sand (%Sa) and clay (%Cl) of soil textural properties.

Two sets of experiments were carried out and are discussed here. These two experiments compare the effects of constant values of the ancillary data. This is done by having experiments using one single farm and a combination of different farms. By using a single farm, the ancillary data, which were collected once throughout the field work (NDVI, Rs, %Si, %Sa and %Cl) would be constant values. When multiple farms were used, these constant values will be variable according to the farms used.

The first experiment used the data from the Pembroke focus farm and the second experiment was conducted using data from a combination of three focus farms: Roscommon, Stanley and Cullingral. As there were nine inputs for the ANN model, the ANN became more complicated. In order for the ANN to learn well, there is a need for more data. Therefore, Pembroke was chosen as it is the largest among the eight focus farms and hence will provide adequate data for the training of the ANN. Experiment 2 requires focus farms of different characteristics in terms of topography and land cover. For these reasons, Roscommon, Stanley, and Cullingral, with the characteristics stated in **Table 7.3** were selected.

Pembroke has a high average vegetation biomass of 1.5 kg/m^2 compared to Roscommon 0.6 kg/m^2, Stanley 0.5 kg/m^2 and Cullingral 0.5 kg/m^2. The average spatial variability of soil moisture for Pembroke was 4.5% v/v, Roscommon 3.3% v/v, Stanley 5.8% v/v and Cullingral 11% v/v. Roscommon was considered as the "control" site with minimum soil moisture heterogeneity. A spatial data resolution of 500 m is used because there were more data available at this resolution than for the previous experiment that used 250 m resolution data. As the ANN model with more inputs is more complicated, more data are needed in order for the ANN to map the relationships between the inputs and the output. Therefore, data at coarser resolution comparing to previous sections were used. The data at 500 m resolution is the coarsest with the desired amount of data available for the study area.

Table 7.3. Characteristics of the data for the focus farms used in the experiments.

Focus Farm : Pembroke (Area : 6400 ha, Topography : Hilly/Gently rolling, Land cover: Wheat and Barley)										
Date	**TbH(K) (max/min)**	**TbV(K) (max/min)**	**SM(v/v) (max/min)**	**VWC (kg/m^2)**	**NDVI**	**Rs**	**%Cl**	**%Si**	**%Sa**	**No. of Data**
8/11	258.7/243.4	277.4/260.3	0.63/0.28	0.54	0.71	0.84	62.5	29.5	8	88
15/11	269.7/256.4	283.2/272.1	0.35/0.14	2.03						88
17/11	270.3/258.1	282.0/271.1	0.36/0.14	0.91						88
22/11	273.7/263.7	284.5/276.1	0.22/0.06	2.41						88
Focus Farm : Roscommon (Area : 940 ha, Topography : Flat/Gently rolling, Land cover: Grassland)										
Date	**TbH(K) (max/min)**	**TbV(K) (max/min)**	**SM(v/v) (max/min)**	**VWC (kg/m^2)**	**NDVI**	**Rs**	**%Cl**	**%Si**	**%Sa**	**No. of Data**
1/11	237.0/205.1	262.9/235.0	0.38/0.19	0.77	0.60	0.62	6.5	8.5	85	11
8/11	244.2/222.9	262.7/253.5	0.26/0.11	0.83						11
15/11	271.0/260.2	285.1/278.4	0.10/0.04	0.48						11
22/11	275.4/269.2	286.3/282.3	0.05/0.01	0.44						11
Focus Farm : Stanley (Area : 720 ha, Topography : Hilly, Land cover: Grassland)										
Date	**TbH(K) (max/min)**	**TbV(K) (max/min)**	**SM(v/v) (max/min)**	**VWC (kg/m^2)**	**NDVI**	**Rs**	**%Cl**	**%Si**	**%Sa**	**No. of Data**
3/11	255.1/243.7	275.1/265.4	0.46/0.23	0.37	0.73	1.07	39.2	39.4	21.4	17
10/11	255.6/241.7	272.4/260.7	0.47/0.21	0.07						17
17/11	268.7/260.4	281.3/274.4	0.25/0.05	0.31						17
24/11	248.4/237.3	267.8/255.2	0.37/0.16	0.29						17
Focus Farm : Cullingral (Area : 220 ha, Topography : Flat, Land cover:Wheat and Barley)										
Date	**TbH(K) (max/min)**	**TbV(K) (max/min)**	**SM(v/v) (max/min)**	**VWC (kg/m^2)**	**NDVI**	**Rs**	**%Cl**	**%Si**	**%Sa**	**No. of Data**
4/11	255.5/249.9	273.2/265.7	0.41/0.11	0.87	0.60	0.65	0	6	94	8
9/11	249.0/240.5	270.0/258.5	0.64/0.14	0.48						8
18/11	275.1/264.8	285.9/277.4	0.24/0.006	0.42						8
25/11	271.8/262.1	281.9/273.6	0.23/0.09	0.36						8

i. Experiment 1: Pembroke

Data obtained for the Pembroke focus farm on 8th Nov and 15th Nov 2005 are used for training of the ANN. To make sure that the data used were representative, data were selected according to dates with a stratified method. This assures that data used are representative of each date. Of the 176 samples available on these two dates, stratification across the dates was used to select 3% (5 samples) of the data for validation and 3% (5 samples) for testing. The BFGS Quasi-Newton algorithm, which produced the lowest RMSE on the testing samples was then taken as the trained ANN. At this stage, the weights and biases were held constant. The contribution of each of the inputs was evaluated by setting the weights of the chosen input to be

zero and the trained ANN was evaluated to examine the correlation R^2 on the other inputs. The incremental contribution of each of the inputs is shown in **Table 7.4**.

Table 7.4. Incremental contribution of each of the inputs for Experiment 1.

Input Excluded	R^2	Incremental Contribution	RMSE (% v/v)
None	0.5031	-	4.09
I1 (TbH)	0.4893	0.0138	3.94
I2 (TbV)	0.4482	0.0549	4.06
I3 (Ts)	0.5041	-0.0010	3.58
I4 (VWC)	0.5311	-0.0280	4.15
I5 (NDVI)	0.5040	-0.0009	4.06
I6 (Roughness)	0.5040	-0.0009	4.06
I7 (%Clay)	0.5031	0	4.09
I8 (%Silt)	0.5031	0	4.09
I9 (%Sand)	0.5031	0	4.09

From **Table 7.4**, the incremental contribution for TbH and TbV are higher in terms of positive correlation compared to the other parameters (i.e. more than one tenth of the contributions of all nine inputs). The incremental contributions of I3(Ts), I4 (VWC), I5 (NDVI), I6 (Roughness), I7 (%Clay), I8 (%Silt), and I9 (%Sand) are very small and hence these inputs are candidates for exclusion From **Table 7.4**, it can be seen that, the adding of the I7 (%Clay), I8 (%Silt) and I9(%Sand) made no contribution to the retrieval accuracy. After all these inputs are excluded from the ANN, the ANN is re-trained to obtain the best parameters and performance. Then the process of checking the incremental contribution of each of the remaining variables is again undertaken with the results shown in **Table 7.5**.

Table 7.5. Incremental contribution of TbH and TbV after exclusion of other inputs.

Input Excluded	R^2	Incremental Contribution	RMSE (%v/v)
None	0.5307	-	3.92
I1 (TbH)	0.2233	0.3074	4.03
I2 (TbV)	0.3576	0.1731	6.32

Table 7.5 shows that the incremental contributions for each of the two inputs are of similar magnitude and the lowest is greater than that one tenth of the largest. Hence, no further exclusion is needed. Note the result for all input features in **Table 7.5** is worse than the result in **Table 7.4** with I3 removed. However the result in **Table 7.5** is more desirable because of the reduction in the number of inputs needed. This results in a network of {2,10,1}, i.e. two inputs, 10 hidden nodes and one output node. To verify that these inputs alone produce either superior or almost the same accuracy with the inclusion of any other ancillary data, the lowest RMSE value for each of a number of combinations of ancillary factors with the brightness temperature is shown in **Table 7.6**.

Table 7.6 shows that using just the brightness temperatures: TbH and TbV, produces the best accuracy for both dates. The ANN model was used to predict the soil moisture for the two different dates (17th Nov. and 22nd Nov.) after training on two previous dates (8th Nov. and 15th Nov.). Although good accuracy was obtained on the training data (3.92%v/v), the accuracy is not better than the desired 4% v/v, for the SMOS mission for the 17th and 22nd of November. With more input used, the accuracy of retrieval is not getting better, compared to using only TbH and TbV as the input. As the conditions were getting drier during the field experiment, the range of soil moisture was different for the testing dates compared to the training date. These results are similar to the results obtained by Angiuli *et al.*(2008) whose ANN model was unable to predict soil moisture values, which were out of range of the training data.

Table 7.6. RMSE testing when using different combinations of inputs.

Combination	RMSE (% v/v)	
	17th Nov	22nd Nov
TbH+TbV	4.93	8.85
TbH+TbV+Ts	12.41	30.58
TbH+TbV+Ts+VWC	6.43	12.52
TbH+TbV+Ts+VWC+NDVI	10.34	10.13
All Nine Inputs	9.21	12.50

ii. Experiment 2: Combination of Roscommon, Stanley and Cullingral Farms

Experiment 1 considered a single farm for which the values of NDVI, RMS roughness value, %Clay, %Silt, and %Sand were constant throughout the whole farm. To investigate whether the exclusions of these parameters are the result of relatively uniform parameters across this farm or because there was little correspondence of the values with other data for each of the particular farms, a combination of farms was used. The ANN was trained using data for the first three dates of each of three farms (Roscommon: 1st, 8th & 15th Nov., Stanley: 3rd, 10th & 17th Nov., Cullingral: 4th, 9th & 18th Nov.). To make sure that the data used for validation and testing are representative of the training data, the stratified method was used whereby it was made sure that data from each date were selected. A total of 108 samples were obtained and of these, six samples were selected for each of the validation and testing samples. The same process of input analysis followed in Experiment 1 was used. The incremental contributions of all nine inputs are shown in **Table 7.7**.

Table 7.7 shows that inputs I1 (TbH), I4 (VWC), I6 (Roughness), and I9 (%Sand) are candidates for exclusion. This results in a network of {5,10,1}. It can be seen that the constant values for %Clay and %Silt do contribute to the mapping of the function using the ANN and hence are not a parameter to be excluded at this stage. After the exclusion of the candidate inputs, the ANN is retrained and results are shown in **Table 7.8**. The inputs I5 (NDVI)

and I7 (%Clay) are now candidates to be excluded. This results in a network of {3,10,1}.

Table 7.7. Incremental contribution of each of the variables in Experiment 2.

Input Excluded	R^2	Incremental Contribution	RMSE (%v/v)
None	0.5210	-	7.31
I1 (TbH)	0.5044	0.0166	7.37
I2 (TbV)	0.3904	0.1306	8.01
I3 (Ts)	0.0030	0.5180	11.68
I4 (VWC)	0.5472	-0.0262	7.21
I5 (NDVI)	0.3629	0.1581	8.21
I6 (Roughness)	0.5774	-0.0564	8.62
I7 (%Clay)	0.0251	0.4959	15.60
I8 (%Silt)	0.2423	0.2787	9.82
I9 (%Sand)	0.4851	0.0359	9.08

Table 7.8. Incremental contributions of each of the variables of network {5,10,1}.

Input Excluded	R^2	Incremental Contribution	RMSE (%V/V)
None	0.5878	-	6.76
I2 (TbV)	0.0096	0.5782	17.41
I3 (Ts)	0.1075	0.4803	16.95
I5(NDVI)	0.5333	0.0545	8.42
I7(%Clay)	0.7655	-0.1777	7.25
I8(%Silt)	0.4255	0.1623	9.44

Table 7.9 shows the results after further training, which results in input I8 (%Silt) being considered for exclusion. The network of size {2,10,1} is again retrained and the results are shown in **Table 7.10**. As the contributions of the two inputs are almost the same, no further reduction is needed. A verification of this combination of inputs compared to other combinations is shown in **Table 7.11**.

Table 7.9. Incremental contributions of each of the variables of network {3,10,1} .

Input Excluded	R^2	Incremental Contribution	RMSE (%v/v)
None	0.6685	-	6.21
I2 (TbV)	0.4133	0.2552	8.57
I3 (Ts)	0.1803	0.4882	17.47
I8(%Silt)	0.8268	-0.1583	10.86

Table 7.10. Incremental contributions of each of the variables of network {2,10,1}.

Input Excluded	R^2	Incremental Contribution	RMSE (%v/v)
None	0.6039	-	6.56
I2 (TbV)	0.3411	0.2628	8.86
I3 (Ts)	0.1826	0.4213	18.08

Table 7.11. Accuracy for different combinations of input.

Combination	RMSE (% v/v)		
	Roscommon (22/11)	Stanley (24/11)	Cullingral (25/11)
TbV+Ts	1.77	9.11	5.86
TbH+TbV	7.56	10.06	5.09
All Nine Inputs	2.06	6.90	7.17

Table 7.11 shows the accuracies obtained with the two inputs selected from Experiment 2, the best inputs combination from Experiment 1, and all nine inputs when the ANN is evaluated using data from different dates to those used for training. It can be seen that TbH was determined to be a good input for a single farm and for multiple farms. Note that TbV gives the best result in combination with TbH in Experiment 1 whereas Ts gave the best result in combination with TbV in Experiment 2. The results show that analysis of the incremental contributions of variables helps to reduce the number of inputs needed, resulting in less complex ANNs. Note that, higher

R^2 values do not mean that the retrieval results are better, as the retrieval values might group at a certain location causing a high R^2 value to be obtained. Therefore, the value of the incremental contribution of a specific variable is the main concern of this technique.

iii. Analysis of results

The two experiments have analyzed the use of brightness temperature and ancillary data for soil moisture retrieval. It is important to analyze the ANN for different combinations of inputs to determine those that improve the accuracy of soil moisture prediction, and those that, could, reduce the performance by essentially confusing the ANN. **Table 7.6** showed that, for one farm, the use of ancillary data reduces the accuracy and hence appears not to be beneficial. **Table 7.11** shows that more inconclusive results for the usefulness of ancillary data occur for a more representative training and testing set of data i.e. over more farms. Through the analysis of the incremental contribution of each input, the best combination of inputs required can be determined.

With the use of ancillary data, and with the incremental contribution of variables to select appropriate input parameters for the ANN model, the prediction accuracy obtained (except for the Roscommon farm that is considered a "control" site) is still worse than the desired 4% v/v when the "trained" ANN is tested on data from a new future date. This shows that the ANN model does not generalize well for future dates.

While these two experiments show that the incremental contribution of a variable can be used for the selection of parameters for the ANN model, the validity of the ancillary data used in the experiments could be an issue as most of the values of the ancillary data used have constant values (see **Section 7.1.4**). Variables that have constant values across a site but which are different for different sites can be used to bias the ANN towards the right result. The same would be true for the same site for different dates. Moreover, from **Table 7.3.**, the number of data available for training is

limited. Therefore, in the next stage of this thesis, only data at 1 km resolution which covers the whole target area of 40 km×40 km (presented in **Section 4.5** and **Section 6.2**) will be used.

7.2 Overview of the Proposed Methodology

From the preliminary experiments results and **Section 5.3.3**, it is concluded that, the problem of using ANN as a soil moisture prediction method is its inability to capture data for future dates, which is out-of-range of the training data, i.e. has higher or lower values than those used for training. This is said to be a problem of capturing the variability of the soil moisture values. However, soil moisture is highly spatially and temporally variable (Western *et al.* 2002). When quantities vary in space or time, the variation can be quantified with a number of characteristics (Western *et al.* 2002). These characteristics include the central tendency (i.e. mean or median) and the spread (i.e. variance or standard deviation).

For this research study, the prediction of soil moisture is over a target area of 40 km×40 km and on two dates, 14th Nov and 21st Nov 2005, which are one and two weeks after the data used for the training of the ANN (7th Nov 2005). This data division ensures that the predictions are done on two totally new dates and on unknown conditions. Moreover, the ability of trained ANN is tested on two real cases. As surface soil moisture variance observed within a square metre can be as large as a whole field (Van Oevelen 1998), the ANN in this research study will have to capture the variance of the soil moisture across a large area (spatial variation) and across different dates (temporal variation).

A technique to accommodate this is to normalise each of the input variables using the mean and standard deviation. As the spatial variability of soil moisture is scale dependent (Nykanen and Foufoula-Georgiou 2001; Richard *et al.* 2004), soil moisture prediction is done using a "window". The details of this methodology are discussed in this chapter.

Different scenarios are used to verify this methodology. **Figure 7.4** summarizes each of these different scenarios. Note the dotted and full lines mean the same but are to show clearly the different paths. From this figure, it can be seen that there are four different scenarios. The data on 7th Nov 2005 are divided into training, validation, and testing sets with each set consisting of 1440 (90%), 80 (5%) and 80 (5%) data samples respectively. The ANN model is first trained using data for the 7th Nov 2005 to obtain the optimum ANN architecture. The input of the ANN is normalized using the mean and the standard deviation values obtained from the input variables. The predicted soil moisture values are de-normalized using the mean and standard deviation of the actual soil moisture values. The RMSE values are then calculated from the actual and de-normalized soil moisture values. This "trained" ANN model is next tested using data for the 14th and 21st Nov 2005 (termed as evaluation cases hereafter). To evaluate the importance of using the normalization and de-normalization factors from the data on each of the evaluation cases, the trained ANN is tested with normalization and de-normalization factors from the training data (scenario **b**. of **Figure 7.4**). The result is compared with the trained ANN model, which uses the normalization and de-normalization factors from the evaluation cases (scenario **a.** of **Figure 7.4**). In **Figure 7.4**, the scenario **d** is the proposed method to optimize the standard backpropagation ANN model for soil moisture retrieval. The importance of the normalization and de-normalization factors in this proposed methodology is verified by testing whether the use of these factors from the training data affects the accuracy (scenario **c.** in **Figure 7.4**). Scenario **a.** and **d.** of **Figure 7.4** also will be used to compare the result of the retrieval of soil moisture without using the "window" method proposed in this research (refer **Section 7.6**).

Note the de-normalisation on the output uses the values we are trying to predict. It is envisaged that some surrogate or indicator for this will be used in future. For example, results for previous dates where we have the input data and corresponding output results may be useful to determine these

values. An alternative is to use some other indicator of soil moisture, perhaps a crude low resolution measure from ground measurements.

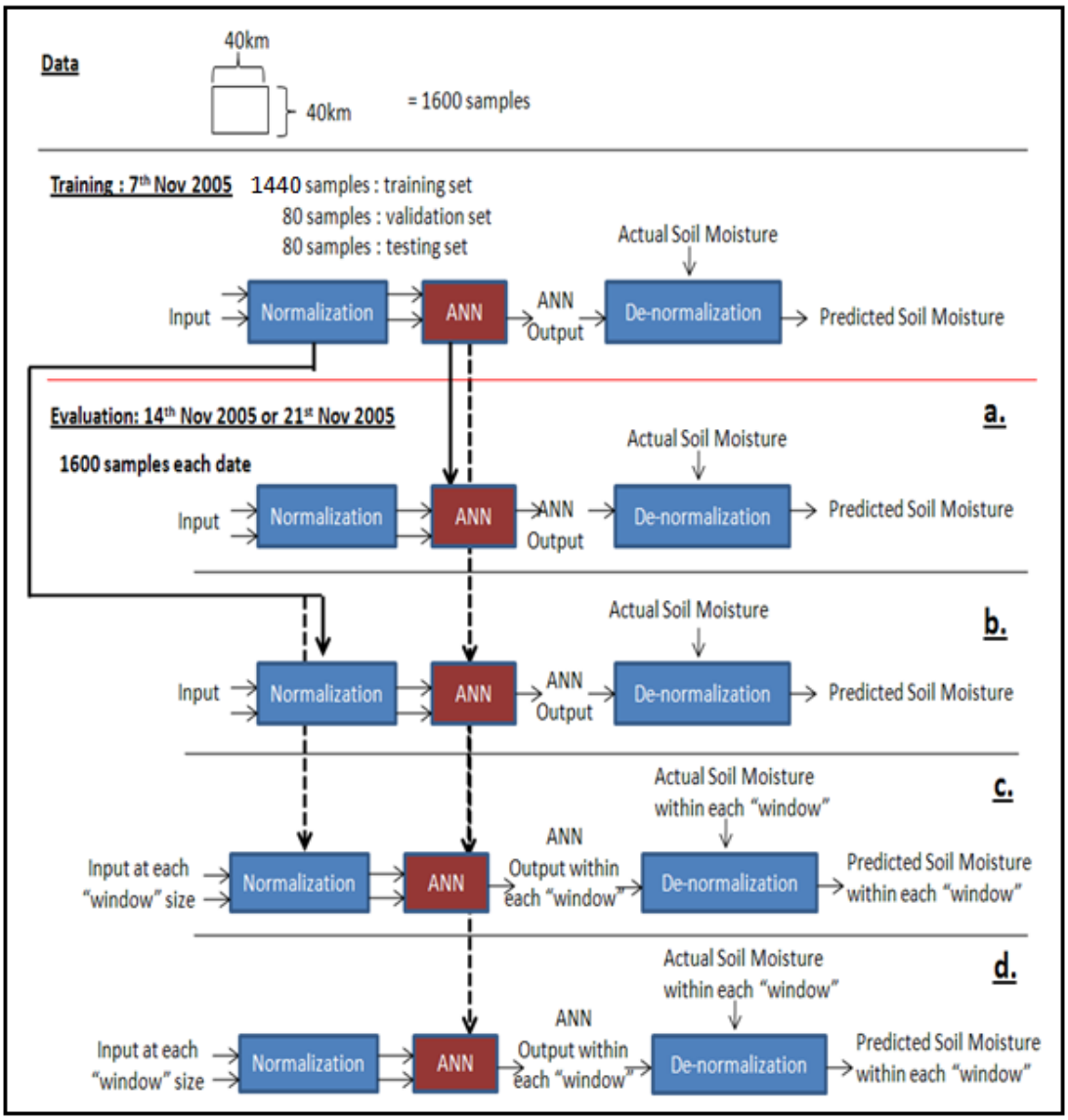

Figure 7.4. Different scenarios (a, b and c) used to verify the proposed methodology (d). Secenario a. Use of normalization factors from the input for the evaluation set data; b. Use of normalization factors from the training data; c. Normalization factors obtained from the training data with addition of the use of "window"; d. Normalization factors obtained from the evaluation set with the use of "window".

7.2.1 Data Division: Training, Validation and Testing Data

The regional data acquired on 31st October 2005, 7th November 2005, 14th November 2005 and 21st November 2005 as discussed in **Chapter 4 (section 4.5)** and **Chapter 6 (section 6.2)** were the target dataset. However, as MODIS

scenes were available for only three of the four days during NAFE'05, only data on the 7th, 14th and 21st November 2005 were considered and discussed in this study. Data were binned into a 1 km reference grid for the whole 40km ×40km area. On occasions where there were missing data, i.e. the data from MODIS acquired when not totally cloud free, the Inverse Distance Weighted (IDW) method was used to interpolate the values based on the surrounding values. IDW is a commonly used technique for interpolation (Steed *et al.* 2004)that is based on the assumption that the interpolating surface should be influenced most by nearby points and less by distant points. As the MODIS/Aqua Surface Reflectance Daily L2G Global data has a resolution of 250 m and the MODIS/Aqua Land Surface Temperature and Emissivity Daily L3 Global data of 1 km, and as the reference grid is chosen to be 1 km, the points that needed to be interpolated will be close. IDW is shown to provide reasonable estimates and is shown in a large number of comparative studies to perform better than kriging-based techniques, an advanced spatial-statistics technique that uses data trends (Weber and Englund 1992; Babak and Deutsch 2009). A total of 1600 (40×40 at 1 km resolution) samples were obtained for each date. To train the ANN model, 1440 samples from the 7th November 2005 are randomly selected for training, and 80 samples (5%) are selected for each of the validation and testing sets. To randomly select samples, the MATLAB routine (**rand( )**) was used. The ANN is trained to minimize the RMSE between the referenced (ground truth) and retrieved (predicted) soil moisture value. At this stage, the weights and bias of the ANN, termed the "trained ANN", are used for evaluation using data of 14th and 21st November 2005 (evaluation cases) (**Figure 7.5**).

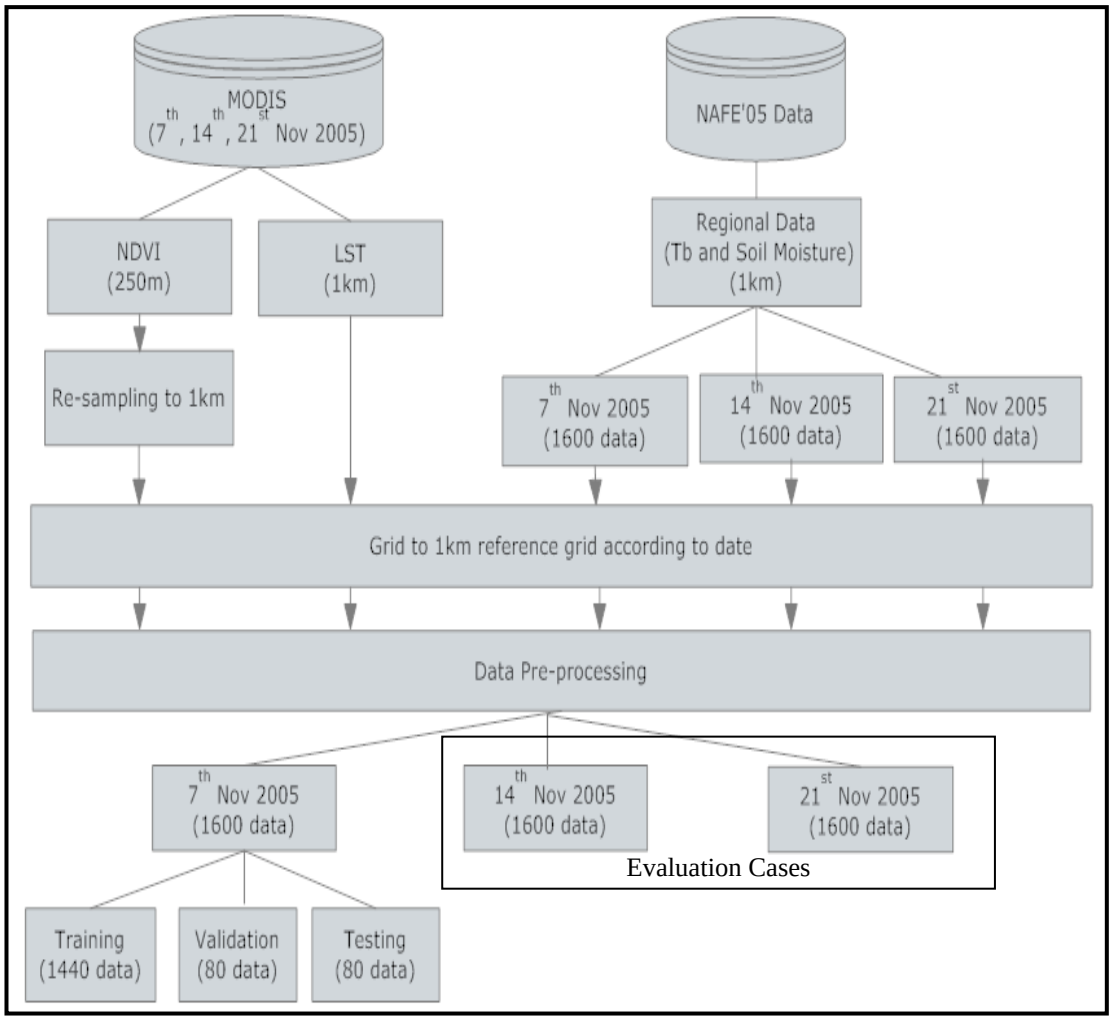

Figure 7.5. Data division process.

7.2.2 Data Pre-processing for ANN: Input Normalization

The input data will be normalized so that they have zero mean and unit standard deviation using:

$$z_{norm} = (x - \bar{x}) \times \left(\frac{\sigma_y}{\sigma_x} \right) + \bar{y} \tag{7.2}$$

where z_{norm} is the normalized feature value, x is the input feature value, $\bar{x}$ is the mean and σ_x is the standard deviation of the input data, $\bar{y}$ is equal to 0, and σ_y is equal to 1. Equation (7.2) can be simplified and written as:

$$z_{norm} = \frac{x - \bar{x}}{\sigma_x} \tag{7.3}$$

Using Equation (7.3), the input data are normalized.

The mean and the standard deviation of the target layer of the ANN model are also calculated for the data de-normalization step.

7.2.3 Data Post-processing: De-normalization

The output of the ANN, which are the normalized soil moisture prediction values, are de-normalized using the mean and standard deviation obtained in **Section 7.2.2.2**. The de-normalization of the normalized soil moisture is calculated based on equation (7.4):

$$y'' = z''_{norm,y}\sigma_y + \bar{y} \tag{7.4}$$

where y'' is the de-normalized soil moisture values, $z''_{norm,y}$ is the predicted soil moisture values in normalized format, σ_y , and $\bar{y}$ is the standard deviation and mean of the soil moisture obtained in **Section 7.2.2.2.**

Figure 7.6. shows the process for the normalized and de-normalized process to pre- and post-processing the data as discussed in **Section 7.2.2** and **7.2.3**. This outlines in more detail the stages shown in **Figure 7.4** showing the equations used.

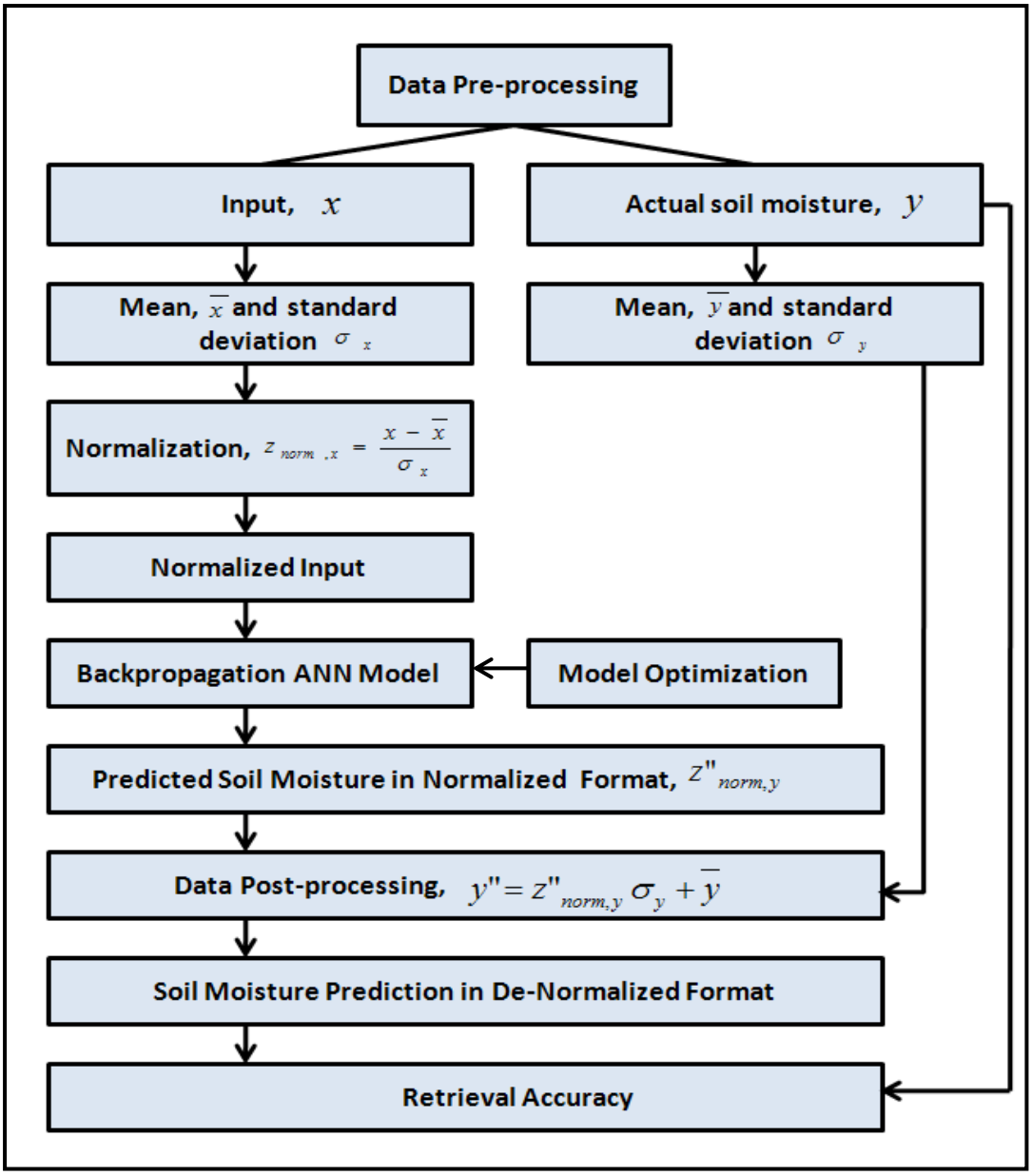

Figure 7.6. The pre- and post-processing of the data.

7.3 Normalization: Training, Validation, Testing and Evaluation Cases Data

The general way of data preprocessing for ANNs is to obtain the standard deviation and mean from the training data, but not for the validation and testing data as the validation and testing data are normalized using the same mean and standard deviation when inputted to the ANN (Sarle 1997). Therefore, generally, the means and standard deviations are computed for each feature over the set of training data, and are used to scale each sample

of the validation and testing data (Priddy and Keller 2005). The performance of the ANN will vary unpredictably if the ANN is trained using normalized data but then tested with unnormalized data.

In contrast to this general way of pre-processing the data, normalization is also done for the validation, testing and evaluation cases data using the mean and standard deviation of the data itself.

The rationale behind this is that as the training is done using a single date, the condition of wetness/dryness for each date will almost certainly differ from the training date (i.e. in this study, the evaluation cases condition differ from the training data). The review of the literature (**Section 5.3.3**) showed that to cover the variety of conditions, electromagnetic models that include much ancillary data, could be used to simulate enough data during training so that the ANN can learn all those unforeseen conditions. However, it is not easy to cover all the unforeseen conditions. On the other hand, the values of mean and standard deviation that represent the variation can be used to overcome the issue of the different conditions on an unforeseen date. For example, different normalization factors were applied for the training and evaluation samples by Minns and Hall (1996) in their rainfall-runoff model. In their study, they pointed out the importance of normalizing data as the ANN they used failed to extrapolate when required to predict values that are out-of-range of the training data. Their research concluded that in practice, the ANN can only be used to predict data that are similar or the same as that which have been "seen" before. In their research, they found that when using the same normalization factor for training and evaluation data (determined from the training data), the results were notably poorer than when different normalization factors were used. The results obtained from their research emphasized the care required in choosing the normalization factors. Moreover, previous work by Chai *et al.* (2008) has shown that the performance of the ANN can be improved if the ANN is presented with the training and testing data of similar statistical mean and standard deviation values.

7.4 Input Data Selection

From **Section 7.1.4**, it is clear that with carefully selected ancillary data, the soil moisture prediction accuracy will be improved using the ANN model. Ancillary data investigated in this study include the Normalized Difference Vegetation Index (NDVI) and soil surface temperature (Ts) from MODIS (refer to S**ection 5.4.1**). NDVI data are calculated from Band 1 and Band 2 of the MODIS/Aqua Surface Reflectance Daily L2G Global 250 m data while the Ts values are obtained from the MODIS/Aqua Land Surface Temperature and Emissivity Daily L3 Global 1 km data. Both of these ancillary data are gridded to the same 1 km reference grid as used in the processing of the brightness temperature and soil moisture data. The sensitivity of the ANN towards the inputs is measured by the change of Root Mean Square Error (RMSE) when an ancillary feature is added to the model. The ANN is initialized and trained repeatedly until the lowest global error between the referenced and computed values is obtained. At this stage, the ANN is assessed using the testing data.

7.5 Neural Network Architecture Determination

There are a number of parameters that need to be determined for the ANN. The number of input and output nodes is directly linked to the application itself. In this thesis, the different input combinations assessed include: (i) H- and V-polarized brightness temperatures (two features), (ii) combination of the dual-polarized brightness temperatures with NDVI (three features), (iii) combination of the dual-polarized brightness temperatures with Ts, (three features) and (iv) combination of the dual polarized brightness temperatures with NDVI and Ts (four features). The output node is the soil moisture value (one output value).

Parameters that need to be determined include the number of hidden layers and the number of hidden neurons in each of the chosen hidden layers. It is known that backpropagation ANNs with one or more hidden

layers can form any arbitrary decision boundary if a sufficient number of neurons is used in the hidden layers (Stinchcombe and White 1989). Multi-Layer Perceptrons (MLPs) with non-linear activation functions and an arbitrarily large number of hidden units suffice for the "universal approximation" property (Hornik *et al.* 1989; Lippmann 1987). However, ANNs with two hidden layers can represent functions of any shape (Lippmann 1987). There is currently no theoretical reason to use neural networks with more than two hidden layers (Heaton 2008). For this reason, the ANN architecture being determined has either one or two hidden layers. Using too few or too many hidden neurons may undermine the application. Too few hidden neurons will cause underfitting to occur, whereby complicated signals within the data are poorly represented by simple models in the ANN. On the other hand, using too many hidden neurons will cause overfitting whereby the neural network has too much information processing capacity to build complex models, such that the limited amount of information contained in the training set is not enough to train all of the neurons in the hidden layers. Moreover, if too many hidden neurons are used, the amount of training time will increase. Currently, the best way to optimize the number of hidden layers and the number of hidden neurons is simply through trial and error (Lakhankar 2006) .

From **Section 7.1.1**, it is found that the Broyden–Fletcher–Goldfarb–Shanno (BFGS) method derived from the Newton method in optimization obtained the best retrieval results when different training algorithms are trained and tested with the same data set. For this reason, the BFGS method is selected. The details of the neural network parameters used in this study are given in **Table 7.12**.

Table 7.12. The training parameters for the BFGS training algorithm.

Performance goal	0.001
Maximum number of epochs to train	200
Minimum performance gradient	1e-10000
Maximum validation failures	5

The number of hidden neurons chosen ranged from 2 to 100 for a single hidden layer case, while for two hidden layers, the same number of hidden neurons were used for each layer (the notation 2:2 means two hidden layers with 2 hidden neurons at each of two layers, and will be used hereafter). Equal number of hidden neurons in each hidden layer is typically used by ANN researchers for soil moisture retrieval. The training of the ANN is repeated until the ANN produces an acceptable accuracy for the testing data.

7.6 Capturing Spatial Variability: Sub-grid

As the surface soil moisture variance observed within a square metre can be as large as a whole field (Van Oevelen 1998), there is a need to determine the size of the area (sub-grid) whereby the ANN can capture the spatial variability within this region. For this purpose, a methodology that utilizes a "window" approach is developed. Using the approach, the prediction of soil moisture will be carried out within the "window" as the prediction process moves from top left corner of the target area of 40 km×40 km, to the right and down, without overlap. The main reason for not overlapping the "window" is because the prediction will be done for each cell within the "window". Thus, overlapping the "window" will cause multiple values being predicted for a single cell. To develop this approach, there is a need to determine the size of the "window".

In order to have two sets of independent data for testing purposes, the data on 14th and 21st Nov 2005 are not used for training. For this reason, the

"window" size selection was determined using only data on 7th Nov 2005. An area of size 20km×20km at the top left of the study area on 7th Nov 2005 is used for the training of the ANN. Among these 400 data samples, 5% or 20 data are randomly selected (again using the MATLAB random number function) for validation and testing. The training of the ANN is repeated until the ANN produces an acceptable accuracy with the testing data. At this stage, the weights and biases are retained for purpose of selecting the "window" size. Different "window" sizes of 2km×2km, 3km×3km, 4km×4km, 5km×5km, 6km×6km, 7km×7km and 8km×8km, for the same date are used for the testing of the effects of the different sizes on the prediction accuracy. The selection of the 20km×20km area for training and testing for getting a trained ANN model can be done at any location on the 40km×40km study area. However, the data use for training and testing should not be from the same area. This is to avoid the ANN being biased by the training data. **Figure 7.7** shows the division of the data on 7th Nov 2005 for the purpose of "window" size selection. From **Figure 7.7**, it is clear that each of the "windows" is a sub-set of another larger "window". By each window being a subset of a bigger window, the effect of adding extra data can be compared across window sizes.

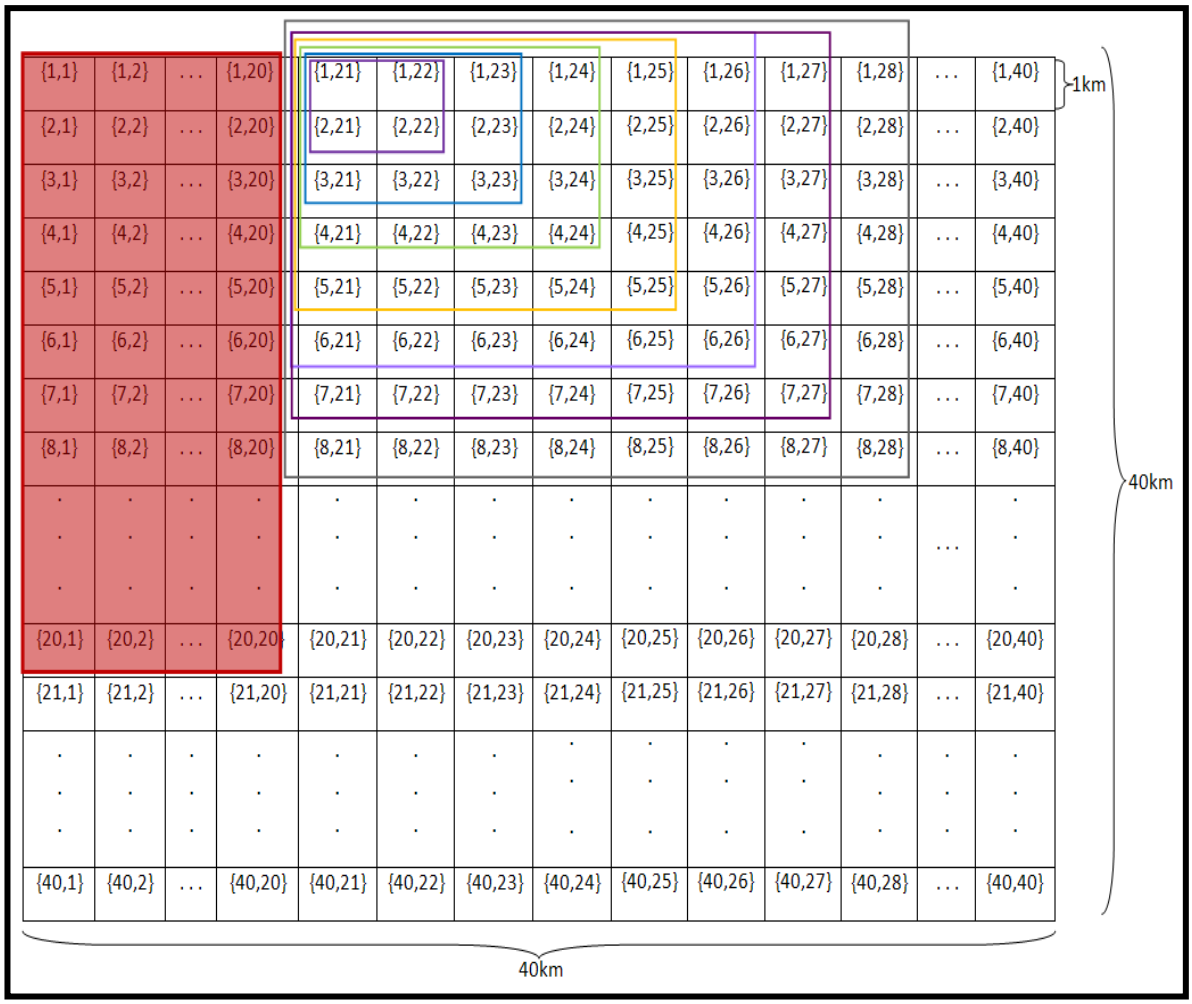

Figure 7.7. "Window" size determination using data from the 7th Nov 2005. The red-filled data were used for the training. The unfilled squares are the location of the "window" used for the size selection.

7.7 Selection of Optimum ANN Architecture, Combination of Inputs and "Window" Size

For the selection of the optimum ANN architecture, the combination of inputs and "window" size, the ANN is trained using the data division as shown in **Figure 7.7.** The experiment for obtaining the optimum features in terms of architecture, inputs and "window" size is conducted at the same time as well as for each of the four different combinations of inputs: TbH & TbV, TbH, TbV & NDVI, TbH, TbV & Ts and TbH, TbV, NDVI & Ts. The best combination of inputs will be selected from these four different combinations. The effect of ancillary information in addition to the brightness temperature can be seen from the experiments for using the four

different combinations of inputs. The results are shown in **Table 7.13** (TbH and TbV as input), **Table 7.14** (TbH, TbV and NDVI), **Table 7.15** (TbH, TbV and Ts) and **Table 7.16** (TbH, TbV, NDVI and Ts).

Table 7.13. The impact on RMSE and R^2 for different numbers of hidden layers, hidden neurons and "window" size when using only TbH and TbV as input.

	Hidden neurons	RMSE (R^2) Testing (%v/v)	RMSE (R^2) for Different "Window" Size (km) (%v/v)						
			2×2	3×3	4×4	5×5	6×6	7×7	8×8
Single Layer	**2**	6.69 (0.34)	1.09 (0.77)	3.26 (0.49)	5.66 (0.54)	6.42 (0.42)	7.04 (0.63)	6.69 (0.31)	6.97 (0.38)
	4	6.45 (0.40)	1.14 (0.77)	3.12 (0.55)	5.35 (0.66)	6.07 (0.56)	6.73 (0.35)	6.38 (0.43)	6.71 (0.47)
	6	6.32 (0.34)	1.37 (0.91)	3.25 (0.30)	4.87 (0.56)	5.74 (0.46)	7.11 (0.20)	6.65 (0.26)	6.78 (0.32)
	8	6.34 (0.33)	1.42 (0.94)	3.75 (0.10)	5.31 (0.43)	5.75 (0.46)	6.89 (0.24)	6.52 (0.28)	6.83 (0.31)
	10	6.23 (0.37)	1.23 (0.63)	2.93 (0.56)	4.56 (0.69)	5.60 (0.49)	6.80 (0.26)	6.28 (0.34)	6.42 (0.41)
	20	5.75 (0.45)	1.42 (0.59)	2.44 (0.63)	**2.86 (0.88)**	4.52 (0.67)	5.75 (0.47)	5.27 (0.53)	5.53 (0.55)
	50	5.4 (0.54)	1.57 (0.62)	2.98 (0.46)	3.57 (0.75)	4.41 (0.68)	5.82 (0.46)	5.23 (0.54)	5.76 (0.51)
	100	5.39 (0.63)	1.44 (0.32)	3.21 (0.40)	3.08 (0.84)	4.51 (0.65)	5.22 (0.58)	4.66 (0.64)	5.21 (0.60)
Two Layers	**2:2**	7.01 (0.29)	1.05 (0.83)	3.70 (0.12)	6.24 (0.29)	6.82 (0.33)	7.33 (0.19)	7.05 (0.24)	7.38 (0.30)
	4:4	6.59 (0.31)	1.32 (0.91)	3.47 (0.23)	5.28 (0.53)	6.01 (0.46)	7.11 (0.20)	6.75 (0.24)	7.03 (0.29)
	5:5	6.42 (0.36)	1.13 (0.70)	3.52 (0.22)	5.60 (0.47)	6.19 (0.39)	6.95 (0.24)	6.56 (0.30)	6.74 (0.38)
	10:10	6.16 (0.37)	1.44 (0.91)	3.64 (0.13)	4.95 (0.55)	5.48 (0.53)	6.87 (0.25)	6.52 (0.28)	6.66 (0.35)
	20:20	5.86 (0.44)	1.44 (0.71)	2.72 (0.52)	3.63 (0.79)	4.61 (0.69)	5.81 (0.47)	5.57 (0.49)	5.92 (0.49)
	50:50	5.73 (0.47)	1.45 (0.74)	2.90 (0.49)	3.50 (0.78)	5.06 (0.56)	6.58 (0.34)	6.02 (0.41)	6.02 (0.47)
	100:100	5.74 (0.47)	1.50 (0.66)	3.16 (0.37)	3.25 (0.82)	3.93 (0.74)	4.68 (0.68)	4.12 (0.72)	5.16 (0.61)

Table 7.14. As for **Table 7.13.** but using TbH, TbV and NDVI as input.

	Hidden neurons	RMSE (R^2) Testing (%v/v)	RMSE (R^2) for Different "Window" Size (km) (%v/v)						
			2×2	3×3	4×4	5×5	6×6	7×7	8×8
Single Layer	**2**	6.30 (0.39)	1.29 (0.80)	2.84 (0.55)	4.58 (0.75)	5.78 (0.55)	6.75 (0.30)	6.37 (0.36)	6.64 (0.41)
	4	5.23 (0.63)	1.43 (0.91)	3.1 (0.36)	5.12 (0.46)	5.93 (0.41)	6.22 (0.40)	5.84 (0.45)	5.76 (0.54)
	6	5.34 (0.54)	1.55 (0.95)	3.09 (0.37)	4.53 (0.58)	5.33 (0.53)	6.23 (0.38)	5.84 (0.43)	5.89 (0.49)
	8	5.50 (0.50)	1.64 (0.88)	2.93 (0.43)	4.01 (0.69)	5.13 (0.58)	6.21 (0.40)	5.94 (0.41)	5.99 (0.48)
	10	5.56 (0.51)	1.41 (0.90)	3.04 (0.38)	4.89 (0.53)	5.50 (0.52)	5.41 (0.59)	5.09 (0.62)	5.19 (0.67)
	20	4.82 (0.64)	1.45 (0.71)	2.55 (0.58)	3.59 (0.80)	5.09 (0.58)	5.60 (0.51)	5.25 (0.55)	5.16 (0.63)
	50	5.46 (0.51)	1.60 (0.95)	3.36 (0.36)	4.49 (0.48)	5.92 (0.42)	6.11 (0.44)	5.57 (0.49)	5.46 (0.57)
	100	5.52 (0.49)	1.87 (1.00)	3.11 (0.49)	4.84 (0.52)	4.61 (0.64)	5.01 (0.61)	4.60 (0.65)	5.01 (0.64)
Two Layers	**2:2**	6.54 (0.39)	1.27 (0.89)	3.34 (0.31)	5.33 (0.63)	6.18 (0.53)	7.04 (0.26)	6.73 (0.30)	7.03 (0.36)
	4:4	5.84 (0.55)	1.32 (0.92)	3.11 (0.39)	5.12 (0.58)	5.86 (0.53)	6.17 (0.50)	5.91 (0.53)	6.12 (0.58)
	5:5	5.53 (0.56)	1.38 (0.86)	2.95 (0.44)	4.74 (0.62)	5.59 (0.52)	5.56 (0.57)	5.30 (0.61)	5.52 (0.65)
	10:10	5.57 (0.50)	1.55 (0.94)	2.60 (0.56)	3.96 (0.76)	5.15 (0.60)	6.46 (0.34)	6.12 (0.38)	6.22 (0.44)
	20:20	5.60 (0.51)	1.46 (0.22)	3.24 (0.31)	5.17 (0.44)	5.59 (0.48)	6.01 (0.43)	5.53 (0.50)	5.50 (0.58)
	50:50	5.27 (0.54)	1.46 (0.72)	2.85 (0.46)	5.27 (0.42)	5.42 (0.50)	5.91 (0.44)	5.44 (0.50)	5.43 (0.57)
	100:100	5.30 (0.54)	1.68 (1.00)	2.72 (0.61)	4.76 (0.53)	4.41 (0.76)	4.90 (0.70)	4.52 (0.71)	4.64 (0.72)

Table 7.15. As for **Table 7.13**. but using TbH, TbV and Ts as input.

	Hidden neurons	RMSE (R^2) Testing (%v/v)	RMSE (R^2) for Different "Window" Size (km) (%v/v)						
			2×2	3×3	4×4	5×5	6×6	7×7	8×8
Single Layer	**2**	6.51 (0.42)	1.11 (0.56)	2.88 (0.67)	5.22 (0.67)	6.34 (0.46)	7.09 (0.24)	6.54 (0.37)	6.76 (0.45)
	4	5.72 (0.46)	1.43 (0.76)	2.93 (0.43)	4.16 (0.65)	5.27 (0.55)	6.09 (0.42)	5.52 (0.50)	5.60 (0.55)
	6	5.98 (0.43)	1.33 (0.87)	3.20 (0.33)	4.66 (0.64)	5.21 (0.59)	6.04 (0.46)	5.66 (0.52)	5.82 (0.56)
	8	5.84 (0.50)	1.38 (0.94)	2.75 (0.50)	4.27 (0.64)	5.56 (0.48)	6.46 (0.33)	5.67 (0.46)	5.59 (0.55)
	10	5.66 (0.48)	1.36 (0.68)	2.56 (0.59)	3.59 (0.77)	5.36 (0.53)	5.93 (0.46)	5.25 (0.56)	5.25 (0.62)
	20	5.73 (0.47)	1.23 (0.68)	2.59 (0.62)	3.68 (0.76)	5.59 (0.47)	6.06 (0.41)	5.20 (0.56)	4.99 (0.66)
	50	5.27 (0.54)	1.33 (0.87)	2.31 (0.66)	3.62 (0.76)	5.30 (0.52)	6.39 (0.39)	5.65 (0.48)	5.55 (0.55)
	100	4.81 (0.62)	1.33 (0.46)	3.63 (0.32)	4.49 (0.60)	5.58 (0.49)	6.07 (0.42)	5.39 (0.51)	5.82 (0.51)
Two Layers	**2:2**	6.75 (0.39)	1.13 (0.63)	3.46 (0.25)	5.70 (0.48)	6.73 (0.46)	7.06 (0.29)	6.79 (0.31)	7.14 (0.34)
	4:4	5.85 (0.50)	1.17 (0.75)	2.64 (0.60)	3.95 (0.78)	5.28 (0.61)	5.85 (0.50)	5.31 (0.60)	5.38 (0.51)
	5:5	6.09 (0.50)	1.12 (0.72)	3.04 (0.50)	4.86 (0.72)	5.84 (0.62)	6.16 (0.53)	5.77 (0.61)	5.95 (0.68)
	10:10	5.93 (0.42)	1.46 (0.92)	2.82 (0.50)	3.92 (0.77)	5.52 (0.52)	6.69 (0.29)	6.01 (0.40)	6.07 (0.38)
	20:20	5.59 (0.48)	1.54 (0.91)	3.50 (0.21)	4.75 (0.53)	5.39 (0.51)	6.27 (0.37)	5.66 (0.46)	5.62 (0.55)
	50:50	5.56 (0.49)	1.46 (0.61)	2.49 (0.63)	2.79 (0.84)	4.56 (0.83)	5.29 (0.56)	4.70 (0.63)	4.84 (0.66)
	100:100	5.08 (0.57)	1.54 (0.39)	3.24 (0.34)	4.61 (0.56)	5.41 (0.50)	5.97 (0.44)	4.99 (0.60)	5.24 (0.62)

Table 7.16. As for **Table 7.13.** but using TbH, TbV, NDVI and Ts as input.

	Hidden neurons	RMSE (R^2) Testing (%v/v)	RMSE (R^2) for Different "Window" Size (km) (%v/v)						
			2×2	3×3	4×4	5×5	6×6	7×7	8×8
Single Layer	**2**	6.45 (0.53)	1.13 (0.35)	3.25 (0.35)	5.86 (0.33)	7.03 (0.17)	7.29 (0.51)	6.71 (0.31)	6.78 (0.47)
	4	5.54 (0.50)	1.51 (0.92)	2.96 (0.41)	4.43 (0.63)	5.53 (0.50)	6.44 (0.34)	6.04 (0.39)	6.08 (0.47)
	6	5.69 (0.60)	1.27 (0.88)	2.81 (0.60)	4.69 (0.77)	5.68 (0.62)	6.34 (0.45)	5.96 (0.52)	6.11 (0.59)
	8	5.78 (0.50)	1.31 (0.91)	2.68 (0.57)	4.01 (0.80)	5.04 (0.71)	5.82 (0.54)	5.52 (0.59)	5.66 (0.63)
	10	5.79 (0.45)	1.41 (0.98)	3.18 (0.33)	4.83 (0.58)	5.71 (0.49)	6.49 (0.33)	6.00 (0.41)	6.03 (0.52)
	20	5.78 (0.46)	1.27 (0.66)	2.97 (0.43)	4.35 (0.68)	5.53 (0.53)	5.88 (0.49)	5.30 (0.58)	5.60 (0.59)
	50	4.96 (0.59)	1.59 (0.95)	3.41 (0.27)	5.21 (0.45)	6.06 (0.38)	6.52 (0.34)	6.05 (0.40)	5.78 (0.51)
	100	4.93 (0.61)	1.54 (0.22)	3.67 (0.22)	3.69 (0.72)	5.47 (0.50)	6.54 (0.35)	5.68 (0.48)	5.62 (0.54)
Two Layers	**2:2**	6.69 (0.48)	1.15 (0.89)	3.43 (0.31)	5.81 (0.55)	6.57 (0.50)	6.94 (0.45)	6.68 (0.48)	7.03 (0.53)
	4:4	6.04 (0.62)	1.22 (1.00)	3.42 (0.23)	6.06 (0.28)	6.79 (0.25)	7.13 (0.22)	6.66 (0.31)	6.76 (0.43)
	5:5	5.31 (0.60)	1.25 (0.74)	3.05 (0.41)	4.48 (0.67)	5.27 (0.62)	6.04 (0.47)	5.54 (0.54)	5.81 (0.58)
	10:10	5.53 (0.56)	1.30 (0.87)	3.09 (0.41)	4.49 (0.70)	5.24 (0.64)	6.05 (0.47)	5.69 (0.53)	5.81 (0.58)
	20:20	5.70 (0.47)	1.37 (0.61)	2.96 (0.43)	4.12 (0.44)	5.10 (0.59)	6.03 (0.43)	5.51 (0.51)	5.95 (0.49)
	50:50	5.48 (0.51)	1.51 (0.95)	3.23 (0.32)	4.10 (0.67)	5.07 (0.60)	6.00 (0.44)	5.66 (0.47)	5.80 (0.51)
	100:100	4.40 (0.68)	1.72 (0.77)	3.21 (0.34)	4.61 (0.55)	6.70 (0.29)	7.21 (0.24)	5.84 (0.44)	5.47 (0.56)

7.7.1 Analysis

The results shown in **Tables 7.13** to **7.16** will be analysed for different "window" sizes, and the ANN architecture in order to select the optimum parameters for the trained ANN model. This trained ANN model will be evaluated using the data from 14th and 21st Nov 2005.

7.7.1.1 "Window" Size

From the four tables, it can be seen that, generally, the retrieval results deteriorate as the "window" size increases. For example, the accuracies deteriorate from 2.44%v/v to 5.53%v/v when the "window" size increases from 2km×2km to 8km×8km (**Table 7.13**). This is due to the inability of the ANN to capture the variability within the larger "window" size. For the combination of TbH and TbV (**Table 7.13**), the largest "window" size where the ANN can obtain the globally acceptable error of less or equal than 4%v/v is 4km×4km with the number of hidden neurons being 20, 50 and 100 for both single and two hidden layers. When the inputs consist of TbH, TbV and NDVI (**Table 7.14**), with a single hidden layer of 20 neurons and two hidden layers of 10 hidden neurons in each layer (10:10), the ANN achieves an acceptable error at the largest "window" size of 4km×4km. The same optimum "window" size is obtained for the case of TbH, TbV and Ts (**Table 7.15**) as inputs and for a single layer of 100 hidden neurons using all four parameters as inputs, i.e. TbH, TbV, NDVI and Ts (**Table 7.16**). As a result of this work, the optimum "window" size will be 4km×4km.

7.7.1.2 ANN Architecture

By looking at the column for 4km×4km "window" size, a decision can be made on the number of inputs and hidden layers and neurons. The lowest RMSE obtained for the "window" size of 4km×4km is 2.79%v/v (R^2 = 0.84) with two hidden layers of 50 neurons in each layer when TbH, TbV and Ts were used as input (**Table 7.15**). For the same "window" size, the use of only TbH and TbV as input results in a RMSE of 2.86%v/v (R^2=0.88) using a single hidden layer of 20 neurons. More hidden neurons used show that the relationship between the inputs and the output is complex. Although this RMSE is slightly higher than the lowest RMSE obtained when Ts is added, fewer resources are needed if the inputs used only consist of the dual-polarized brightness temperature. Moreover, according to Vonk *et al.* (1997) less complex neural networks are preferred over complex ones, providing

they have similar performance. Therefore, a single hidden layer of 20 hidden neurons is preferred compare to two hidden layers of 50 neurons in each layer. **Figure 7.8** shows the graph of the RMSE obtained when different combinations of inputs are used with this architecture. From this graph, it is clearly seen that TbH and TbV give the best RMSE value. The use of the ancillary information does not aid much in improving the accuracy of the retrieval. This might be because the data used for these two dates are not totally cloud free.

The ANN architecture chosen will be of two inputs (TbH and TbV), a single hidden layer of 20 neurons and 1 output.

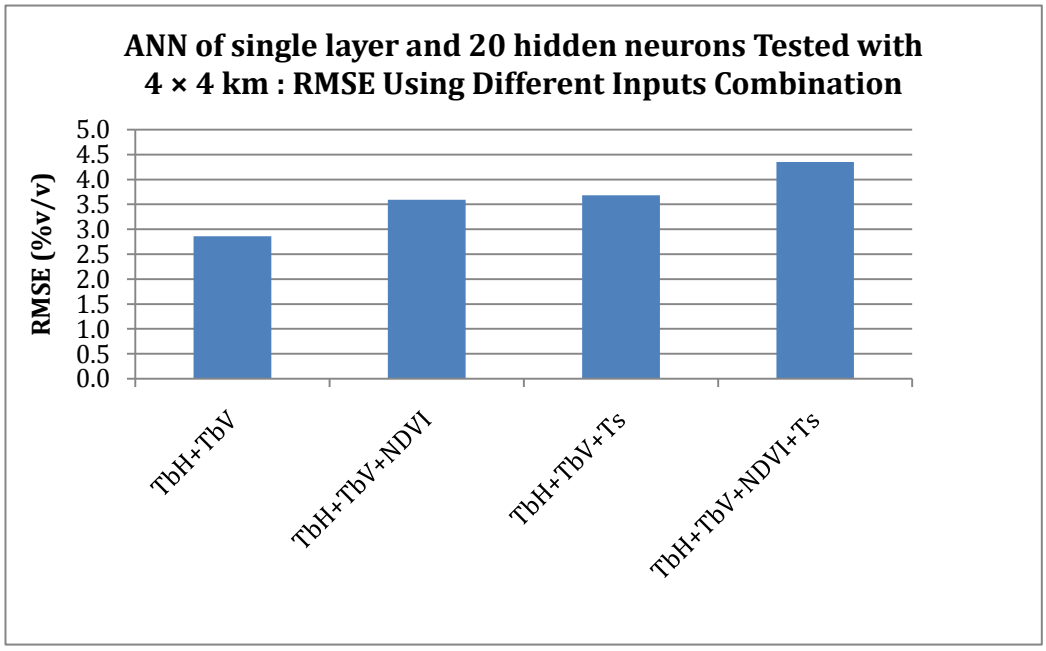

Figure 7.8. Comparison between different combinations of inputs for a single layer ANN with 20 hidden neurons and verification on 4km×4km pixels.

7.8 Testing: Evaluation Cases

With the architecture (number of neurons and hidden layer and the number of inputs) and the defined "window" size, the ANN is evaluated using the data of 14th and 21st Nov 2005. The condition of the field is totally different during the evaluation dates. The mean and standard deviation for each date are given in **Table 7.17**, showing that the training data on 7th November 2005

is "wetter" compared to the verification cases on 14th and 21st November 2005.

After the ANN is trained using the data of date 7th Nov 2005, the ANN is evaluated. During the evaluation, the prediction process is carried out at each "window" of 4km×4km. This "window" starts from the top left corner of the target area moving to the right, down and to the end of the image.

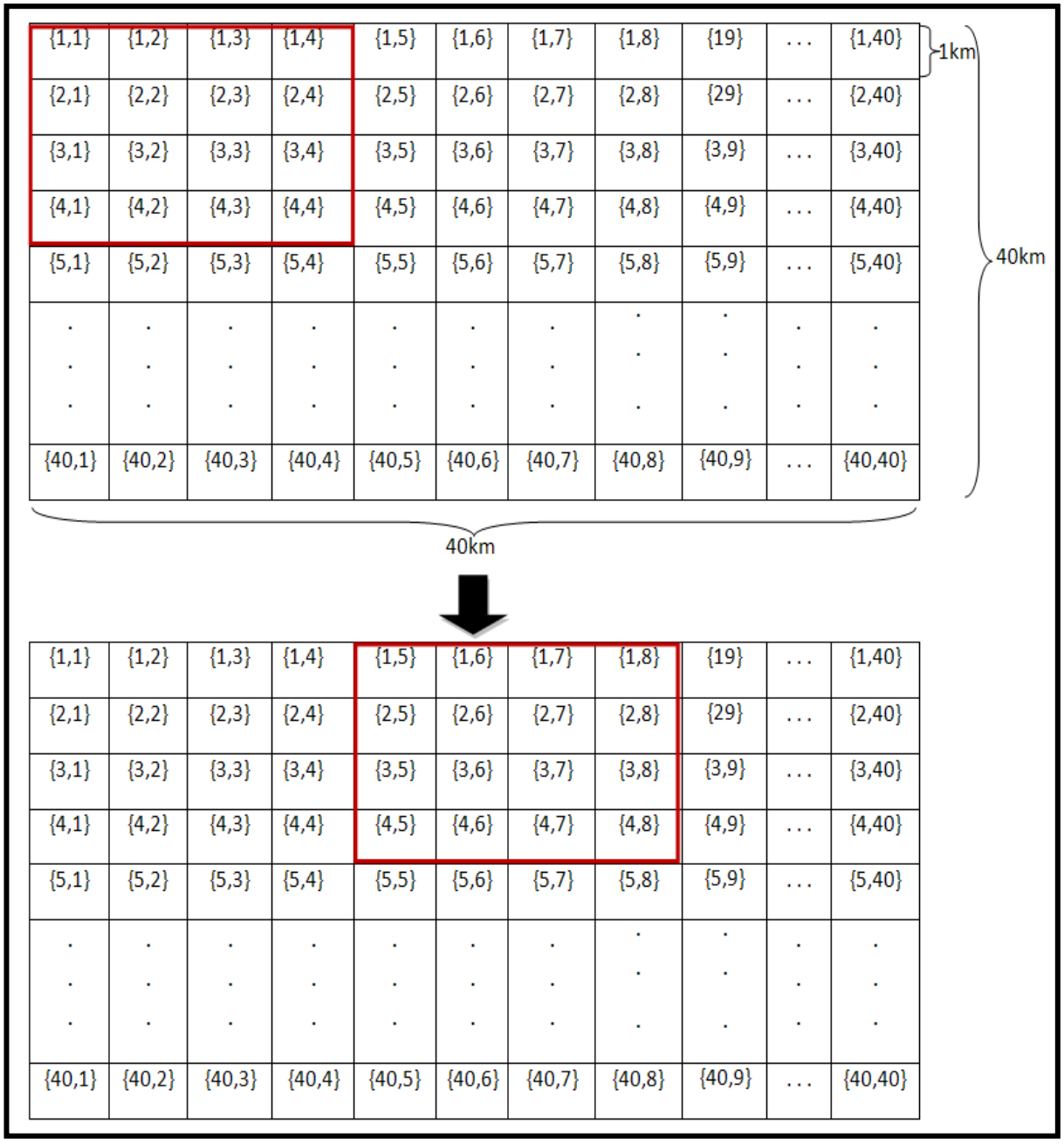

Figure 7.9. The start position of the 4km×4km "moving window" and its position after one move in the horizontal direction.

Table 7.17. Statistical mean and standard deviation for the dual polarized brightness temperature and soil moisture values used for training (7th Nov) and evaluation (14th Nov and 21st Nov).

Date	TbH (K)		TbV (K)		Soil Moisture (v/v)	
	Mean	Standard deviation	Mean	Standard deviation	Mean	Standard deviation
7th Nov 05	241.5	10.1	261.4	7.8	0.39	0.12
14th Nov 05	266.0	6.5	279.3	5.4	0.18	0.10
21st Nov 05	271.3	3.9	282.6	3.1	0.16	0.08

Figure 7.9 shows the start position of the 4km×4km "moving window" and the position of the window after one step of horizontal movement. The mean and standard deviation of the soil moisture within the window will be used as the de-normalization factors for the corresponding output of the ANN model.

Using this methodology, the RMSE values between the actual and predicted value were 3.9 %v/v with $R^2 = 0.85$for the 14th and 3.4%v/v with $R^2 = 0.81$for the 21st November 2005. The actual and predicted soil moisture maps are shown in **Figure 7.10a** and **Figure 7.10b** while the correlation relationships are shown using scatter plots in **Figure 7.11**. It can be seen from the soil moisture variation map (iii. of **Figure 7.10**) that the maximum difference between the actual and predicted soil moisture was 0.24 v/v. The locations where such large differences happened were very few. The correlation coefficients chart shows that the predicted and actual soil moisture values are highly correlated.

From this, it can be concluded that, with the use of TbH and TbV as inputs, the ANN manages to capture the variability of soil moisture by incorporating the use of mean and standard deviation of soil moisture as the normalization factors for the ANN and prediction process, which is divided into each defined "window" size.

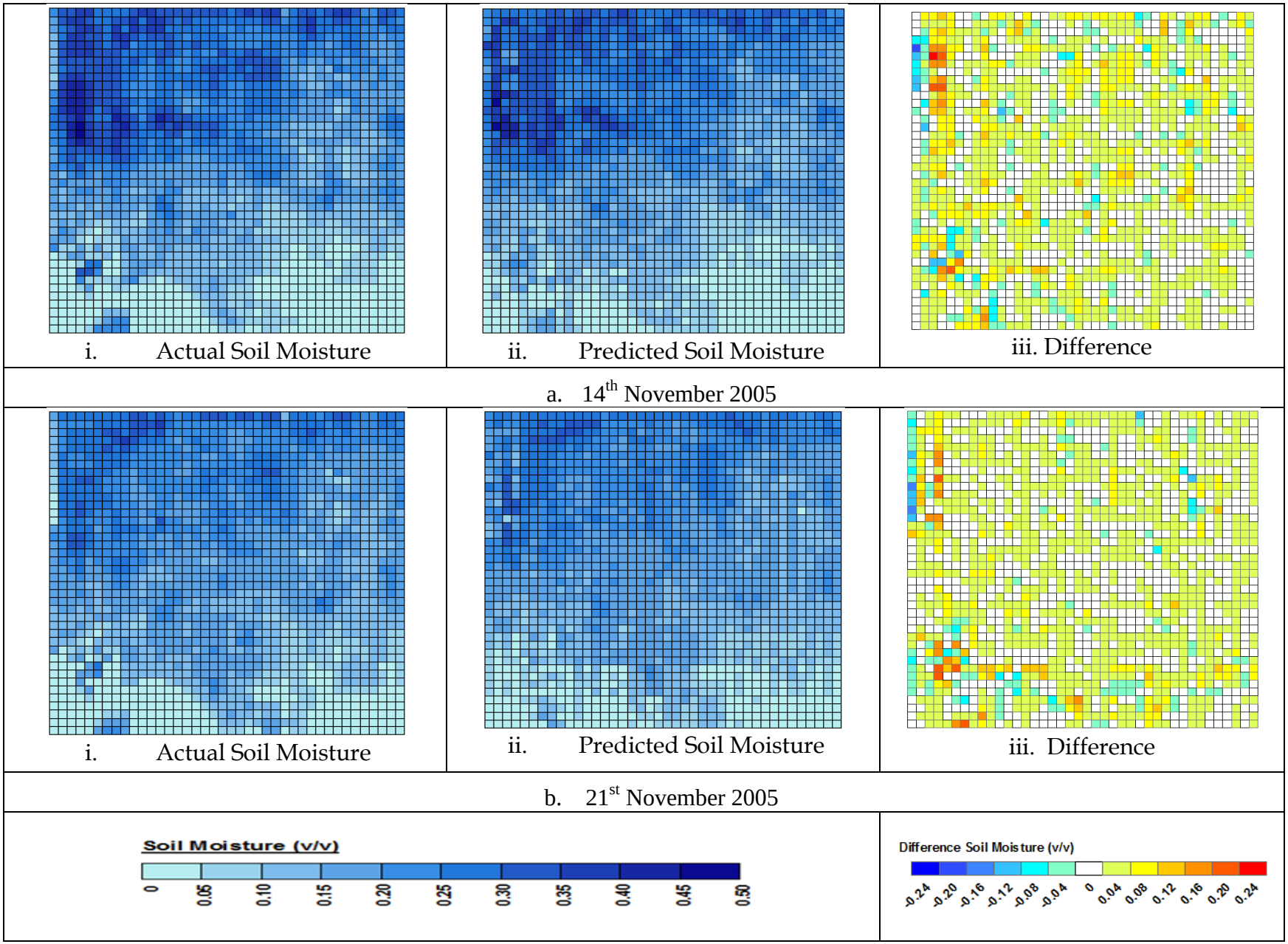

Figure 7.10. Actual and predicted soil moisture map at 1 km resolution on a. 14th November 2005, and b. 21st November 2005.

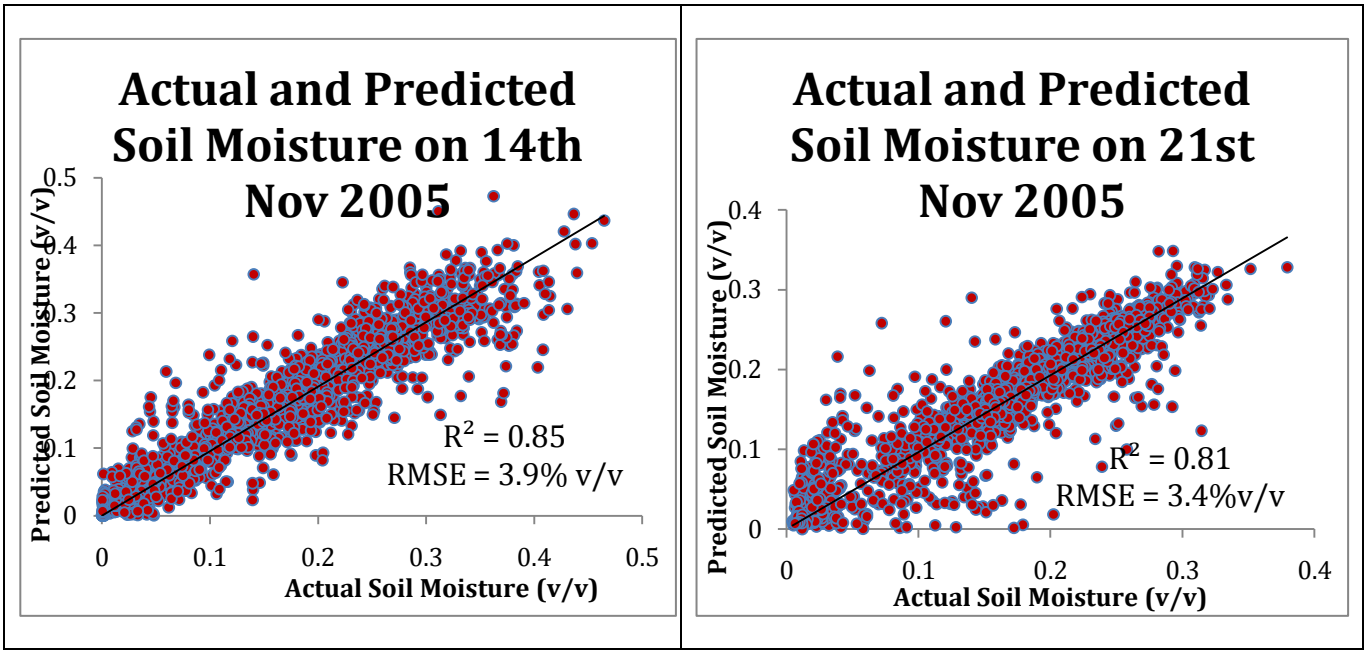

Figure 7.11. Actual and predicted soil moisture map at 1km resolution on a. 14th November 2005, and b. 21st November 2005.

7.9 Methodology Verification

As the proposed methodology requires the mean and standard deviation within a specific "window" size, the dependency of these values on the applicability of the ANN model for practical use is needed to be verified. Moreover, the use of different normalization factors is needed to be justified. To verify the use of different normalization factors and the prediction process within the defined "window", a series of experiments were conducted. These are explained in the following sections.

7.9.1 Same Normalization Factors

In the first experiment, the general way of applying the same normalization factors from the training data are conducted. The ANN, trained using data of 7th Nov 2005, consisting of 2 inputs, 1 hidden layer of 20 neurons and 1 output is used (see **Section 7.8)**. The verification is divided into two categories: (i) without "window" and (ii) with "window". For the category without "window", the retrieval of soil moisture will be done for

the whole study area of 40km×40km. Each 1km×1km cell is evaluated in a raster fashion from top left to bottom right. For with "window", the cell from each "window" is evaluated in a raster fashion from top left to bottom right inside the window. During the verification of these two categories, the data are normalized using the same factors obtained from the training data (7th Nov 2005). The overview of this testing is shown in **Figure 7.12.** From this figure, it can be seen that the data on 7th Nov 2005 is divided into training, validation and testing. For training set, the normalization and de-normalization factors are obtained from the inputs and output of the data. This is the same for the validation and testing data. The training, validation and testing data are used to develop a trained ANN model. This trained model is next evaluated using data from 14th and 21st Nov 2005. The normalization factors for these evaluation sets are obtained from the training data. As discussed earlier, to verify the methodology, two categories of the testing are carried out (**Figure 7.12**). The results are shown in **Table 7.18.** For **Category I: Without "window"**, the retrieval accuracy is calculated for the whole 40km×40km target area, while for **Category II: With "window"**, the retrieval accuracy the average of accuracy for each of the "window" for the whole 40km×40km target area.

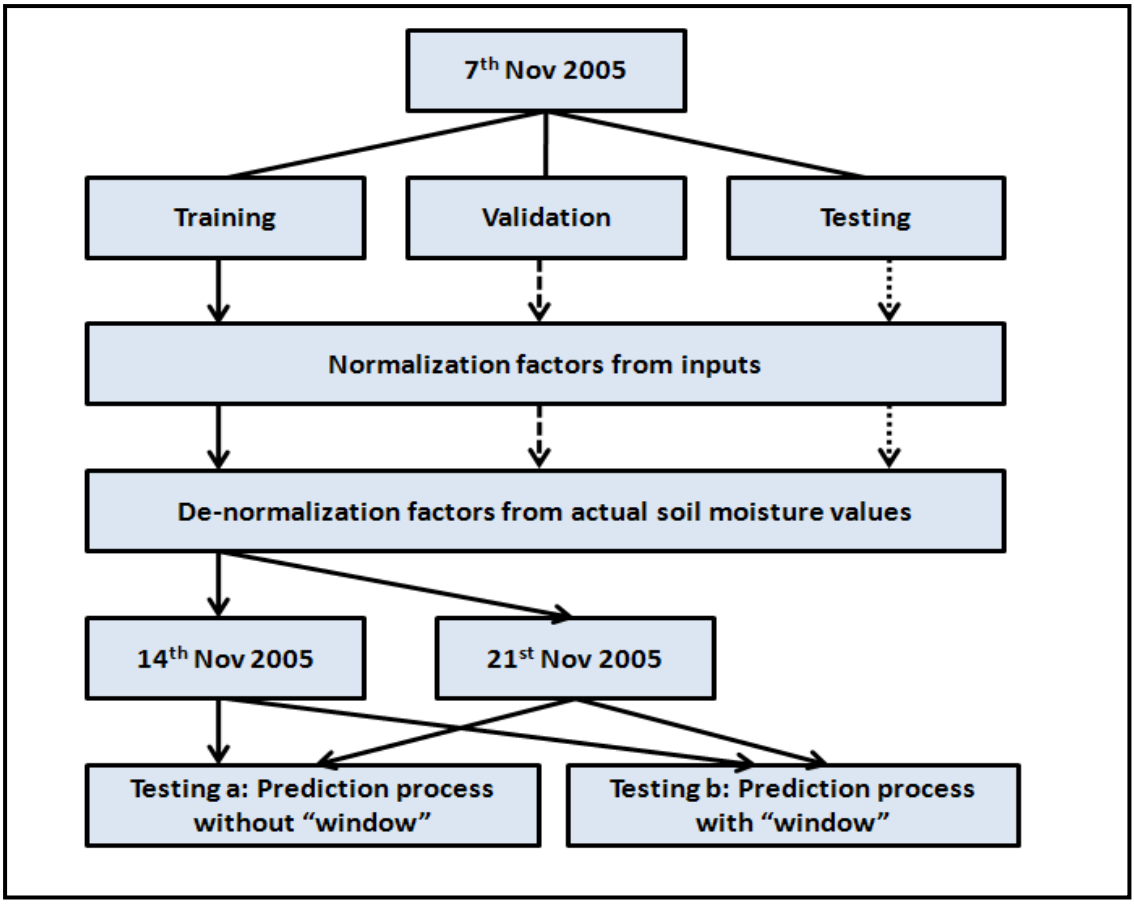

Figure 7.12. Process of verifying the methodology for using different normalization factors and regions.

Table 7.18. Results of using the same normalization factors from the training data for cases of with and without "window".

Category I : Without " Window"		
Date	RMSE (%v/v)	R^2
14th November 2005	6.1	0.78
21st November 2005	8.8	0.53
Category II : With "Window"		
Date	RMSE (%v/v)	R^2
14th November 2005	6.1	0.78
21st November 2005	8.8	0.53

The RMSE and R^2 values for each categories at each evaluation date are shown in **Table 7.18**. From **Table 7.18**, it is clear that with same normalization factors across the dates, the retrieval accuracy was around 6.1

to 8.8%v/v, which was worse than the desired target error. The retrieval accuracies for either using or not the "window" show the same values as expected because the two evaluation methods are identical in terms of the processing for each cell.

7.9.2 Different Normalization Factors

To verify whether the conclusion from **Section 7.9.1** stands, a further analysis is carried out using different normalization factors for each evaluation date. In this case the retrieval of the 1km resolution soil moisture is done for the whole 40km×40km at once, i.e. without "moving window". For this experiment, the temporal variation is captured using the different normalization factors but the spatial variation is neglected (i.e. without the use of the "moving window"). The results of this experiment are shown in **Table 7.19**. From **Table 7.19**, it can be seen that, the retrieval accuracy is improved (comparing to **Table 7.18**), although it is still worse than the desired retrieval accuracy of 4%v/v .

Table 7.19. Results of using different normaliization factors without different regions within the 40km×40km target area (compare to **Table 7.18**).

Date	RMSE (%v/v)	R^2
14th November 2005	5.5	0.72
21st November 2005	4.6	0.65

7.10 Dependency: Accuracy of Mean and Standard Deviation Values

Prior information required by this proposed methodology are the mean and standard deviation of the soil moisture at each of the 4km×4km "windows". While this research initially assumed such information was equal to the values calculated from the actual soil moisture within the "window", such data will not be available in practice, and the mean and standard deviation of soil moisture within the "window" will need to be estimated by alternative

methods. Consequently, the sensitivity of results to the accuracy of these values needs to be assessed. In the past, retrieval of land surface parameters using passive microwaves had utilized a multiple linear-regression method (Njoku and Li 1999). If we assume a linear relationship between the input variables and the soil moisture, then a regression model can be used to predict the values of soil moisture used for normalization and hence act as a surrogate. Therefore, a multiple linear-regression method is investigated to estimate the soil moisture values using TbH, TbV, NDVI and Ts values.

For each of the evaluation dates (14th and 21st Nov 2005), 18 data samples (1%) of the data are randomly selected for the regression. The rationale behind the small number of data selected is to simulate a situation where these data are ground-truth samples. With more data selected, the regression formula will be more accurate, but at the same time, more sample points will need to be taken if ground sampling has taken place. The RMSE and R^2 between the actual and regressed soil moisture values are shown in **Table 7.20**. The regressed soil moisture values are correlated to the actual soil moisture with $R^2 \geq 0.50$, and the RMSE values are more than 4%v/v.

Table 7.20. Comparison of RMSE and R^2 for the regressed and actual soil moisture values.

Date	RMSE (%v/v)	R^2
14th November 2005	8.3	0.77
21st November 2005	6.0	0.70

The trained ANN, as in **Section 7.8,** is evaluated using the regressed soil moisture values. The results are given in **Table 7.21.** The predicted soil moisture values using the ANN produce errors that are similar to the error between the regressed and actual soil moisture values. The results show that the accuracy of the predicted soil moisture with this methodology depends highly on the mean and standard deviation values used.

Table 7.21. The RMSE and R^2 values obtained using the ANN.

Date	Regressed and Predicted SM		Actual and Predicted SM	
	RMSE (%v/v)	**R^2**	**RMSE (%v/v)**	**R^2**
14th November 2005	4.2	0.66	7.8	0.67
21st November 2005	1.4	0.92	5.8	0.53

7.11 Conclusions

This chapter has presented a methodology that captures the temporal variability of soil moisture using different normalization factors and spatial variability using a "window" method, yielding soil moisture retrieval with an acceptable error. The effects of using different normalization factors both with and without a "window" are also shown and discussed. Compared to the general ANN application for soil moisture retrieval, the combination of these two methods has solved the problem of "out-of-range" conditions when the trained ANN is used to retrieve results for future data, which are totally new and not previously "seen" by the ANN during the training process. The "out-of-range" problem is mainly due to the inability of the ANN to capture the spatial and temporal variability of the soil moisture. Temporal variability is a common condition in soil moisture prediction problems when the prediction is needed on a different date to that used in the training process, as it is not easy to cover all the conditions during the training. Spatial variability occurs as soil moisture values can vary greatly even within a square metre. For temporal variability, the trained ANN model is able to predict soil moisture of an unknown future date which is almost certain to have a pattern different from the training data ("out-of-range" condition). For spatial variability, the ANN model is shown to be able to predict soil moisture for each cell at different 1km locations on the 40km×40km study area.

Despite the encouraging results, the main challenge of this method is the estimation of the variability in terms of the mean and standard deviation of the soil moisture at the optimum window size as the de-normalization factors for the ANN. The actual soil moisture values will not be available for future dates so some means of predicting them or using surrogate is needed. In this thesis, the mean and standard deviation within a pre-determined window size is calculated using the actual soil moisture values within the window. A method of predicting the soil moisture values from input data for de-normalization is evaluated using multiple linear-regression. The soil moisture values are regressed using the TbH, TbV, Ts and NDVI with a selected number of samples and the mean and standard deviation values within the window are calculated with the regressed soil moisture values. The results show that, the proposed approach depends greatly on the accuracy of the mean and standard deviation of the soil moisture values. Therefore, the practicality of this method depends on a highly accurate method in retrieving the mean and standard deviation of the soil moisture values within the optimum window size.

Chapter 8

Downscaling of Soil Moisture

Downscaling procedures offer the possibility that the desired fine scale statistical properties of soil moisture fields can be inferred from coarse-scale data. A novel approach using an ANN to downscale soil moisture is presented in this chapter. An introduction to the problem of downscaling has been presented in **Section 5.3.2** and the general methodology used for downscaling in this research was outlined in **Section 5.4.2.** In the literature, the term disaggregation is used to refer to downscaling and hence, in this chapter, the word downscaling and disaggregation can be regarded as interchangeable.

8.1 Overview

The basic principle of the proposed methodology in capturing the spatial and temporal variability of soil moisture in **Section 7.2** is also used for the downscaling of soil moisture retrieval. For the purposes of this study, the downscaling scale is from 20 km to 1 km. The linear relationship between the soil evaporative efficiency and near surface soil moisture approach by Merlin *et al* (2008b) is adopted in this study and is discussed below. This relationship is incorporated into the ANN model that will be used for downscaling purposes. A description of this relationship is first presented, followed by outlining how this relationship is incorporated into the ANN model. Different results of testing and verification of this methodology are presented.

8.2 Soil Evaporative Efficiency and Near Surface Soil Moisture

This section of the thesis will explore the approach by Merlin *et al.* (2008b).

8.2.1 Deterministic Downscaling Approach

A deterministic approach for downscaling of soil moisture from ≈40 km resolution SMOS observations was developed from 1 km resolution MODIS data by Merlin *et al.* (2008b). The disaggregation scale was fixed at 10 km. In further work, Merlin *et al.* disaggregated microwave-derived soil moisture from 40 km to 4 km using MODIS data with a resulting RMSE of 2.6% v/v (Merlin *et al.* 2009). The 1 km resolution airborne L-band brightness temperatures from the NAFE 2006 experiment were used to generate a time series of eleven clear sky 40 km by 60 km near-surface soil moisture observations to represent SMOS pixels across the three-week experiment. The NAFE 2006 experiment was similar to the NAFE 2005 experiment but covered a different site. The overall RMSE between downscaled and observed soil moisture varies between 1.4% v/v and 1.8% v/v with soil moisture values ranging from 0 to 15% v/v.

The linear relationship derived from MODIS by Merlin *et al.* (2008b) and physically-based model predictions of soil evaporative efficiency is:

$$\theta = \theta_{SMOS} + \theta_C \frac{\Delta\beta_{MODIS}}{\mathbf{1} - \beta_{MODIS}} \tag{8.1}$$

where:

θ	downscaled soil moisture
θ_{SMOS}	SMOS-scale soil moisture
β_{MODIS}	MODIS-derived soil evaporative efficiency
$\Delta\beta_{MODIS}$	difference between MODIS-derived soil evaporative efficiency and its integrated value at the SMOS scale ($\int d\beta/d\theta \, d\theta$)
θ_C	characteristic volume fraction

$\Delta\beta_{MODIS}$ is calculated using:

$$\beta_{MODIS} = \frac{T_{max} - T_{MODIS}}{T_{max} - T_{min}} \tag{8.2}$$

where:

T_{max}	soil temperature at minimum soil moisture
T_{min}	soil temperature at maximum soil moisture
T_{MODIS}	soil skin temperature derived from MODIS data at the time of interest

T_{MODIS} is calculated using the triangle approach (Price 1980; Carlson *et al.* 1995):

$$T_{MODIS} = \frac{T_{surf,MODIS} - f_{veg}T_{veg}}{1 - f_{veg}} \tag{8.3}$$

where

$T_{surf,MODIS}$	MODIS surface skin temperature
T_{veg}	vegetation skin temperature
f_{veg}	vegetation fraction cover

and the vegetation fraction cover, f_{veg} is defined as:

$$f_{veg} = \frac{NDVI_{MODIS} - NDVI_{min}}{NDVI_{max} - NDVI_{min}} \tag{8.4}$$

where:

$NDVI_{MODIS}$	MODIS observed NDVI
$NDVI_{\min}$	minimum NDVI values for a particular scene
$NDVI_{\max}$	maximum NDVI values for a particular scene

In the study by Merlin *et al.* (2008b), the $NDVI_{\min}$ and $NDVI_{\max}$ were assumed to be constant over time within the study area, T_{veg} , T_{max} , T_{min} were assumed to be uniform within the study area but varying over time. Parameters $NDVI_{\min}$ and $NDVI_{\max}$ were determined from the 16-day NDVI product within the SMOS pixel. Vegetation temperature T_{veg} was estimated at the time of overpass (10.00am. or 1.00pm.) as the minimum temperature

reached at maximum *NDVI* (f_{veg}=1). Minimum temperature T_{min} was used as it could be estimated either over fully vegetated pixels by assuming $T_{\min} \approx T_{veg}$ or over water bodies as the minimum temperature reached at minimum *NDVI*. Parameter T_{max} was the value extrapolated along the dry edge of the triangle. A typical $NDVI / T_{surf,MODIS}$ scatter plot is shown in **Figure 8.1.** The upper edge of the triangle is defined as dry-edge.

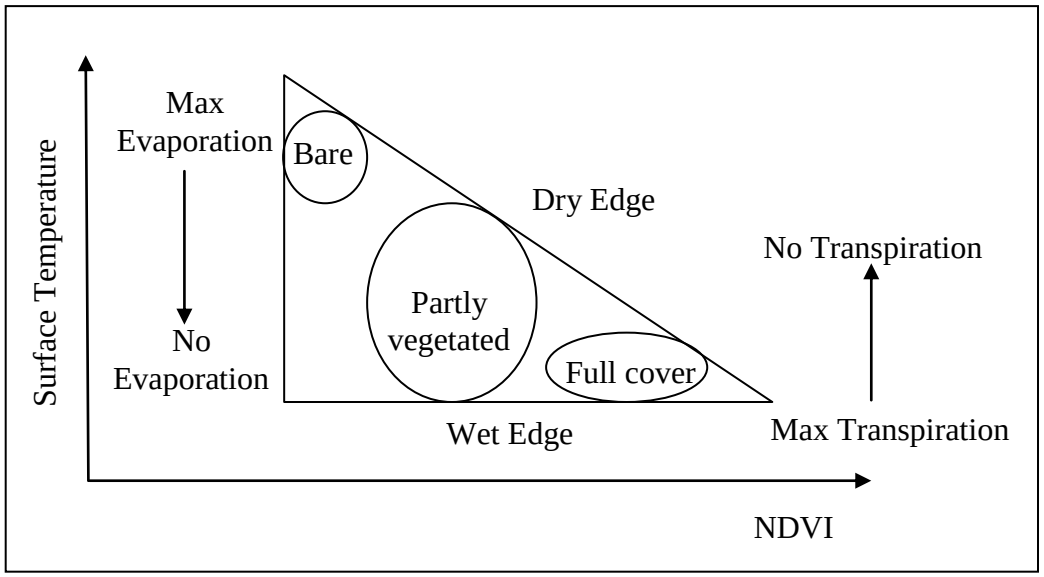

Figure 8.1. Simplified NDVI/Surface temperature space (Lambin and Ehrlich 1996).

Equation (8.1) can be further simplified to:

$$\theta = \theta_{SMOS} + \theta_C SMP_{MODIS} \tag{8.5}$$

with:

$$SMP_{MODIS} = \frac{\Delta\beta_{MODIS}}{1 - \beta_{MODIS}} \tag{8.6}$$

From Equation (8.2), by assuming that T_{max} and T_{min} are mostly uniform within the SMOS pixel and the integral $\int dT/d\theta \, d\theta$ is approximately equal to the areal average of T_{MODIS} (designated as T_{SMOS}), SMP_{MODIS} can be computed as:

$$SMP_{MODIS} = \frac{T_{SMOS} - T_{MODIS}}{T_{MODIS} - T_{min}} \tag{8.7}$$

The characteristic water fraction θ_C is computed as:

$$\theta_c = \theta_{c0}(1 + \gamma / r_{ah}) \tag{8.8}$$

where: θ_{c0} (% v/v) and γ (s/m) are two soil dependent parameters and r_{ah} (s/m) is the aerodynamic resistance over bare soil, given the roughness and the wind speed at a reference height of 2 m. The empirical parameter θ_{c0} controls the soil's capacity to retain moisture under optimal evaporative conditions, i.e. when wind speed is zero or r_{ah} is infinite. In other words, the higher θ_{c0} is, the slower the soil dries.

8.3 The ANN Downscaling Approach

In order for the ANN to learn the downscaling relationship in Equation (8.5), the ANN will need three values as input: θ_{SMOS}, θ_C and SMP_{MODIS} and the output of soil moisture at desired downscaled resolution, θ. The value of θ_{SMOS} is obtained by aggregating the soil moisture value at the desired resolution from the L-band derived soil moisture value. The value of SMP_{MODIS} is calculated from the MODIS/Aqua Land Surface Temperature and Emissivity Daily L3 Global (1 km resolution) data to derive the $T_{surf,MODIS}$, T_{SMOS}, T_{max} and T_{min} values. The values for $NDVI_{\min}$ and $NDVI_{\max}$ are derived from Band 1 and Band 2 of the MODIS/Aqua Surface Reflectance Daily L2G Global (250m resolution) data. The value of θ_C depends on the value of wind speed and is soil dependent but is unavailable for the NAFE'05 data used in this study. In this study, the ANN is used to learn the relationship between θ, θ_{SMOS} and SMP_{MODIS} without the value of θ_C and maps a function between these three variables through the learning process

for the ANN. The ANN will calibrate the values of θ_C in the relationship mapped between the θ, θ_{SMOS} and SMP_{MODIS}.

An analogy for this phenomena is a set of data of a function $y = mx + 3$. For a particular situation, let the value of $m = 2$. By supplying the values of x and the value 3 as the inputs, and the calculated y values for the corresponding x values, the ANN can map a function between the inputs and output using a linear model. This simple scenario becomes more complicated when m is a parameter, which is dependent on other factors, i.e. the value of m will change. The value of θ_C is related to wind speed and two soil dependent parameters, and hence the "complicated" scenario in the analogy happens when this linear relationship is adopted in the ANN model without having the value of θ_C.

Figure 8.2 shows the summary of the steps carried out in this downscaling study. This follows the general downscaling approach as presented in **Section 5.4.2**.

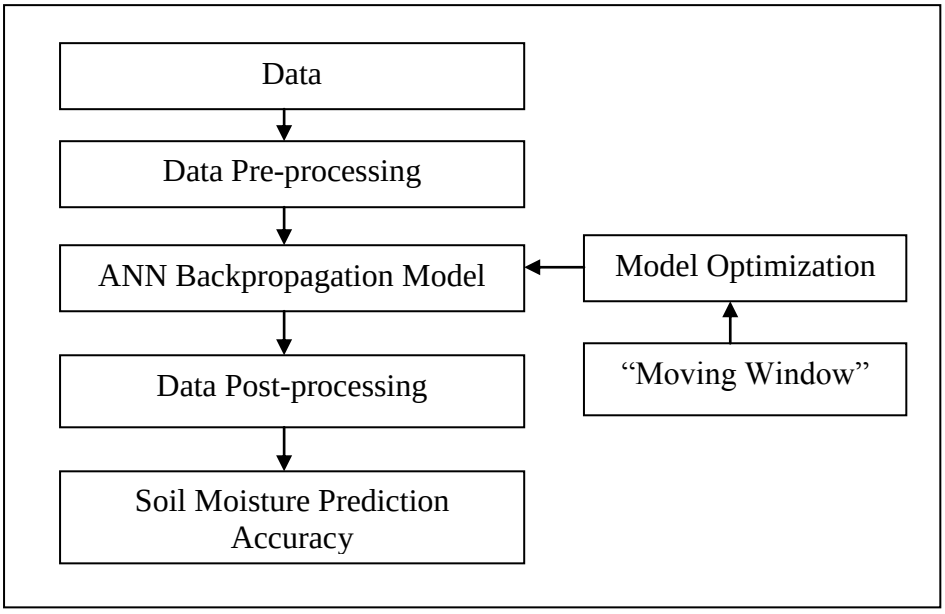

Figure 8.2. The general process in the proposed methodology used in this downscaling study.

8.3.1 Data Preparation

As the NAFE'05 field experiment was carried out over a single area of 40km × 40km, downscaling from 40 km to 1 km will result in the input of the ANN with a constant value of θ_{SMOS} together with 1600 different values of SMP_{MODIS} to predict 1600 different soil moisture θ values at 1 km. As constant values of θ_{SMOS} fail to provide useful information, to avoid this, the area of 40km × 40km is further divided into 20km × 20km "grids". The 20km × 20km grids (each called "20 km area" hereafter) are chosen to cover as much as possible the whole 40km × 40km study area. In order to have more θ_{SMOS} data, it would be better to have as many as possible 20 km areas so that the ANN can better learn the relationship. However, there is no rule of thumb for how large the data should be. Therefore, for the purpose of this study, seven 20 km areas are selected. In order to cover as much as possible the whole study area, the easiest way is to divide the study area into the four 20 km area of Grid 1 to Grid 4 of **Figure 8.3**. Another three 20 km areas are defined by choosing areas which overlap the underlining four grids. Although there may be reasons for deciding on which areas to choose as the overlapping ones, the three extra ones were randomly selected. This is shown as Grid 5 to 7 in **Figure 8.3**. From the seven 20 km areas selected, all seven areas are used for the training phase while for evaluation purpose, only Grid 1 to Grid 4 are used. The 1 km soil moisture product within the 20 km area is aggregated to form the coarse scale soil moisture value (20 km resolution).

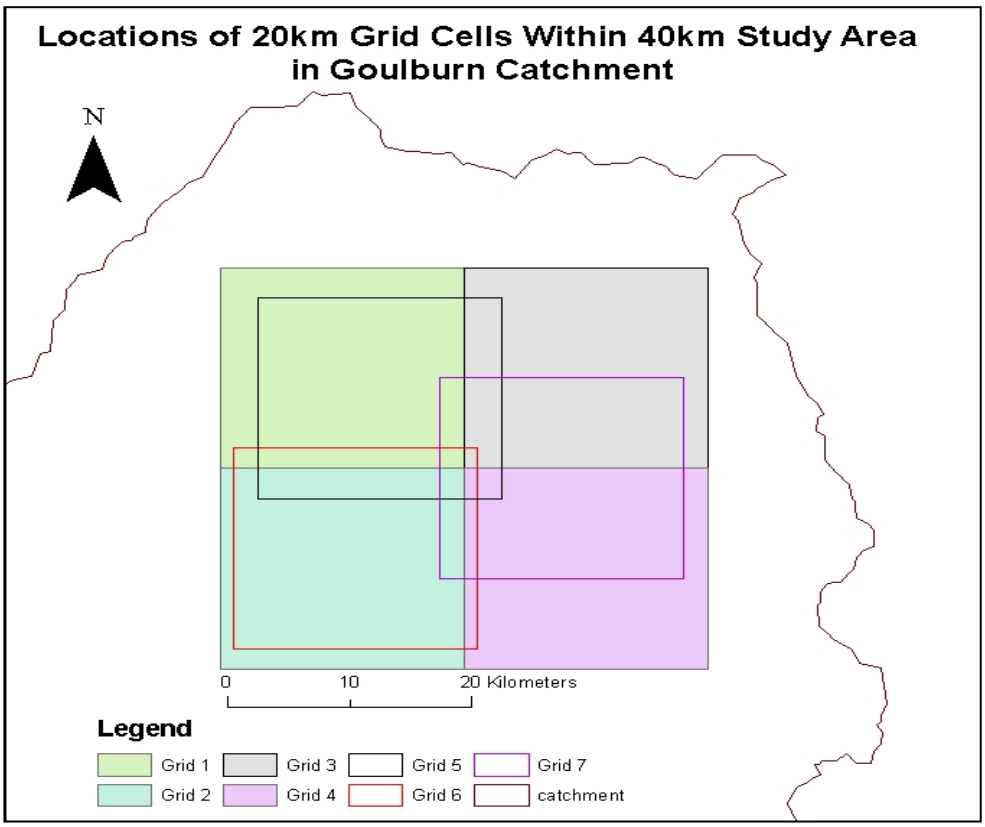

Figure 8.3. Locations of the seven selected 20 km areas on the 40km×40km study area.

8.3.1.1 Data Division: Training, Validation and Testing Sets

The regional data acquired on 7th, 14th and 21st Nov 2005 are used (see **Section 6.1**). For each of the 20 km areas, there will be one similar θ_{SMOS} value for all the 400 SMP_{MODIS} values at 1 km resolution. During the training phase, the data on the 7th November 2005 are used. With the 2800 data points available on this date, 140 or 5% of the data is randomly selected (again using the MATLAB random number function previously mentioned) for each of validation and testing sets while the remaining 90% of the data are kept for training. The data on the 14th and 21st November 2005 are kept as the evaluation cases. The data division process is shown using a schematic diagram in **Figure 8.4**.

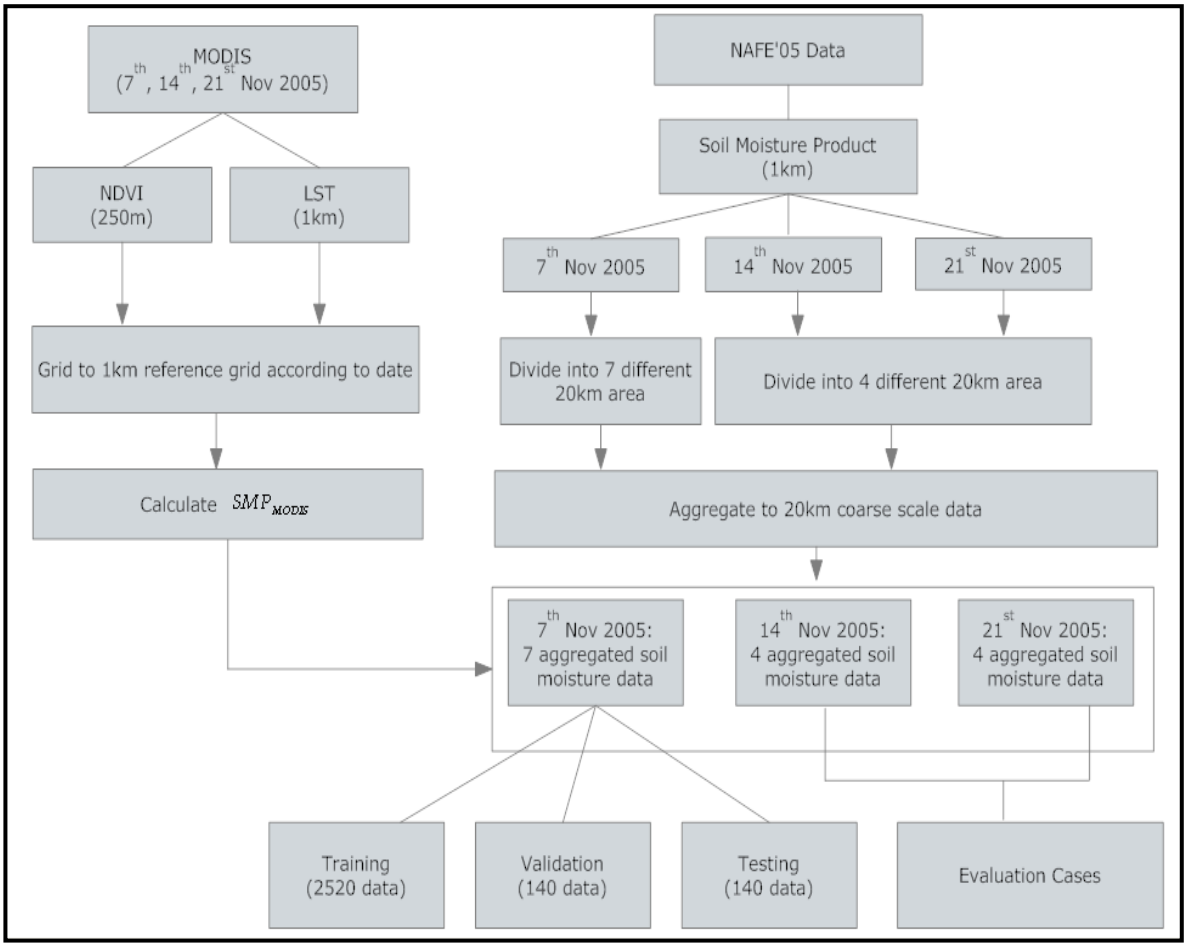

Figure 8.4. Schematic diagram showing the data division process for the downscaling methodology.

8.3.2 ANN Architecture

The inputs of the ANN are θ_{SMOS} and SMP_{MODIS}, while the output is θ. The number of nodes in the input and output layers are determined by the number of input and output parameters. However, a decision needs to be made regarding the number of hidden layers and the number of hidden neurons in each of the hidden layers. The Broyden-Fletcher-Goldfarb-Shanno (BFGS) training algorithm is used, which gave the best results for soil moisture retrieval (**Section 7.1.1**).

The details of the neural network parameters used in this study are given in **Table 8.1**.

Table 8.1. The training parameters for the BFGS training algorithm.

Performance goal	0.001
Maximum number of epochs to train	1000
Minimum performance gradient	1e-10000
Maximum validation failures	100

8.3.3 Data Pre and Post-processing for ANN

The justification and procedures for the process of normalization have been presented in **Section 3.3 and 7.2.2**. The mean and standard deviation values are used as the normalization and de-normalization factors (**Section 7.2.2** and **7.2.3**, **Figure 7.5**).

8.3.4 Window Size Selection

To select the optimum window size, i.e. size when the desired disaggregation accuracy is at most 4% v/v, the data on 7th Nov 2005 is used in the training phase while Grid 1 of 14th Nov 2005 is used for the evaluation phase. This is shown in **Figure 8.5.** Not all the grids of 14th Nov 2005 are used as this is a process of selecting the window size. Moreover, those grids, which are not used will be useful to evaluate the ability of the trained ANN model on unseen data. Increasing "window" sizes are assessed: 2km×2km , 3km×3km and so on. The grid cells for 2km×2km window are: {A1, A2, B1, B2} while the grid cells for the 3km×3km window are {A1, A2, A3, B1, B2, B3, C1, C2, C3} which means that the window of size 2km×2km is the subset of the window size of 3km×3km (**Figure 8.6**). The same relationship exists between the window sizes of 3km×3km, 4km×4km and 5km×5km and so on. With such relationships, the variances of the results obtained, if any, are caused by the new cells in the larger window. Moreover, the new cells added in the larger windows are close to the smaller sub-set of the larger window. The topography, land uses, and soil texture conditions of the new cells are expected to be similar to those for the smaller sub-sets. Therefore, the

variance of the soil moisture is not expected to change much across window sizes.

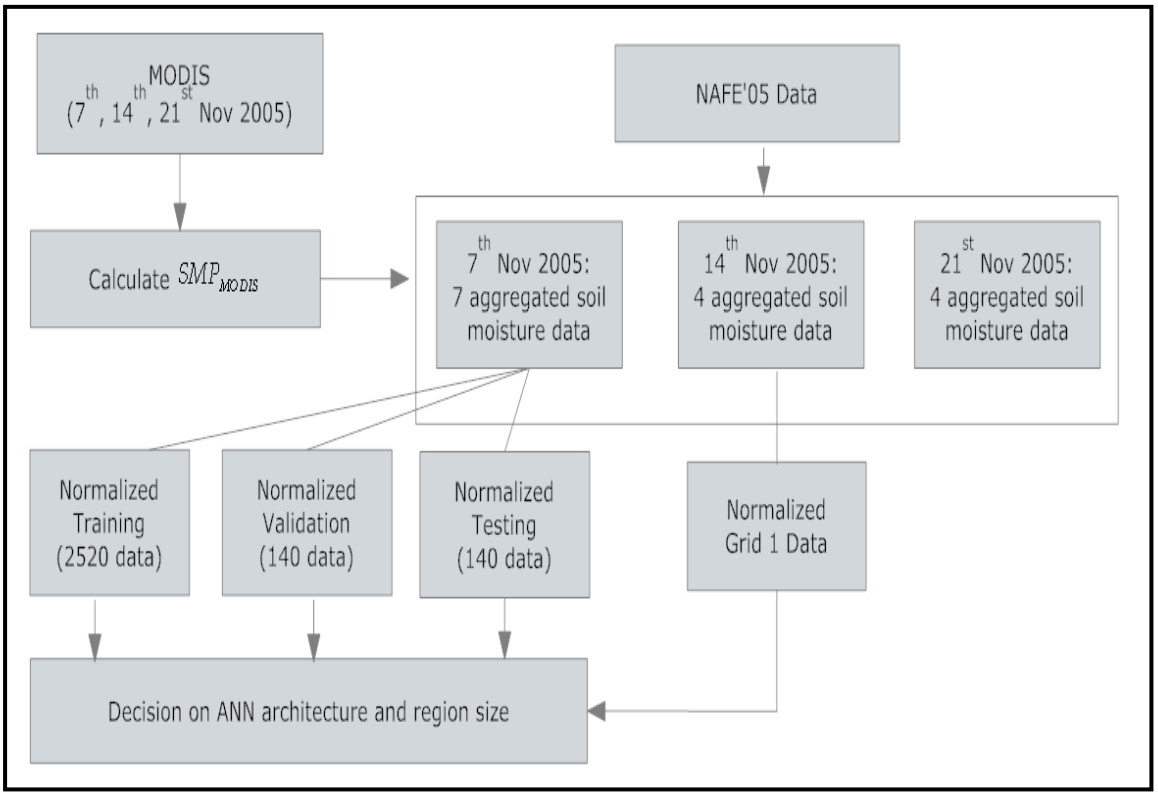

Figure 8.5. The data division used for selecting the optimum ANN architecture and window size.

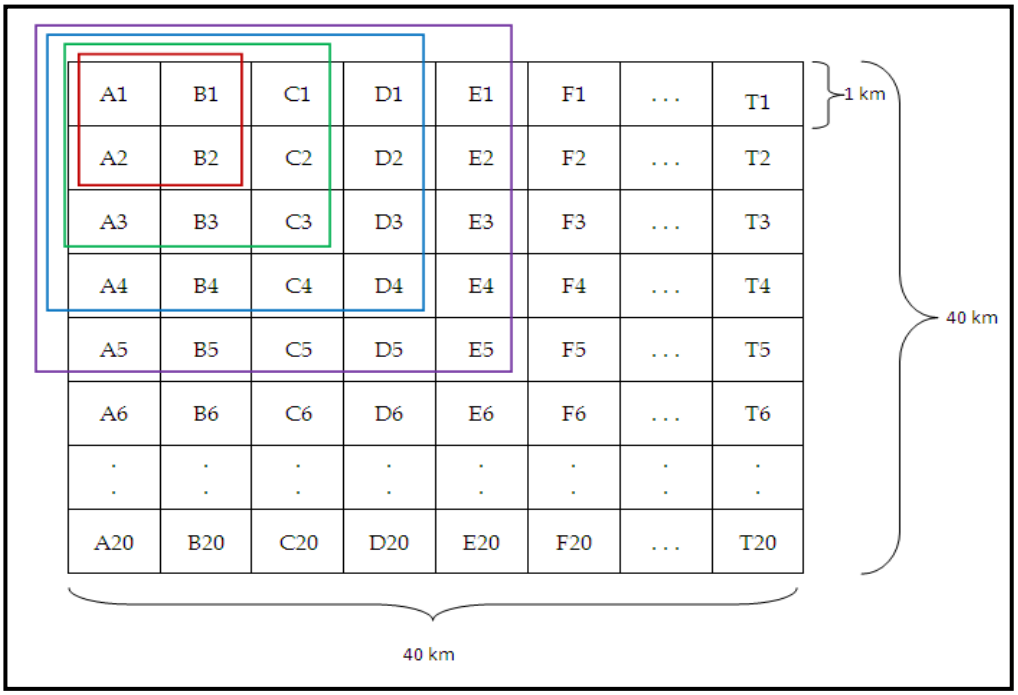

Figure 8.6. The different window sizes used for the selecting the optimum ANN architecture and window size using data from Grid 1 of 14th Nov 2005.

Table 8.2. The effects of using different numbers of hidden neurons for one and two layers in the ANN architecture when tested on different "window"sizes of Grid 1 on 14th Nov 2005.

	Hidden Neuron	RMSE After training (% v/v) (R^2)	RMSE (%v/v) (R^2) for Different "Window" Sizes 2×2 km	3×3 km	4×4 km	5×5 km
One Layer	2	8.15 (0.74)	4.09 (0.29)	4.69 (0.22)	6.47 (0.05)	6.48 (0.12)
	4	8.12 (0.74)	4.07 (0.55)	4.84 (0.20)	6.50 (0.002)	6.52 (0.02)
	6	8.11 (0.74)	3.89 (0.54)	4.84 (0.15)	6.60 (0.20)	6.49 (0.0002)
	8	8.03 (0.75)	3.80 (0.55)	4.76 (0.18)	6.56 (7.3E-06)	6.51 (0.02)
	10	7.75 (0.76)	**3.56 (0.46)**	4.59 (0.22)	6.45 (0.003)	6.21 (0.02)
	20	7.75 (0.76)	5.55 (0.13)	6.24 (0.18)	7.43 (0.13)	7.42 (0.13)
	50	7.55 (0.77)	6.02 (0.12)	6.93 (0.24)	6.31 (1E-08)	6.31 (0.12)
	100	7.50 (0.78)	5.08 (0.26)	5.77 (0.26)	6.37 (0.10)	6.60 (0.14)
Two Layers	2:2	8.19 (0.73)	4.44 (0.17)	4.90 (0.25)	6.48 (0.09)	6.57 (0.13)
	4:4	8.12 (0.74)	3.84 (0.38)	4.49 (0.27)	6.64 (0.08)	6.69 (0.11)
	5:5	8.00 (0.75)	5.00 (0.11)	5.63 (0.15)	6.66 (0.10)	6.88 (0.04)
	10:10	7.76 (0.76)	3.67 (0.40)	4.46 (0.27)	6.54 (0.05)	6.62 (0.05)
	20:20	7.76 (0.72)	4.67 (0.04)	5.33 (0.19)	6.37 (0.11)	6.49 (0.14)

8.3.5 Selection of ANN architecture and "Window" Size

The ANN of different architecture is first trained using the training data. For each different architectures, the trained ANN model is next tested on the next different "window" size. Using the data division shown in **Figure 8.5** and the different window size in **Figure 8.6**, testing is carried out to select the optimum ANN architecture, i.e. the number of hidden layers and neurons in the hidden layers. The results are shown in **Table 8.2**. Note the RMSE after training, is for the best ANN from the training, testing and validation stage. Only the results of four "window" sizes: 2km×2km , 3km×3km , 4km×4km and 5km×5km, are shown as the result deteriorate greatly for larger window sizes. The RMSE for the testing data are shown to be low (column 3 of **Table**

8.2). This might be because the testing data which are randomly selected from the training data are not representative of the training data.

From **Table 8.2**, it can be seen that, the prediction results deteriorate as the window size increases. For example, for single layer of two hidden neurons, the RMSE values deteriorate from 4.09% v/v for 2km×2km "window" size to 4.69%v/v at 3km×3km, to 6.47%v/v and 6.48%v/v for 4km×4km and 5km×5km, respectively. This is as expected, as soil moisture variance observed within a square meter can be as large as a whole field (Van Oevelen 1998), depending on homogeneity. However for the site evaluated here, for a bigger "window" size, the soil moisture variance will be higher comparing to a smaller "window" size because of a lack of homogeneity. As the variance increases, the ANN is unable to capture this variability, causing the retrieval accuracy to deteriorate.

For a single hidden layer of 10 neurons, the best RMSE obtained is 3.56% v/v with a correlation coefficient, R^2 = 0.46 for the 2km×2km "window" size. For two hidden layers of 10 neurons in each layer, it is 3.67% v/v with R^2 = 0.40 for the 2km×2km "window" size. The results show that the use of two hidden layers gives little improvement in the accuracy of predictions indicating that a more complex model is unnecessary. In addition to this, when the "window" size increases, the RMSE values increase. This was because the training was carried out using 20km×20km area and the testing carried out using various window sizes. The bigger the window the harder it is to capture the increased variability of the site. This shows that without the use of the "window" during prediction process, the ANN would not work well. This is verified in the later testing discussed in the **Section 8.3.6**.

With this testing, the optimum ANN architecture is set to be 10 neurons in one single hidden layer with an optimum "window" size of 2km×2km (shown in bold in **Table 8.2**).

8.3.6 Testing: Evaluation Cases

With the architecture (number of neurons and hidden layer) and the size of the "window" defined, this methodology is evaluated using the data of the 14th and 21st Nov 2005.

During the evaluation, the prediction process is carried out using a "window" of size 2km×2km. The prediction process is carried out within the "window" before moving to the next location. This "window" starts from the top left corner of the target area, moving to the right, down in a raster scanning fashion to the end of the 20 km area. **Figure 8.7** shows the start of the "window" of size 2km×2km in one of the 20 km area and the position of the next window after this location. The mean and standard deviation of the actual soil moisture within the "window" will be used as the de-normalization factors for the output of the ANN model.

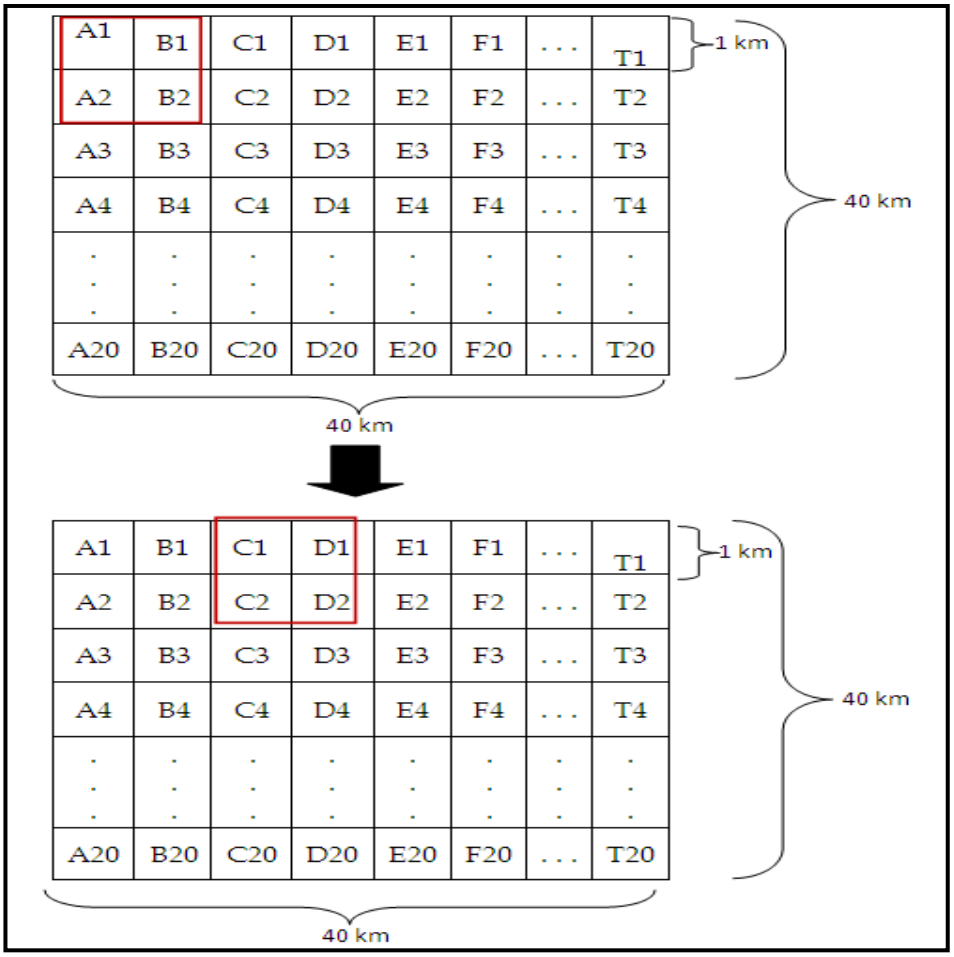

Figure 8.7. The the first and second 2km×2km moving windows and its moving direction.

Table 8.3. The RMSE values obtained for each of the 20×20 km grids in the 40×40 km target area.

Date	Grid (20×20 km)	RMSE (%v/v)
14th Nov 2005	Grid 1	3.5
	Grid 2	3.4
	Grid 3	2.3
	Grid 4	1.8
21st Nov 2005	Grid 1	2.7
	Grid 2	2.9
	Grid 3	2.0
	Grid 4	2.3

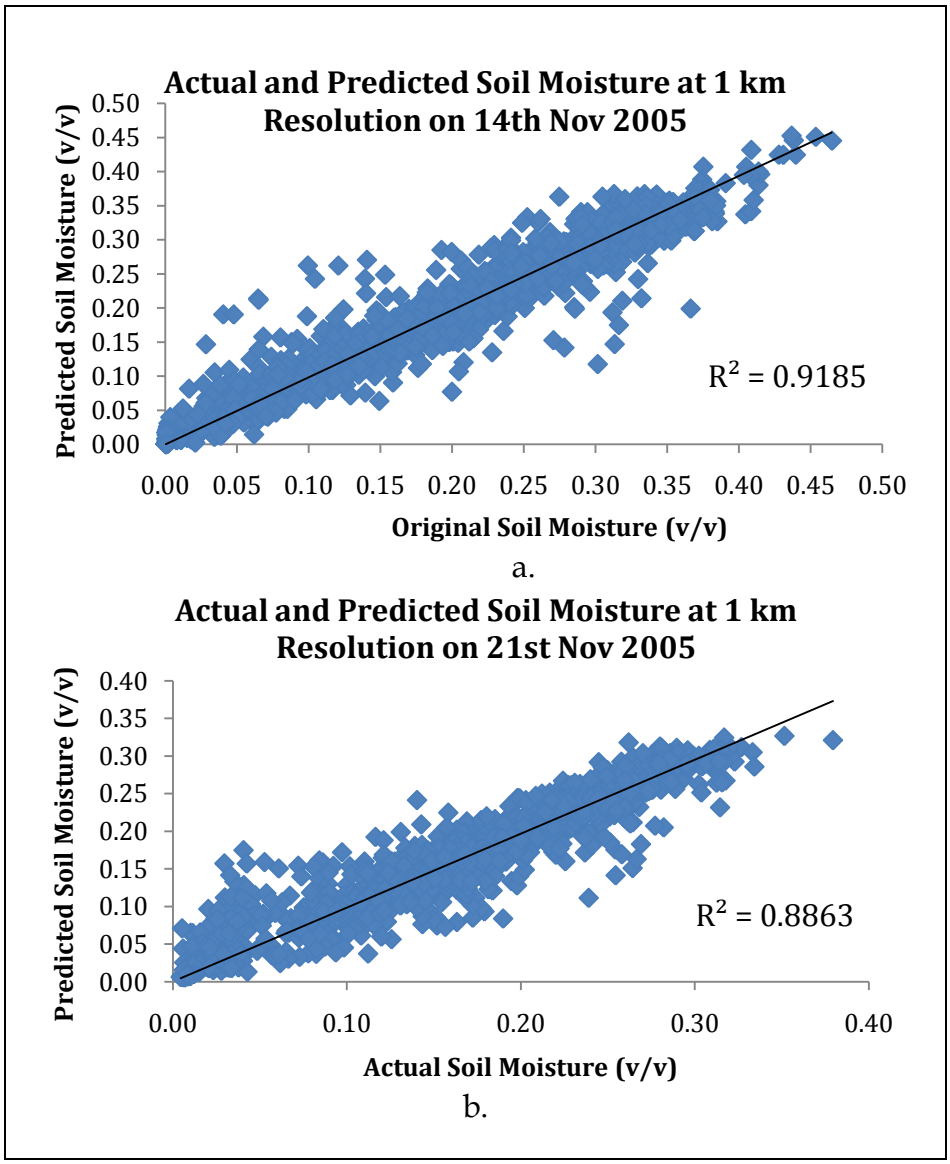

Figure 8.8. The relationship between actual and predicted soil moisture after applying the disaggregation method on a. 14th Nov 2005, and b. 21st Nov 2005.

Using this methodology, the RMSE between the actual and predicted values for each of the four grids of the 14th and 21st November 2005 are shown in **Table 8.3**. The correlations of the actual and predicted soil moisture are shown using scatter plots in **Figure 8.8**. The actual and predicted soil moisture maps are shown in **Figure 8.9** show reasonable correspondence between the actual and predicted maps. From the spatial difference of the soil moisture map, generally, the predicted soil moisture using this methodology is slightly lower compared to the actual soil moisture as evidenced by the large number of cells of positive difference.

From **Table 8.9** , it can be seen that the RMSE values range from 1.8% v/v to 3.5% v/v. **Figure 8.10** shows the standard deviation values for each of the 2 km×2 km "windows" in each 20 km area for each evaluation date. From this figure, it can be seen that the variability of soil moisture for Grids 3 and 4 for both dates is smaller, resulting in a maximum RMSE of 2.3% v/v. Grids 1 and 2 show greater soil moisture variability for both dates (**Figure 8.10**). With higher variability, the RMSE values obtained are higher. The RMSE values (see **Figure 8.10** for grids 1 and 2 on both dates) show that the ANN model fails to capture the variability of the soil moisture when the variability of the soil moisture is high. In other words, even with the use of 2km×2km "window", the capabilities of the ANN in capturing the soil moisture variability is shown to be low, and hence the ANN might not be able to generalize well if the downscaling is done for the whole target area (i.e. without the use of "window"). To verify this conclusion, further analyses are carried out in **Section 8.4**.

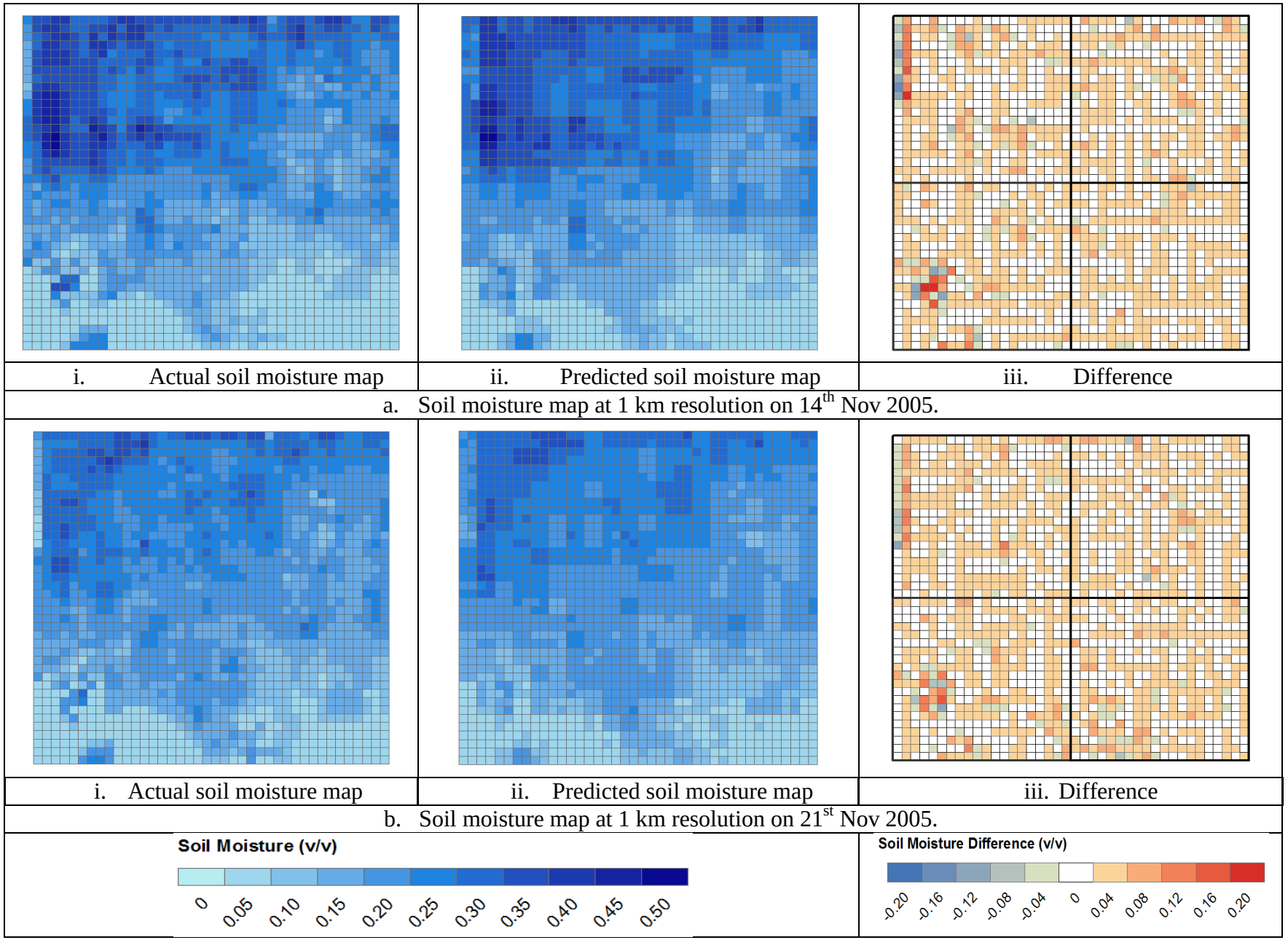

Figure 8.9. The actual and predicted soil moisture maps at 1 km resolution after applying the downscaling methodology. The difference between the actual and predicted soil moisture for each date is also shown.

8.4 Methodology Verification

The methodology proposed in this chapter is a combination of the use of "windows" and the different normalization factors for downscaling using an ANN model. To verify the use of different normalization factors and the "window" methods for downscaling of soil moisture in this chapter, three verification experiments are conducted. The first experiment will verify the use of the same normalization factors from training data with the "windowing" method, the second experiment focuses on the same normalization factors from training data without "windows", and the third experiment will verify the use of different normalization factors without "windows". The ANN consisting of 2 inputs, 1 hidden layer of 10 neurons and 1 output which is trained using the data from the 7th Nov 2005 of **Section 8.3.6.** will be used.

8.4.1 Same Normalization Factors from Training Data With Windows

The mean and standard deviation from the training data are used for the evaluation cases (see **Section 7.2**). During the prediction process, the "window" of size 2 km×2 km is used. To de-normalize the data, the mean and standard deviation values of the actual soil moisture values of the training data are used (see **Section 7.2**). The results are shown in **Table 8.4**. From this table, it is seen that the retrieval results range from 14.97%v/v to 63.72%v/v. The RMSE values show that the ANN is not generalizing as the error is larger than the range of soil moisture on the target area (0% v/v to 50% v/v) (see **Section 8.4.2**, **Figure 8.11**).

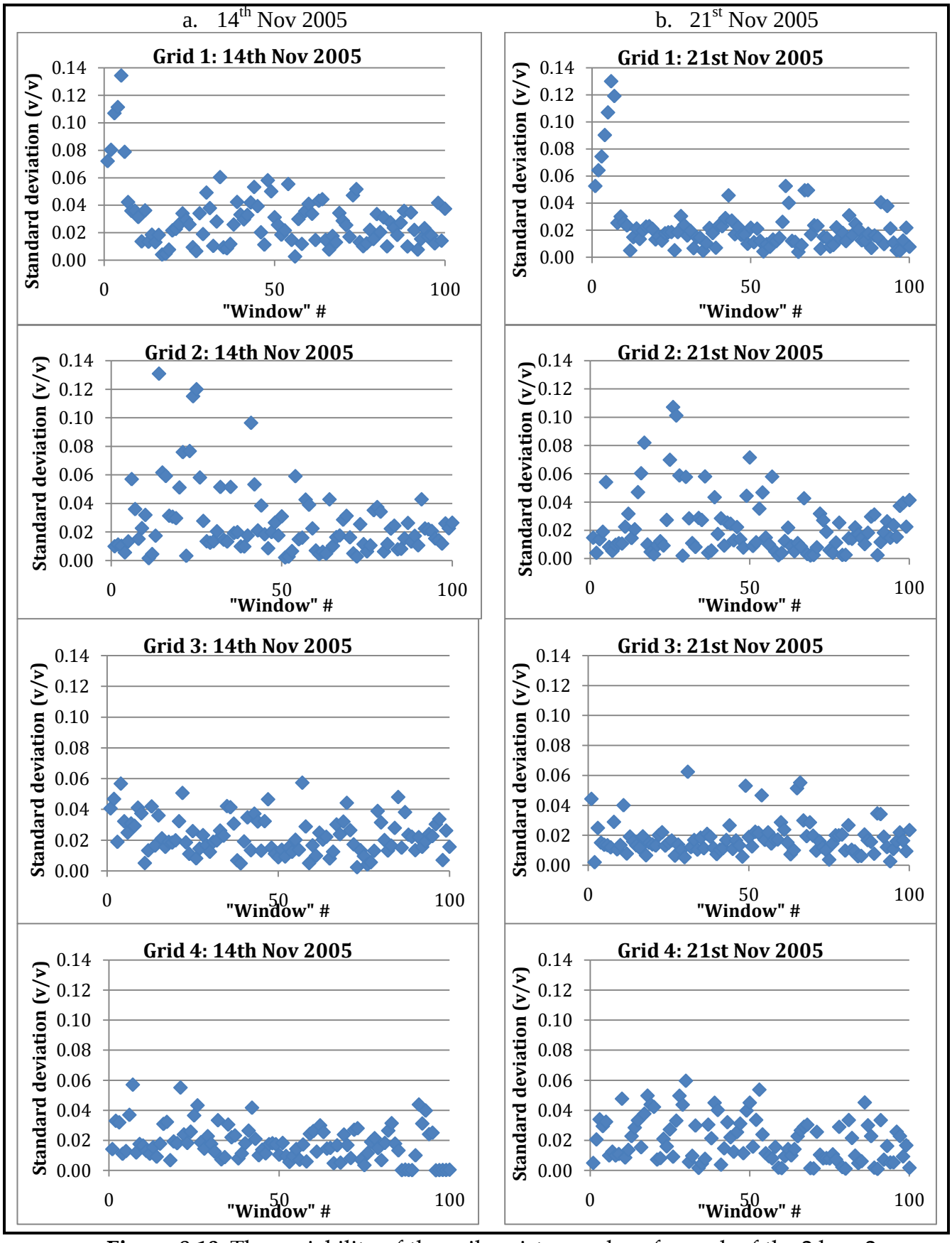

Figure 8.10. The variability of the soil moisture values for each of the 2 km×2 km "window" on each 20 km area.

Table 8.4. Prediction of 1 km using 2 km×2 km "moving windows" using the normalization factors from the training set.

Date	Grid	RMSE (%v/v)	R^2
14th November 2005	1	17.23	0.0005
	2	45.48	0.04
	3	31.78	0.0002
	4	55.33	0.10
21st November 2005	1	18.04	0.09
	2	56.18	0.22
	3	14.97	0.04
	4	63.72	0.06

8.4.2 Normalization Factors from Training Data Without "Moving Windows"

The importance of "moving windows" is verified using both the normalization factors obtained from the training data and the retrieval of the soil moisture of the 20 km area, i.e. the use of same normalization factors and not using "window". The results are shown in **Table 8.5**.

Table 8.5. Disaggregation to 1 km resolution using the same normalization factors from the training set without the use of "moving windows".

Date	Grid	RMSE (%v/v)	R^2
14th November 2005	1	31.46	0.001
	2	53.43	0.06
	3	53.03	0.02
	4	57.13	0.24
21st November 2005	1	50.94	0.20
	2	56.19	0.20
	3	29.31	0.10
	4	63.72	0.06

Comparing to **Table 8.4**, it can be seen that the disaggregation results deteriorate without the use of "windows" (**Table 8.5**). For example, the RMSE on 14th Nov 2005 for Grid 1 deteriorates from 17.23%v/v to 31.46%v/v, Grid 2 from 45.48%v/v to 53.43%v/v, Grid 3 from 31.78%v/v to

53.03%v/v and Grid 4 from 55.33%v/v to 57.13%v/v. The same trend goes for the four grids on 21st Nov 2005. In fact, the RMSE values show that the ANN is not generalizing as the error is larger than the range of soil moisture on the target area (0% v/v to 50% v/v). For example, from **Figure 8.11**, the actual and predicted soil moisture for Grid 4 of 21st Nov 2005 shows that, the predicted soil moisture is mostly in the range of 0.65 v/v to 0.85 v/v, which is virtually constant with regards to the actual soil moisture values, i.e. a horizontal straight line. Hence, a low R^2 value. Therefore, from **Table 8.4** and **Table 8.5**, it can be concluded that, the use of "windows" during the disaggregation process improves the retrieval accuracy. The effects of normalization factors in pre- and post-processing of the ANN data is verified using the experiment below (**Section 8.4.3**).

8.4.3 Different Normalization Factors Without "Moving Windows"

As the proposed methodology used different normalization factors, there is a need to verify the importance of this method in the proposed methodology. Therefore, a further analysis of the normalization factors on the disaggregation accuracy is carried out using different normalization factors. The disaggregation is done without the use of "moving windows", i.e. for the whole 20 km area at once. The pre- and post-processing of the data for the ANN is done using the mean and standard deviation of each of the 20 km areas for each date, i.e. the pre- and post-processing of ANN for Grid 1 on 14th Nov 2005 is done using the mean and the standard deviation of the data on this grid, and so on. The disaggregation results are shown in **Table 8.6**.

Table 8.6. Disaggregation results at 1 km resolution without "moving windows" with the use of mean and standard deviation values from each of 20 km regions.

Date	Grid	RMSE (%v/v)	R^2
14th November 2005	1	7.29	0.003
	2	9.02	0.06
	3	7.77	0.05
	4	8.24	0.01
21st November 2005	1	5.80	0.14
	2	8.67	0.10
	3	5.79	0.04
	4	7.53	0.05

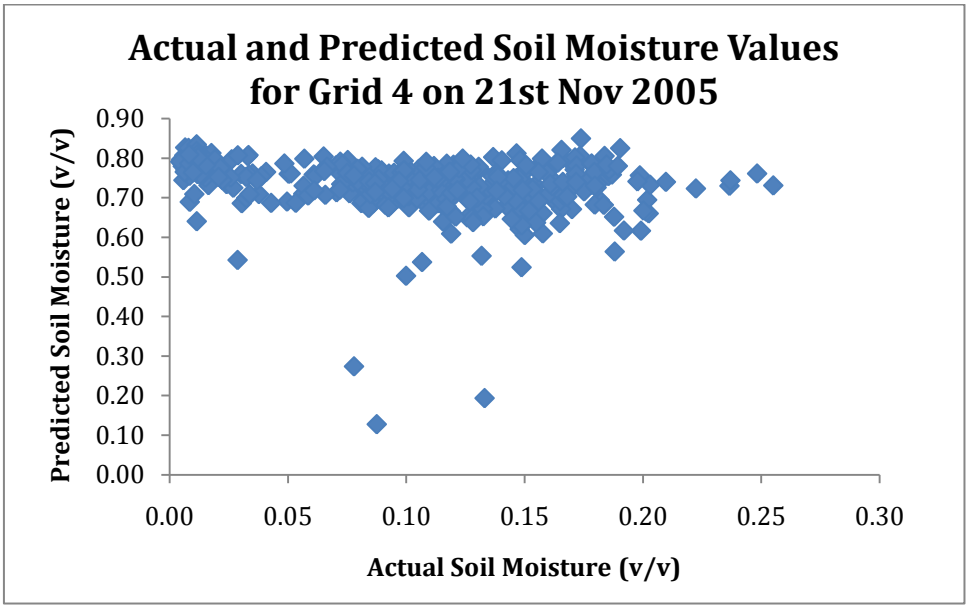

Figure 8.11. Actual and predicted soil moisture values for Grid 4 on 21st Nov 2005.

Comparing **Table 8.4** and **Table 8.5**, the retrieval accuracies increase. For example, the retrieval accuracy for Grid 1 on 14th Nov 2005 is 17.23%v/v when the retrieval is done using the normalization factor of the training set and with the use of 2km×2km "window" (**Table 8.4**). This result deteriorates to 31.46%v/v when the normalization factors of the training set are used without the 2km×2km "window" (**Table 8.5**). With the use of different

normalization factors, but without the 2km×2km "window", the retrieval accuracy is better, i.e. 7.29%v/v (**Table 8.6**). Therefore, it is concluded that the disaggregation to 1 km resolution improves significantly when the normalization factors are obtained from the data itself. The retrieval result is the best when different normalization factors are used together with the 2km×2km "window" (**Table 8.3**).

8.5 Sensitivity to Mean and Standard deviations

The proposed methodology utilized the mean and standard deviation of the soil moisture at the "window" size to de-normalize the disaggregation results from the ANN model. The 1 km soil moisture product is used to calculate the mean and the standard deviation values within the "window". The dependency of the proposed methodology on the accuracy of these two parameters is verified by simulating the mean and standard deviation values using a multiple regression model. Using the H- and V-polarized brightness temperature (TbH and TbV), the NDVI and Land Surface Temperature (LST) from MODIS/Aqua, the soil moisture values at 1 km resolution are regressed. The mean and standard deviation values within the "window" are calculated based on the regressed soil moisture values.

Table 8.7. RMSE and R^2 between the regressed and actual soil moisture values.

Date	Grid	RMSE (%v/v)	R^2
14th November 2005	1	6.4	0.13
	2	10.5	0.15
	3	6.3	0.27
	4	9.1	0.43
21st November 2005	1	4.3	0.29
	2	8.7	0.001
	3	3.1	0.57
	4	6.1	0.23

For each of the dates (7th, 14th and 21st Nov 2005), 18 data (around 1%) of the data are randomly selected (using the MATLAB random number function) for the regression. The rationale behind the small number of data selected is to simulate a situation where these data are ground-truth samples. With more data selected, the regression formula will be more accurate, but at the same time, more sample points will need to be taken if ground sampling has taken place (see **Section 7.10**). **Table 8.7** shows the RMSE and R^2 values for each of the 20 km areas for each date. The disaggregation is carried out with the 2km×2km "windows" and the results are shown in **Table 8.8**.

From **Table 8.8**, it can be seen that the RMSE values between actual and predicted soil moisture are similar to the RMSE values between the regressed and predicted soil moisture values in **Table 8.7**. As the predicted soil moisture values (using the ANN model) are very close to the regressed soil moisture values (using the linear regression model), the RMSE values between the actual and predicted soil moisture exhibit similar RMSE values. From this experiment, it is shown that the accuracy of the disaggregated soil moisture with this methodology depends greatly on the accuracy of the mean and standard deviation values used.

Table 8.8. The RMSE and R^2 values obtained using the ANN for disaggregation.

Date	**Grid**	**Regressed and Predicted SM**		**Actual and Predicted SM**	
		RMSE (%v/v)	**R^2**	**RMSE (%v/v)**	**R^2**
14th November 2005	1	2.6	0.74	6.2	0.14
	2	2.9	0.53	10.5	0.15
	3	2.6	0.73	6.3	0.30
	4	2.6	0.71	9.1	0.50
21st November 2005	1	1.5	0.82	4.3	0.28
	2	1.8	0.45	8.7	0.00
	3	1.7	0.82	3.1	0.58
	4	1.8	0.72	6.1	0.25

8.6 Conclusions

This chapter has presented a novel ANN approach that utilizes the variability in terms of the mean and standard deviation values as the de-normalization factors in the ANN model with "windows" method to disaggregate soil moisture values from 20 km to 1 km resolution. This model improves the ability of the ANN to capture the variability of soil moisture values when disaggregated from coarse resolution data. The method has shown to achieve RMSE values ranging from 1.8%v/v to 3.5%v/v, with an average of 2.7%v/v. The benefit of this method is in terms of the minimum input variables required.

The challenges of this approach include the following:

1. The number of data needed to train the ANN in order for the ANN to learn the relationship between the θ, θ_{SMOS} and SMP_{MODIS}. The number of data should be large enough in order for the ANN to map the function. In the approach proposed in this thesis, as the data are only available on three different dates, and with the aim of this thesis of developing an ANN model which can be tested with at least two real problems (see **Section 3.7**), the target area of 40 km×40 km is divided into seven 20 km areas for training in order to avoid the problem of supplying constant values to the ANN model.

2. The variability values, i.e. mean and standard deviation values, at the "window" size for the de-normalization purpose. In this study, the mean and standard deviation values are estimated from the actual soil moisture values and from multiple linear-regression. However, in real life, the estimation of the mean and standard deviation values of actual soil moisture at the "window" size, especially at a size as small as 2km×2km, will need to be further investigated. One possible solution towards this challenge is to use radar data that promises higher resolution data. It is believed that by incorporating radar data of a higher resolution, this methodology will be able to disaggregate soil moisture to a resolution finer than the resolution of the radar data. By incorporating both passive and active microwave data, the accuracy of this methodology for disaggregation purpose will therefore

depend on the accuracy of the radar data in order to disaggregate to a resolution finer than the radar resolution. The minimum input variables required for this methodology is the main advantage of this approach. An alternative approach is discrete possibly sparse ground sampling of soil moisture or a surrogate.

With SMOS having a resolution of around 40km×40km, it is argued that this method can lead to the disaggregation of the data to 2 km resolution (20 times as suggested in this chapter) at an accuracy of around 3% v/v, provided an acceptable mean and standard deviation accuracies (around 3% v/v) at a resolution of around 4km×4km can be obtained. In fact Merlin *et al.* (2008b) have proposed that their method can also downscale 20 times. The performance of achieving this using the ANN approach will require further investigation.

Chapter 9

Conclusions, Contributions and Future Work

9.1 Conclusions

This research can be divided into two main parts: i. scale-to-scale soil moisture predictions; and, ii. soil moisture disaggregation from coarse scale resolution data. From the results of this study, it is clear that passive microwave remote sensing has significant capabilities in estimating soil moisture in faster and more reliable ways and with sufficient accuracy using ANNs. The data used in this research is generally at 1 km resolution. The main reason for using data at this resolution is that there is a large amount of data available for the sites of interest, which enables the ANN model to reliably and representatively learn and map the relationship between sensed input data and output predictions. The ANN is trained using a single date: 7th Nov 2005, and was verified using data from two different dates: 14th and 21st Nov 2005. Good performance for the evaluation cases demonstrate the ability of ANN to generalize to other dates.

The microwave response to surface characteristics is not only strongly dominated by the volumetric surface soil moisture, but also by vegetation attenuation and the effective surface temperature (Kerr *et al.* 2001). In this research, the influence of these two factors was studied in terms of their effects on the accuracy of the soil moisture retrieval using ANNs. The backpropagation neural network model, a popular form of ANN and the most commonly used ANN model for soil moisture retrieval, is used in this research. The NDVI and the surface temperature were combined with the

dual-polarized brightness temperature to form the input for the ANN model. The architecture of the ANN in terms of the number of hidden neurons and hidden layers was analysed using different combinations of these inputs.

A novel approach, which utilizes the mean and the standard deviation values as the de-normalization factors for the output of the ANN was developed to capture the temporal variability of the soil moisture values. This approach is combined with a methodology that predicts soil moisture values at a pre-determined "window" size within the target area to capture the spatial variability of the soil moisture values. The optimum "window" size for the spatial variability statistics where the ANN manages to obtain an RMSE of less than or equal to the globally acceptable retrieval error of 4% v/v was analysed. This approach is adopted for both the scale-to-scale and the downscaling methods for soil moisture prediction. For scale-to-scale retrieval, the retrieval results are 3.9%v/v and 3.4%v/v for data on 14th Nov and 21st Nov 2005, respectively, while for downscaling, the average RMSE value obtained is 2.7%v/v.This method shows that an ANN can be used both for scale-to-scale and downscaling methods of soil moisture prediction. In addition to this, it was also shown that the ANN is able to maintain stable prediction results when independent and new data sets are used. For scale-to-scale retrieval, the optimum "window" size was determined to be 4km×4km with an ANN consisting of a single hidden layer of 20 neurons while for downscaling purpose, it is 2km×2km.

The addition of satellite derived data such as NDVI and land surface temperature (LST) derived from MODIS data produced little improvement in the scale-to-scale predictions, although these two parameters have been used to retrieve soil moisture from passive microwave through the "universal triangle" method by Hossain and Easson (2008)

The soil moisture spatial variability is mainly affected by physical properties such as climate, soil texture, vegetation, and topography in natural catchment or agricultural areas (Mohanty and Skaggs 2001). In this work, as the study area only covers an area of 40km×40km, the climate factor

can be neglected. Jacobs *et al.* (2004) and Mohanty and Skaggs (2001) concluded that topography is a crucial physical factor in understanding surface soil moisture variability. Teuling and Troch (2005) pointed out that soil and vegetation may be important factors that can increase or decrease soil moisture variance. There is therefore a need to incorporate these factors into soil moisture prediction using ANN models. In this research, this was done by incorporating the mean and standard deviation of the actual soil moisture values as the de-normalization factors and the "window" method in the ANN model. The ANN was shown to capture the temporal and spatial variation with this methodology. Multiple linear-regression was investigated as a method of determining the mean and standard deviation from the input data for standardisation with the result that if the estimates were poor, then the prediction of soil moisture was poor.

For disaggregation of soil moisture, the linear relationship between the soil evaporative efficiency and near-surface soil moisture approach by Merlin *et al.* (2008b) was incorporated into the ANN model. The soil moisture at the desired downscaled resolution, θ, can be written as a linear relationship between the soil moisture at SMOS scales or a coarse scale θ_{SMOS}, characteristic volume fraction θ_C, and the SM_MP_O value (**Chapter 8**). As θ_C is not available for the NAFE'05 data, the ANN model learns to map the relationship between the target θ and the inputs of θ_{SMOS} and SM_MP_O. The spatial and temporal variability in terms of the mean and the standard deviation of the soil moisture were used as the de-normalization factors for the ANN model. Using the same principle as in the scale-to-scale soil moisture retrieval in **Chapter 7**, the spatial variability of soil moisture is captured using a method that predicts soil moisture at a pre-determined "window" size. During training, as the data were not organized according to the spatial location and not using the "windows" method, the RMSE values obtained are high. Different "window" sizes were used to determine the optimum size and this was found to be 2km×2km with 10 hidden neurons in

a single hidden layer. This novel approach was used to disaggregate a total of eight different 20km×20km coarse scale soil moisture data sets from the 14th and 21st Nov 2005 to 1 km soil moisture data. The disaggregation accuracies obtained were between 1.8 %v/v and 3.5% v/v of RMSE. This shows that this novel approach is applicable to disaggregate soil moisture from 20 km to 1 km using an ANN without the need to incorporate any empirical parameters.

9.2 Contributions

The contributions of this research to the problem of passive microwave soil moisture prediction using the ANN approach can be summarized with respect to the objectives identified in **Section 1.3**:

i. A methodology to predict soil moisture at 1 km resolution using 1 km input data. The methodology developed is capable of capturing the spatial and temporal variability of soil moisture and provide a stable and encouraging results when it was used on data of different dates on the same target area. This solves the common issue of not being able to work with data, which are "out-of-range" with the ANN model.

ii. The use of ancillary data, i.e. NDVI and LST data in this research study, as the input of the ANN model is shown to produce minimal improvement to the prediction accuracy for scale-to-scale soil moisture prediction. Therefore, only the dual-polarized brightness temperatures are used to predict soil moisture in this thesis.

iii. A methodology for the downscaling of soil moisture from 20 km to 1 km resolution using the ANN model. This developed model shows that the downscaling of soil moisture data can be done using only data from two satellites, i.e. MODIS and passive microwave data, without the incorporation of data obtained empirically.

The main contribution of this thesis is the development of a novel approach, which aids the ANN's generalization ability across different dates with encouraging and stable results. This approach utilizes the mean and standard deviation of ground truth soil moisture values as the de-normalization factors in the ANN model and "windows" method during the prediction process. It is found that the use of the mean and standard deviation as the de-normalization factors and the "moving window" methodology manages to capture the temporal variability and the effects of topography, vegetation and soil. With this innovative approach, the ANN is able to account for spatial variations in soil type and temporal variation in soil moisture condition. This methodology is applied to both scale-to-scale and disaggregation soil moisture retrieval methods with the use of two evaluation cases, which are neither: i. a subset obtained from the training data, nor, ii. data, which are modelled within the constraints of the conditions on the training data. The use of two evaluation cases verifies the capability of this methodology for soil moisture retrieval to generalise over time and locations within the same target area.

9.3 Future Directions

Although the use of mean and the standard deviation values of the soil moisture as the de-normalization factors and the "window" method in the prediction process have showed their capabilities in improving the retrieval accuracy, further exploration of the practicality of this methodology is needed. This is mainly due to the dependency of this methodology on the accuracy of the mean and standard deviation values of the ground truth soil moisture data as shown in **Section 7.10** and **Section 8.5**. The corresponding mean and standard deviation values used in this research study are calculated by using the soil moisture values at 1 km. Therefore, there is room for improvement, such as the development of an algorithm to predict the mean and standard deviation at the pre-determined "window" size. Further work is required to determine good surrogates for the actual soil moisture.

This is an important task in order for this methodology to be practical. One possible solution towards this challenge is to use radar data that should produce higher resolution data.

Moreover, as the data used in this work focus only on a single site, further testing is needed to assess the applicability of such an approach for a wider range of surface conditions, especially over heavily vegetated areas.

As only field experiment data were used in this research, it is necessary to examine the capability of this methodology using the SMOS satellite data. This is especially important for the methodology of downscaling soil moisture data. In this research, as the data from the field experiment were only from a single site area of 40km×40km, the problem of data inadequacy resulted in dividing this site into different 20km×20km regions. Although the results obtained were very encouraging, and with an expectation that the method can be applied to downscale data from the SMOS satellite (~40km resolution) to 2 km resolution (20 times as suggested in this thesis) at an accuracy of ~3% v/v (provided the mean and standard deviation at a resolution of 4km×4km can be obtained at an accuracy of around 3% v/v), further verification of the practicality of this approach is needed.

In addition to this, as the selection of the BFGS algorithm was based on analysis using inputs on TbH and TbV, it will be interesting to verify that the BFGS algorithm continues to outperform the other algorithms for each of the ancillary input scenarios. Recently partial mutual information and gamma testing have been used in other applications for help with input selection. It is worth exploring the usefulness of these techniques for soil moisture estimation.

References

Angiuli, E., F. del Frate, and A. Monerris. 2008. *IEEE International Geoscience and Remote Sensing Symposium, 2008 (IGARSS 2008), Application of Neural Networks to Soil Moisture Retrievals from L-Band Radiometric Data*.

Atluri, V., H. Chih-Cheng, and T. L. Coleman. 1999. *IEEE Southeastcon '99. Proceedings. , An artificial neural network for classifying and predicting soil moisture and temperature using Levenberg-Marquardt algorithm*.

Babak, O., and C. Deutsch. 2009. Statistical approach to inverse distance interpolation. *Stochastic Environmental Research and Risk Assessment* 23 (5): 543-553.

Barbier, C. 2003. SAR Image Data Processing at CSL: an Overview. *REVUE HF* (Part 1): 41-50.

Barnes, W. L., X. Xiong, and V. V. Salomonson. 2003. Status of terra MODIS and aqua modis. *Advances in Space Research* 32 (11): 2099-2106.

Behari, J. 2005. *Microwave Dielectric Behaviour of Wet Soils*: Springer.

Berger, M., Y. Kerr, J. Font, J.-P. Wigneron, J.-C. Calvet, K. Saleh, E. Lopez-Baeza, L. Simmonds, P. Ferrazzoli, B. v. d. Hurk, P. Waldteufel, F. Petitcolin, A. v. d. Griend, E. Attema, and M. Rast. 2003. Measuring the Moisture in the Earth's Soil - Advancing the Science with ESA's SMOS Mission. *ESA Bulletin* (115): 40-45.

Best, B. 1990. *An Overview of Neural Networks*. http://www.benbest.com/computer/nn.html (accessed 10 Feb 2008)

Bolten, J., W. Crow, X. Zhan, T. Jackson, C. Reynolds, and B. Doom. 2006. *IEEE International Conference on Geoscience and Remote Sensing Symposium, 2006 (IGARSS 2006). The Application of AMSR-E Soil Moisture for Improved Global Agricultural Assessment and Forecasting*.

Bolten, J. D., V. Lakshmi, and E. G. Njoku. 2003. Soil moisture retrieval using the passive/active L- and S-band radar/radiometer. *IEEE Transactions on Geoscience and Remote Sensing* 41 (12): 2792-2801.

Burke, E. J., and L. P. Simmonds. 2001. A simple parameterisation for retrieving soil moisture from passive microwave data. *Hydrology and Earth System Sciences* Vol. 5 (NUMB 1): 39-48.

Calla, O. P. N., D. Bohra, R. Vyas, B. S. Purohit, R. Prasher, A. Loomba, and N. Kumar. 2008. *International Conference on Recent Advances in Microwave Theory and Applications, 2008. MICROWAVE 2008., Measurement of soil moisture using microwave radiometer*.

Carlson, T. 2007. An Overview of the "Triangle Method" for Estimating Surface Evapotranspiration and Soil Moisture from Satellite Imagery. *Sensors* 7 (8): 1612-1629.

Carlson, T. N., R. R. Gillies, and E. M. Perry. 1994. A method to make use of thermal infrared temperature and NDVI measurements to infer surface soil. *Remote Sensing Reviews* 9: 161-173.

Carlson, T. N., R. R. Gillies, and T. J. Schmugge. 1995. An interpretation of methodologies for indirect measurement of soil water content. *Agricultural and Forest Meteorology* 77 (3-4): 191-205.

Chai, S.-S., B. Veenendaal, G. West, and J. P. Walker. 2008. Input Pattern According to Standard Deviation of Backpropagation Neural Network: Influence on Accuracy of Soil Moisture Retrieval. In *IEEE International Geoscience and Remote Sensing Symposium, 2008 (IGARSS 2008)*

Chang, D.-H., and S. Islam. 2000. Estimation of Soil Physical Properties Using Remote Sensing and Artificial Neural Network. *Remote Sensing of Environment* 74 (3): 534-544.

Chanzy, A., S. Raju, and J. P. Wigneron. 1997. Estimation of soil microwave effective temperature at L and C bands. *IEEE Transactions on Geoscience and Remote Sensing* 35 (3): 570-580.

Chauhan, N. S. 1997. Soil moisture estimation under a vegetation cover: combined active passive microwave remote sensing approach. *International Journal of Remote Sensing* 18 (5): 1079 - 1097.

Chauhan, N. S., S. Miller, and P. Ardanuy. 2003. Spaceborne soil moisture estimation at high resolution: a microwave-optical/IR synergistic approach. *International Journal of Remote Sensing* 24 (22): 4599-4622.

Chiang, Y.-M., L.-C. Chang, and F.-J. Chang. 2004. Comparison of static-feedforward and dynamic-feedback neural networks for rainfall-runoff modeling. *Journal of Hydrology* 290 (3-4): 297-311.

Choudhury, B. J., and R. E. Golus. 1988. Estimating soil wetness using satellite data. *International Journal of Remote Sensing* 9 (7): 1251 - 1257.

Choudhury, B. J., T. J. Schmugge, A. Chang, and R. W. Newton. 1979. Effect of Surface Roughness on the Microwave Emission From Soils *Journal of Geophysical Research* Vol. 84 (No. C59): 5699-5706.

Connor, L. N., P. S. Chang, Z. Jelenak, N. Y. Wang, and T. P. Mavor. 2004. *IEEE International Geoscience and Remote Sensing Symposium, 2004 (IGARSS '04)*, *WindSat validation datasets: an overview*.

Crosson, W. L., C. A. Laymon, R. Inguva, and C. Bowman. 2002. Comparison of two microwave radiobrightness models and validation with field measurements. *IEEE Transactions on Geoscience and Remote Sensing* 40 (1): 143-152.

Curtis, J. O. 2001. A durable laboratory apparatus for the measurement of soil dielectric properties. *IEEE Transactions on Instrumentation and Measurement* 50 (5): 1364-1369.

Davis, D. T., Z. Chen, L. Tsang, J. N. Hwang, and A. T. C. Chang. 1993. Retrieval of snow parameters by iterative inversion of a neural network. *IEEE Transactions on Geoscience and Remote Sensing* 31 (4): 842-852.

Davis, D. T., and H. Jenq-Neng. 1997. Solving inverse problems by Bayesian neural network iterative inversion with ground truth incorporation. *IEEE Transactions on Signal Processing* 45 (11): 2749-2757.

Davis, D. T., C. Zhengxiao, H. Jenq-Neng, L. Tsang, and E. Njoku. 1995. Solving inverse problems by Bayesian iterative inversion of a forward model with applications to parameter mapping using SMMR remote sensing data. *IEEE Transactions on Geoscience and Remote Sensing* 33 (5): 1182-1193.

Dawson, C. W., and R. Wilby. 1998. An artificial neural network approach to rainfall-runoff modelling. *Hydrological Sciences Journal* 43 (1): 47-66.

Dawson, M. S., A. K. Fung, and M. T. Manry. 1997. A robust statistical-based estimator for soil moisture retrieval from radar measurements. *IEEE Transactions on Geoscience and Remote Sensing* 35 (1): 57-67.

Del Frate, F., P. FERRAZZOLI, and G. SCHIAVON. 2003. Retrieving soil moisture and agricultural variables by microwave radiometry using neural networks. *Remote Sensing of Environment* 84: 174-183.

Del Frate, F., P. Ferrazzoli, G. Schiavon, J. P. Wigneron, and A. Chanzy. 1999. *IEEE 1999 International Geoscience and Remote Sensing Symposium, 1999. IGARSS '99 Proceedings., Retrieving agricultural variables by microwave radiometry using a neural network algorithm trained by a physical model*.

Demuth, H., M. Beale, and M. Hagan. 2009. *Neural Network Toolbox 6, User's Guide*. Nattick, MA: Mathworks Inc.

Dobson, M. C., and F. T. Ulaby. 1986. Active Microwave Soil Moisture Research. *IEEE Transactions on Geoscience and Remote Sensing* GE-24 (1): 23-36.

Dobson, M. C., F. T. Ulaby, M. T. Hallikainen, and M. A. El-Rayes. 1985. Microwave Dielectric Behavior of Wet Soil-Part II: Dielectric Mixing Models. *IEEE Transactions on Geoscience and Remote Sensing* GE-23 (1): 35-46.

Drusch, M., E. F. Wood, and T. J. Jackson. 2001. Vegetative and Atmospheric Corrections for the Soil Moisture Retrieval from Passive Microwave Remote Sensing Data: Results from the Southern Great Plains Hydrology Experiment 1997. *Journal of Hydrometeorology* 2 (2): 181-192.

Du, Y., F. T. Ulaby, and M. C. Dobson. 2000. Sensitivity to soil moisture by active and passive microwave sensors. *IEEE Transactions on Geoscience and Remote Sensing* 38 (1): 105-114.

Elman, J. L. 1990. Finding structure in time. *Cognitive Science* 14 (2): 179-211.

Elshorbagy, A., and K. Parasuraman. 2008. On the relevance of using artificial neural networks for estimating soil moisture content. *Journal of Hydrology* 362 (1-2): 1-18.

Engman, E. T. 1991. Applications of microwave remote sensing of soil moisture for water resources and agriculture. *Remote Sensing of Environment* 35 (2-3): 213-226.

Engman, E. T., and N. Chauhan. 1995. Status of microwave soil moisture measurements with remote sensing. *Remote Sensing of Environment* 51 (1): 189-198.

Entekhabi, D., E. G. Njoku, P. Houser, M. Spencer, T. Doiron, K. Yunjin, J. Smith, R. Girard, S. Belair, W. Crow, T. J. Jackson, Y. H. Kerr, J. S. Kimball, R. Koster, K. C. McDonald, P. E. O'Neill, T. Pultz, S. W. Running, S. Jiancheng, E. Wood, and J. van Zyl. 2004. The hydrosphere State (hydros) Satellite mission: an Earth system pathfinder for global mapping of soil moisture and land freeze/thaw. *IEEE Transactions on Geoscience and Remote Sensing* 42 (10): 2184-2195.

. *ESA Water Mission SMOS*. 2009. http://www.esa.int/esaMI/smos/SEMNEYAOE1G_0.html (accessed 5 Nov 2009).

Escorihuela, M. J., P. de Rosnay, Y. H. Kerr, and J. C. Calvet. 2007. Influence of Bound-Water Relaxation Frequency on Soil Moisture Measurements. *IEEE Transactions on Geoscience and Remote Sensing* 45 (12): 4067-4076.

Fernando, J. P. 1988. Dynamics and architecture for neural computation. *J. Complex.* 4 (3): 216-245.

Ferrazzoli, P., and L. Guerriero. 1995. Modeling microwave emission from vegetation-covered surfaces: a parametric analysis. In *Passive Microwave Remote Sensing of Land--Atmosphere Interactions*, ed. B. Choudhury, Y. Kerr, E. Njoku and P. Pampaloni.

Ferrazzoli, P., J. P. Wigneron, L. Guerriero, and A. Chanzy. 2000. Multifrequency emission of wheat: Modeling and applications. *IEEE Transactions on Geoscience and Remote Sensing* 38 (6): 2598-2607.

Fischman, M. A., and A. W. England. 1999. Sensitivity of a 1.4 GHz direct-sampling digital radiometer. *IEEE Transactions on Geoscience and Remote Sensing* 37 (5): 2172-2180.

Fung, A. K. 1994. *Microwave Scattering and Emission Models and Their Applications*. Norwood, MA: Artech House.

Gaiser, P. W., K. M. St Germain, E. M. Twarog, G. A. Poe, W. Purdy, D. Richardson, W. Grossman, W. L. Jones, D. Spencer, G. Golba, J. Cleveland, L. Choy, R. M. Bevilacqua, and P. S. Chang. 2004. The WindSat spaceborne polarimetric microwave radiometer: sensor

description and early orbit performance. *IEEE Transactions on Geoscience and Remote Sensing* 42 (11): 2347-2361.

Ghedira, H., M. Bernier, and T. B. M. J. Ouarda. 2000. *IEEE 2000 International Geoscience and Remote Sensing Symposium, 2000. Proceedings. IGARSS 2000. , Application of neural networks for wetland classification in RADARSAT SAR imagery*.

Ghedira, H., T. Lakhankar, N. Jahan, and R. Khanbilvardi. 2004. *IEEE International Geoscience and Remote Sensing Symposium, 2004. IGARSS '04. Proceedings. , Combination of passive and active microwave data for soil moisture estimates*.

Grant, J. P., J. P. Wigneron, A. A. Van de Griend, M. Guglielmetti, K. Saleh, and M. Schwank. 2007a. *IEEE International Geoscience and Remote Sensing Symposium, 2007(IGARSS 2007), Calibration of L-MEB for soil moisture retrieval over forests*.

Grant, J. P., J. P. Wigneron, A. A. Van de Griend, A. Kruszewski, S. S. Søbjærg, and N. Skou. 2007b. A field experiment on microwave forest radiometry: L-band signal behaviour for varying conditions of surface wetness. *Remote Sensing of Environment* 109 (1): 10-19.

Hallikainen, M. T., F. T. Ulaby, M. C. Dobson, M. A. El-Rayes, and W. Lil-Kun. 1985. Microwave Dielectric Behavior of Wet Soil-Part 1: Empirical Models and Experimental Observations. *IEEE Transactions on Geoscience and Remote Sensing* GE-23 (1): 25-34.

Haykin, S. 1994. *Neural Network: A Comprehensive Foundation*. New York: Macmillan.

Heaton, J. 2008. *Introduction to Neural Networks with Java, 2nd Edition*. Edited by K. Smith: Heaton Research, Inc.

Hebb, D. O. 1949. *The organization of behavior: a neuropsychological theory*. New York: Wiley.

Hemakumara, M., J. Kalma, J. Walker, and G. Willgoose. 2004. Downscaling of low resolution passive microwave soil moisture observations. In *Proceedings of the 2nd international CAHMDA workshop on: The Terrestrial Water Cycle: Modelling and Data Assimilation Across Catchment Scales*, edited by A. J. Teuling, H. Leijnse, P. A. Troch, J. Shef-field and E. F. Wood. Princeton, NJ.

Hopfield, J. J. 1982. Neural Networks and Physical Systems with Emergent Collective Computational Abilities. *Proceedings of the National Academy of Sciences of the United States of America* 79 (8): 2554-2558.

Hornik, K., M. Stinchcombe, and H. White. 1989. Multilayer feedforward networks are universal approximators. *Neural Netw.* 2 (5): 359-366.

Hossain, A., and G. Easson. 2008. *IEEE International Geoscience and Remote Sensing Symposium, 2008. IGARSS 2008. , Evaluating the Potential of VI-*

LST Triangle Model for Quantitative Estimation of Soil Moisture using Optical Imagery.

Jackson, T., J. Du, R. Bindlish, M. Cosh, L. Li, and P. Gaiser. 2008. *Proceeding of the Catchment-Scale Hydrological Modelling and Data Assimilation International Workshop*, *WindSat passive microwave soil moisture retrievals*. Melbourne, Australia.

Jackson, T. J. 2001. Multiple resolution analysis of L-band brightness temperature for soil moisture. *IEEE Transactions on Geoscience and Remote Sensing* 39 (1): 151-164.

Jackson, T. J., D. Entekhabi, and E. Njoku. 2005. The Hydros mission and validation of soil moisture retrievals. *Geophysical Research Abstracts* Vol. 7.

Jackson, T. J., and A. Y. Hsu. 2001. Soil moisture and TRMM microwave imager relationships in the Southern Great Plains 1999 (SGP99) experiment. *IEEE Transactions on Geoscience and Remote Sensing* 39 (8): 1632-1642.

Jackson, T. J., A. Y. Hsu, and P. E. O'Neill. 2002. Surface Soil Moisture Retrieval and Mapping Using High-Frequency Microwave Satellite Observations in the Southern Great Plains. *Journal of Hydrometeorology* vol. 3, no. 6: 688-699.

Jackson, T. J., A. Y. Hsu, A. Van de Griend, and J. R. Eagleman. 2004. Skylab L-band microwave radiometer observations of soil moisture revisited. *International Journal of Remote Sensing* 25 (13): 2585 - 2606.

Jackson, T. J., and D. E. Le Vine. 1996. Mapping surface soil moisture using an aircraft-based passive microwave instrument: algorithm and example. *Journal of Hydrology* 184 (1-2): 85-99.

Jackson, T. J., D. M. Le Vine, A. Y. Hsu, A. Oldak, P. J. Starks, C. T. Swift, J. D. Isham, and M. Haken. 1999. Soil moisture mapping at regional scales using microwave radiometry: the Southern Great Plains Hydrology Experiment. *IEEE Transactions on Geoscience and Remote Sensing* 37 (5): 2136-2151.

Jackson, T. J., D. M. Le Vine, C. T. Swift, and T. J. Schmugge. 1995a. Large scale mapping of soil moisture using the ESTAR passive microwave radiometer. *Remote Sensing of Environment* 53: 27-37.

Jackson, T. J., and P. E. O'Neill. 1987. Salinity Effects on the Microwave Emission of Soils. *IEEE Transactions on Geoscience and Remote Sensing* GE-25 (2): 214-220.

Jackson, T. J., P. E. O'Neill, W. P. Kustas, E. Bennett, and C. T. Smith. 1995b. *IEEE International Geoscience and Remote Sensing Symposium, 1995 (IGARSS '95)*, *Passive microwave observation of diurnal soil moisture at 1.4 and 2.65 GHz*.

Jackson, T. J., and T. J. Schmugge. 1989. Passive microwave remote sensing system for soil moisture: some supporting research. *IEEE Transactions on Geoscience and Remote Sensing* 27 (2): 225-235.

Jackson, T. J., and T. J. Schmugge. 1995. Surface soil moisture measurement with microwave radiometry. *Acta Astronautica* 35 (7): 477-482.

Jackson, T. J., and T. J. Schmugge. 1996. Remote sensing applications to hydrology: soil moisture. *Hydrological Sciences Journal* 41(4): 517-530.

Jacobs, J. M., B. P. Mohanty, E.-C. Hsu, and D. Miller. 2004. SMEX02: Field scale variability, time stability and similarity of soil moisture. *Remote Sensing of Environment* 92 (4): 436-446.

Jensen, C. A., R. D. Reed, R. J. Marks, II, M. A. El-Sharkawi, J. Jae-Byung, R. T. Miyamoto, G. M. Anderson, and C. J. Eggen. 1999. Inversion of feedforward neural networks: algorithms and applications. *Proceedings of the IEEE* 87 (9): 1536-1549.

Jha, G. K. 2007. Artificial Neural Networks and Its Applications. http://www.iasri.res.in/ebook/EBADAT/5-Modeling%20and%20Forecasting%20Techniques%20in%20Agriculture/5-ANN_GKJHA_2007.pdf. (accessed 10 September 2007)

Jones, L. A., J. S. Kimball, K. C. McDonald, S. T. K. Chan, E. G. Njoku, and W. C. Oechel. 2007. Satellite Microwave Remote Sensing of Boreal and Arctic Soil Temperatures From AMSR-E. *IEEE Transactions on Geoscience and Remote Sensing* 45 (7): 2004-2018.

Judge, J., L. M. Abriola, and A. W. England. 2003. Numerical validation of the land surface process component of an LSP/R model. *Advances in Water Resources* 26: 733-746.

Junlei, S., W. Dianhong, L. Nianjun, C. Li, D. Lan, and Z. Ke. 2008. *Digital Image Computing: Techniques and Applications, 2008. DICTA '08., Soil Moisture Prediction with Feature Selection Using a Neural Network*.

Kaashoek, J. F., and H. K. Van Dijk. 2002. Neural Network Pruning Applied to Real Exchange Rate Analysis. *Journal of Forecasting* 21 (8): 559-77.

Kaheil, Y. H., M. K. Gill, M. McKee, L. A. Bastidas, and E. Rosero. 2008. Downscaling and Assimilation of Surface Soil Moisture Using Ground Truth Measurements. *IEEE Transactions on Geoscience and Remote Sensing* 46 (5): 1375-1384.

Kasischke, E. S., J. M. Melack, and M. Craig Dobson. 1997. The use of imaging radars for ecological applications--A review. *Remote Sensing of Environment* 59 (2): 141-156.

Kawanishi, T., T. Sezai, Y. Ito, K. Imaoka, T. Takeshima, Y. Ishido, A. Shibata, M. Miura, H. Inahata, and R. W. Spencer. 2003. The Advanced Microwave Scanning Radiometer for the Earth Observing System (AMSR-E), NASDA's contribution to the EOS for global energy and

water cycle studies. *IEEE Transactions on Geoscience and Remote Sensing* 41 (2): 184-194.

Kerr, Y. 2007. Soil moisture from space: Where are we? *Hydrogeology Journal* 15: 117-120.

Kerr, Y. H., P. Waldteufel, J. P. Wigneron, J. Martinuzzi, J. Font, and M. Berger. 2001. Soil moisture retrieval from space: the Soil Moisture and Ocean Salinity (SMOS) mission. *IEEE Transactions on Geoscience and Remote Sensing* 39 (8): 1729-1735.

Kevin, J. L., H. W. Alex, and E. H. Geoffrey. 1990. A time-delay neural network architecture for isolated word recognition. *Neural Netw.* 3 (1): 23-43.

Kim, G., and A. P. Barros. 2002. Downscaling of remotely sensed soil moisture with a modified fractal interpolation method using contraction mapping and ancillary data. *Remote Sensing of Environment* 83: 400-413.

Kohonen, T. 1982. Self-organized formation of topologically correct feature maps. *Biological Cybernetics* 43 (1): 59-69.

Lakhankar, T. 2006. Estimation of Soil Moisture Using Microwave Remote Sensing Data. Phd Thesis, Graduate Faculty in Engineering, The City University of New York

Lakhankar, T., H. Ghedira, and R. Khanbilvardi. 2006a. Non-Parametric Tools for Soil Moisture Mapping Using Active Microwave Data. In *American Meteorological Society (AMS) Annual Meetings*. Georgia, Atlanta, USA.

Lakhankar, T., H. Ghedira, and R. Khanbilvardi. 2006b. Soil Moisture Retrieval from Radarsat Data: A Neuro-Fuzzy Approach. In *IEEE International Conference on Geoscience and Remote Sensing Symposium, 2006. IGARSS 2006*.

Lakhankar, T., H. Ghedira, M. Temimi, M. Sengupta, R. Khanbilvardi, and R. Blake. 2009. Non-parametric Methods for Soil Moisture Retrieval from Satellite Remote Sensing Data. *Remote Sensing* 1 (1): 3-21.

Li, L., and P. Gaiser. 2007. WindSat soil moisture algorithm and validation. In *IEEE International Geoscience and Remote Sensing Symposium, 2007. IGARSS 2007*.

Li, L., J. Vivekanandan, C. H. Chan, and T. Leung. 1997. Microwave radiometric technique to retrieve vapor, liquid and ice. I. Development of a neural network-based inversion method. *IEEE Transactions on Geoscience and Remote Sensing* 35 (2): 224-236.

Limaye, A. S., W. L. Crosson, C. A. Laymon, and E. G. Njoku. 2004. Land cover-based optimal deconvolution of PALS L-band microwave brightness temperatures. *Remote Sensing of Environment* 92 (4): 497-506.

Lippmann, R. 1987. An introduction to computing with neural nets. *ASSP Magazine, IEEE* 4 (2): 4-22.

Lixin, Z., S. Jiancheng, L. Suhong, and Z. Kaiguang. 2002. *IEEE International Geoscience and Remote Sensing Symposium, 2002 (IGARSS '02), The statistical inversion algorithm of bare surface soil moisture for the AMSR using C-band IEM simulated emissivity*.

. *LP DAAC: Land Processes Distributed Active Archive Center*. 1999. https://lpdaac.usgs.gov/ (accessed 14 June 2007)

Macelloni, G., S. Paloscia, P. Pampaloni, E. Santi, and M. Tedesco. 2003. Microwave radiometric measurements of soil moisture in Italy. Copernicus GmbH.

Maier, H. R., and G. C. Dandy. 2000. Neural networks for the prediction and forecasting of water resources variables: a review of modelling issues and applications. *Environmental Modelling and Software* 15 (1): 101-124.

Mattikalli, N. M., E. T. Engman, L. R. Ahuja, and T. J. Jackson. 1998. Microwave remote sensing of soil moisture for estimation of profile soil property. *International Journal of Remote Sensing* 19 (9): 1751 - 1767.

Mätzler C, and A. Standley. 2000. Technical note: Relief effects for passive microwave remote sensing. *International Journal of Remote Sensing* 21: 2403-2412.

Mecklenburg, S., Y. Kerr, J. Font, and A. Hahne. 2008. The Soil Moisture and Ocean Salinity (SMOS) Mission– An overview. *Geophysical Research Abstracts* (vol. 10).

Merlin, O., A. Al Bitar, J. P. Walker, and Y. Kerr. 2009. A sequential model for disaggregating near-surface soil moisture observations using multi-resolution thermal sensors. *Remote Sensing of Environment* 113 (10): 2275-2284.

Merlin, O., A. Chehbouni, J. P. Walker, R. Panciera, and Y. H. Kerr. 2008a. A Simple Method to Disaggregate Passive Microwave-Based Soil Moisture. *IEEE Transactions on Geoscience and Remote Sensing* 46 (3): 786-796.

Merlin, O., A. G. Chehbouni, Y. H. Kerr, E. G. Njoku, and D. Entekhabi. 2005. A combined modeling and multispectral/multiresolution remote sensing approach for disaggregation of surface soil moisture: application to SMOS configuration. *IEEE Transactions on Geoscience and Remote Sensing* 43 (9): 2036-2050.

Merlin, O., J. P. Walker, A. Chehbouni, and Y. Kerr. 2008b. Towards deterministic downscaling of SMOS soil moisture using MODIS derived soil evaporative efficiency. *Remote Sensing of Environment* 112 (10): 3935-3946.

Meyer, C. M., and W. A. Maul. 1991. The Application of Neural Networks to the SSME Startup Transient. In *27th Joint Propulsion Conference cosponsored by AIAA, SAE, ASME, and ASEE*. Sacramento, California.

Minns, A. W., and M. J. Hall. 1996. Artificial neural networks as rainfall-runoff models. *Hydrological Sciences Journal* 41 (3): 399-418.

Mission Objectives and Scientific Requirements of the SMOS Mission. 2003. http://esamultimedia.esa.int/docs/SMOS_MRD_V5.pdf.(accessed 12 March 2008)

Mo, T., B. J. Choudhury, T. J. Schmugge, and T. J. Jackson. 1982. A Model for Microwave Emission from Vegetation covered Fields. *Journal of Geophysical Research* 87: 11229-11237.

Mohanty, B. P., and T. H. Skaggs. 2001. Spatio-temporal evolution and time-stable characteristics of soil moisture within remote sensing footprints with varying soil, slope, and vegetation. *Advances in Water Resources* 24 (9-10): 1051-1067.

Moran, M. S., C. D. Peters-Lidard, J. M. Watts, and S. McElroy. 2004. Estimating soil moisture at the watershed scale with satellite-based radar and land surface models. *Canadian Journal of Remote Sensing* 30: 1-22.

Narayan, U., V. Lakshmi, and E. G. Njoku. 2004. A simple algorithm for spatial disaggregation of radiometer derived soil moisture using higher resolution radar observations. In *IEEE International Geoscience and Remote Sensing Symposium, 2004. IGARSS '04. Proceedings*.

Navarkhele, V. V., S. T. Nakade, and A. A. Shaikh. 2006. A dielectric approach to determine water content in soil using microwave transmission technique at J-band. *Journal of the Indian Institute of Science* 86 (Number 6): 723-729.

Nemani, R., L. Pierce, S. Running, and S. Goward. 1993. Developing satellite-derived estimates of surface moisture status. *Journal of Applied Meteorology* 32 (3): 548-557.

Newton, R., and J. Rouse, Jr. 1980. Microwave radiometer measurements of soil moisture content. *IEEE Transactions on Antennas and Propagation* 28 (5): 680-686.

Newton, R. W., Q. R. Black, S. Makanvand, A. J. Blanchard, and B. R. Jean. 1982. Soil Moisture Information And Thermal Microwave Emission. *IEEE Transactions on Geoscience and Remote Sensing* GE-20 (3): 275-281.

Nissen, S. 2007. *Implementation of a Fast Artificial Neural Network Library (FANN)*. Department of Computer Science University of Copenhagen (DIKU).

Njoku, E. G., and D. Entekhabi. 1996. Passive microwave remote sensing of soil moisture. *Journal of Hydrology* 184 (1-2): 101-129.

Njoku, E. G., T. J. Jackson, V. Lakshmi, T. K. Chan, and S. V. Nghiem. 2003. Soil moisture retrieval from AMSR-E. *IEEE Transactions on Geoscience and Remote Sensing* 41 (2): 215-229.

Njoku, E. G., and L. Li. 1999. Retrieval of land surface parameters using passive microwave measurements at 6-18 GHz. *IEEE Transactions on Geoscience and Remote Sensing* 37 (1): 79-93.

Noborio, K. 2001. Measurement of soil water content and electrical conductivity by time domain reflectometry: a review. *Computers and Electronics in Agriculture* 31 (3): 213-237.

Notarnicola, C., M. Angiulli, and F. Posa. 2008. Soil Moisture Retrieval From Remotely Sensed Data: Neural Network Approach Versus Bayesian Method. *IEEE Transactions on Geoscience and Remote Sensing* 46 (2): 547-557.

Nykanen, D. K., and E. Foufoula-Georgiou. 2001. Soil moisture variability and scale-dependency of nonlinear parameterizations in coupled land-atmosphere models. *Advances in Water Resources* 24 (9-10): 1143-1157.

Okamura, S. 2000. Microwave Technology for Moisture Measurement. *Subsurface Sensing Technologies and Applications* 1 (2): 205-227.

Oldak, A., T. J. Jackson, and Y. Pachepsky. 2002. Using GIS in passive microwave soil moisture mapping and geostatistical analysis. *International Journal of Geographical Information Science* 16 (7): 681 - 698.

Orr, G., N. Schraudolph, and F. Cummins. 1999. Lecture Notes. In *CS-449: Neural Networks*. Salem, Oregon. Willamette University.

Ottlé, C., D. Vidal-Madjar, and G. Girard. 1989. Remote sensing applications to hydrological modeling. *Journal of Hydrology* 105 (3-4): 369-384.

Owe, M., R. de Jeu, and J. Walker. 2001. A methodology for surface soil moisture and vegetation optical depth retrieval using the microwave polarization difference index. *IEEE Transactions on Geoscience and Remote Sensing* 39 (8): 1643-1654.

Owe, M., and R. A. M. de Jeu. 2001. *IEEE International Geoscience and Remote Sensing Symposium, 2001 (IGARSS '01), Retrieving surface soil moisture and vegetation optical depth from satellite microwave observations*.

Owe, M., and Rathbun. 1999. Estimating soil moisture from satellite microwave observations: Past and ongoing projects, and relevance to GCIP. *Journal of geophysical research* 104 (e1): 1917.

Paloscia, S., G. Macelloni, and E. Santi. 2006. Soil Moisture Estimates From AMSR-E Brightness Temperatures by Using a Dual-Frequency Algorithm. *IEEE Transactions on Geoscience and Remote Sensing* 44 (11): 3135-3144.

Paloscia, S., G. Macelloni, E. Santi, and M. Tedesco. 2002. *IEEE International Geoscience and Remote Sensing Symposium, 2002. IGARSS '02., The*

capability of microwave radiometers in retrieving soil moisture profiles: an application of artificial neural networks.

Pampaloni, P., and S. Paloscia. 1986. Microwave Emission and Plant Water Content: A Comparison between Field Measurements and Theory. *IEEE Transactions on Geoscience and Remote Sensing* GE-24 (6): 900-905.

Panciera, R. 2009. Effect of Land Surface Heterogeneity on Satellite Near-surface Soil Moisture Observations (Phd Thesis in preparation), Dept. of Civil and Environmental Engineering, The University of Melbourne, Melbourne

Panciera, R., J. P. Walker, J. D. Kalma, E. J. Kim, J. M. Hacker, O. Merlin, M. Berger, and N. Skou. 2008. The NAFE'05/CoSMOS Data Set: Toward SMOS Soil Moisture Retrieval, Downscaling, and Assimilation. *IEEE Transactions on Geoscience and Remote Sensing* 46 (3): 736-745.

Panciera, R., J. P. Walker, J. D. Kalma, E. J. Kim, K. Saleh, and J.-P. Wigneron. 2009. Evaluation of the SMOS L-MEB passive microwave soil moisture retrieval algorithm. *Remote Sensing of Environment* 113 (2): 435-444.

Panciera, R., J. P. Walker, O. Merlin, J. D. Kalma, and E. Kim. 2006. *30th Hydrology and Water Resources Symposium, Scaling Properties of L-band Passive Microwave Soil Moisture: From SMOS to Paddock Scale*. he Institute of Engineers Australia, Launceston, Australia.

Patterson, D. 1996. *Artificial Neural Networks*. Singapore: Prentice Hall.

Pellarin, T., J. C. Calvet, and J. P. Wigneron. 2003. Surface soil moisture retrieval from L-band radiometry: a global regression study. *IEEE Transactions on Geoscience and Remote Sensing* 41 (9): 2037-2051.

Pellenq, J., J. Kalma, G. Boulet, G. M. Saulnier, S. Wooldridge, Y. Kerr, and A. Chehbouni. 2003. A disaggregation scheme for soil moisture based on topography and soil depth. *Journal of Hydrology* 276 (1-4): 112-127.

Posa, F., C. Notarnicola, and M. Angiulli. 2004. Soil parameters retrieval from remotely sensed data: efficiency of neural network and Bayesian approaches. In *Geoscience and Remote Sensing Symposium, 2004. IGARSS '04. Proceedings. 2004 IEEE International*.

Price, J. C. 1980. The Potential of Remotely Sensed Thermal Infrared Data to Infer Surface Soil Moisture and Evaporation. *Water Resour. Res.* 16 (4): 787-795.

Priddy, K. L., and P. E. Keller. 2005. *Artificial Neural Networks: An Introduction*. Vol. 68. Washington: SPIE-International Society for Optical Engineering.

Pulliainen, J., J. P. Karna, and M. Hallikainen. 1993. Development of geophysical retrieval algorithms for the MIMR. *IEEE Transactions on Geoscience and Remote Sensing* 31 (1): 268-277.

Richard, M. P., J. S. Price, S. K. Carey, and J. M. Waddington. 2004. Statistical characterization of the spatial variability of soil moisture in a cutover peatland. *Hydrological Processes* 18 (1): 41-52.

Robinson, D. A., S. B. Jones, J. M. Wraith, D. Or, and S. P. Friedman. 2003. A Review of Advances in Dielectric and Electrical Conductivity Measurement in Soils Using Time Domain Reflectometry. *Vadose Zone J* 2 (4): 444-475.

Robinson, I. S. 2000. Space Techniques For Remote Sensing Of Environmental Risks In Seas And Oceans. *Surveys in Geophysics* 21 (2): 317-328.

Rosenblatt, F. 1957. *The perceptron : A perceiving and recognizing automaton*. Cornell Aeronautical Laboratory.

Roth, K., R. Schulin, H. Flühler, and W. Attinger. 1990. Calibration of Time Domain Reflectometry for Water Content Measurement Using a Composite Dielectric Approach. *Water Resour. Res.* 26 (10): 2267-2273.

Rüdiger, C., G. Hancock, H. M. Hemakumara, B. Jacobs, J. D. Kalma, C. Martinez, M. Thyer, J. P. Walker, T. Wells, and G. R. Willgoose. 2007. Goulburn River experimental catchment data set. *Water Resour. Res.* 43.

Rumelhart, D. E., G. E. Hinton, and R. J. Williams. 1986. Learning representations by back-propagating errors. *Nature* 323 (6088): 533-536.

Saleh, K., J.-P. Wigneron, P. de Rosnay, J.-C. Calvet, and Y. Kerr. 2006. Semi-empirical regressions at L-band applied to surface soil moisture retrievals over grass. *Remote Sensing of Environment* 101 (3): 415-426.

Sandells, M. J., I. J. Davenport, and R. J. Gurney. 2008. Passive L-band microwave soil moisture retrieval error arising from topography in otherwise uniform scenes. *Advances in Water Resources* 31 (11): 1433-1443.

Sandholt, I., K. Rasmussen, and J. Andersen. 2002. A simple interpretation of the surface temperature/vegetation index space for assessment of surface moisture status. *Remote Sensing of Environment* 79 (2-3): 213-224.

Sarle, W. S., ed. 1997. *Neural Network FAQ, part 1 of 7: Introduction, periodic posting to the Usenet newsgroup comp.ai.neural-nets*. ftp://ftp.sas.com/pub/neural/FAQ.html (accessed 7 April 2007)

Savtchenko, A., D. Ouzounov, S. Ahmad, J. Acker, G. Leptoukh, J. Koziana, and D. Nickless. 2004. Terra and Aqua MODIS products available from NASA GES DAAC. *Advances in Space Research* 34 (4): 710-714.

Schamschula, M. P., W. L. Crosson, C. Laymon, R. Inguva, and A. Steward. 2002. *Automation Congress, 2002 Proceedings of the 5th Biannual World, Disaggrregation of remotely sensed soil moisture using neural networks*.

Schlenz, F., A. Loew, and W. Mauser. 2008. *IEEE International Geoscience and Remote Sensing Symposium, 2008. IGARSS 2008., Soil Moisture Retrieval*

from Passive Microwave Data: A Sensitivity Study Using a Coupled Svat-Radiative Transfer Model at the Upper Danube Anchor Site.

Schmugge, T. 1983a. Remote Sensing of Soil Moisture with Microwave Radiometers. *Transactions of the American Society of Agricultural Engineers* Vol. 26 (No. 3): 748-753.

Schmugge, T. 1990. *Measurements of Surface Soil Moisture and Temperature*, *In Remote Sensing of Biosphere Functioning*: Springer-Verlag, New York.

Schmugge, T. 1996. *IEEE International Geoscience and Remote Sensing Symposium, 1996 (IGARSS '96), Applications of passive microwave observations of surface soil moisture*.

Schmugge, T. 1998. Applications of passive microwave observations of surface soil moisture. *Journal of Hydrology* 212-213: 188-197.

Schmugge, T., T. J. Jackson, W. P. Kustas, and J. R. Wang. 1992. Passive microwave remote sensing of soil moisture - Results from HAPEX, FIFE and MONSOON 90 *ISPRS Journal of Photogrammetry and Remote Sensing* 47 (2-3): 127-143.

Schmugge, T., P. E. O'Neill, and J. R. Wang. 1986. Passive Microwave Soil Moisture Research. *IEEE Transactions on Geoscience and Remote Sensing* GE-24 (1): 12-22.

Schmugge, T. J. 1983b. Remote Sensing of Soil Moisture: Recent Advances. *IEEE Transactions on Geoscience and Remote Sensing* GE-21 (3): 336-344.

Schmugge, T. J., and T. J. Jackson. 1992. A dielectric model of the vegetation effects on the microwave emission from soils. *IEEE Transactions on Geoscience and Remote Sensing* 30 (4): 757-760.

Schneeberger, K., C. Stamm, C. Matzler, and H. Fluhler. 2003. *IEEE International Geoscience and Remote Sensing Symposium, 2003. IGARSS '03. Proceedings. , Estimating soil hydraulic properties from time series of L-band measured water contents*.

Schneeberger, K., C. Stamm, C. Matzler, and H. Fluhler. 2004. Ground-based dual-frequency radiometry of bare soil at high temporal resolution. *IEEE Transactions on Geoscience and Remote Sensing* 42 (3): 588-595.

Schultz, G. A. 1988. Remote sensing in hydrology. *Journal of Hydrology* 100 (1-3): 239-265.

Sharkov, E. A. 2003. *Passive Microwave Remote Sensing of Earth: Physical Foundation*. Chichester, UK: Praxis Publishing Ltd.

Shou-Fang, L., L. Yuei-An, W. Wen-Jun, J. P. Wigneron, and L. Jann-Bin. 2002. Retrieval of crop biomass and soil moisture from measured 1.4 and 10.65 GHz brightness temperatures. *IEEE Transactions on Geoscience and Remote Sensing* 40 (6): 1260-1268.

Simmonds, L. P. 1998. Estimating near-surface soil water content from passive microwave remote sensing - an application of MICRO-SWEAT. *Hydrological sciences journal* 43 (4): 521-536.

Simmonds, L. P., and E. J. Burke. 1998. Estimating near-surface soil water content from passive microwave remote sensing - an application of MICRO-SWEAT. *Hydrological Sciences Journal* 43 (4): 521-536.

Singh, V. P., and M. Fiorentino. 1996. *Geographical Information System in Hydrology*: Kluwer Academic Publishers.

Specht, D. F. 1988. Probabilistic neural networks for classification, mapping, or associative memory. In *IEEE International Conference on Neural Networks*.

Specht, D. F. 1991. A general regression neural network. *IEEE Transactions on Neural Networks* 2 (6): 568-576.

St. Germain, K. M., and P. W. Gaiser. 2000. *IEEE Aerospace Conference Proceedings Spaceborne polarimetric microwave radiometry and the Coriolis WindSat system*.

Steed, A., S. Spinello, B. Croxford, and R. Milton. 2004. *Theory and Practice of Computer Graphics, 2004. Proceedings, Data visualization within urban models*.

Stinchcombe, M., and H. White. 1989. *International Joint Conference on Neural Networks, 1989. IJCNN., Universal approximation using feedforward networks with non-sigmoid hidden layer activation functions*. Washington, DC, USA.

Stogryn, A. P., C. T. Butler, and T. J. Bartolac. Ocean surface wind retrievals from special sensor microwave imager data with neural networks. *J. Geophys. Res.* 99.

Su, Z. B. 2006. Microwave remote sensing of soil moisture. http://envisat.esa.int/envschool_2006/lectures/su2.pdf. (accessed 6 May 2007)

Swingler, K. 1996. *Applying Neural Networks: A Practical Guide*. London: Academic Press Limited.

Tan, H. 2004. *ASTER-Advanced Spaceborne Thermal Emission and Reflection Radiometer*. http://asterweb.jpl.nasa.gov/ (accessed 14 November 2008)

Teuling, A. J., and P. A. Troch. 2005. Improved understanding of soil moisture variability dynamics. *Geophys. Res. Lett.* 32.

Thomas, J. J. 1993. III. Measuring surface soil moisture using passive microwave remote sensing. *Hydrological Processes* 7 (2): 139-152.

Tien, K. J. C., J. Judge, and J. M. Jacobs. 2004. *IEEE International Geoscience and Remote Sensing Symposium, 2004 (IGARSS '04). Proceedings., Passive*

microwave remote sensing of soil moisture, evapotranspiration, and vegetation properties during a growing season of cotton.

Timm, L. C., D. T. Gomes, E. P. Barbosa, K. Reichardt, M. D. d. Souza, and J. F. Dynia. 2006. Neural network and state-space models for studying relationships among soil properties. *Scientia Agricola* 63: 386-395.

Tsang, L., Z. Chen, S. Oh, R. J. Marks, II, and A. T. C. Chang. 1992. Inversion of snow parameters from passive microwave remote sensing measurements by a neural network trained with a multiple scattering model. *IEEE Transactions on Geoscience and Remote Sensing* 30 (5): 1015-1024.

Tsegaye, T. D., W. L. Crosson, C. A. Laymon, M. P. Schamschula, and A. D. Johnson. 2003. Application of a Neural Network-Based Spatial Disaggregation Scheme for Addressing Scaling of Soil Moisture. . In *Scaling Methods in Soil Physics*, ed. Y. Pachepsky, D. E. Radcliffe and H. M. E. Selim: CRC Press LCC, Boca Raton, Florida, USA.

Turchin, V. F. 1977. *The Phenomenon of Science:a cybernetic approach to human evolution*. Columbia University Press.

Uitdewilligen, D. C. A., W. P. Kustas, and P. J. van Oevelen. 2003. Estimating surface soil moisture with the scanning low frequency microwave radiometer (SLFMR) during the Southern Great Plains 1997 (SGP97) hydrology experiment. *Physics and Chemistry of the Earth, Parts A/B/C* 28 (1-3): 41-51.

Ulaby, F. T., P. C. Dubois, and J. van Zyl. 1996. Radar mapping of surface soil moisture. *Journal of Hydrology* 184 (1-2): 57-84.

Ulaby, F. T., R. K. Moore, and A. K. Fung. 1986. *Microwave Remote Sensing, Active and Passive, vol.III: From Theory to Applications*: Artech House, Massachusettes.

Ulaby, F. T., M. Razani, and M. C. Dobson. 1983. Effects of Vegetation Cover on the Microwave Radiometric Sensitivity to Soil Moisture. *IEEE Transactions on Geoscience and Remote Sensing* GE-21 (1): 51-61.

Van Oevelen, P. J. 1998. Soil moisture variability: a comparison between detailed field measurements and remote sensing measurement techniques. *Hydrological Sciences Journal* 43 (4): 511-520.

Vinnikov, K. Y., A. Robock, N. A. Speranskaya, and C. A. Schlosser. 1996. Scales of temporal and spatial variability of midlatitude soil moisture. *J. Geophys. Res.* 101: 7163-7174.

Voltz, M. 1997. Spatial variability of soil moisture regimes at different scales: implications in the context of precision agriculture. *CIBA Foundation Symposium. John Wiley & Sons Ltd* (210): 18-37.

Vonk, E., L. C. Jain, and R. P. Johnson. 1997. *Automatic generation of a neural network architecture using evolutionary computation*. London: World Scientific Publishing Co. Pte. Ltd. .

Wagner, W., G. Bloeschl, P. Pampaloni, J.-C. Calvet, B. Bizzarri, J.-P. Wigneron, and Y. Kerr. 2007. Operational readiness of microwave remote sensing of soil moisture for hydrologic applications. *Hydrol. Res.* 38 (1): 1-20.

Walker, J. P. 1999. Estimating Soil Moisture Profile Dynamics From Near-Surface Soil Moisture Measurements And Standard Meteorological Data. Phd Thesis, Civil, Surveying and Environmental Engineering, The University of Newcastle, New South Wales.

Walker, J. P., and R. Panciera. 2005. *National Airborne Field Experiment 2005: Experiment Plan*. Department of Civil and Environmental Engineering, The University of Melbourne.

Walker, J. P., G. R. Willgoose, and J. D. Kalma. 2004. In situ measurement of soil moisture: a comparison of techniques. *Journal of Hydrology* 293 (1-4): 85-99.

Wang, J. R. 1987. Microwave Emission from Smooth Bare Fields and Soil Moisture Sampling Depth. *IEEE Transactions on Geoscience and Remote Sensing* GE-25 (5): 616-622.

Wang, J. R., and B. J. Choudhury. 1995. *Passive microwave radiation from soil: examples of emission models and observations*. Edited by B. J. Choudhury, Y. H. Kerr, E. G. Njoku and P. Pampaloni, *Passive Microwave Remote Sensing of Land-Atmosphere Interactions*: VSP Publishing, Utrecht.

Wang, J. R., E. T. Engman, M. Tsan, T. J. Schmugge, and J. C. Shiue. 1987. The Effects of Soil Moisture, Surface Roughness, and Vegetation on L-Band Emission and Backscatter. *IEEE Transactions on Geoscience and Remote Sensing* GE-25 (6): 825-833.

Wang, J. R., P. E. O'Neill, T. J. Jackson, and E. T. Engman. 1983. Multifrequency Measurements of the Effects of Soil Moisture, Soil Texture, And Surface Roughness. *IEEE Transactions on Geoscience and Remote Sensing* GE-21 (1): 44-51.

Wang, J. R., and T. J. Schmugge. 1980. An Empirical Model for the Complex Dielectric Permittivity of Soils as a Function of Water Content. *IEEE Transactions on Geoscience and Remote Sensing* GE-18 (4): 288-295.

Wang, X., and Z. Zhang. 2005. *Geoscience and Remote Sensing Symposium, 2005. IGARSS '05. Proceedings. , A review: theories, methods and development of soil moisture monitoring by remote sensing*.

Weber, D., and E. Englund. 1992. Evaluation and comparison of spatial interpolators. *Mathematical Geology* 24: 381-391.

Wei, L., B. Zhang, and M. Wang. 2007. Effects of antecedent soil moisture on runoff and soil erosion in alley cropping systems. *Agricultural Water Management* 94 (1-3): 54-62.

Werbos, P. J. 1990. Backpropagation through time: what it does and how to do it. *Proceedings of the IEEE* 78 (10): 1550-1560.

Western, A. W., R. B. Grayson, and G. Blöschl. 2002. Scaling of Soil Moisture: A Hydrologic Perspective. *Annual Review of Earth and Planetary Sciences* 30 (1): 149-180.

Widrow, B., and M. E. Hoff. 1960. *IRE WESCON Convention Record*, *Adaptive Switching Circuits*.

Wigneron, J.-P., P. Waldteufel, A. Chanzy, J. Calvet, and Y. Kerr. 2000. Two-D microwave interferometer retrieval capabilities of over land surfaces (SMOS Mission). *Remote Sensings Environment* 73 (3): 270-282.

Wigneron, J. P., J. C. Calvet, T. Pellarin, A. A. Van de Griend, M. Berger, and P. Ferrazzoli. 2003. Retrieving near-surface soil moisture from microwave radiometric observations: current status and future plans. *Remote Sensing of Environment* 85 (4): 489-506.

Wigneron, J. P., Y. Kerr, P. Waldteufel, K. Saleh, M. J. Escorihuela, P. Richaume, P. Ferrazzoli, P. de Rosnay, R. Gurney, J. C. Calvet, J. P. Grant, M. Guglielmetti, B. Hornbuckle, C. Mätzler, T. Pellarin, and M. Schwank. 2007. L-band Microwave Emission of the Biosphere (L-MEB) Model: Description and calibration against experimental data sets over crop fields. *Remote Sensing of Environment* 107 (4): 639-655.

Williams, R. J., and D. Zipser. 1989. A Learning Algorithm for Continually Running Fully Recurrent Neural Networks. *Neural Computation* 1 (2): 270-280.

Wu, S. T. S. 1996. *Geoscience and Remote Sensing Symposium, 1996 (IGARSS '96)*, *Microwave remote sensing of land surfaces soil moisture at Global Hydrology and Climate Center*.

Xiwu, Z., P. R. Houser, J. P. Walker, and W. T. Crow. 2006. A method for retrieving high-resolution surface soil moisture from hydros L-band radiometer and Radar observations. *IEEE Transactions on Geoscience and Remote Sensing* 44 (6): 1534-1544.

Yuei-An, L., J. F. Galantowicz, and A. W. England. 1999a. A land surface process/radiobrightness model with coupled heat and moisture transport for prairie grassland. *IEEE Transactions on Geoscience and Remote Sensing* 37 (4): 1848-1859.

Yuei-An, L., L. Shou-Fang, and W. Wen-June. 2001. Retrieving soil moisture from simulated brightness temperatures by a neural network. *IEEE Transactions on Geoscience and Remote Sensing* 39 (8): 1662-1672.

Yuei-An, L., Y. C. Tzeng, and K. S. Chen. 1999b. A neural-network approach to radiometric sensing of land-surface parameters. *IEEE Transactions on Geoscience and Remote Sensing* 37 (6): 2718-2724.

Zhang, G. P. 2007. Avoiding Pitfalls in Neural Network Research. *IEEE Transactions on Systems, Man, and Cybernetics - Part C: Applications and Reviews* 37 (1): 3-16.

Zhao, K. G., J. C. Shi, L. X. Zhang, L. M. Jiang, Z. J. Zhang, J. Qin, Y. J. Yao, and J. C. Hu. 2003. *IEEE International Geoscience and Remote Sensing Symposium, 2003. IGARSS '03. Proceedings. , Retrieval of bare soil surface parameters from simulated data using neural networks combined with IEM.*

Zhen, L., S. Jiancheng, and G. Huadong. 2002. *IEEE International Geoscience and Remote Sensing Symposium, 2002 (IGARSS '02), Measuring soil moisture change with vegetation cover using passive and active microwave data.*